The Superconducting and Magnetic Properties of the Iron-Chalcogenides

Dissertation

zur

Erlangung der naturwissenschaftlichen Doktorwürde
(Dr. sc. nat.)

vorgelegt der

Mathematisch-naturwissenschaftlichen Fakultät

der

Universität Zürich

von

Markus Michael Bendele
aus
Deutschland

Zürich, 2012

Promotionskomitee

Prof. Dr. Hugo Keller (Vorsitz)
Dr. Rustem Khasanov
Prof. Dr. Elvezio Morenzoni
Prof. Dr. Roman Puzniak

Meinem Vater

Die vorliegende Arbeit wurde von der Mathematisch-naturwissenschaftlichen Fakultät der Universität Zürich auf Antrag von Prof. Dr. Hugo Keller als Dissertation angenommen.

Abstract

Superconductivity is a remarkable phenomenon that was discovered exactly 100 years ago by H. Kamerlingh-Onnes. Many famous physicists such as N. Bohr, W. Heisenberg, or A. Einstein, to name only a few, tried for more than 50 years to describe the mechanism that leads to superconductivity. Only in 1957 a theory was suggested by J. Bardeen, L. Cooper, and J. Schrieffer, that was widely accepted. 25 years ago the striking finding of high temperature superconductivity in copper based materials, the so-called cuprates, by J. G. Bednorz and K. A. Müller revolutionized the field of superconductivity. The superconducting transition temperature increased within a short period of time from 23 K in the materials known till then to approximately 140 K in the cuprates. Since the discovery a great effort has been made towards the understanding of the mechanism of high temperature superconductivity and the microscopic pairing mechanism. However, it remains one of the biggest mysteries in physics. Obviously the high temperature superconductors bear still lots of surprises as ten years ago the diborides were discovered to be superconducting and recently, only three years ago, the finding of the iron-based high temperature superconductors attracted again the attention to the field. To find the microscopic mechanism leading to superconductivity in the iron-based high temperature superconductors might help to resolve the mystery of high temperature superconductivity in general.

This thesis is focused on the simplest of the iron-based high temperature superconductors, namely the binary Fe*Ch* family. Here *Ch* stands for the chemical elements belonging to the chalcogenide group like Sulfur (S), Selenium (Se), and Tellurium (Te). It is the simplest among this class because of its simple crystallographic structure consisting of a stack of Fe*Ch* layers. Furthermore, it is an ideal modeling system for the other iron-based superconductors because of its simplicity and its similarity with their electronic structure.

The electronic phase diagrams of the Fe*Ch* family contain the appearance of different ground states. Whereas the mother compounds are in general antiferromagnetically ordered, the material becomes superconducting after going through a region where superconductivity and magnetism coexist. In the framework of this thesis, the Fe*Ch* system was tuned solely by changing the lattice either by hydrostatic or chemical pressure and without introducing additional charge carriers. The muon spin rotation/relaxation/resonance (μSR) technique in combination with ac and dc magnetization experiments is an ideal tool to investigate the superconducting and magnetic states and the interplay in a sense of competition and/or coexistence between them. It can be seen that the system is extremely sensitive to pressure. $FeSe_{1-x}$ at ambient pressure is superconducting and nonmagnetic. Upon applying hydrostatic pressure the superconducting transition temperature increases and exhibits one of the biggest pressure effects known. Surprisingly, the compound features the appearance of magnetism that coexists on atomic length scales with superconductivity at high pressures.

A similar effect is observed if chemical pressure is applied by substituting Se by the isovalent Te. First the superconducting transition temperature increases, then the system becomes magnetic and superconducting at the same time, and finally it turns into an antiferromagnet. This suggests that the lattice plays a very important role in determining whether the system is superconducting, magnetic, or both at the same time as already minor changes lead to drastic differences in electronic characteristics.
In order to find hints for the pairing mechanism leading to superconductivity in the iron-based high temperature superconductors, the temperature dependence of the superfluid density and the resulting superconducting gap structure were examined. It is seen that all of the iron-based superconductors, including the FeCh, have multiple gaps that open below the critical temperature T_c. Interestingly, the gap to T_c ratio is similar in all the iron-based superconductors. A further important hint to the pairing mechanism may come from isotope exchange experiments. They in fact showed that the transition temperature is dependent on the isotope mass, which strongly suggests that the lattice effects play a major role in the pairing mechanism.

Zusammenfassung

Die Supraleitung ist ein bemerkenswertes Phänomen, das vor 100 Jahren vor H. Kamerlingh-Onnes entdeckt wurde. Daraufhin haben viele berühmte Physiker wie zum Beispiel N. Bohr, W. Heisenberg oder A. Einstein, versucht den Mechanismus, welcher zur Supraleitung führt, zu beschreiben. Dies gelang jedoch erst 1957 J. Bardeen, L. Cooper und J. Schrieffer. Vor 25 Jahren haben J. G. Bednorz und K. A. Müller das Feld der Supraleitung mit der Entdeckung der Hochtemperaturesupraleitung revolutioniert. Danach erhöhte sich die supraleitende Sprungtemperatur innerhalb kurzer Zeit von 23 K, auf einen Wert von ca. 140 K. Seither sind grosse Anstrenungen unternommen worden, den Mechanismus der Hochtemperatursupraleitung und den mikroskopischen Paarungsmechanismus zu beschreiben. Dies ist jedoch bis heute nicht gelungen und die Supraleitung bleibt eines der grössten Rätsel der Physik, welches immer noch viele Überraschungen birgt. So wurde vor 10 Jahren entdeckt, dass die Diboride supraleitend sind und vor nur drei Jahren wurde die Entdeckung von Supraleitung in eisenbasierten Materialien gefeiert. Indem der Paarungsmechanismus, der zur Supraleitung führt, in den Letztgenannten gefunden wird, können Rückschlüsse auf alle Klassen gemacht werden und möglicherweise das Rätsel der Hochtemperatursupraleitung im Generellen gelöst werden.

In dieser Arbeit wird der Fokus auf das Fe*Ch* System, die einfachste Familie der Eisenbasierten Hochtemperatursupraleitern, gelegt. Hierbei steht *Ch* als Akronym für die chemischen Elemente welche zur Gruppe der Chalkogenide gehören. Das sind zum Beispiel Schwefel (S), Selen (Se) oder Tellur (Te). Fe*Ch* wird aufgrund seiner einfachen Kristallstruktur, die nur aus einer Stapelung aus Fe*Ch* Schichten besteht, als das einfachste System bezeichnet. Zusätzlich ist es ein ideales Modellsystem für die anderen Familien der Eisenbasierten Hochtemperatursupraleiter gerade wegen dieser Einfachheit und der sich extrem ähnlichen elektronischen Struktur zwischen allen Familien.

Die elektronischen Phasendiagramme der Fe*Ch* Familie beinhalten das Auftreten von verschiedenen Phasen wie Magnetismus oder Supraleitung. Während die Muttersubstanzen im Allgemeinen antiferromagnetisch geordnet sind, werden die Materialien in der Regel supraleitend nachdem sie eine Region der Koexistenz zwischen Supraleitung und Magnetismus durchlaufen haben. In dieser Arbeit wurde das Fe*Ch* System nur durch Änderungen am Kristallgitter manipuliert. Hierfür wurde entweder hydrostatischer Druck in einer Druckzelle oder chemischer Druck durch Substitution von Se durch das isovalente Te angelegt ohne zusätzliche Ladungsträger in das System einzufügen. Die Myon Spin Rotation/Relaxation/Resonanz (μSR) Technik in Kombination mit ac und dc Magnetisierungsmessungen ist eine optimale Kombination um den supraleitenden und magnetischen Zustand zu untersuchen und wie die Beiden miteinander interagieren im Sinne von Koexistieren und/oder in Konkurenz zueinander stehen. Dabei stellte sich heraus, dass das System extrem sen-

sitiv auf Druck reagiert. $FeSe_{1-x}$ ist bei Umgebungsdruck ausschliesslich supraleitend und nicht magnetisch. Indem Druck angelegt wird, erhöht sich die supraleitende Sprungtemperatur und das System zeigt einen der grössten Druckeffekte, die in der Natur bekannt sind. Überraschenderweise wird es zusätzlich bei hohen Drücken magnetisch und Magnetismus und Supraleitung koexistieren in $FeSe_{1-x}$ auf atomaren Längenskalen. Einen ähnlichen Effekt kann man durch die Substitution von Se durch das isovalente Te beobachten. Zunächst steigt die supraleitende Sprungtemperatur an, anschliessend wird das System supraleitend und magnetisch zugleich und schliesslich tritt es in eine Phase, die ausschliesslich antiferromagnetisch ist. Diese Beobachtungen lassen den Schluss zu, dass in der Fe*Ch* Familie das Kristallgitter eine aussergewöhnlich wichtige Rolle zu spielen scheint, da bereits kleinste Änderungen am System zu drastischen Effekten an den elektronischen Eigenschaften führen. Um Hinweise auf den mikroskopischen Paarungsmechanismus, welcher zur Supraleitung in den eisenbasierten Hochtemperatursupraleitern führt, zu finden wurde die Temperaturabhängigkeit der suprafluiden Dichte und die daraus resultierende Struktur der Energielücke untersucht. Es stellt sich herraus, dass alle eisenbasierten Supraleiter einschliesslich Fe*Ch* mehrere Energielücken aufweisen. Interessanterweise ist das Verhältnis der Energielücke zur Sprungtemperatur in allen eisenbasierten Supraleitern ähnlich zueinander. Ein weiterer Hinweis auf den Paarungsmechanismus liefern Isotopenaustausch Experimente. Sie zeigten, dass die supraleitende Sprungtemperatur von der Isotopenmasse abhängt, was eindeutig die Wichtigkeit des Gitters zum Paarungsmechanismus hervorhebt.

Contents

1 Introduction

After the liquefaction of helium by H. K. Onnes in 1908 [1] he investigated the resistivity of metals at low temperature. In doing so, he discovered in 1911 that the electrical resistivity of mercury drops to zero below a critical temperature $T_c \simeq 4.19\,\mathrm{K}$ [2]. First he called the phenomenon "supraconductivity" and only later adopted the term "superconductivity". In the following years more superconducting materials as e.g. lead with a $T_c \simeq 7\,\mathrm{K}$ or niobium nitride with $T_c \simeq 16\,\mathrm{K}$ were found.

An important step in understanding superconductivity was made in 1933, when W. Meissner and R. Ochsenfeld discovered an effect called the "Meissner effect" [3]. In a weak magnetic field it is expelled completely from the inside of the superconductor below T_c, independent on the cooling history. Accordingly, superconductors are not only perfect conductors but also perfect diamagnets which lead to the conclusion that superconductivity is a thermodynamic phase. Shortly after, in 1935 F. and H. London developed the first phenomenological theory describing the thermodynamic properties of a superconductor [4, 5]. In this theory the zero resistance and the Meissner effect were described. Fifteen years later, in 1950 V. Ginzburg and L. Landau developed the Ginzburg-Landau theory that combined Landau's theory of second order phase transitions with a wave function that characterizes the superconducting state [6]. As was shown later by A. Abrikosov [7] it was the first theory specifying type I and type II superconductors by introducing the coherence length. It had great success explaining the macroscopic properties of a superconductor.

A major role to describe the mechanism behind superconductivity played the finding of the isotope effect in 1950 when E. Maxwell [8] and C. A. Reynolds *et al.* [9] discovered it in mercury at about the same time independently. It indicates that the electron-phonon interaction is a main ingredient of the mechanism leading to superconductivity. Actually, this was afterwards described by the first widely-accepted theory explaining the effect of superconductivity that was advanced in 1957 by J. Bardeen, L. Cooper, and J. Schrieffer [10, 11]. The so-called BCS theory explains superconductivity close to absolute zero, whereas the supercurrent consists of Cooper pairs, *i.e.* pairs of electrons that are interacting with each other through the exchange of phonons. It was awarded the Nobel prize in 1972. In 1959 shortly after the development of the BCS-theory L. Gor'kov showed that the microscopic BCS theory reduces to the phenomenological Ginzburg-Landau theory close to T_c [12]. After the theoretical description of superconductivity by the BCS theory and the knowledge, what properties a superconductor should have to reach a high T_c (high density of states at the Fermi level, a strong electron phonon interaction, and a high Debye temperature) T_c increased only marginally to the record of 23 K found in Nb_3Ge in 1973. However, the BCS theory reveals that the maximum value of T_c can not be higher than 30 K [13].

In 1986 the striking discovery of the cuprate high-temperature superconductivity in Ba-La-

Cu-O by J. G. Bednorz and K. A. Müller attracted the attention of the scientific community [14]. This lead to the class of the cuprate high temperature (HTC) superconductors which reached superconducting transition temperatures higher than 77 K, the boiling point of nitrogen. Till now the highest T_c is 135 K at ambient pressure [15] and reaches 164 K at high pressure [16]. The name HTC superconductors came up because T_c is higher than the supposed BCS value of 30 K and the fraction T_c/T_F (T_F Fermi temperature) is larger than in elemental, or classical superconductors as mercury or lead. However, after 25 years of research the origin of high temperature superconductivity is still not clear, and the HTC superconductors cannot be explained by the BCS theory. But there are hints that instead of electron-phonon interaction as in the conventional superconductors it is rather a polaronic mechanism [17, 18, 19] and instead of pure s-wave, rather mixed d- plus s-wave pairing is substantial [19, 20].

Over a decate later, in 2001 the binary MgB_2 was found to be superconducting at $T_c \simeq 39$ K [21]. It still is a HTC superconductor, but compared to the cuprates it is a more conventional one in the sense of electron-phonon mediated high temperature superconductivity in which not only one superconducting gap opens. It was shown that MgB_2 is a two-gap superconductor [22]. Again the field of superconductivity gained major interest when in 2008 the iron-based HTC superconductors were discovered with T_c reaching values up to 56 K [23]. Also here the microscopic origin of superconductivity is not explained yet. But it seems that the iron-based superconductors are again multi-gap superconductors with a complicated gap structure, whereas the exact symmetry of the gap still is under discussion [24].

For understanding high temperature superconductivity it is important to compare the different classes with each other. All of the high temperature superconductors share some important features like e.g. the layered structure and the resulting pronounced, temperature dependent anisotropic behavior, a small coherence length, competing order parameters, and possible multi-gap superconductivity. But there are also important differences between the classes as the iron-based HTC superconductors have metallic parent compounds while the parent compounds of the cuprates are in general insulators. Furthermore, the anisotropy of the iron-based materials is in general lower than the one of the cuprates and the temperature dependences of the anisotropy parameters of the magnetic penetration depth and the coherence length are opposite in the iron-based superconductors compared to MgB_2. Another important difference is the order parameter that is d+s-wave in the cuprates, s+s in MgB_2 and most probably $s_\pm$ in the iron-based superconductors, whereas in the latter Fermi surface nesting seems to play a major role. Hence, to understand the mechanism leading to superconductivity and the fundamental question whether the origin is similar, it is important to investigate the superconducting and magnetic properties and the interplay of both of them of these systems in detail. Especially in the iron-based HTC superconductors there are large regions of coexistence of superconductivity and magnetic order in the phase diagrams. Among the iron-based superconductors the FeCh (Ch = chalcogenide) system is an ideal system to study, since it is the simplest one due to the layered crystallographic structure with no separating layers between the superconducting ones (see Chapter 4) and the similarity of the Fermi-surface topology with that of other iron-based superconductors [25]. Muon spin rotation (μSR) in combination with magnetization measurements is an op-

timal tool to investigate the superconducting properties of the system and the interplay of superconductivity and magnetism.
In Chapter 2 a general introduction to some important phenomenological parameters and phenomena of superconductivity is given, forming a basis for the subsequent discussion of the techniques and results. Chapter 3 gives an overview on the μSR technique and its sensitivity to characteristic parameters for the different classes of materials. The following chapter 4 presents the superconducting and magnetic properties of the FeCh system and the preparation of the samples. Furthermore, the influence of hydrostatic and chemical pressure as well as the influence of excess Fe on the system is discussed. Chapter 5 deals with the iron isotope effect on the superconducting transition temperature in $FeSe_{1-x}$. As already mentioned above, the isotope effect played a major role in finding a theory for conventional superconductors. Also in the iron-based superconductors it might give a major hint at the pairing mechanism.

2 Basic properties of superconductors

Superconductors exhibit two main characteristics below the critical temperature (superconducting transition temperature) T_c: They are perfect conductors, meaning that the resistivity is unmeasurable small and they are perfect diamagnets, that expel a magnetic field up to a critical field H_c completely from their interior which is known as the Meissner effect. In this chapter the basics of the theory of superconductors are introduced. The interested reader is referred to more comprehensive textbooks [26, 27, 28].

2.1 Introduction to superconductivity

A mathematical model to describe superconductivity is based on Landau's theory of second order phase transitions [29]. Motivated by the London theory, showing that superconductors behave as though governed by a macroscopic wave function, Ginzburg and Landau introduced a complex, spatially varying order parameter. It is characterized by a complex pseudo-wave function $\psi(r)$ with $|\psi(r)|^2 = n_s(r)$, whereas n_s is the superconducting carrier density. According to the Landau theory the total free energy f of a system can be reduced by entering a new phase. Following the Ginzburg-Landau postulate the free energy density f can be expressed in the superconducting state of a spatially inhomogeneous superconductor in an applied magnetic field in a series of the form [6]:

$$f(\mathbf{H}) = f_{n0} + \alpha |\psi|^2 + \frac{\beta}{2} |\psi|^4 + \frac{1}{2m^*} \left| \left(\frac{\hbar}{i} \nabla - e^* \mathbf{A} \right) \psi \right|^2 + \frac{\mu_0 \mathbf{H}^2}{2}. \tag{2.1}$$

Here m^* denotes the effective mass and e^* the charge of the superfluid carriers, i.e. $m^* = 2m$ and $e^* = 2e$ for Cooper pairs in metals, f_{n0} is the normal state free energy, $\psi = |\psi| \exp[i\varphi]$ the complex, macroscopic order parameter of the superconducting phase, and α and β the expansion coefficients from the Landau theory of phase transitions.
Integration of the free energy over the whole sample volume and minimization by variation of ψ and $\mathbf{A}$ leads to the Ginzburg-Landau equations:

$$\alpha\psi + \beta |\psi|^2 + \frac{1}{2m^*} \left(\frac{\hbar}{i} \nabla - e^* \mathbf{A} \right)^2 \psi = 0 \tag{2.2}$$

$$\mathbf{J}_s = \frac{e^*}{m^*} |\psi|^2 (\hbar \nabla \varphi - e^* \mathbf{A}) = e^* |\psi|^2 \mathbf{v}_s \tag{2.3}$$

Here $\mathbf{v}_s$ denotes the average carrier velocity and $\mathbf{J}_s$ the density of circulating supercurrents. The Ginzburg-Landau theory contains two characteristic length scales. The 2^{nd} Ginzburg-Landau equation [Eq. (2.3)] represents the expression for the supercurrent density and is

analogous to

$$\mathbf{J}_s = -\frac{n_s^* e^{*2}}{m_e^*}\mathbf{A} \tag{2.4}$$

obtained within the generalized London theory [4]. The length scale derived from that equation is the London penetration depth

$$\lambda_{\mathrm{L}} = \sqrt{\frac{m_e^*}{\mu_0 n_s^* e^{*2}}} \tag{2.5}$$

which describes perfect conductivity, the Meissner effect, and flux quantization.
The 1^{st} Ginzburg-Landau equation [Eq. (2.2)] describes implicitly the spatial variation of $\psi(r)$, yielding an equation that has the dimension of length:

$$\xi_{\mathrm{GL}} = \sqrt{\frac{\hbar^2}{2m^*\alpha}} \tag{2.6}$$

This is the second characteristic length scale in the Ginzburg-Landau theory, called the Ginzburg-Landau coherence length ξ_{GL}.
The ratio of the two characteristic length scales is denoted as the Ginzburg-Landau parameter

$$\kappa = \frac{\lambda_{\mathrm{L}}}{\xi_{\mathrm{GL}}} \tag{2.7}$$

that is independent of temperature in classical superconductors. It allows to distinguish between two types of superconductors: type-I and type-II superconductors [26]. In the introduction to this chapter it was mentioned that superconductors behave as perfect diamagnets expelling the applied field H_{appl} completely up to a critical field H_{c} where superconductivity is suppressed. This behavior is called the Meissner effect but it is valid only for type-I superconductors for which $\kappa < 1/\sqrt{2}$. However, there are also type-II superconductors for which $\kappa > 1/\sqrt{2}$ and that show a completely different behavior. As long as H_{appl} is smaller than the lower critical field H_{c1}, type-I and type-II superconductors behave the same. But as soon as $H_{\mathrm{appl}} > H_{\mathrm{c1}}$ the magnetic field partly penetrates a type-II superconductor and forms the so-called mixed state or Shubnikov phase. Only when H_{appl} reaches the value of the upper critical field H_{c2} that is usually much higher than H_{c} in a type-I superconductor superconductivity is suppressed. Generally, in the mixed state a regular arrangement of normal conduction regions containing a single flux quantum $\Phi_0 = \pi\hbar/e$ is formed, denoted as the flux line lattice.

2.2 Energy gap and excitation spectrum

Bardeen, Cooper, and Schrieffer [10, 11] proposed in their BCS theory a weak attractive force between electrons, that is caused by the electron-phonon interaction. This causes an instability at the Fermi ground state of the electron gas and bound pairs of electrons are formed that have opposite momentum and opposite spin. Such an electron pair is called a Cooper-pair which has the spacial size of the order of the coherence length ξ_0 [30]. They are much larger than the interparticle distance and thus they are highly overlapping. The

formation of the Cooper pairs leads to a gain of energy which gives rise to a gap at the Fermi energy.
The following equation determines the temperature dependence of the superconducting gap parameter. It follows from the BCS theory and has to be solved numerically for $T > 0$ [26]:

$$\frac{1}{N(0)V} = \int_{-\hbar\omega_\mathrm{D}}^{\hbar\omega_\mathrm{D}} \frac{\tanh\frac{\sqrt{\xi_k^2+\Delta_k^2}}{2k_BT}}{\sqrt{\xi_k^2+\Delta_k^2}} \mathrm{d}\xi_k. \tag{2.8}$$

Here, $(\xi_k^2 + \Delta_k^2)^{1/2}$ is the excitation energy of a fermion quasi particle, whereas $\xi_k = E - E_\mathrm{F}$ (E_F is the Fermi energy) and Δ_k is the energy gap, $N(0)$ and V are the density of states at the Fermi level and the electron-phonon interaction strength, respectively.
For $T = 0$ it can be evaluated that the gap is comparable to k_BT_c:

$$\frac{2\Delta(0)}{k_BT_\mathrm{c}} = 3.5. \tag{2.9}$$

However, experimentally it is found in classical superconductors that the values of $2\Delta(0)$ range from $3k_BT_\mathrm{c}$ to $4.5k_BT_\mathrm{c}$.
For weak coupling superconductors $\Delta(T)/\Delta(0)$ is a monotonically decreasing function of T/T_c from 1 to 0. One sees from Eq. (2.8) that near $T = 0$ the temperature dependence of $\Delta(T)$ is very weak. This implies that the gap is nearly constant close to $T = 0$ and changes only when a significant number of quasi-particles are thermally excited. At the same time at $T \approx T_\mathrm{c}$ the superconducting gap closes relatively fast by following the relation:

$$\Delta(T) \simeq 1.74\Delta(0)\sqrt{1-\frac{T}{T_\mathrm{c}}} \tag{2.10}$$

One finds that the temperature dependence of the density of charge carriers n_s depends on the temperature evolution of the gap parameter Δ^2. The calculations yield that on the one hand $\Delta(0)$ is half of the energy gap of the superconductor and on the other hand it also determines the number of Cooper pairs [26].

3 Muon spin rotation/relaxation/resonance (μSR)

The acronym μSR stands for "muon spin rotation/relaxation/resonance". This technique, which has found a wide application in solid states physics, makes possible to study magnetism, superconductivity, diffusion processes, kinetics and molecular dynamics, and semiconductivity. In this chapter a brief introduction to the μSR technique is given, and its application to the study of magnetic materials and the internal field distributions in type-II superconductors is discussed. The interested reader is referred to more comprehensive textbooks [31, 32].

3.1 Introduction

The muon is a particle belonging to the family of the leptons with an average lifetime of $\tau_\mu \simeq 2.2\,\mu$s. The muon mass is about $1/9^{\text{th}}$ of the proton mass or, alternatively, about 200 times the electron mass. The muon is the decay product of pions that are produced upon bombarding nucleons with other nucleons. At the Paul Scherrer Institute (PSI Villigen, Switzerland) this is performed by accelerating protons with a 590 MeV cyclotron that hit a carbon target. There, the following reactions are taking place:

$$\begin{aligned}
\mathrm{p}+\mathrm{p} &\rightarrow \mathrm{p}+\mathrm{n}+\pi^+ \\
&\rightarrow \mathrm{d}+\pi^+ \\
&\rightarrow \mathrm{p}+\mathrm{p}+\pi^0 \\
\mathrm{p}+\mathrm{n} &\rightarrow \mathrm{p}+\mathrm{n}+\pi^0 \\
&\rightarrow \mathrm{p}+\mathrm{p}+\pi^- \\
&\rightarrow \mathrm{n}+\mathrm{n}+\pi^+
\end{aligned}$$

All the resulting pions (π^+, π^-, and π^0) have a spin $S = 0$. Solely the π^+ and π^- are decaying into muons whereas the π^0 decays into two γ rays:

$$\begin{aligned}
\pi^+ &\rightarrow \mu^+ + \nu_\mu \\
\pi^- &\rightarrow \mu^- + \overline{\nu}_\mu \\
\pi^0 &\rightarrow \gamma + \gamma
\end{aligned}$$

Due to the spin conservation, and since the pions have a spin 0 and the neutrinos a spin 1/2, the spin of the muons is equal to 1/2. Furthermore, as solely left-handed ν_μ exist, the pion decay violates parity leading to the production of 100 % spin polarized muons. Due

to the negative helicity of the neutrino, the muon spin points to opposite direction of its momentum.
For μSR experiments in condensed matter physics, positively charged μ^+ are used. They come to rest at interstitial lattice positions as a free particle after the thermalization process. On the other hand, negative charged muons μ^- form an excited muonic atom where the muon behaves as a heavy electron. After an averaged lifetime of $\tau_\mu \simeq 2.2\,\mu$s, the muon μ^+ decays into a positron e^+, an electron-neutrino ν_e, and a muon-antineutrino $\overline{\nu}_\mu$, as the lepton number and the charge must be conserved:

$$\mu^+ \quad \rightarrow \quad e^+ + \nu_e + \overline{\nu}_\mu$$

This decay, as the pion decay, occurs via the weak interaction, and as the neutrinos have a negative helicity and the antineutrinos a positive, the decay positron tends to be emitted along the muon spin direction at the time of the decay.

Roughly speaking, there are three key properties of the muon making μSR possible: (i) the muon is 100% spin polarized, (ii) the positron is preferentially emitted along the direction of the muon spin at decay time, and (iii) the muon has a magnetic moment and its spin precesses around a magnetic field with the Larmor frequency.

3.2 Principle of μSR

The μSR method is based on the observation of the time evolution of the muon spin polarization $P(t)$ of muons, that are implanted into a sample. The basic principle of a μSR experiment is illustrated in Fig. 3.1. At the time of the muon implantation into the sample, a clock triggered by the muon detector is started. In the local magnetic field the muons spin starts to precess with the Larmor frequency ω_L until it decays and emits a positron. The latter is then detected by one of the positron-detectors which stops the clock. As a result a histogram as a function of time is generated for the forward ($N_F(t)$, forward with respect to the spin) and the backward ($N_B(t)$) detectors:

$$N_{F(B)}(t) = N_0 \exp[-t/\tau_\mu] \cdot (1 + A_{max} P(t) \cdot \hat{n}_{F(B)}), \tag{3.1}$$

where

$$P(t) = \frac{\langle I(t) \cdot \hat{n} \rangle}{|I(0)|} \tag{3.2}$$

is the polarization function with the unit vector $\hat{n}$ with respect to the direction of the incoming muon spin polarization $I(0)$. To get the time evolution of the muon polarization either the exponential decay component due to the muon decay can be fitted or the asymmetry can be obtained from:

$$A(t) = A_{max} P(t) = \frac{N_F(t) - \beta N_B(t)}{N_F(t) + \beta N_B(t)}. \tag{3.3}$$

Here, the function $A(t)$ is the asymmetry, that contains the information about the physics whereas A_{max} depends on different experimental factors, such as the detector solid angle,

efficiency, absorption, and scattering of positrons in the material. The values typically lie between 0.25 and 0.3. The parameter β is introduced to take into account the different efficiency of the positron-detectors and needs to be determined by calibration.
Two different types of muon beams are used for μSR: continuous beams like at PSI and TRIUMF (Canada) and pulsed beams like the ones at ISIS (U.K.) and J-PARC (Japan). In a continuous beam a nearly continuous source of spin-polarized muons are implanted one at a time into the sample and for each individual muon its decay positron is counted. That limits the muon implantation rate since the corresponding muon/positron events need to be clearly differentiate from another pair. However, the paramount advantage of this type of muon beam is the small time resolution of $\approx 100\,\mathrm{ps}$ which give the possibility to investigate large magnetic fields and fast relaxing signals. On the other hand, in a pulsed beam a bunch of muons are implanted into the sample at the same time, with the conditions that the muon pulse must be considerably shorter than the lifetime of the muons and that the pulse repetition period must be much longer than the muon lifetime. A pulsed beam cannot compete with a continuous beam measuring fast relaxing μSR signals or μSR spectra in high magnetic fields, since the pulses have typically a width of 80 ns. The advantages on the other hand are, that one can use the entire amount of incoming muons, a lower background due to the absence of accidental double events, and by synchronizing the muon beam with e.g. an RF field one has the possibility to study resonance effects.

3.3 Muons in materials

Two different magnetic field configurations for μSR experiments are used: (i) the transverse-field (TF) μSR and (ii) the longitudinal (LF) and zero-field (ZF) μSR. In the TF configuration an external magnetic field $\vec{B}_{\mathrm{ext}}$ is applied perpendicular to the original muon polarization, whereas in LF μSR the field is applied along the initial muon spin direction, and in ZF μSR no field is applied.

3.3.1 Muons in magnetic materials

Muons are ideal local probes to study problems in magnetism like determining the internal field distributions and the magnetic ground state of systems. This is performed by ZF μSR (zero applied field, see above). For the muons stopping in magnetically ordered systems, their spins precess in the local field B_{loc} with the Larmor frequency $\omega_\mu = \gamma_\mu \cdot B_{\mathrm{loc}}$ ($\gamma_\mu = 2\pi \cdot 135.5\,\mathrm{MHz/T}$ is the gyromagnetic ratio of the muon), yielding a precessing signal directly proportional to B_{loc}. Due to their large magnetic moment the muons are very sensitive to small magnetic fields ($\simeq 10^{-5}\,\mathrm{T}$, i.e. values of the order of magnetic fields created by nuclear moments). As the muons are stopping at well defined crystallographic sites, but randomly in the sample, the μSR technique can be utilized to check the coexistence of different types of ground states at the microscopic level. If different ground states are present in a sample, they will be characterized in the μSR spectrum by different components with amplitudes proportional to the corresponding volume fractions. This makes the technique extremely

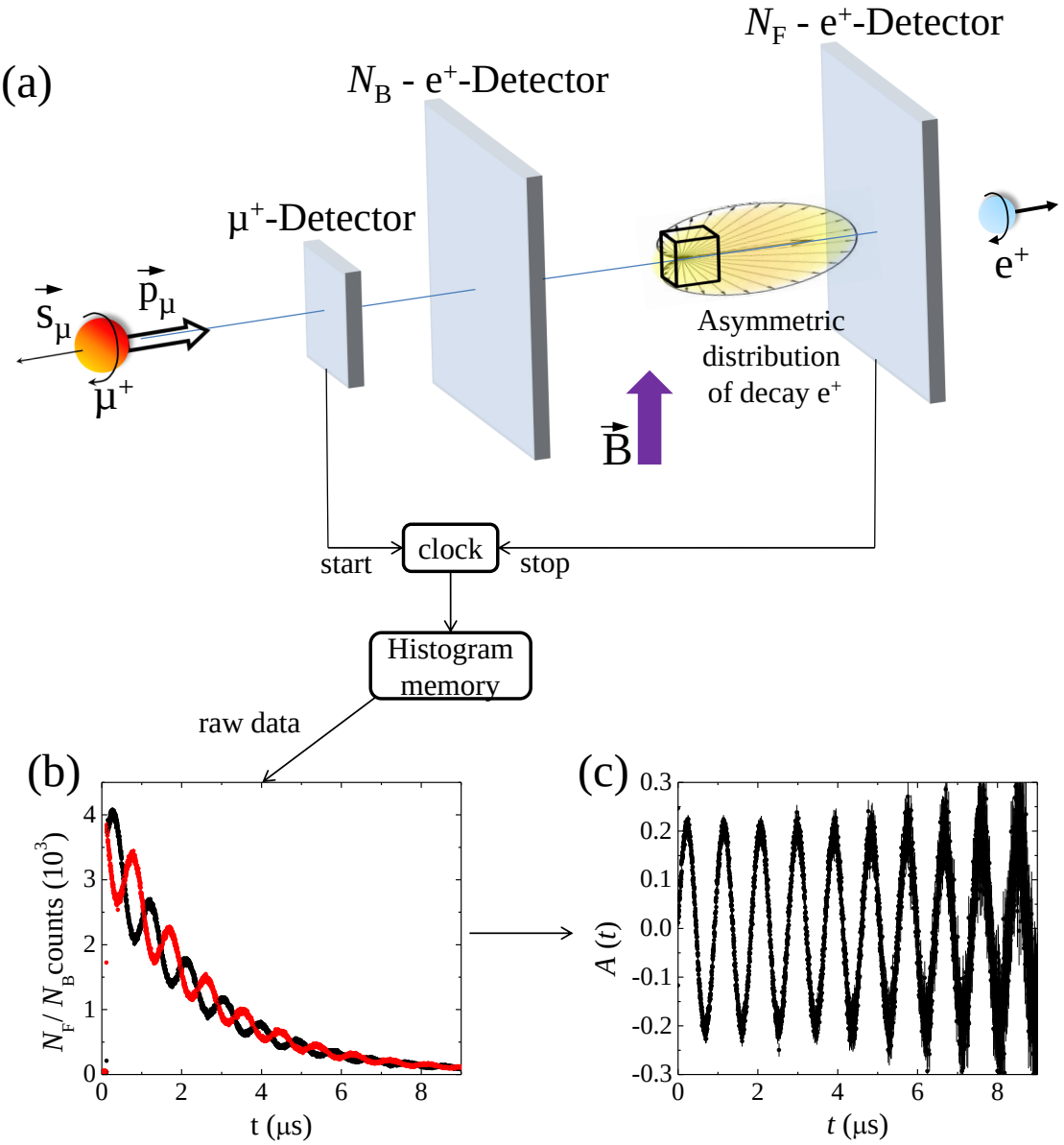

Figure 3.1: Principle of a μSR experiment as explained in the text. (a) shows the simplified experimental setup of a beamline: A spin polarized muon is implanted in the sample that is placed between the forward and the backward positron detector. In the transverse field (TF) configuration the external field B_{ext} is applied perpendicular to the initial muon spin polarization, whereas in longitudinal field μSR experiments the external field is applied parallel to the muon spin polarization. In zero-field μSR no field is applied, and the muon precesses only in the local magnetic field of the sample B_{loc}. A clock is started at the time the muon enters the muon detector/sample and stopped again as soon as the decay positron is detected. (b) The number of detected positrons as a function of time for both individual detectors. The histograms still contain the natural life-time decay of the muons. (c) The asymmetry signal obtained from the forward and backward positron detector with the help of Eq. 3.3.

useful in the case where the sample consists of multiple phases or if an incomplete magnetic ordering occurs.
To get a flavor of why the muon is able to study randomness and dynamics in magnetic materials some aspects of spin precession are hereafter considered. If the magnetic field at the muon site is at an angle ϑ to the initial muon spin direction, the muon spin will precess around the direction of the field along a cone with angular aperture ϑ. The decay positron asymmetry is then given by:

$$A(t) = A_{\max}\left[\cos^2\vartheta + \sin^2\vartheta\cos\left(\gamma_\mu B_{\mathrm{loc}} t\right)\right]. \tag{3.4}$$

In the case of a polycrystal, the direction of the local internal field is random with respect to the initial polarization. Averaging over all directions yields

$$A(t) = A_{\max}\left[\frac{1}{3} + \frac{2}{3}\cos\left(\gamma_\mu B_{\mathrm{loc}} t\right)\right]. \tag{3.5}$$

If the internal field is not constant, but is Gaussian distributed around zero with a width Δ/γ_μ, one obtains the well-known formula

$$A(t) = A_{\max}\left[\frac{1}{3} + \frac{2}{3}\left(1-\Delta^2 t^2\right)\exp\left[-\Delta^2 t^2/2\right]\right], \tag{3.6}$$

developed by Kubo and Toyabe [33]. This relaxation function falls from its initial value to a minimum and recovers to an average value $A(t \to \infty) = 1/3 A_{\max}$. Obviously, the form of the internal field distribution will strongly affect the form of the observed μSR time spectrum, e.g. if the magnetic order is incommensurate with the crystal lattice, the muon spin relaxation follows a Bessel function [34, 35].
If there is a variation of the field strength, different muons will precess with different frequencies, leading to a dephasing so that the oscillations will be damped. The bigger this variation is, the larger is the damping until the oscillations vanish. However, such an effect could also arise from fluctuations either of the internal field or due to muon diffusion. The origin of the vanishing of the oscillations can be determined by so called longitudinal field (LF) measurements, where the field is applied parallel to the initial muon spin direction [36]. Already relatively low magnetic fields ($B_{\mathrm{ext}} \leq 10 \times B_{\mathrm{loc}}$) have a large effect in the case of static magnetism or weak dynamics, but less effect if the dynamics are fast.

3.3.2 Muons in superconducting materials

Using the μSR technique important length scales of superconductors can be measured, namely the magnetic penetration depth λ and the coherence length ξ (see Chapter 2) [37]. If a type II superconductor is cooled below T_{c} in an applied magnetic field $H_{\mathrm{c1}} < H < H_{\mathrm{c2}}$ a vortex lattice is formed which in general is incommensurate with the crystal lattice and the vortex cores will be separated by much larger dimensions than those of the unit cell. Because the implanted muons stop at given crystallographic sites, they will randomly probe the field distribution of the vortex lattice.

Such measurements need to be performed in an applied field perpendicular to the muon spin (TF configuration). In the normal state, all muons precess with the frequency $\omega = \gamma_\mu B_{\text{ext}}$ and the field distribution is ideally a δ-peak (some broadening may occur due to the nuclear moments leading to a depolarization rate σ_{nm}, see below). In the superconducting state, however, the muons will sample the field distribution created by the vortex lattice. Muons stopping close to a vortex core experience larger fields than the ones stopping in between vortices. The field distribution sensed by the muons will result in a damping of the muon precession signal. The larger the penetration depth of the superconductor (characterizing the decay of the field around a vortex), the smaller is the magnetic field variation and thus the damping. The field distribution created by the vortices is highly asymmetric as shown in Fig. 3.2. It turns out, that a sum of oscillating signals with Gaussian damping is a reasonable approximation if the probed field distribution is due to an ordered or only weakly disordered vortex lattice [38]. In this case the muon asymmetry is described by:

$$A(t) = \sum_{i=1}^{n} A_i \exp[-\sigma_i^2 t^2/2] \cos(\gamma_\mu B_i t + \varphi). \tag{3.7}$$

Here A_i are the asymmetries, σ_i the Gaussian depolarization rates, and B_i the average fields of the components i. φ is the common initial phase of the muon spins with respect to the muon detector. The total asymmetry $A = \sum_{i=1}^{n} A_i$ and the second central moment of the corresponding field distribution is given by:

$$\left\langle \Delta B^2 \right\rangle = \frac{\sigma^2}{\gamma_\mu^2} = \frac{1}{A} \sum_{i=1}^{n} A_i \left(\sigma_i^2/\gamma_\mu^2 + (B_i - \langle B \rangle)^2 \right), \tag{3.8}$$

with the corresponding first moment of the field distribution:

$$\langle B \rangle = \frac{1}{A} \sum_{i=1}^{n} A_i B_i. \tag{3.9}$$

The depolarization of the muon spin ensemble is assumed to be caused only by the inhomogeneous field distribution of the vortex lattice and random nuclear moments. The contribution from the vortex state is given by $\sigma_{\text{sc}}^2 = \sigma^2 - \sigma_{\text{nm}}^2$, where σ_{nm} is the depolarization of the nuclear moments obtained above T_{c}. For further interpretation, the magnetic penetration depth λ is evaluated from the depolarization rate σ_{sc} by the relation [39]:

$$\sigma_{\text{sc}} = 4.83 \times 10^4 \, (1-b) \left[1 + 3.9 \, (1-b)^2 \right]^{\frac{1}{2}} \lambda^{-2}, \tag{3.10}$$

where $b = \langle B \rangle / B_{\text{c2}}$ is the reduced upper critical field of the type-II superconductor. Thus, the relaxation rate of the observed precession signal can be used to determine the magnetic penetration depth. The determination of λ by μSR can be considered as a bulk technique, in contrast to many techniques that probe λ only from the surface.
A different, more advanced approach is to describe the spatial field distribution of the magnetic field in the vortex state by a Fourier series:[40, 41, 38]

$$B(\mathbf{r}) = \langle B \rangle \sum_{\mathbf{G}} \exp\left[-i\mathbf{G}\mathbf{r}\right] B_{\mathbf{G}}(\lambda, \xi), \tag{3.11}$$

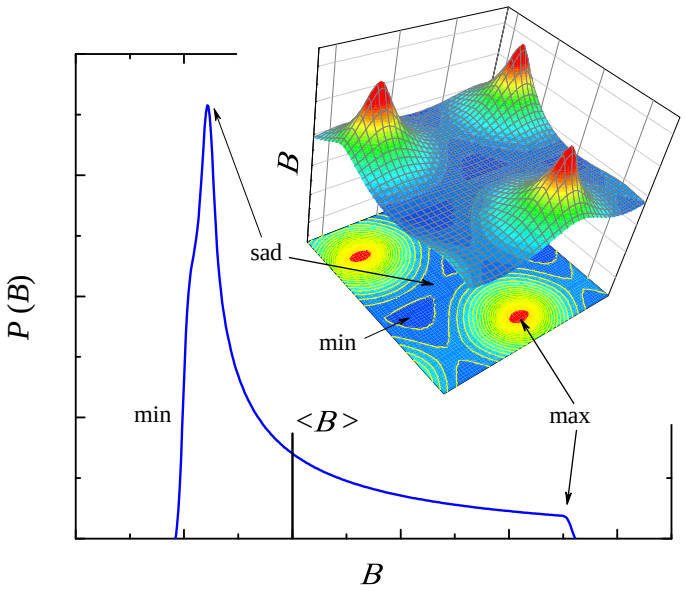

Figure 3.2: Field distribution $P(B)$ of a perfect regular vortex lattice. The inset corresponds to the spatial distribution.

where $\mathbf{r}$ is the vector coordinate in the plane perpendicular to the applied field, $\mathbf{G}$ the reciprocal lattice vectors of a two-dimensional hexagonal vortex lattice, and $B_{\mathbf{G}}$ the Fourier components. The field distribution $P(B)$ is probed by the muons by random sampling of $B(\mathbf{r})$ leading to the following asymmetry function:

$$A(t) = A_{\max} \exp\left[-\sigma_{\mathrm{g}}^2 t^2/2\right] \int P(B) \cos\left(\gamma_\mu B t + \varphi\right) \mathrm{d}B. \tag{3.12}$$

Here the Gaussian prefactor takes the broadening of the field distribution by e.g. nuclear dipole fields or weak pinning into account [42], whereas in the above described Gaussian approximation only the nuclear moments are taken into account and one assumes a perfect vortex lattice.

4 The Fe*Ch* system

This chapter is focused on the superconducting and magnetic phases, their properties, and their competition, coexistence, and interplay in the Fe*Ch* system (*Ch* = chalcogen S, Se, Te), which is the most simple among the Fe-based superconductors discovered in 2008 [23]. First an introduction to the Fe-based superconductors is given, followed by a detailed description of the preparation procedure. Then the hydrostatic as well as the chemical pressure effect on $FeSe_{1-x}$ and finally the influence of excess Fe on the physical properties is discussed.

4.1 Fe-based superconductors

In the year 2008 Kamihara *et al.* discovered superconductivity in the iron based compound $LaFeAsO_{1-x}F_x$ with a superconducting transition temperature $T_c \simeq 26\,K$ [23]. It is worth to mention, that superconductivity in the isostructural $LaFePO_{1-x}F_x$ was observed earlier by the same group in 2006 with $T_c \simeq 5\,K$ [43]. But at that time even the fact that Fe-based or Fe-containing materials become superconducting was not noteworthy, as e.g. the Fe-containing U_6Fe [44] or the skutterudites XFe_4P_{12} [45, 46] with T_c's up to 7 K were already known. Yet only the later discovery captured the imagination of physicists and chemists worldwide as high transition temperatures can be reached although elemental iron is a ferromagnet. By applying pressure in the $LaFeAsO_{1-x}F_x$ compound T_c increases even further to $\sim 43\,K$ [47]. The compound grows in the primitive tetragonal ZrCuSiAs-type (1111-type) structure [48] and contains FeAs layers with Fe atoms in a square planar lattice arrangement tetrahedrally coordinated by As atoms. The FeAs layers alternate with the LaO layers along the *c*-axis. Remarkably, by replacing the non-magnetic La by magnetic rare earth metals such as Sm, Nd, or Ce, the transition temperature T_c even increased further to its current highest value in the Fe-based compounds of $\simeq 56\,K$ in $SmFeAsO_{1-x}F_x$ [49, 50, 51, 52, 53]. The materials with the highest T_c's differ from the ones with a lower T_c in a sense that application of pressure decreases T_c in the materials with the highest T_c. This leads to the conclusion that there is an optimal ion height above the Fe-plane [54].
Shortly after the discovery of the high T_c's in the 1111 family of Fe-based superconductors, other superconducting families with similar FeAs layers were found. The $Ba_{1-x}K_xFe_2As_2$ compound in the body-centered-tetragonal $ThCr_2Si_2$ (122-type) structure shows so far a maximum of $T_c \simeq 38\,K$ for $x \simeq 0.4$ [55]. Subsequently, by replacing the Ba/K by other elements (e.g. Cs, Sr, Na, Rb, Eu) various related compounds were discovered [53, 56, 57, 58, 59]. They are, however, separated only by a single layer consisting of one atom. Other similar superconducting materials such as LiFeAs (111-type) containing FeAs layers were also reported during that time [60, 61]. Meanwhile even more complicated systems as the $(Fe_2As_2)(Ae_4M_2O_6)$ (22426, *Ae* = alkaline earth metal and *M* = transition metal) and

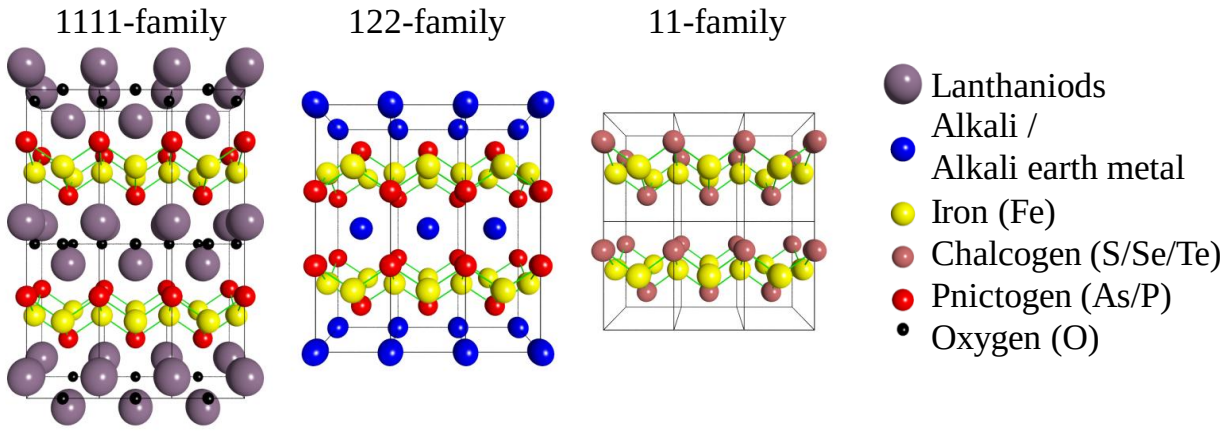

Figure 4.1: Comparison of the crystal structures of the 1111-type, the 122-type, and the 11-type. All crystal structures consist of the superconducting M_2X_2 layers separated by insulating layers. Each of the M_2X_2 layers consists of a square lattice of M atoms that is tetrahedrally coordinated by X atoms. The figure is adopted from [72].

$(Fe_2As_2)(Ae_3M_2O_5)$ (22325) were detected [62, 63].

Even the binary compound α-$FeSe_{1-x}$ (11-type) with a layered structure was found to be superconducting at $T_c \simeq 8\,K$ [64]. From the first point of view it could be argued that $FeSe_{1-x}$ is not a high temperature superconductor as T_c is that low but after a short time it was found upon studying the pressure effect, that T_c is very sensitive on chemical (substitution of Se by isovalent Te or S) or hydrostatic pressure and reaches values of 36 K at $p \simeq 9\,GPa$ [65, 66, 67, 68].

Very recently superconductivity at about 30 K was reported in the FeSe-layer compound $K_{0.8}Fe_{2-x}Se_2$ [69] by intercalating potassium in a solid state reaction between the FeSe layers whereas the substitution of K by e.g. Cs or Rb did not change T_c [69, 70, 71]. This system is isostructural to the 122-type materials and thus might allow a direct comparison of the Se-based 122- to the As-based 122-type of Fe-based superconductors.

The crystal structures of the three most often studied types, namely the 1111-type, the 122-type, and the 11-type are shown in Fig. 4.1. They consist of a superconducting layer that is identical for all of them and has the composition M_2X_2, where M is a metal atom and X is either a pnictogen Pn = P, As, Sb or a chalcogen Ch = S, Se, Te. At high temperatures the layers consist of a square lattice of M atoms tetrahedrally coordinated by X atoms that can undergo a orthorhombic distortion at low temperatures controlled by the actual doping. Depending on the type of superconductor the superconducting M_2X_2 layers are separated by layers of different thickness. Therefore, the 11-type is considered to be the most simple one among all the Fe-based superconductors, as it consists of FeCh layers only without any separating atoms.

The origin of superconductivity in the Fe-based materials still needs to be resolved. Already shortly after the discovery of superconductivity in $LaFeAsO_{1-x}F_y$ calculations indicated that conventional electron-phonon coupling is not sufficient to explain the high transition

temperatures [73]. Several experiments show that the Fe-based superconductors are multi-band materials in which several gaps open in the superconducting state (for a summary of the experiments see e.g. [74]). However, after three years of research no consensus of an universal gap symmetry has been reached. Already small changes in the electronic structure can lead to a significant diversity in the superconducting gap structure like gaps with nodes in some materials or nodeless gaps in others [24]. Nevertheless, the general symmetry class of the order parameter of most or even all of the Fe-based superconductors may be the same s-wave type. Some recent studies, however, also propose a d-wave symmetry, where nodes are on the hole pockets due to symmetry reasons and involve a sign change after 90° rotation [24, 75, 76]. But nevertheless the symmetry properties are distinct from the gap structure. Gaps with the same symmetry might have a different structure: The isotropic and fully gaped s-wave states s_{++} [77] and $s_{\pm}$ [78, 79] differ only by a relative phase shift π in the latter case between the hole and electron pockets. There is one more s case, the so-called nodal $s_{\pm}$ case [24, 75, 80], in which the gap is shown to vanish at certain points on the electron pockets but the overall sign is still opposite to the hole pockets. However, several publications proposing theoretical models for superconductivity and magnetism in Fe-based superconductors argue that within them the observed coexistence of a spin density wave and superconductivity is easily possible in the sign changing $s_{\pm}$ state whereas in the s_{++} state its only possible in a very narrow range of parameters [24, 81, 82, 83].

But even if the pairing symmetry would be known it does not itself imply a specific mechanism leading to superconductivity, although it appears to rule out electron-phonon interaction [84, 85, 86]. But this conclusion could be a bit premature, because a significant Fe-isotope effect on T_c was observed [87, 88, 89, 90, 91]. This indicates that superconductivity is somehow coupled to an electron-phonon interaction. Furthermore, it seems that Fermi surface nesting plays a major role in determining the gap properties of the Fe-based systems [92].

It has been shown by inelastic neutron scattering studies that spin fluctuations occur above T_c in the Fe-based superconductors, whereas all FeAs compounds show a diffraction peak at the same wave vector $Q_{\text{nesting}} = (\frac{1}{2}, \frac{1}{2})$ r.l.u. (reciprocal lattice units) (see e. g. [93] and references therein). This is the nesting wave vector between the electron and hole Fermi surface. But also the FeCh system exhibits magnetic fluctuations in the superconducting samples above T_c along the same nesting wave vector Q_{nesting} [93, 94, 95, 96]. This, on the other hand, seems to point towards an antiferromagnetic spin fluctuation model for the pairing mechanism which would be consistent with the fully gapped $s_{\pm}$ pairing symmetry [97].

However, it appears that the suggested nodal states "may be impurity or 'accidental' effects rather than intrinsic features of the Fe-based superconductors" [93].

Attention has shifted from the 1111 to the 122 and especially to the 11 compounds, even though they have a lower T_c. The particular interest in the 11-type has several reasons like e.g. the simplicity of the system or mainly the availability of large single crystals allowing a more definite characterization of the physical properties [66].

4.2 Synthesis of $FeSe_{1-x}$

Two different routes to synthesize superconducting $FeSe_{1-x}$ were proposed. The first one is the so-called "low-temperature synthesis" (LTS) that uses Se and Fe powders as starting materials in a temperature range of $400 - 700\,°C$ [64]. Therefore, the Fe and Se powders were mixed and cold-pressed and afterwards the mixtures were sealed in quartz ampules. The $FeSe_{1-x}$ was then prepared in a solid state reaction by heating it up to $700\,°C$, slow cooling to room temperature, followed by intermediate grinding in an inert atmosphere and annealing at $400\,°C$ [64, 68, 98].

The second method is the "high-temperature synthesis" (HTS) starting from Fe pieces and Se shots that were first heated to $750\,°C$. Then the material is molten at $1075\,°C$ followed by a fast decrease in temperature down to $420\,°C$ and quenched afterwards. To complete the HTS the samples were annealed again in a new ampule at temperatures between $300\,°C$ and $500\,°C$ followed again by quenching [99].

Surprisingly, in the beginning the $FeSe_{1-x}$ samples synthesized by the LTS and HTS techniques were found to be rather different despite of $T_c \simeq 8\,K$ for both methods. Whereas in the LTS samples superconductivity was found first in a rather extended range of nominal Se content up to $x = 0.18$ in the HTS samples superconductivity was detected only in a very narrow region in the phase diagram ($0.01 \geq x \geq 0.025$). In addition, McQueen *et al.* reported that below $300\,°C$ the tetragonal - and superconducting $FeSe_{1-x}$ converts into a hexagonal not superconducting NiAs-type phase [99]. Therefore, the samples were quenched from temperatures above $300\,°C$ in the HTS. Whereas no special care for fast cooling of LTS samples needs to be taken [64, 98, 100]. In order to resolve these controversies, Pomjakushina *et al.* performed comparative studies of $FeSe_{1-x}$ synthesized by both the LTS and HTS method [98]. The magnetization measurements showed a $T_c \simeq 8\,K$ for all $FeSe_{1-x}$ samples prepared both by LTS and HTS (the superconducting transition of one LTS sample is displayed in Fig. 4.2). The neutron powder diffraction (NPD) measurements on the same samples revealed that there is only one superconducting stoichiometry, namely $FeSe_{0.980(3)}$ [98]. Any deviation of the nominal stoichiometry from this one leads to an increase of secondary impurity phases. This is confirmed by the magnetization measurements above T_c that show a magnetization $M_{magn} = 0$ only for the sample with the nominal composition $FeSe_{0.98}$. As seen in the inset of Fig. 4.2, the more the nominal stoichiometry deviates from $x = 0.02$ the larger is M_{magn} above T_c. Additionally, it is seen that M_{magn} scales with the amount of impurities detected by NPD.

By studying the temperature dependence of the crystal structure NPD revealed a second-order phase transition from a tetragonal to an orthorhombic phase on cooling at $T \sim 100\,K$. Yet the Fe-Se-Fe bond angles become different in the low-temperature phase, the Se-height above the Fe-plane stays constant [98, 100].

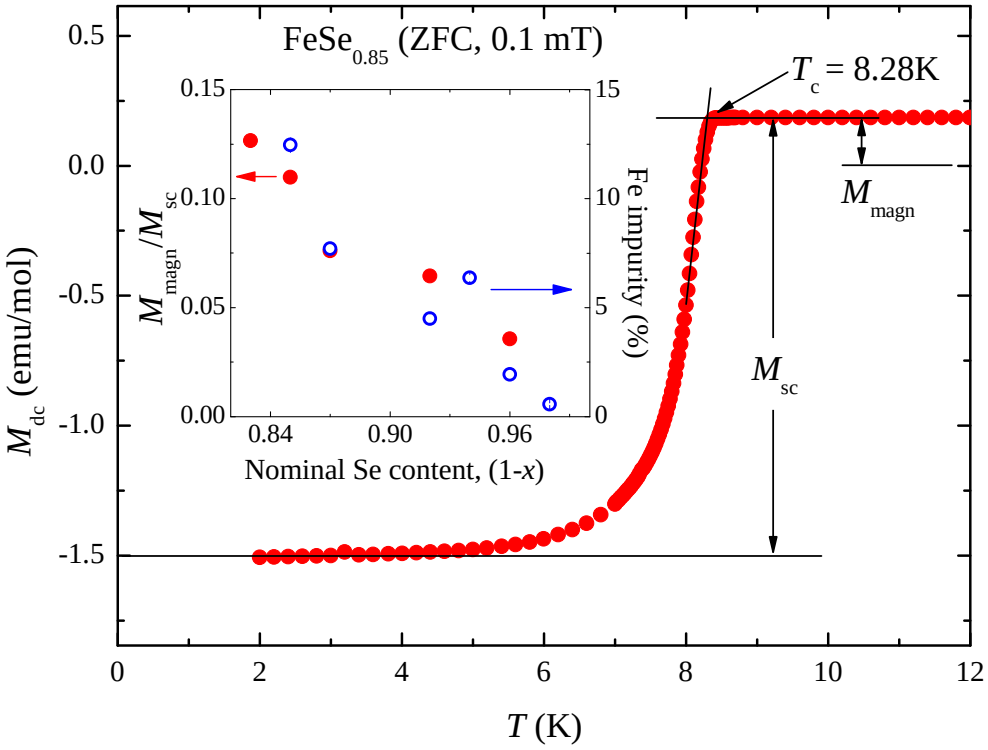

Figure 4.2: Temperature dependence of the dc magnetization M_{dc} of $FeSe_{0.85}$ (after zero field cooling in $\mu_0 H = 0.1\,\mathrm{mT}$). The superconducting transition temperature T_c, the superconducting M_{SC} and the magnetic M_{magn} responses of the sample are determined as shown in the figure. The inset shows the dependencies of $M_{\mathrm{magn}}/M_{\mathrm{SC}}$ and Fe impurity concentration as a function of the nominal Se content. After [98].

4.3 Hydrostatic pressure effect

The superconducting transition temperature of $FeSe_{1-x}$ was found to be only $T_c \simeq 8\,\mathrm{K}$ [64]. Shortly after, pressure dependent studies of the electronic and magnetic phase diagram revealed one of the largest pressure effects on T_c known at present. The transition temperature reaches values of $T_c \approx 37\,\mathrm{K}$ at $p \approx 9\,\mathrm{GPa}$, demonstrating that $FeSe_{1-x}$ is in fact a high temperature superconductor [68, 101]. Furthermore, it was discovered that superconductivity disappears at very high pressures ($p \geq 9\,\mathrm{GPa}$), which is connected to a structural phase transition to a more densely packed hexagonal phase [68].

A more detailed investigation of $T_c(p)$ with finer pressure steps at low pressures up to $\sim 2.5\,\mathrm{GPa}$ revealed a nonlinear increase. The pressure dependence of T_c exhibits a local maximum at $p \simeq 0.8\,\mathrm{GPa}$ followed by a decrease of T_c to a local minimum at $p \simeq 1.2\,\mathrm{GPa}$ [102, 103, 104]. At higher pressures ($p \geq 1.2\,\mathrm{GPa}$) T_c increases again (see Fig. 4.3). It was shown that in the region where T_c decreases static magnetic order develops in $FeSe_{1-x}$ and competes with superconductivity [102]. But as soon as the local minimum is reached and T_c increases again, superconductivity and the fully developed magnetism coexist within the

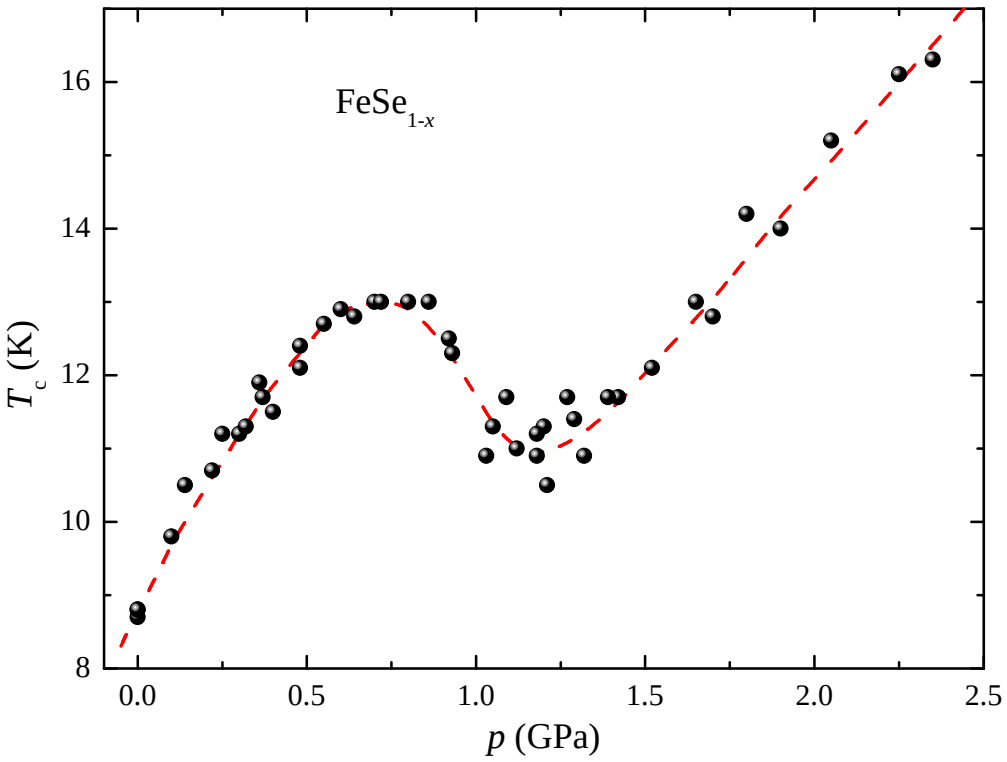

Figure 4.3: Dependence of the superconducting transition temperature T_c on pressure p of $FeSe_{1-x}$ [102, 105, 106]. Clearly, T_c increases almost linearly at low pressures up to $p \simeq 0.8$ PGa where a local maximum is observed. A further increase of the pressure leads to a decrease of T_c to a local minimum at $p \simeq 1.2$ GPa followed by an anew increase of T_c to the highest pressure investigated. The red dotted line is a guide to the eyes. After [102, 105].

whole sample volume.

The dc and ac measurements at ambient pressure without the pressure cell, performed in a SQUID magnetometer and a PPMS ac susceptometer showed that the samples are bulk superconductors with a susceptibility of $\chi \simeq -1.3$. By assuming each grain has a shape of a sphere and taking the corresponding demagnetization factor of $N = 1/3$ into account, leads to an ideal response of a superconductor of $\chi \simeq -1$. The measurements of the pressure dependence of T_c were performed in a double wall pressure cell especially designed for μSR measurements made from MP35 alloy. A frequency of $\nu_{ac} = 94$ Hz and an ac amplitude of $\mu_0 H_{ac} \approx 0.1$ mT was used for all measurements. It is well known that weak links can occur and that it can be checked for them by frequency and amplitude dependent measurements. None of the measurements gave an indication for weak links [105]. To determine the ac response under pressure reliably, the coils were directly wound on the pressure cell and the signal was normalized to the one obtained in a SQUID magnetometer. Based on these measurements the conclusion is that $FeSe_{1-x}$ is a bulk superconductor for all pressures investigated with a superconducting volume fraction of $\simeq 100\%$, as the ac response was constant up to the highest pressure investigated.

The superfluid density response was studied in transverse field (TF, $\mu_0 H = 0.01$ T) μSR

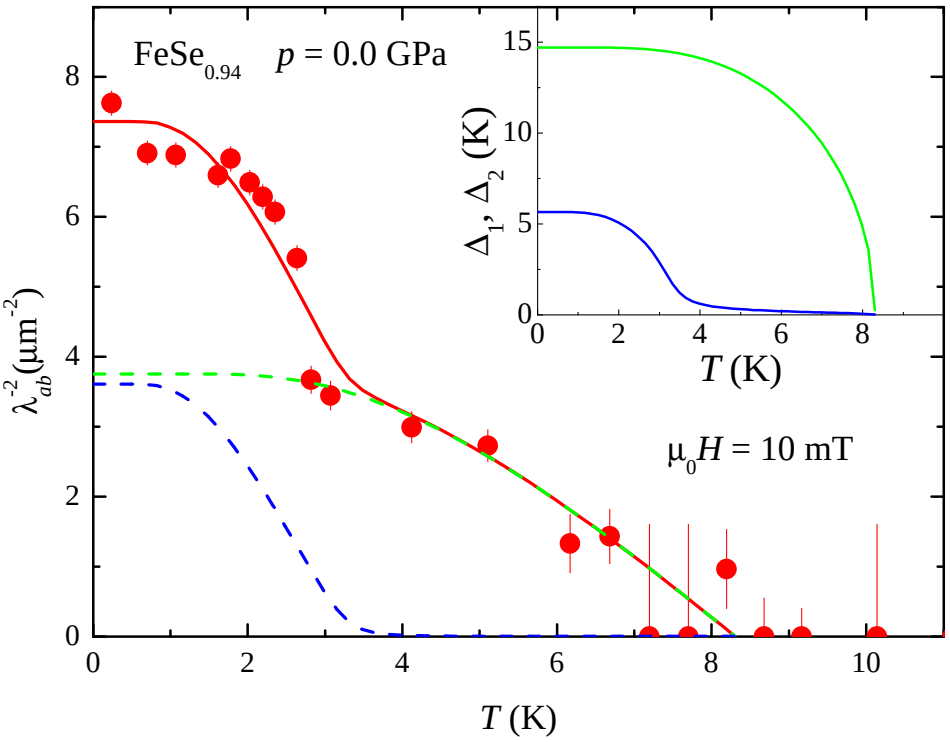

Figure 4.4: Temperature dependence of $\lambda_{ab}^{-2} \propto \rho_s = n_s/m*$ of $FeSe_{0.94}$ measured at ambient pressure in a CuBe pressure cell. Approximately 50% of the signal originates from the sample. The solid and dashed lines are the theoretical curves obtained within the framework of the γ-model [107, 108, 109]. The inset show the corresponding temperature dependencies of the large (Δ_1) and the small (Δ_2) gap. After [110].

experiments via the measurement of the in-plane magnetic penetration depth λ_{ab}. The superfluid density ρ_s can be expressed in terms of $\rho_s = n_s/m^*_{ab} \propto \lambda_{ab}^{-2}$ (n_s is the charge carrier density and m^*_{ab} is the carrier mass).

In a powder sample the magnetic penetration depth λ can be extracted from the Gaussian muon-spin depolarization rate $\sigma_{\rm sc}(T) \propto 1/\lambda^2(T)$, which probes the second moment of the magnetic field distribution in the superconductor in the mixed state. $\sigma_{\rm sc}$ can be converted into λ_{ab} via [39]:

$$\sigma_{\rm sc}^2/\gamma_\mu^2 = 0.00126\,\Phi_0^2/\lambda_{ab}^4, \tag{4.1}$$

where $\Phi_0 = 2.068 \cdot 10^{-15}$ Wb is the magnetic flux quantum and $\gamma_\mu = 2\pi$ 135.5 MHz/T is the muon gyromagnetic ratio.

The measured $\lambda_{ab}^{-2}(T)$ of $FeSe_{0.94}$ at ambient pressure is shown in Fig. 4.4. Note that the determination of $\lambda_{ab}(T)$ was possible only for $p \lesssim 0.9$ GPa. At higher pressures the emergence of static, temperature dependent magnetism does not allow to obtain $\lambda_{ab}^{-2}(T)$ with a sufficient precision [102].

The experimentally obtained $\lambda_{ab}^{-2}(T)$ was analyzed within the framework of the so-called two-band weak coupling γ-model that accounts for the interband and intraband coupling, the partial densities of states at the Fermi level, and the Fermi velocities [109]. It allows

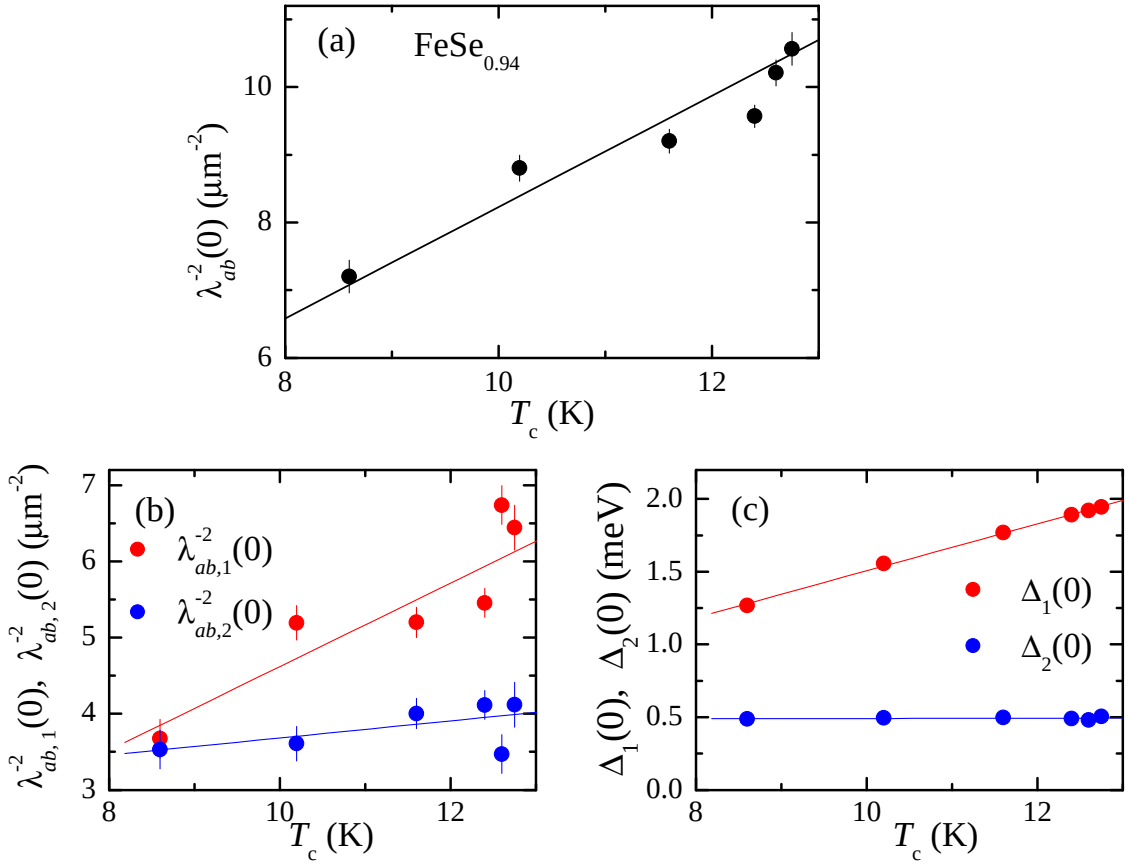

Figure 4.5: (a) Dependence of the superfluid density $\lambda_{ab}^{-2} \propto \rho_s = n_s/m^*$ on the superconducting transition temperature T_c that depends almost linear on pressure in the region shown. (b) Relative contribution of the superfluid density of the large gap $\lambda_{ab,1}^{-2}(0)$ and the small gap $\lambda_{ab,2}^{-2}(0)$ to the total superfluid density $\lambda_{ab}^{-2}(0)$ as a function of T_c. (c) Dependence of the zero-temperature values of the large gap $\Delta_1(0)$ and the small gap $\Delta_2(0)$ on T_c. After [110].

to evaluate self-consistently the temperature dependence of both superconducting energy gaps and the superfluid density. The theoretical superfluid density, calculated within the framework of the weak-coupling γ-model is shown as a solid red line in Fig. 4.4. The green and blue dashed lines represent the contributions of the large and the small gap to the superfluid density $\lambda_{ab,1}^{-2}(T)$ and $\lambda_{ab,2}^{-2}(T)$, respectively. The dependence of the superconducting gaps Δ_1 and Δ_2 on T are shown in the inset of Fig. 4.4.

The dependence of $\lambda_{ab}^{-2}(0)$, $\lambda_{ab,1}^{-2}(0)$ and $\lambda_{ab,2}^{-2}(0)$, and $\Delta_1(0)$ and $\Delta_2(0)$ on T_c (or pressure) are shown in Figs. 4.5 (a), (b), and (c). In Fig. 4.5 (a) the tendency of an increasing superfluid density $\rho_s \propto \lambda_{ab}^{-2}$ with increasing T_c is seen, following an Uemura relation which has been established for various Fe-based superconductors [111]. Figures 4.5 (b) and (c) show that the electronic bands are affected very differently by the pressure. Whereas the large gap $\Delta_1(0)$ and the corresponding $\lambda_{ab,1}^{-2}(0)$ show a strong dependence on T_c and increase almost linear, the small gap $\Delta_2(0)$ and the corresponding $\lambda_{ab,2}^{-2}(0)$ are hardly affected. Taking this together with the interband coupling constant that is estimated to be of the order of $\sim 10^{-4}$ or even less, one may conclude that the pressure effect on T_c and λ_{ab}^{-2} is mainly determined

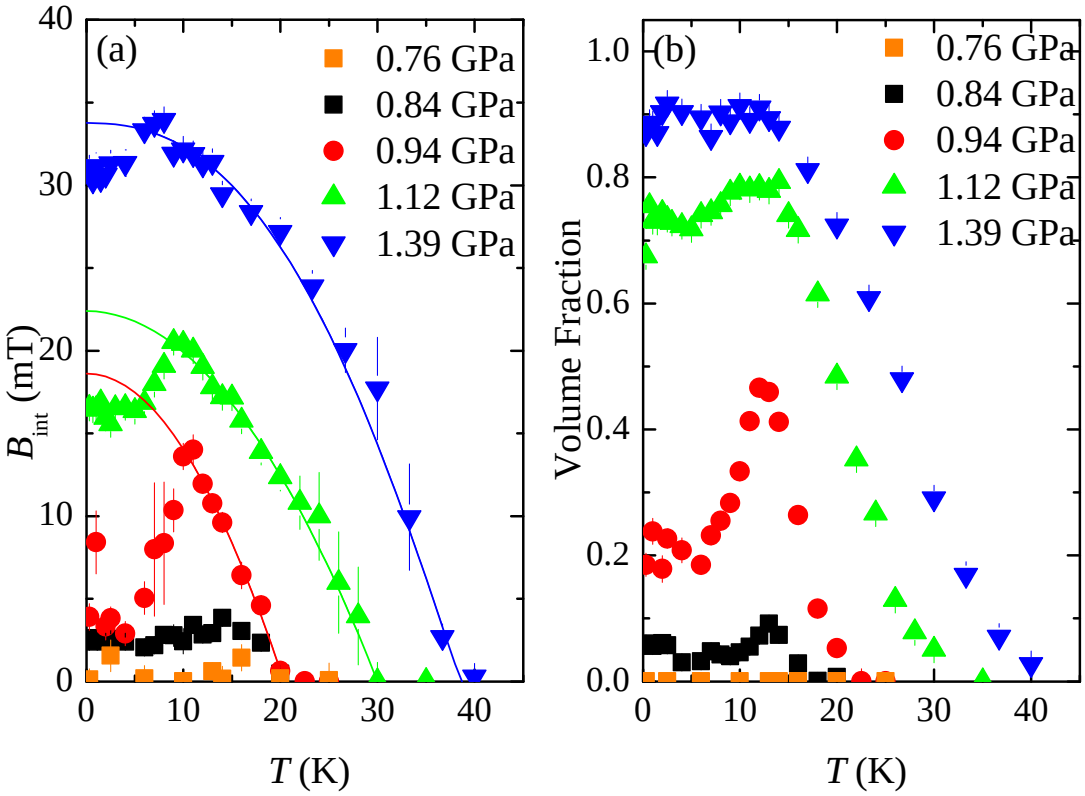

Figure 4.6: Temperature dependence of (a) the internal magnetic field at the muon stopping site B_{int} and (b) the magnetic volume fraction of $FeSe_{1-x}$ for various pressures. The solid lines in (a) are a fit of $B_{\mathrm{int}}(T)$ in the region $T_{\mathrm{c}} \leq T \leq T_{\mathrm{N}}$ to $B_{\mathrm{int}}(T) = B_{\mathrm{int}}(0)[1-(T/T_{\mathrm{N}})^{\alpha}]^{\beta}$ (α and β are power exponents). After [102].

by the bands exhibiting the large superconducting gap.

The magnetic response of $FeSe_{1-x}$ under pressure was studied in ZF μSR experiments. Three different pressure regions with different magnetic and superconducting states emerge in the sample. In the low-pressure region ($0 \leq p \lesssim 0.8\,\mathrm{GPa}$) in which T_{c} increases almost linear with p (see Fig. 4.3) no static magnetic ordering was observed to the lowest temperatures investigated ($T \simeq 0.3\,\mathrm{K}$).

For pressures above $\simeq 0.8\,\mathrm{GPa}$ a spontaneous muon spin precession is observed indicating that static long range magnetic order in the μSR time scale is present below the Néel temperature T_{N}. The oscillation is found to be best described by a zeroth-order spherical Bessel function, archetypical for incommensurate magnetic order [112]. However, as soon as superconductivity emerges the magnetic order is suppressed again, which is reflected in the temperature dependences of the internal magnetic field B_{int} that is proportional to the order parameter (Fig. 4.6(a)) and in the volume fraction (Fig. 4.6(b)) for different pressures. With increasing pressure an increase of both the volume fraction and the order parameter is observed. Furthermore, magnetism is less suppressed in the superconducting state.

At pressures higher than $p \geq 1.2\,\mathrm{GPa}$ the magnetic volume fraction is close to 100% and

stays constant even in the superconducting state. Also B_{int} does not decrease in the superconducting state any more, and the magnetic order becomes commensurate, as the μSR time spectra are best described by a cosine with zero initial phase. Additionally, with increasing pressure B_{int} increases further to the highest pressure investigated [102].
In an earlier study Medvedev *et al.* did not observe the occurrence of magnetic order in $FeSe_{1-x}$ under pressure by means of Mössbauer spectroscopy [101]. As already described in Section 4.2 two different methods HTS and LTS for the sample preparation are used so far. Medvedev *et al.* prepared the samples following the HTS method, whereas the μSR studies were done on samples prepared by the LTS method. To exclude that this discrepancy is a result of the different preparation procedures, samples for the μSR measurements were synthesized following exactly the HTS method proposed by McQueen *et al.* [99]. Both experiments lead to the same result allowing the conclusion that in the pressure and temperature range investigated by Medvedev *et al.* [101] no magnetic order appears [105, 106].
Up to now it is not clear what kind of magnetic order develops in $FeSe_{1-x}$ under pressure. Thus calculations of the muon stopping sites at different pressures combined with a symmetry analysis were performed to check for possible magnetic structures that were proposed. The muon stopping site calculations, using a modified Thomas-Fermi approach [113], revealed only one possible muon stopping site. It is located on the line connecting the Se-Se ions along the *c*-direction.
The studies of the crystal structure under pressure revealed a stronger reduction of the *c*-axis than of the *a*- and *b*-axis. This results in an increase of the Fe-Se-Fe bond angle that in accordance with the semi-empirical Goodenough-Kanamori rules can be interpreted as a tendency to antiferromagnetic exchange [114, 115, 116]. Knowing that a very small variation of the Fe-As-Fe bond angle gives rise to a drastic change of the magnetic exchange integral in the *R*FeAsO compounds [117]. This leads to the occurrence of a ferromagnetic type of order along the *a*-axis and antiferromagnetic along the *b*-axis in $FeSe_{1-x}$ under pressure. The minimal model accounting for this feature includes a doubling of the primitive cell along the *b*-direction with magnetic propagation vectors $K_I = (0; \pi/\tau_y; \pi/2\tau_z)$ or $K_{II} = (0; \pi/\tau_y; 0)$. However, other simpler possible magnetic vectors such as $K_0 = (0; 0; 0)$ and $K_{III} = (0; 0; \pi/2\tau_z)$ should also be considered.
The calculations of the magnitude and symmetry of the dipole fields of the Fe subsystem at the muon site for different pressures yield an increase of the internal field at the muon stopping site. This was observed in the experiments (see Fig. 4.6) only for the K_I and K_{II} translation symmetries, whereas for the K_0 and K_{III} translation symmetries the internal field decreases. Comparison of both possible magnetic structures K_I and K_{II} with the experimental data leads to magnetic fields along the *z*-coordinate of the size $B_z(K_I) = 354.6 \cdot m_y(K_I)$ and $B_z(K_{II}) = 334.3 \cdot m_y(K_{II})$, respectively. Both magnetic structures K_I and K_{II} provide similar and very low values of the magnetic moment per Fe atom $\mu \approx 0.2\mu_B$ at the lowest temperatures and at the highest pressure investigated in this study ($p \simeq 2.4\,\text{GPa}$) [105].
In order to test the proposed models neutron powder diffraction experiments were performed at $p = 4.4(5)\,\text{GPa}$. To obtain the position of the possible magnetic peak the background of the diffraction patterns taken at 5 and 150 K were normalized to each other and then

subtracted. However, no difference peak of magnetic origin was observed. Simulations of the proposed magnetic structures with the expected magnetic moments at $p = 4.4(5)\,\mathrm{GPa}$ resulted in magnetic reflections much smaller than the background signal [105].

The electronic phase diagram studied up to $p \simeq 2.5\,\mathrm{GPa}$ is shown in Fig. 4.7. At low pressures below $p \leq 0.8\,\mathrm{GPa}$ the samples are only superconducting and show an almost linear increase of T_c from $\sim 8\,\mathrm{K}$ at ambient pressure to $\sim 13\,\mathrm{K}$ at $\simeq 0.8\,\mathrm{GPa}$. At higher pressures static magnetic in the muon time scale order occurs below $T_\mathrm{N} > T_\mathrm{c}$ that first competes and coexists with superconductivity and then, for $p \gtrsim 1.2\,\mathrm{GPa}$, coexists only with superconductivity. In the intermediate pressure range ($0.8 \leq p \leq 1.2\,\mathrm{PGa}$) the competition is evident from two observations: First, as a function of pressure T_c is suppressed as soon as magnetic order appears, leading to the local maximum of T_c at $p \simeq 0.8\,\mathrm{GPa}$ (see Fig. 4.3). However, the superconducting volume fraction stays 100% for all pressures investigated. Second, the magnetic order present above T_c is parially (or even fully) suppressed by the onset of superconductivity. This is evident in the decrease of the internal magnetic field B_int and the decrease of the magnetic volume fraction shown in Fig. 4.6 [102, 105]. Above $p \simeq 1.2\,\mathrm{GPa}$ magnetism is fully established, and both T_N and the magnetic moment increase with increaing pressure.

The appearance of antiferromagnetic order has also been seen by NMR experiments [118]. An increase of $1/TT_1$ close to T_c is observed at low pressures ($p = 0$ and $0.7\,\mathrm{GPa}$) indicating antiferromagnetic modes of spin fluctuations that are strongly enhanced towards T_c. This leads to the conclusion that $FeSe_{1-x}$ is in close proximity to a magnetic instability. At higher pressures ($p = 1.4$ and $2.2\,\mathrm{GPa}$, where μSR observes static magnetic ordering) the $1/TT_1$ data reveal a broad hump significantly above T_c. Furthermore, the integrated intensity of the NMR signal begins to decrease at temperatures of $\sim 34\,\mathrm{K}$ in $1.4\,\mathrm{GPa}$ and $\sim 50\,\mathrm{K}$ in $2.2\,\mathrm{GPa}$ in excellent agreement with the μSR data. The disappearance of the NMR signal below a peak of $1/TT_1$ is a typical sign for a magnetic phase transition [118].

Keeping in mind that the superconducting volume fraction is 100% for all pressures measured and that the magnetic volume fraction reaches 100% at pressures above $1.2\,\mathrm{GPa}$ indicates that both ground states coexist in the whole sample volume. The data does not show any signature for macroscopic phase separation into superconducting and magnetic regions bigger than a few nm size, as observed e.g. in $Ba_{1-x}K_xFe_2As_2$ [119] or $LaFeAsO_{1-x}F_x$ [120]. Moreover, no sublattice that could order magnetically is present while the superconducting FeAs layers are not magnetically ordered, as e.g. in Ce- or Sm1111 [121, 122]. All these findings point rather to an atomic coexistence of the order parameters as it is seen e.g. in $FeTe_{1-x}Se_x$ [123] or $Ba(Fe_{1-x}Co_x)_2As_2$ [124]. Furthermore, it seems that the two ground states stabilize each other with pressure, since T_c, T_N, and B_int are all increasing hand in hand with increasing pressure. A comparison with the newly discovered $RFe_{2-x}Se_2$ 245 system (R = K, Cs, Rb) where superconductivity and magnetism coexist and which has the same crystallographic structure as the 122 family, rises the question whether the magnetic order in $FeSe_{1-x}$ under pressure and the magnetic order in the 245 system are of similar origin [125, 126]. In the 245 system the superconducting transition temperatures reaches $T_\mathrm{c} \simeq 32\,\mathrm{K}$ and superconductivity seem to coexists with magnetism occuring at $T_\mathrm{N} \approx 500\,\mathrm{K}$ with a rather large magnetic moment of $3\mu_B$ per Fe atom [127].

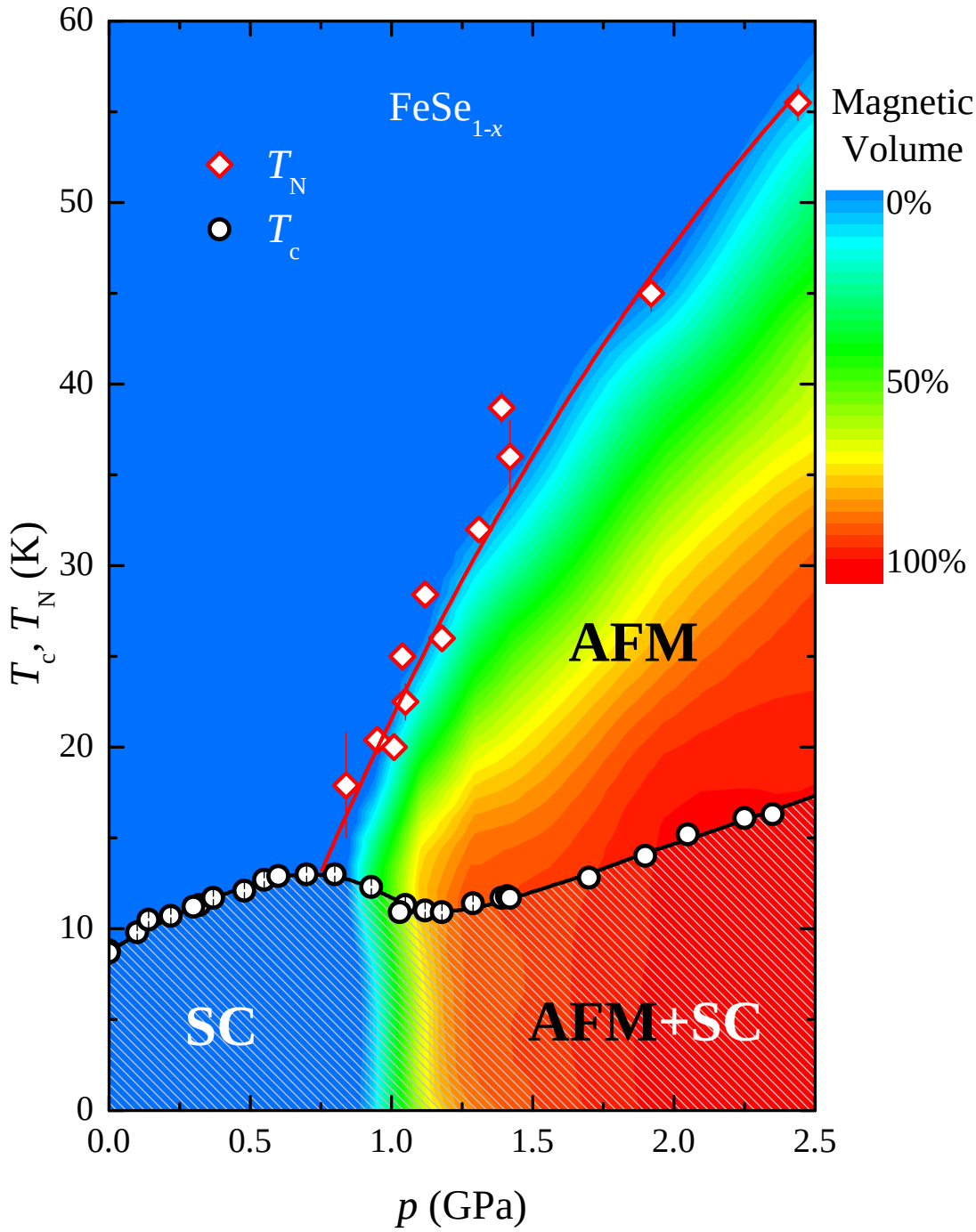

Figure 4.7: Pressure dependence of the superconducting transition temperature T_c, the magnetic ordering temperature T_N, and the superconducting and magnetic volume fractions (the superconducting volume is 100% for all pressures investigated) obtained by ac susceptibility and muon spin rotation experiments for $FeSe_{1-x}$. The lines marking the pressure dependence of T_c and T_N are guides to the eyes. SC and AFM denote the superconducting and magnetic states of the samples, respectively. The nonmagnetic state is indicated by the blue area. After [102] and [105].

Knowing that $FeSe_{1-x}$ is a two gap superconductor [110, 128] a possible scenario of an atomic coexistence of superconductivity and magnetism has recently been proposed by Vorontsov *et al.* [81, 83, 129] and Cvetkovic and Tesanovic [130]. They proposed a region where superconductivity and magnetic order can coexist. In this region the magnetic order can be commensurate only in a rather small parameter range where the Fermi surface nesting is not perfect, the bands are supposed to have an elliptical shape, and the chemical potential is supposed to shift.

4.4 Chemical pressure effect and role of Fe

Application of hydrostatic pressure is not the only possibility to increase T_c in the 11-system. Very shortly after superconductivity was found in α-$FeSe_{1-x}$ [64] at $T_c \simeq 8\,K$ it was realized that substitution of Se by the isovalent Te or S, so to say applying chemical pressure, leads to an increase of T_c up to $\simeq 14\,K$ at a substitution level of $\approx 50\%$ Se by Te [66]. Furthermore, it was discovered that large single crystals of $Fe_ySe_xTe_{1-x}$ can be grown for $0 \leq x \leq 0.5$ [66]. The availability of large superconducting single crystals made it possible to study the anisotropic superconducting properties of $Fe_ySe_xTe_{1-x}$. They were grown by the Bridgman method by mixing the appropriate amounts of Fe, Se, and Te powders together. The mixed powder was then pressed into a rod that was put to a double wall ampule and evacuated. The ampule was placed into a vertical furnace with a temperature gradient and heated to $T = 1200\,°C$. The melt was kept for 4 hours at that temperature. Afterwards, the samples were cooled down to $750\,°C$ with a rate of $4\,°C/h$, followed by a fast cooling ($\sim 50\,°C/h$) to room temperature. The so-obtained crystals were easily cleaved from the as-grown crystal along the *ab* plane.

The superconducting properties of $Fe_ySe_xTe_{1-x}$ were studied by means of magnetization measurements on a piece of the crystal with the nominal stoichiometry $FeSe_{0.5}Te_{0.5}$ and a mass of about 200 mg. A sharp transition to the superconducting state at $T_c = 14.6\,K$ was detected. However, the large difference between the field cooled and zero field cooled magnetization is a signature, that strong vortex pinning is present. This is in agreement with the weakly field dependent and pronounced critical current density of the order of $10^7\,A/m^2$ [111].

The temperature dependence of the lower critical field H_{c1} was determined from magnetization measurements with the field applied parallel and perpendicular to the *ab*-plane yielding the zero temperature values of $H_{c1}^{\parallel ab}(0) = 2.0(2)\,mT$ and $H_{c1}^{\parallel c}(0) = 4.5(3)\,mT$. From these values the zero temperature magnetic penetration depths were estimated to $\lambda_{ab}(0) \approx 460(100)\,nm$ and $\lambda_c(0) \approx 1100(300)\,nm$. These values are in good agreement with the penetration depths obtained by μSR [111].

The temperature dependence of the magnetic penetration depth in both crystallographic directions was determined also by μSR. This was done by applying the field once parallel and once perpendicular to the *ab*-plane, but always perpendicular to the muon spin. The so obtained anisotropic μSR line shapes were analyzed with the help of the Ginzburg-Landau model [38]. The temperature dependence of the magnetic penetration depth is shown in

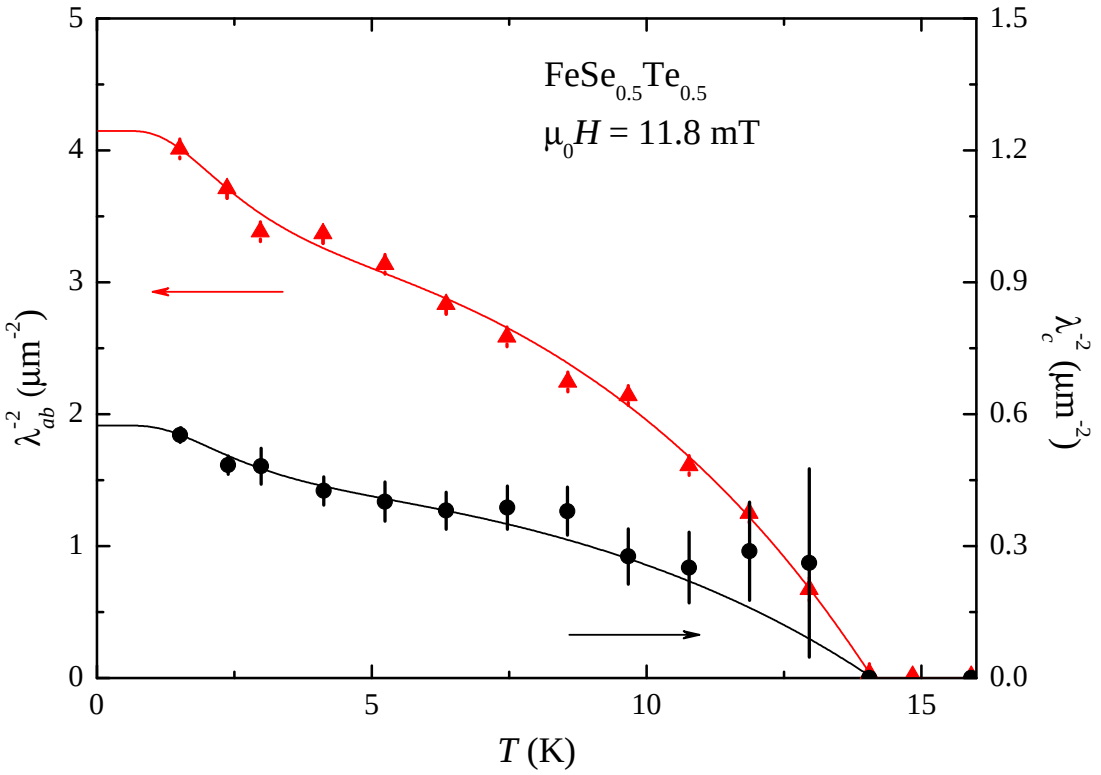

Figure 4.8: Temperature dependence of the penetration depth components λ_{ab} and λ_c of single crystal $FeSe_{0.5}Te_{0.5}$. The solid lines represend fits to the α-model. After [111].

Fig. 4.8. It was best described by a $s+s$-wave model within the framework of the so-called α-model [131] that assumes that λ^{-2} is a linear combination of two terms. The zero temperature values of the magnetic penetration depth were determined to be $\lambda_{ab}(0) = 491(8)\,\mathrm{nm}$ and $\lambda_c(0) = 1320(14)\,\mathrm{nm}$ [111], consistent with previous μSR results [132].

From the temperature dependence of λ_{ab} and λ_c the gap to T_c ratios $2\Delta_S^0/k_\mathrm{B}T_\mathrm{c} = 0.84(4)$ and $2\Delta_L^0/k_\mathrm{B}T_\mathrm{c} = 4.3(1)$ were obtained. These values are in fair agreement with μSR results of $FeSe_{0.5}Te_{0.5}$ [132] and the results obtained by other methods [135, 136]. They are also very close to what is reported for isotstructural $FeSe_{1-x}$ (see above and Refs. [110] and [128]). Furthermore, Evtushinski *et al.* pointed out that most of the Fe-based superconductors exhibit two-gap superconductivity with a large gap of $2\Delta_L^0/k_\mathrm{B}T_\mathrm{c} = 7(2)$ and a small gap of $2\Delta_S^0/k_\mathrm{B}T_\mathrm{c} = 2.5(1.5)$ [74]. The corresponding values of $FeSe_{0.5}Te_{0.5}$ are at the lower limit of these estimations.

Moreover, from the T-dependence of λ_{ab} and λ_c obtained from μSR the magnetic penetration depth anisotropy parameter γ_λ was extracted. It is within the error the same as the one deduced from H_{c1} measurements by a SQUID (see Fig. 4.9). Both techniques yield a T-dependent γ_λ that increases with decreasing temperature from 1.6 at T_c to 2.6 at $T = 1.6\,\mathrm{K}$. While γ_λ increases with decreasing temperature, the anisotropy parameter of the upper critical field $\gamma_{H_{c2}}$ determined by resistivity measurements decreases with decreasing temperature [133, 134]. The observed T-dependence of the anisotropy parameters γ_λ and

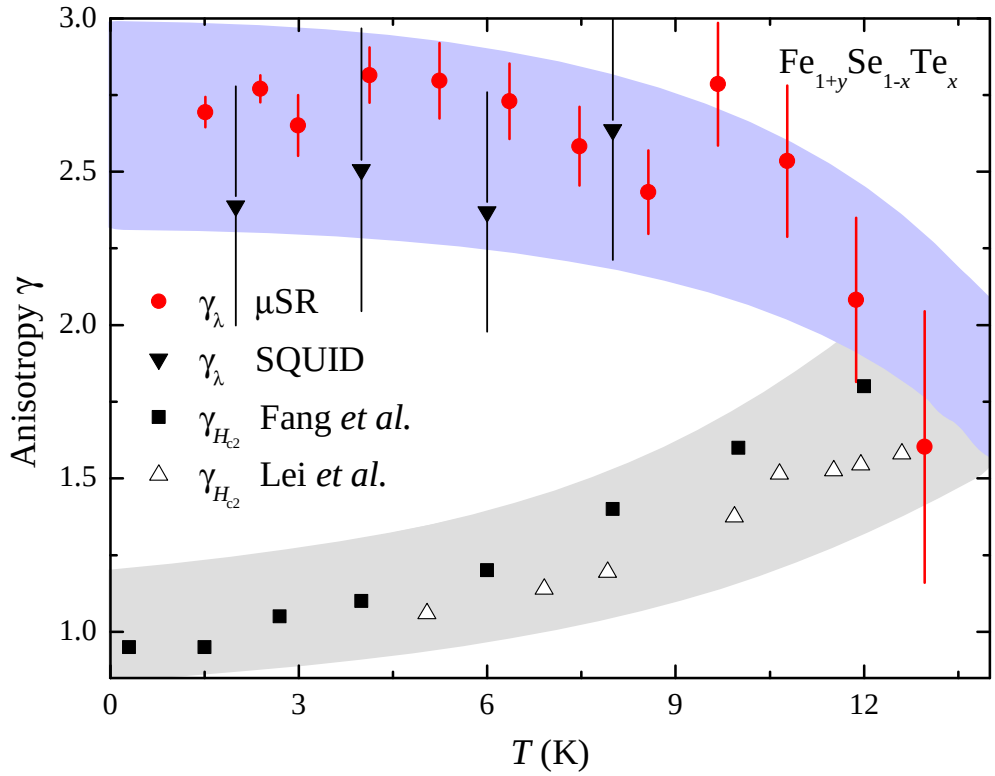

Figure 4.9: Temperature dependence of the magnetic penetration depth anisotropy parameter $\gamma_\lambda = \lambda_c/\lambda_{ab}$ derived from μSR and SQUID measurements on single crystalline $FeSe_{0.5}Te_{0.5}$ and the upper critical field H_{c2}-anisotropy parameter $\gamma_{H_{c2}} = H_{c2}^{\parallel ab}/H_{c2}^{\perp ab}$ obtained from resistivity measurements [133, 134]. The lines are guides to the eyes. After [111].

$\gamma_{H_{c2}}$ is similar to the one seen earlier by Weyeneth *et al.* in the 1111 family [137, 138]. However, superconductivity in $FeSe_{0.5}Te_{0.5}$ is much more isotropic suggesting that the direct electronic coupling of the Fe_2Se_2 layers in the 11 family is more effective than the coupling through the LnO layers in the 1111 Fe-based systems [111]. Such an anisotropic behavior was also observed in the known two-gap superconductor MgB_2, however, there γ_λ and $\gamma_{H_{c2}}$ have reversed sign: γ_λ decreases with decreasing temperature while $\gamma_{H_{c2}}$ increases.

The value of $\lambda_{ab}^{-2}(0)$ for $FeSe_{0.5}Te_{0.5}$ extracted from μSR data as well as the values of $\lambda_{ab}^{-2}(0)$ obtained for various Fe-based superconductors fall on the Uemura plot [140] (see Fig. 4.10) within the limits of hole-doped and electron-doped cuprates [141]. This suggests that the pairing mechanism in the Fe-based superconductors is unconventional as in the cuprates.

The maximum T_c in $Fe_ySe_xTe_{1-x}$ is reached at a substitution level of $\sim 50\%$. A further increase of $1-x$ leads to the appearance of magnetic order in the system, whereas superconductivity and magnetism coexist on atomic length scale in the region of $0.55 \lesssim 1-x \lesssim 0.6$. Above ($1-x \gtrsim 0.6$) only incommensurate magnetic order is present with traces of superconductivity [123]. With increasing amount of Te in the system T_N is increasing from $T_N \simeq 3\,K$ at $1-x \simeq 0.45$ to 33 K at $1-x \simeq 0.9$. For $1-x \gtrsim 0.9$ no traces of superconductivity are detected in the system and the magnetic order changes to commensurate long range antifer-

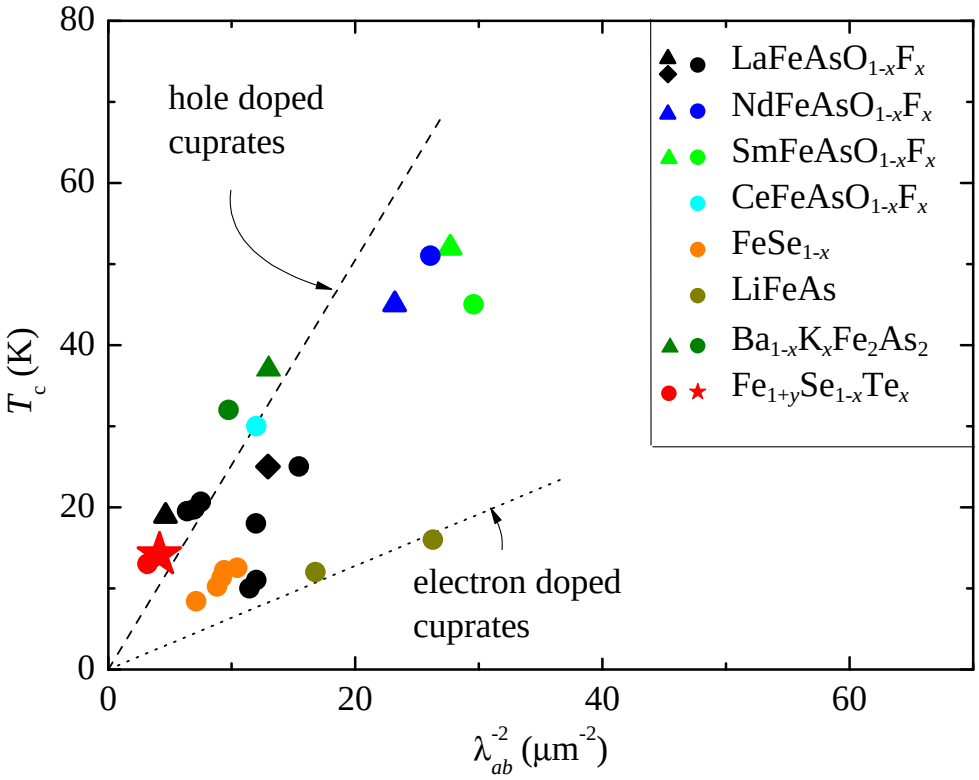

Figure 4.10: Uemura plot for a selection of Fe-based high temperature superconductors. The Uemura relation observed for underdoped cuprates is included for comparison (dashed line: hole doped, dotted line: electron doped cuprates). After [111] and references therein.

romagnetic order. In pure FeTe $T_N = 70\,K$ and coincides with a structural transition making the phase transition first order like with a hysteretic behavior [123]. The corresponding electronic phase diagram is shown in Fig. 4.11 (a).

Interestingly, the superconducting and magnetic properties of $Fe_ySe_xTe_{1-x}$ not only depend on the Se:Te ratio x but also strongly on the Fe content y [142]. This was studied systematically by keeping x constant to $x = 0.25$ and varying y in the range $0.9 \leq y \leq 1.1$ [139]. As can be seen in the phase diagram in Fig. 4.11 (b), for $y \lesssim 1$ (low Fe content region) bulk superconductivity is established and coexists with incommensurate magnetism. In this Fe deficient region, the magnetic correlations of the Fe magnetic moments are more short ranged as compared to the region of excess Fe and thus magnetic order is less well coordinated. Hence, only the reduction of the Fe content results in a reduction of the magnetic correlations and the system becomes superconducting. However, it seems unlikely that the excess Fe atoms acts as isolated magnetic moments that destroy superconductivity. They may act as magnetic electron donors that suppress superconductivity and induce weakly localized electronic states [139].

Combining both the phase diagram of $Fe_{1.03}Se_xTe_{1-x}$ and the one of $Fe_ySe_{0.25}Te_{0.75}$ leads to a tentative three-dimensional phase diagram shown in Fig. 4.11 (c). It is seen that Fe_yTe is always antiferromagnetically ordered [143, 144]. Upon substituting Te by Se the

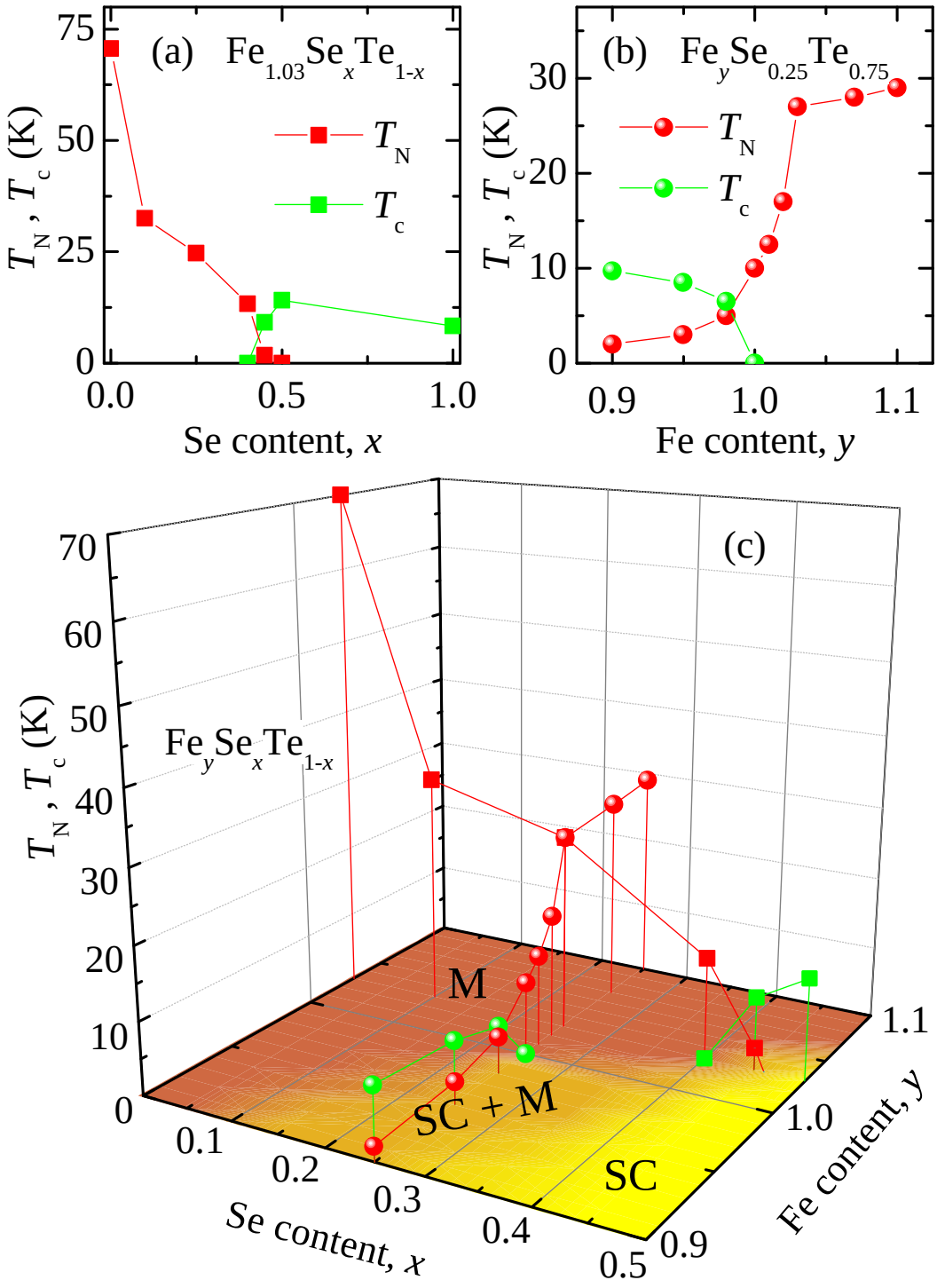

Figure 4.11: (a) Phase diagram of $Fe_{1.03}Se_xTe_{1-x}$ as a function of x. The datum of $FeSe_{1-x}$ is taken from Ref. [128]. (b) Variation in T_c and T_N in $Fe_ySe_{0.25}Te_{0.75}$ as a function of y. (c) The three dimensional phase diagram of T_c and T_N of $Fe_ySe_xTe_{1-x}$ as a function of x and y. M and SC denotes the magnetic and superconducting phases, respectively. With increasing amount of Se superconductivity is established, whereas it strongly depends on the amount of Fe in the system. After [123] and [139].

order becomes weaker and superconductivity occurs and finally the system is a pure bulk superconductor. The superconducting and magnetic behavior of $Fe_ySe_xTe_{1-x}$ can therefore not only be tuned by substituting Te with Se, but also by adjusting the Fe content. It is suggested that superconductivity has to be of multi-band nature, where different doping channels may be involved [111].

4.5 Related publications to Chapter 4

4.5.1 Paper I: Synthesis, crystal structure, and chemical stability of the superconductor $FeSe_{1-x}$

This work is published in:

E. Pomjakushina, K. Conder, V. Pomjakushin, M. Bendele, and R. Khasanov, *Synthesis, crystal structure, and chemical stability of the superconductor $FeSe_{1-x}$*, Phys. Rev. B **80**, 024517 (2009).

Abstract:

We report on a comparative study of the crystal structure and the magnetic properties of $FeSe_{1-x}$ ($x = 0.0 - 0.15$) superconducting samples by neutron powder-diffraction and magnetization measurements. The samples were synthesized by two different methods: a low-temperature one using powders as a starting material at $T \simeq 700\,^{\circ}\mathrm{C}$ and a high-temperature method using solid pieces of Fe and Se at $T \simeq 1075\,^{\circ}\mathrm{C}$. The effect of a starting (nominal) stoichiometry on the phase purity of the obtained samples, the superconducting transition temperature T_c, as well as the chemical stability of $FeSe_{1-x}$ at ambient conditions were investigated. It was found that in the Fe-Se system, a stable phase exhibiting superconductivity at $T_c \simeq 8\,\mathrm{K}$ exists in a narrow range of selenium concentration ($FeSe_{0.974\pm0.005}$).

URL: http://link.aps.org/doi/10.1103/PhysRevB.80.024517
DOI: 10.1103/PhysRevB.80.024517
PACS: 74.70.-b, 74.72.-h, 61.05.fm, 74.25.Ha

PHYSICAL REVIEW B **80**, 024517 (2009)

Synthesis, crystal structure, and chemical stability of the superconductor $FeSe_{1-x}$

E. Pomjakushina,[1,*] K. Conder,[1] V. Pomjakushin,[2] M. Bendele,[3,4] and R. Khasanov[4]
[1]*Laboratory for Developments and Methods, PSI, 5232 Villigen, Switzerland*
[2]*Laboratory for Neutron Scattering, ETHZ and PSI, 5232 Villigen, Switzerland*
[3]*Physik-Institut der Universität Zürich, Winterthurerstrasse 190, 8057 Zürich, Switzerland*
[4]*Laboratory for Muon Spin Spectroscopy, PSI, 5232 Villigen, Switzerland*
(Received 12 May 2009; revised manuscript received 10 July 2009; published 30 July 2009)

We report on a comparative study of the crystal structure and the magnetic properties of $FeSe_{1-x}$ (x =0.0–0.15) superconducting samples by neutron powder-diffraction and magnetization measurements. The samples were synthesized by two different methods: a "low-temperature" one using powders as a starting material at $T \simeq 700$ °C and a "high-temperature" method using solid pieces of Fe and Se at $T \simeq 1075$ °C. The effect of a starting (nominal) stoichiometry on the phase purity of the obtained samples, the superconducting transition temperature T_c, as well as the chemical stability of $FeSe_{1-x}$ at ambient conditions were investigated. It was found that in the Fe-Se system, a stable phase exhibiting superconductivity at $T_c \simeq 8$ K exists in a narrow range of selenium concentration ($FeSe_{0.974\pm0.005}$).

DOI: 10.1103/PhysRevB.80.024517 PACS number(s): 74.70.−b, 74.72.−h, 61.05.fm, 74.25.Ha

I. INTRODUCTION

The discovery of Fe-based superconductors has attracted considerable attention to the pnictides. Superconductivity is detected now in various pnictide families as, e.g., the single-layer $ReO_{1-x}F_xFeAs$ (Re=La, Ce, Pr, Nd, Sm, Gd, Tb, Dy, Ho, and Y),[1–7] the double-layer MFe_2As_2 (M=Ba, Sr, and Ca),[8–12] the oxygen free single-layer LiFeAs,[13–15] etc. The common structural feature of all these materials is the Fe-As layers consisting of a Fe square planar sheet tetrahedrally coordinated by As. Recently, superconductivity with a transition temperature of $T_c \simeq 8$ K was discovered in β-$FeSe_{1-x}$ with the PbO structure.[16] This compound also has a Fe square lattice with Fe atoms tetrahedrally coordinated by Se similar to the structure of FeAs layers in the single- and the double-layer pnictides. In this respect $FeSe_{1-x}$, consisting of the "superconducting" Fe-Se layers only, can be considered as a prototype of the known families of Fe-As-based superconductors and, consequently, is a good model system to study mechanisms leading to the occurrence of superconductivity in this class of materials.

As is stated in the literature, there are two different routs to synthesize superconducting $FeSe_{1-x}$. The first one uses Se and Fe powders as the starting material and is performed in sealed silica tubes at 400–700 °C.[16] Hereafter we call it the "low-temperature synthesis" (LTS). This method, however, was shown to result in samples with a relatively high amount of impurities. According to Ref. 16, $FeSe_{1-x}$ with x=0.18 was found to consist of a superconducting phase and a small amount of elemental selenium, iron oxide, and iron silicide (reaction product with silica ampoule). For a higher average selenium content (x=0.12), some amount of hexagonal (NiAs-type) FeSe phase was detected in addition to impurity phases listed above. The superconducting transition temperature was found to be at $\simeq 8$ K, being independent of the initial Se content. The second procedure proposed in the recent work of McQueen *et al.*[17] starts from Fe pieces and Se shot. The Fe and Se pieces sealed in silica ampoule were first held at 750 °C (3–5 days) then heated up to 1075 °C (3 days) followed by a fast decrease down to 420 °C and quenched. The synthesis was completed by an additional annealing of the sample (sealed in a new ampoule) at 300–500 °C followed by quenching. Superconductivity was found to exist only in a very narrow range of stoichiometry. For $FeSe_{0.99}$, ($Fe_{1.01}Se$) magnetization measurements showed $T_c \sim 8.5$ K, whereas T_c for $FeSe_{0.98}$ ($Fe_{1.02}Se$) decreased down to ~5 K and went to zero (at least down to 0.6 K) for $FeSe_{0.97}$ ($Fe_{1.03}Se$).[17] Hereafter, we call this procedure the "high-temperature synthesis" (HTS). In comparison with LTS, the samples prepared by HTS do not contain iron oxide impurities.[17]

Surprisingly, the $FeSe_{1-x}$ samples synthesized by LTS and HTS techniques were found to be rather different. Indeed, in LTS samples superconductivity was found in a rather extended range of Se content (at least up to x=0.18),[16,18] while for the HTS superconductivity was detected only in a very narrow region corresponding to $0.01 \leq x \leq 0.025$.[17] In addition, McQueen *et al.*[17] reported that below 300 °C the tetragonal $FeSe_{1-x}$ converts into a hexagonal (NiAs-type) phase, which is not superconducting. Therefore, quenching from temperatures above 300 °C was used for synthesizing HTS samples. On the other hand, no special care for fast cooling of LTS samples needs to be taken.[16,18] In order to resolve these controversies, we performed comparative studies of the superconducting $FeSe_{1-x}$ samples synthesized by both methods (LTS and HTS) described above. We have improved a method of synthesis using powder starting materials and investigated the effect of stoichiometry on the phase purity of the obtained samples and its superconducting transition temperature. Based on the neutron powder-diffraction (NPD) data, we have revised the Fe-Se concentration phase diagram proposed by Okamoto.[19]

II. EXPERIMENTAL DETAILS

AC and DC magnetization (M_{AC}/M_{DC}) measurements were performed using Quantum Design physical property measurement system (PPMS) and magnetic property mea-

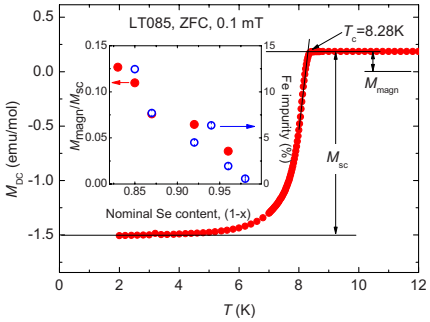

FIG. 1. (Color online) Temperature dependencies of the DC magnetization (M_{DC}, zero-field cooling, 0.1 mT) of LT085 sample. The superconducting transition temperature T_c, the superconducting (M_{SC}), and the magnetic (M_{magn}) responses of the sample are determined as shown in the figure. The inset shows dependencies of M_{magn}/M_{SC} and Fe impurity concentration as a function of the nominal Se content.

surement system (MPMS) at temperatures ranging from 2 to 300 K. The AC field amplitude and the frequency were 0.1 mT and 1000 Hz, respectively. The DC magnetization experiments were performed after zero-field cooling and field cooling the samples at $\mu_0 H$=0.1 mT. The superconducting transition temperature T_c was determined as an intersection of the linearly extrapolated $M_{AC}(T)[M_{DC}(T)]$ with the M =const line (see Fig. 1).

NPD experiments were carried out at the SINQ spallation source at the Paul Scherrer Institute (PSI, Switzerland) using the high-resolution diffractometer for thermal neutrons HRPT (Ref. 20) (the neutron wavelengths λ=1.494 and 1.155 Å). The refinements of the crystal structure parameters were done using the FULLPROF program,[21] with the use of its internal tables for neutron-scattering lengths.

III. RESULTS AND DISCUSSION

A. Sample synthesis

Two types of samples using the LTS and the HTS procedures were prepared. Samples of a nominal composition $FeSe_{0.85}$, $FeSe_{0.87}$, $FeSe_{0.92}$, $FeSe_{0.96}$, $FeSe_{0.98}$, and FeSe (LT085, LT087, LT092, LT096, LT098, and LT100) were prepared by a solid-state reaction similar to that described in Refs. 16 and 18. The cold-pressed mixtures of Fe and Se powders were sealed in quartz ampoules and then heated up to 700 °C followed by annealing at 400 °C. Powders of Fe and Se of a minimum purity of 99.99% were used as starting materials.

Sample $FeSe_{0.94}$ (HT094) was synthesized similar to the route of McQueen *et al.*[17]—by solid-state reaction using pieces of Fe and Se of a minimum purity of 99.99%. The sample was heated in the sealed quartz ampoule up to 1075 °C followed by annealing at 400 °C. In contrast to McQueen *et al.*,[17] no quenching from high temperatures was made. The sample was cooled down to the room temperature at a rate of 200 °C/h.

Note that for the samples synthesized by both LTS and HTS techniques, all the grindings/pelletizings were performed under helium atmosphere. The samples studied in the present work are listed in Table I.

B. Crystal structure and impurity phases

The crystal structure of the main (superconducting) phase and the concentration of the impurity phases were determined by means of neutron powder diffraction. First, we present the results obtained for the $FeSe_{1-x}$ samples with nominal Se contents $0.85 \leq 1-x \leq 0.98$ (LT085–LT098 and HT094). Room-temperature NPD experiments show that all these samples contain the same tetragonal phase $FeSe_{1-x}$ (space group $P4/nmm$) as a main phase. The refined selenium occupancy (selenium stoichiometry) is about 0.974(2) and is *independent* of the starting composition and the route of the synthesis (LTS; HTS). A typical example of the Rietveld refinement of NPD data is shown in Fig. 2 for the LT098 sample. Impurity phases are hexagonal FeSe (space group $P6_3mmc$) in a quantity of ~1% (molar %) and Fe (space group $Im3m$). Amount of the metallic Fe was found to decrease monotonically with increasing Se content from ≃12.5% for $FeSe_{0.85}$ to ≃0.5% for $FeSe_{0.98}$. Note that for all the samples studied, the presence of any oxides was not detected. The "cleanest" sample is LT098 which contains, in total, less than 2% of the secondary phases and has a nominal composition $FeSe_{0.98}$; the same as is refined for the main tetragonal phase $FeSe_{0.975(3)}$. The amount of impurity phases found in the samples, the refined stoichiometry of the main tetragonal phase, and its unit-cell parameters are listed in Table I. It is worth to mention that the samples showing the largest deviation from the average stoichiometry (LT85 and LT100) contain also a relatively large amount of the impurity phases. Therefore, the refined Se occupancy can have some systematic error for these samples. Most NPD measurements were performed with the wavelength λ=1.494 Å because it provides the optimal conditions for refining the structure parameters of the main phase (large q range) and determination of the impurity phases (good resolution). To further check for the possible systematic error in the Se occupancy due to its correlation with the atomic displacement parameters, measurements of the most pure sample with yet shorter wavelength λ=1.155 Å were performed. The refined Se occupancy was found to be 0.980(3), implying that the systematic error is smaller than 0.005. To better visualize the improvements of the refinement as a function of the Se occupancy $(1-x)$, we have calculated the Bragg R factor as a function of $(1-x)$. The structure refinements were performed with all parameters varied except for the fixed value of the occupancy in the range 0.95–1.0. The resulting dependence $R_{Bragg}(1-x)$ (inset in Fig. 2) nicely shows a minimum around the freely refined value of Se occupancy. Table II shows structure parameters and reliability factors for three samples of $FeSe_{1-x}$. The sample labeled LT085a that is a degraded on air sample LT085 is presented for comparison and will be discussed in Sec. III D.

We are quite convinced by our structure model because the refinements were really improved if the Se occupancy

TABLE I. Summary of the neutron powder-diffraction and magnetization results for $FeSe_{1-x}$ samples prepared by LTS and HTS methods. Note that the sample LT085a is the air-degraded sample LT085.

Sample name	Nominal composition	T_c (K)	Refined composition phase content (molar %)	Unit-cell parameters of the tetragonal phase (Å)
LT085a	$FeSe_{0.85}$		$FeSe_{0.994(11)}$ ($P4/nmm$) 71.75 ± 1.75%	a=3.774 13(14)
			Fe ($Im3m$) 26.23 ± 0.85%	c=5.521 41(31)
			FeSe ($P6_3/mmc$) 2.02 ± 0.38%	
LT085	$FeSe_{0.85}$	8.28	$FeSe_{0.963(5)}$ (P4/nmm) 86.38 ± 0.98%	a=3.773 20(4)
			Fe ($Im3m$) 12.46 ± 0.33%	c=5.524 96(9)
			FeSe ($P6_3/mmc$) 1.16 ± 0.18%	
LT087	$FeSe_{0.87}$	8.34	$FeSe_{0.979(4)}$ (P4/nmm) 91.53 ± 0.91%	a=3.772 80(4)
			Fe ($Im3m$) 7.70 ± 0.23%	c=5.523 03(8)
			FeSe ($P6_3/mmc$) 0.77 ± 0.14%	
LT092	$FeSe_{0.92}$	8.44	$FeSe_{0.976(4)}$ (P4/nmm) 94.50 ± 0.89%	a=3.773 35(4)
			Fe ($Im3m$) 4.50 ± 0.21%	c=5.523 68(8)
			FeSe ($P6_3/mmc$) 1.00 ± 0.13%	
HT094	$FeSe_{0.94}$	8.21	$FeSe_{0.977(3)}$ (P4/nmm) 92.91 ± 0.70%	a=3.772 94(4)
			Fe ($Im3m$) 6.36 ± 0.16%	c=5.524 21(7)
			FeSe ($P6_3/mmc$) 0.73 ± 0.09%	
LT096	$FeSe_{0.96}$	8.43	$FeSe_{0.978(4)}$ (P4/nmm) 96.02 ± 1.07%	a=3.773 38(5)
			Fe ($Im3m$) 1.94 ± 0.23%	c=5.524 15(11)
			FeSe ($P6_3/mmc$) 2.04 ± 0.19%	
LT098	$FeSe_{0.98}$	8.21	$FeSe_{0.975(3)}$ (P4/nmm) 98.31 ± 0.59%	a=3.773 81(2)
			Fe ($Im3m$) 0.57 ± 0.05%	c=5.523 30(5)
			FeSe ($P6_3/mmc$) 1.12 ± 0.08%	
LT100	$FeSe_1$	~8	$FeSe_{0.968(3)}$ (P4/nmm) 83.03 ± 0.61%	a=3.773 53(4)
			Fe ($Im3m$) 0.46 ± 0.05%	c=5.523 82(7)
			Fe_7Se_8 ($P3_121$) 16.51 ± 0.28%	

was released and the refined composition exactly corresponded to the starting composition that gave the cleanest final sample as we explained above. However, there is an alternative structure that also would correspond to Se deficiency of the initial composition observed in the isostructural $Fe_{1.125}Te$,[22] where the extra Fe atoms are located at the interstitial cites ($2c$) ($1/4, 1/4, z$), $z \simeq 0.5$. We have made the refinements in this model for the best sample LT098 and found that this model does not fit to our experimental data at all. The above described procedure used to obtain the plot in the inset of Fig. 2 shows that the R factor $R_{\mathrm{Bragg}}(x_{\mathrm{Fe}})$ steadily increases with the increase in the Fe occupancy x_{Fe} from 3.99 for $x_{\mathrm{Fe}}=0.01$ to more than 4.4 for $x_{\mathrm{Fe}}>0.03$.

The results of the structural analysis were further confirmed by magnetic-susceptibility measurements. As follows from Table I, all FeS_{1-x} samples ($0<x\leq 0.15$) have almost the same transition temperatures ($T_c \sim 8.2-8.4$ K) and, consequently, very similar doping (concentration of charge carriers). In addition, the paramagnetic offset (M_{magn}) seen at $T>T_c$ was found to decrease with increasing Se content just following the dependence of Fe impurity phase as the function of the nominal Se content $1-x$ (see the inset in Fig. 1). Note that in Ref. 23 the observation of the paramagnetic offset at $T>T_c$ as well as the static magnetic contribution seen in zero-field muon-spin rotation experiments were attributed to the presence of Fe impurities.

By increasing the Fe:Se ratio up to 1:1, the situation was drastically changed. The Rietveld refinement of NPD data on FeSe (LT100) sample reveals that the main tetragonal phase content is substantially decreased down to ≃83.03%. The content and the composition of the impurity phases were also changed: only 0.46% of Fe and, instead of a hexagonal NiAs-type phase ≃16.51% of the trigonal Fe_7Se_8 (space group $P3_121$) was detected. Magnetization experiments also show a substantial decrease in the superconducting fraction, which was found to be of about 10% at $T=3$ K.

Studies of the crystal structure of the main phase as a function of temperature were performed on the sample LT085 in the temperature range 20–300 K on both cooling and heating. Figure 3 shows the lattice constants a and b and the unit-cell volume as a function of temperature. At temperature $T=100$ K, there is a transition from the tetragonal to orthorhombic structure on cooling similar as observed in Ref. 18. The low-temperature structure is well refined in the space group $Cmma$. The building block of the crystal structure is $SeTe_4$ square pyramid with Se atom in the apex. In the high-temperature phase the pyramid is regular, whereas in the orthorhombic phase the neighboring Fe-Se-Fe bond angles become different as shown in Fig. 4. The Se-Fe bond length amounts to 2.386(2) Å at low temperature and it is not changed at the transition. Neither temperature hysteresis nor the unit-cell volume jump was observed indicating that

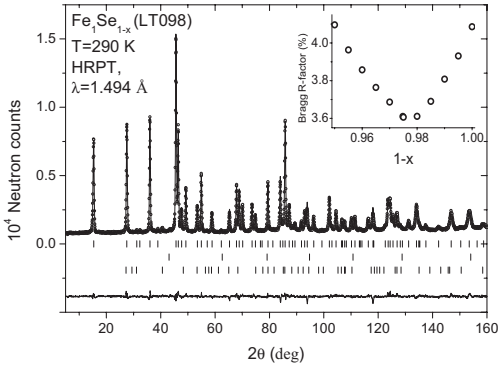

FIG. 2. The Rietveld refinement pattern and difference plot of the neutron-diffraction data for the sample $FeSe_{0.98}$ (LT098) at T =290 K measured at HRPT with the wavelength λ=1.494 Å. The rows of ticks show the Bragg-peak positions for the main phase and two impurity phases. The main tetragonal phase corresponds to 0.975(3) Se content. The inset shows Bragg R factor plotted versus Se occupancy. See text for details.

the transition is of the second-order type. The transition temperature in our sample $FeSe_{0.963(5)}$ (100 K) is different from the one reported for $FeSe_{0.91}$ (70 K) (Ref. 18) that might be related to the different Se stoichiometry. However, as described above our synthesis techniques always produce the main tetragonal phase with approximately the same concentration with the average value of about x=0.974.

C. Phase diagram

In this section, stoichiometry of the main phase and the phase composition of the studied samples are discussed

TABLE II. Structural parameters of the $FeSe_{1-x}$ main phase of the "cleanest" sample LT098, the sample with largest impurity admixture LT085, and the degraded sample LT085a (discussed in Sec. III D) at 290 K. Space group $P4/nmm$ (no. 129), origin choice 2. Fe in ($2b$) position (1/4,3/4,1/2); Se in ($2c$) position $(1/4, 1/4, z)$ The atomic displacement parameters for Fe and Se were constrained to be the same. The Bragg R factor is given for the main phase; the other reliability factors are given for the whole refinement.

	LT098	LT085	LT085a
a(Å)	3.77381(2)	3.77320(4)	3.77413(14)
c(Å)	5.52330(5)	5.52496(9)	5.52141(31)
c/a	1.46359	1.46426	1.46296
z-Se	0.23268(14)	0.2331(3)	0.2334(8)
occupancy	0.975(2)	0.963(5)	0.99(1)
B(Å^2)	1.01(1)	1.09(2)	1.54(5)
R_{Bragg}	3.61	5.83	8.35
χ^2	2.63	1.61	1.54
R_{wp}	4.21	3.83	4.53
R_{exp}	2.60	3.02	3.65

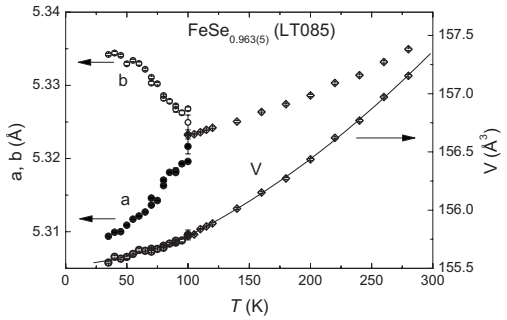

FIG. 3. a,b unit-cell parameters and unit-cell volume V as a function of temperature. In the tetragonal phase, the lattice constant is multiplied by $\sqrt{2}$.

based on the existing Fe-Se binary phase diagrams elaborated by Okamoto[19] and McQueen *et al.*[17] Figure 5 shows a combined phase diagram based on the previously published data.[17,19] Lines correspond to the part of the binary phase diagram reported in Ref 19. The stripe centered at around 49.5 at. % of Se corresponds to a range of existence of tetragonal above 300 °C and hexagonal $FeSe_{1-x}$ (NiAs-type) below 300 °C as proposed in Ref. 17. The circles correspond to the samples with different nominal Se content studied in this work. The refined selenium stoichiometry $(1-x)$ of the main superconducting phase for all the investigated samples are plotted in the inset. The existence range of the nonstoichiometric $FeSe_{1-x}$ as proposed in Ref. 17 is also shown. The average stoichiometry of the superconducting phase was determined to be $FeSe_{0.974(2)}$ (the error bar represents the statistical error). The average Se concentration is represented by the vertical line in the inset and it is very close to that for the most pure sample LT098 [$FeSe_{0.975(3)}$], which is shown by the solid point in the inset.

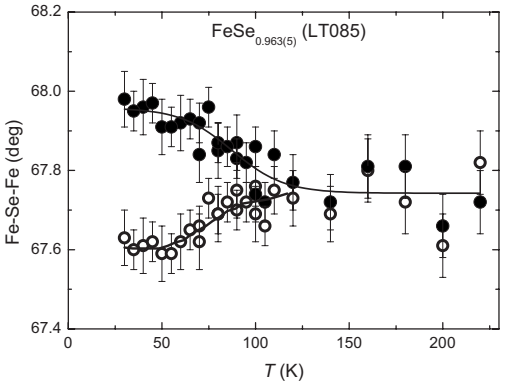

FIG. 4. Fe-Se-Fe bond angles as a function of temperature in $FeSe_{0.963(5)}$. The refinements of the diffraction data were made assuming low-symmetry phase (space group *Cmma*). The high-temperature crystal structure is tetragonal and both Fe-Se-Fe angles would be the same by symmetry in $P4/nmm$ group.

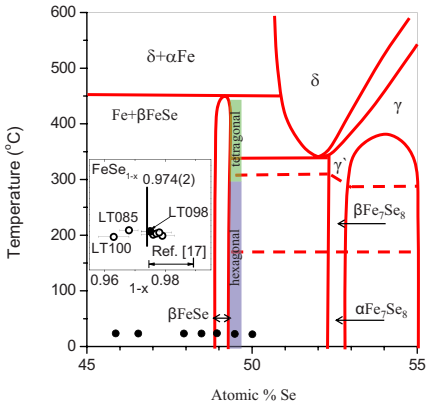

FIG. 5. (Color online) The Fe-Se phase diagram after Okamoto (Ref. 19) (lines) and McQueen *et al.* (Ref. 17) (vertical colored stripe). The black circles correspond to the nominal composition of the samples studied in the present work. In the inset, the refined selenium stoichiometry $(1-x)$ of the main superconducting phase found in all the investigated samples is plotted together with the range of the existence of nonstoichiometric $FeSe_{1-x}$ as proposed in Ref. 17. See text for details.

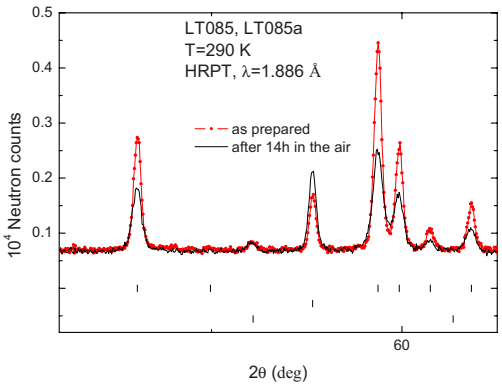

FIG. 6. (Color online) Neutron powder-diffraction pattern of LT085 and LT085a samples at $T=290$ K measured at HRPT with the wavelength $\lambda=1.886$ Å. The red dotted curve corresponds to the as-prepared sample (LT085). The solid black curve was obtained after exposing the sample for 14 h in the air (LT085a). See text for details.

From the data presented in Fig. 5, the following important statements emerge: (i) the stability field of the superconducting *tetragonal* β-FeSe phase as proposed in Ref. 17 does not overlap with that reported in Ref. 19. According to Ref. 17, the tetragonal phase exists only at high temperatures, but it is transformed to the hexagonal one below 300 °C; (ii) all the samples studied in our work contain the superconducting tetragonal phase as the main phase with almost the same average stoichiometry ($FeSe_{0.974(2)}$) (see the inset in Fig. 5 and Table I) and display the same $T_c \simeq 8$ K. This is in disagreement with the results of Ref. 17 because the compounds with the stoichiometries shown by points in the inset of Fig. 5 would have to display lower (~5 K) or even vanishing T_c; (iii) the present work demonstrates that there is no need for quenching from high temperatures (300–450 °C) in order to get a stable at room temperature and pure tetragonal phase. According to our NPD studies, the $FeSe_{0.98}$ (LT098) sample contains, in total, less than 2% of impurity phases. Consequently, our data do not prove an existence of tetragonal-hexagonal phase transition on cooling at ~300 °C as proposed in Ref. 17; (iv) our data suggest very narrow range or even strictly defined stoichiometry of the superconducting tetragonal $FeSe_{1-x}$ phase. It looks that the composition of this phase is located between the fields proposed in both Refs. 17 and 19. An additional confirmation of the correct locus of the tetragonal phase on the phase diagram comes from an investigation of a phase composition of the LT100 sample (nominally $FeSe_{1.00}$). According to the phase diagram,[19] this sample should be in the two phase region (βFeSe-αFe_7Se_8) at room temperature. Using a lever rule ~18% Fe_7Se_8 would be expected being in a good agreement with 16.5% as found from NPD data (see Table I).

D. Chemical stability of FeSe

In order to study the chemical stability of FeSe samples, the LT085 sample was powderized and stored in air for 14 h (LT085a) and then measured by means of NPD. In Fig. 6, the Rietveld refinement of a neutron-diffraction pattern of LT085a sample (solid line) together with as-prepared LT085 sample (dotted curve) taken at room temperature are presented. The sample underwent drastic changes after exposing in air. Volume fraction of the main tetragonal phase was decreased from 93% down to 84%, whereas the quantity of Fe increases from 6% up to 13%, at the same time the increase of the of the hexagonal phase content was not so pronounced. The diffraction peaks of the main phase of LT085a sample show severe broadening and, at the same time, the atomic displacement parameters (Debye-Waller factor) increase by 1.5 times, thus, implying the presence of both large scale defects (e.g., dislocations or the presence of new-phase particles) and point defects (e.g., vacancies).[24] Additionally, it was found that the stoichiometry of the main phase becomes almost 1:1 (Fe:Se). The integral counting rates (scale factors) further reveal that about 20–30 % of the main phase was lost (most probably, it became amorphous).

In order to figure out the reason of $FeSe_{1-x}$ degradation, additional experiments were performed. The $FeSe_{0.98}$ (LT098) sample was divided in three parts. Each of them was further powderized and exposed in pure helium, oxygen, and air atmosphere. Figure 7 shows $M_{DC}(T)$ curves obtained for the different parts of the sample. It is obvious that both air and oxygen lead to a dramatic degradation of the superconducting properties. Indeed, the superconducting volume fraction decreases by more than a factor of 5, while the T_c onset shifts to the lower temperature. At the same time, the superconducting transition becomes very broad—the magnetization decreases continuously from T_c down to 2 K. We suppose, therefore, that by exposing FeSe sample in the air or in

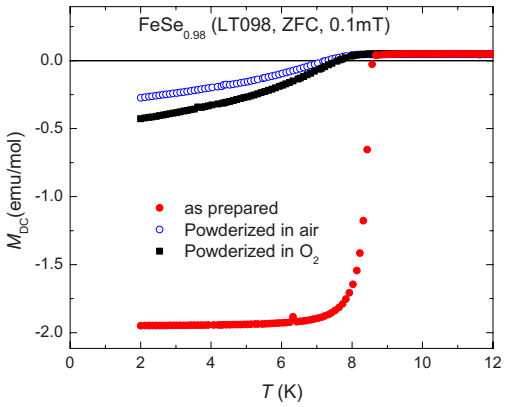

FIG. 7. (Color online) Temperature dependencies of the DC magnetization (M_{DC}, zero-field cooling, 0.1 mT) of LT098 sample. The experimental data correspond to the sample: (●) as prepared; (○) powderized/exposed in the air; and (■) powderized/exposed in pure oxygen.

the oxygen atmosphere it decomposes by oxidizing (most probably forming SeO_2).

IV. CONCLUSIONS

A comparative study of the crystal structure and the magnetic properties of the superconductor $FeSe_{1-x}$ synthesized at lower temperatures from powders and at higher temperatures from pieces of metal was performed. The effect of a starting (nominal) stoichiometry on a phase purity of the obtained samples and their superconducting transition temperatures T_c was studied. On the base of our neutron powder-diffraction data, we have revised the Fe-Se concentration phase diagram proposed by Okamoto.[19] In particular, we have found that in the Fe-Se system a stable phase exhibiting superconductivity at $T_c \sim 8$ K exists in the narrow range of selenium concentration ($FeSe_{0.974\pm0.005}$).

As revealed by the NPD study, at $T \sim 100$ K $FeSe_{1-x}$ undergoes a second-order structural phase transition from a tetragonal phase (space group $P4/nmm$) to an orthorhombic (space group $Cmma$) on cooling. Fe-Se-Fe bond angles in the $FeSe_4$ pyramids become different in low-temperature phase, whereas the Fe-Se bond lengths are not changed at the transition.

The chemical stability of FeSe samples exposed in air and in pure oxygen atmosphere was studied. It was found that after exposing in air the structure gets many defects, as revealed by NPD diffraction peaks broadening and the large increase in the atomic displacement parameters. The amount of both impurity phases increases about two times reaching 26% for metallic iron and 2% for the hexagonal FeSe. This leads to a dramatic degradation of the superconducting properties, which was proved by magnetization measurements.

ACKNOWLEDGMENTS

The authors are grateful to Hugo Keller for helpful discussions. This study was partly performed at Swiss neutron spallation SINQ of Paul Scherrer Institute PSI (Villigen, PSI). We acknowledge the allocation of the beam time at the HRPT diffractometer of the Laboratory for Neutron Scattering (ETHZ & PSI, Switzerland). The authors thank the NCCR MaNEP project and the Swiss National Science Foundation for the support of this study.

*ekaterina.pomjakushina@psi.ch

[1] Y. Kamihara, T. Watanabe, M. Hirano, and H. Hosono, J. Am. Chem. Soc. **130**, 3296 (2008).
[2] C. Wang, L. Li, S. Chi, Z. Zhu, Z. Ren, Y. Li, Y. Wang, X. Lin, Y. Luo, S. Jiang, X. Xu, G. Cao, and Z. Xu, EPL **83**, 67006 (2008).
[3] Z.-A. Ren *et al.*, EPL **83**, 17002 (2008).
[4] A. S. Sefat, M. A. McGuire, B. C. Sales, R. Jin, J. Y. Howe, and D. Mandrus, Phys. Rev. B **77**, 174503 (2008).
[5] G. F. Chen, Z. Li, D. Wu, G. Li, W. Z. Hu, J. Dong, P. Zheng, J. L. Luo, and N. L. Wang, Phys. Rev. Lett. **100**, 247002 (2008).
[6] H. Wen, G. Mu, L. Fang, H. Yang, and X. Zhu, EPL **82**, 17009 (2008).
[7] J. Yang, X. Shen, W. Lu, W. Yi, Z. Li, Z. Ren, G. Che, X. Dong, L. Sun, F. Zhou, and Z. Zhao, New J. Phys. **11**, 025005 (2009).
[8] M. Rotter, M. Tegel, D. Johrendt, I. Schellenberg, W. Hermes, and R. Pottgen, Phys. Rev. B **78**, 020503(R) (2008).
[9] M. Rotter, M. Tegel, and D. Johrendt, Phys. Rev. Lett. **101**, 107006 (2008).
[10] G. F. Chen, Z. Li, G. Li, W. Z. Hu, J. Dong, X. D. Zhang, P. Zheng, N. L. Wang, and J. L. Luo, Chin. Phys. Lett. **25**, 3403 (2008).
[11] N. Ni, S. Nandi, A. Kreyssig, A. I. Goldman, E. D. Mun, S. L. Bud'ko, and P. C. Canfield, Phys. Rev. B **78**, 014523 (2008).
[12] M. S. Torikachvili, S. L. Bud'ko, N. Ni, and P. C. Canfield, Phys. Rev. Lett. **101**, 057006 (2008).
[13] G. Wu, H. Chen, Y. L. Xie, Y. J. Yan, T. Wu, R. H. Liu, X. F. Wang, D. F. Fang, J. J. Ying, and X. H. Chen, Phys. Rev. B **78**, 092503 (2008).
[14] M. J. Pitcher, D. R. Parker, P. Adamson, S. J. C. Herkelrath, A. T. Boothroyd, M. R. Ibberson, M. Brunelli, and S. J. Clarke, Chem. Commun. (Cambridge) **2008**, 5918.
[15] J. H. Tapp, Z. Tang, B. Lv, K. Sasmal, B. Lorenz, P. C. W. Chu, and A. M. Guloy, Phys. Rev. B **78**, 060505(R) (2008).
[16] F.-C. Hsu, J.-Y. Luo, K.-W. Yeh, T.-K. Chen, T.-W. Huang, P. M. Wu, Y.-C. Lee, Y.-L. Huang, Y.-Y. Chu, D.-C. Yan, and M.-K. Wu, Proc. Natl. Acad. Sci. U.S.A. **105**, 14262 (2008).
[17] T. M. McQueen, Q. Huang, V. Ksenofontov, C. Felser, Q. Xu, H. Zandbergen, Y. S. Hor, J. Allred, A. J. Williams, D. Qu, J. Checkelsky, N. P. Ong, and R. J. Cava, Phys. Rev. B **79**, 014522

(2009).
[18] S. Margadonna, Y. Takabayashi, M. T. McDonald, K. Kasperkiewicz, Y. Mizuguchi, Y. Takano, A. N. Fitch, E. Suard, and K. Prassides, Chem. Commun. (Cambridge) **2008**, 5607.
[19] H. Okamoto, J. Phase Equilib. **12**, 383 (1991).
[20] P. Fischer, G. Frey, M. Koch, M. Könnecke, V. Pomjakushin, J. Schefer, R. Thut, N. Schlumpf, R. Bürge, U. Greuter, S. Bondt, and E. Berruyer, Physica B **276-278**, 146 (2000).
[21] J. Rodríguez-Carvajal, Physica B **192**, 55 (1993).
[22] D. Fruchart, P. Convert, P. Wolfers, R. Madar, J. P. Senateur, and R. Fruchart, Mater. Res. Bull. **10**, 169 (1975).
[23] R. Khasanov, K. Conder, E. Pomjakushina, A. Amato, C. Baines, Z. Bukowski, J. Karpinski, S. Katrych, H.-H. Klauss, H. Luetkens, A. Shengelaya, and N. D. Zhigadlo, Phys. Rev. B **78**, 220510(R) (2008).
[24] M. A. Krivoglaz, *X-Ray and Neutron Diffraction in Nonideal Crystals* (Springer-Verlag, Berlin, 1996).

4.5.2 Paper II: Pressure Induced Static Magnetic Order in Superconducting $FeSe_{1-x}$

This work is published in:

M. Bendele, A. Amato, K. Conder, M. Elender, H. Keller, H.-H. Klauss, H. Luetkens, E. Pomjakushina, A. Raselli, and R. Khasanov, *Pressure Induced Static Magnetic Order in Superconducting $FeSe_{1-x}$*, Phys. Rev. Lett. **104**, 087003 (2010).

Abstract:

We report on a detailed investigation of the electronic phase diagram of $FeSe_{1-x}$ under pressures up to 1.4 GPa by means of ac magnetization and muon-spin rotation. At a pressure $\simeq 0.8$ GPa the nonmagnetic and superconducting $FeSe_{1-x}$ enters a region where static magnetic order is realized above T_c and bulk superconductivity coexists and competes on short length scales with the magnetic order below T_c. For even higher pressures an enhancement of both the magnetic and the superconducting transition temperatures as well as of the corresponding order parameters is observed. These exceptional properties make $FeSe_{1-x}$ to be one of the most interesting superconducting systems investigated extensively at present.

URL: http://link.aps.org/doi/10.1103/PhysRevLett.104.087003
DOI: 10.1103/PhysRevLett.104.087003
PACS: 74.70.-b, 74.25.Jb, 76.75.+i

PRL **104,** 087003 (2010) PHYSICAL REVIEW LETTERS week ending 26 FEBRUARY 2010

Pressure Induced Static Magnetic Order in Superconducting $FeSe_{1-x}$

M. Bendele,[1,2] A. Amato,[1] K. Conder,[3] M. Elender,[1] H. Keller,[2] H.-H. Klauss,[4] H. Luetkens,[1] E. Pomjakushina,[3] A. Raselli,[3] and R. Khasanov[1,*]

[1]*Laboratory for Muon Spin Spectroscopy, Paul Scherrer Institut, CH-5232 Villigen PSI, Switzerland*
[2]*Physik-Institut der Universität Zürich, Winterthurerstrasse 190, CH-8057 Zürich, Switzerland*
[3]*Laboratory for Developments and Methods, Paul Scherrer Institute, CH-5232 Villigen PSI, Switzerland*
[4]*IFP, TU Dresden, D-01069 Dresden, Germany*

(Received 25 September 2009; published 25 February 2010)

We report on a detailed investigation of the electronic phase diagram of $FeSe_{1-x}$ under pressures up to 1.4 GPa by means of ac magnetization and muon-spin rotation. At a pressure $\simeq 0.8$ GPa the nonmagnetic and superconducting $FeSe_{1-x}$ enters a region where static magnetic order is realized above T_c and bulk superconductivity coexists and competes on short length scales with the magnetic order below T_c. For even higher pressures an enhancement of both the magnetic and the superconducting transition temperatures as well as of the corresponding order parameters is observed. These exceptional properties make $FeSe_{1-x}$ to be one of the most interesting superconducting systems investigated extensively at present.

DOI: 10.1103/PhysRevLett.104.087003 PACS numbers: 74.70.−b, 74.25.Jb, 76.75.+i

The phase diagram of the recently discovered Fe-based high-temperature superconductors (HTS) [1] share a common feature with cuprates and heavy fermions. The parent compounds of the Fe-based HTS, such as, LnOFeAs (Ln = La, Ce, Pr, Sm) [2–9], AFe_2As_2 (A = Ba, Sr, Ca) [10–13] and Fe(SeTe) [14,15] exhibit long-range static magnetic order. Upon doping or application of pressure (chemical or external), magnetism is suppressed and superconductivity emerges. Recent investigations revealed, however, that the structurally most simple binary compound $FeSe_{1-x}$ is an exception of this rule [16]. Different from the other Fe-based HTS, $FeSe_{1-x}$ did not seem to exhibit static magnetic order for pressures up to about 30 GPa [16]. Yet, short-range spin fluctuations, which are strongly enhanced towards T_c, were observed [17]. The superconducting transition temperature of $FeSe_{1-x}$ was found to increase continuously to $\simeq 37$ K at 7–9 GPa. For higher pressures a decrease is observed with $T_c \simeq 6$ K approaching 20 GPa [16,18]. Subsequent experiments with finer pressure steps revealed, however, a local minimum on $T_c(p)$ at 1.5 GPa of unexplained nature [19].

In this Letter we report on a detailed study of the evolution of the superconducting and magnetic properties of $FeSe_{1-x}$ as a function of pressure and temperature through a combination of ac susceptibility and muon-spin rotation (μSR) techniques. Two samples with the nominal composition $FeSe_{0.94}$ and $FeSe_{0.98}$ were investigated. The obtained phase diagram of $FeSe_{1-x}$ was found to be separated into three distinct regions. At low pressures, $0 \leq p \lesssim 0.8$ GPa, the samples are nonmagnetic and T_c increases monotonically with increasing pressure. In the intermediate pressure region, $0.8 \leq p \lesssim 1.0$ GPa, $T_c(p)$ decreases with increasing pressure and static magnetism develops. In this region of the phase diagram the superconducting and the magnetic order parameters coexist and compete on a short length scale. Incommensurate magnetic order, which sets in above T_c, becomes partially (or even fully) suppressed below $T_c(p)$. At higher pressures, $p \gtrsim 1.0$ GPa, $T_c(p)$ shows a tendency to rise again. The magnetic order becomes commensurate and both bulk magnetism and bulk superconductivity coexist within the whole sample volume.

$FeSe_{1-x}$ samples with the nominal composition $FeSe_{0.94}$ and $FeSe_{0.98}$ were prepared by solid state reaction similar to that described in Refs. [20–22]. Powders of minimum purity 99.99% were mixed in appropriate ratios, pressed, and sealed in a double-walled quartz ampoule. The pressed rod was heated up to 700 °C followed by annealing at 400 °C [22].

The pressure was generated in a piston-cylinder type of cell especially designed to perform muon-spin rotation experiments under pressure [23]. As a pressure transmitting medium 7373 Daphne oil was used. The pressure was measured *in situ* by monitoring the pressure shift of the superconducting transition temperature of Pb or/and In. Two types of cells, the first one made from CuBe alloy [maximum pressures $p_{max}(300\ \mathrm{K}) \simeq 1.4$ GPa and $p_{max}(7\ \mathrm{K}) \simeq 1.1$ GPa] and the second one made from MP35 alloy [$p_{max}(300\ \mathrm{K}) \simeq 1.7$ GPa and $p_{max}(7\ \mathrm{K}) \simeq 1.4$ GPa], were used.

ac susceptibility measurements were performed by using a home made ac magnetometer with a measuring field $\mu_0 H_{ac} \sim 0.1$ mT and frequency $\nu = 96$ Hz. In order to keep the position of the sample unchanged during the series of ac susceptibility under pressure measurements, the excitation and the two pickup coils were wound directly on the cell. To ensure that the ac signal was entirely determined by the Meissner response of individual grains and not by the Josephson type of weak links between them, measurements of the ac susceptibility as a function of ν ($49 \leq \nu \leq 599$ Hz) and H_{ac} ($0.02 \leq \mu_0 H_{ac} \leq 0.5$ mT) at $T = 2.5$ K on a standard Quantum Design PPMS instru-

PRL **104,** 087003 (2010) PHYSICAL REVIEW LETTERS week ending 26 FEBRUARY 2010

ment were performed. The experiments reveal that the ac magnetization (M_{ac}) scales linearly with H_{ac} and is independent on ν as expected for a superconductor in the Meissner state.

The zero-field muon-spin rotation (ZF μSR) experiments were carried out at the μE1 beam line at the Paul Scherrer Institute, Switzerland for the temperatures ranging from 0.25 to 50 K. The typical counting statistics were $\sim 7 \times 10^6$ positron events for each particular data point.

The response of the superconducting state of $FeSe_{1-x}$ to pressure was studied in ac susceptibility (χ_{ac}) experiments, Fig. 1. The transition temperature T_c, Fig. 1(b), shows a nonmonotonic increase with a local minimum at $p \simeq 1.2$ GPa, similar to $T_c(p)$ reported in [19]. Figure 1(c) depicts $-\chi_{ac}(T)(1-N)$ at $T = 6$ K. Here N denotes the demagnetization factor which, assuming a spherical shape of the sample grains, was taken to be equal to $1/3$. For temperatures lower than T_c, $|\chi_{ac}(T)(1-N)|$ is close, but slightly smaller than unity which could caused by penetration of the ac magnetic field on a distance λ from the surface of each individual grain (λ is the magnetic penetration depth). This reveals that within the pressure range studied the superconductivity is bulk by occupying close to 100% of the whole sample volume.

The magnetic response of $FeSe_{1-x}$ was studied in ZF μSR experiments, which is a well known technique to study magnetically ordered phases where the muon acts as a magnetic microprobe. The μSR experiments in ZF provide information on the internal magnetic field(s) [magnetic order parameter(s)] and on the magnetically ordered volume fraction [24]. In the following we discuss the ZF μSR data for the three different pressure regions.

In the low-pressure region, $0 \leq p \lesssim 0.8$ GPa, where T_c increases with increasing p, the ZF μSR time spectra prove the absence of long-range magnetic order for all temperatures as exemplified by the identical weakly damped spectra for $T = 0.24$ K, near $T_c(p)$ and 20 K, see $p = 0.0$ and $p = 0.76$ GPa data in Fig. 2(a). The solid lines in Fig. 2(a) correspond to a two-component fit:

$$A^{ZF}(t) = A_S^{ZF}(t) + A_{PS}^{ZF}(t) \quad (1)$$

with the first component describing the sample response and the second one representing the contribution of the pressure cell (ZF responses of the CuBe and MP35 cells are described in [23]). The sample contribution is well fitted to the single-exponential decay function:

$$A_S^{ZF}(t) = A_{S,0}^{ZF} e^{-\Lambda_0 t}, \quad (2)$$

(Λ_0 is the exponential relaxation rate), thus revealing that very diluted and randomly oriented magnetic moments exist in the sample volume which can be attributed to small traces of Fe impurities; see Ref. [25].

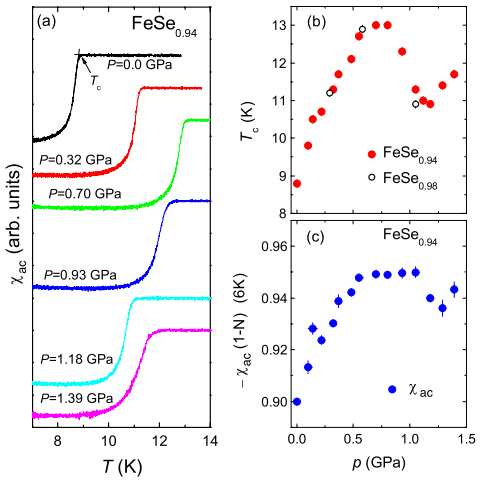

FIG. 1 (color online). (a) Temperature dependence of χ_{ac} of $FeSe_{0.94}$ measured at (from the top to the bottom) $p = 0.0$, 0.32, 0.7, 0.93, 1.18, and 1.39 GPa. The transition temperature T_c is determined from the intersection of straight line fits to the data above and below the transition. (b) Dependence of T_c on p of $FeSe_{0.94}$ and $FeSe_{0.98}$. (c) Pressure dependence of the normalized ac susceptibility $-\chi_{ac}(1-N)$ at $T = 6$ K.

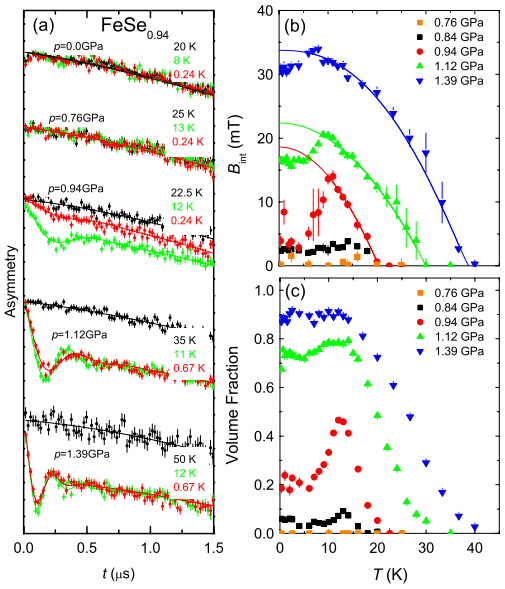

FIG. 2 (color online). (a) Zero-field μSR time spectra of $FeSe_{0.94}$ measured at (from the top to the bottom) $p = 0.0$, 0.76, 0.94, 1.12, and 1.39 GPa. Dependence of the internal field at the muon stopping site B_{int} which is proportional to the magnetic order parameter (b), and the magnetic volume fraction (c), on temperature at various pressures. The solid lines in panel (b) are the fit of $B_{int}(T)$ in the region $T_c(p) \leq T \leq T_N$ to $B_{int}(T) = B_{int}(0)[1-(T/T_N)^{\alpha}]^{\beta}$ (α and β are the power exponents).

In the intermediate pressure region, $0.8 \leq p \lesssim 1.0$ GPa, the spontaneous muon-spin precession is clearly observed in the ZF μSR time spectra; see $p = 0.94$ GPa data in Fig. 2(a). Therefore, static magnetic order is established below the Néel temperature T_N. The analysis of the μSR data was made by accounting for the separation of the sample into magnetically ordered regions with muons experiencing a static local field and nonmagnetic (paramagnetic) regions:

$$A_S^{\mathrm{ZF}}(t) = A_{S,0}^{\mathrm{ZF}}[m(\tfrac{2}{3}j_0(\gamma_\mu B_{\mathrm{int}}t)e^{-\Lambda_T t} + \tfrac{1}{3}e^{-\Lambda_L t}) + (1-m)e^{-\Lambda_0 t}]. \quad (3)$$

Here m is the magnetic volume fraction of the sample, j_0 is a zeroth order Bessel function, $\gamma = 2\pi 135.5$ MHz/T is the muon gyromagnetic ratio, and Λ_T and Λ_L are the exponential relaxation rates longitudinal and transverse to the initial muon-spin polarization. The oscillating part of the signal was found to be good described by a Bessel function, which is archetypical for incommensurate magnetic order [26]. The dependence of the internal field B_{int}, corresponding to the magnetic order parameter, and the magnetic volume fraction on temperature are shown in Figs. 2(b) and 2(c).

For pressures above 1.0 GPa we observe a further increase of the magnetic volume fraction and of the internal magnetic field B_{int}, Fig. 2. Additionally, we find that the μSR line shape is better described by a damped cosine with zero initial phase rather than by a Bessel function:

$$A_S^{\mathrm{ZF}}(t) = A_{S,0}^{\mathrm{ZF}}[m(\tfrac{2}{3}\cos(\gamma_\mu B_{\mathrm{int}}t)e^{-\Lambda_T t} + \tfrac{1}{3}e^{-\Lambda_L t}) + (1-m)e^{-\Lambda_0 t}]. \quad (4)$$

This suggests that in the high pressure region the magnetic order becomes commensurate.

Figure 3 summarizes our results on the magnetism and superconductivity in an electronic phase diagram for $FeSe_{1-x}$. The magnetic order coexists and competes with superconductivity for $p \gtrsim 0.8$ GPa. Above this pressure long-range magnetic order is established below $T_N > T_c$ and bulk superconductivity sets in below T_c. The competition of the two ground states in this pressure range is evident from the following two observations: First, as a function of pressure T_c is weakened as soon as magnetic order appears, leading to the local maximum at $p \simeq 0.8$ GPa in $T_c(p)$; second, as a function of temperature B_{int}, as well as the magnetic volume fraction, decrease below T_c showing that the magnetism, which develops at higher temperatures, becomes partially (or even fully) suppressed by the onset of superconductivity. The superconducting volume fraction is close to 100% for all pressures, Fig. 1(c), while the magnetic fraction increases continuously and reaches ≃90% at the highest pressure investigated $p \simeq 1.39$ GPa, Fig. 2(c). In other words, both ground states coexist in the full sample volume at $p = 1.39$ GPa. Our data do not provide any indication for macroscopic phase separation into superconducting and magnetic clusters (bigger than a few nm in size), as observed, e.g., for $Ba_{1-x}K_xFe_2As_2$ [27]. Actually, the data rather point to a coexistence of both order parameters on an *atomic* scale. This scenario is compatible with the itinerant two-band models of Fe-based HTS proposed recently by Vorontsov *et al.* [28] and Cvetkovic and Tesanovic [29]. According to these models the transition between the magnetic and the superconducting states may involve the formation of the intermediate phase, where both superconductivity and magnetism coexist.

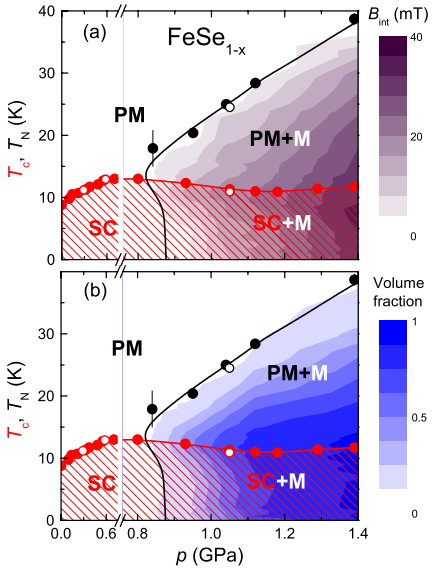

FIG. 3 (color online). (a) Pressure dependence of the superconducting transition temperature T_c, the magnetic ordering temperature T_N, and the internal field B_{int} (magnetic order parameter) obtained in ac susceptibility and muon-spin rotation experiments. (b) Pressure dependence of T_N, T_c, and the magnetic volume fraction. The $T_c(p)$ and $T_N(p)$ lines are guides for the eye. The closed and the open symbols refer to $FeSe_{0.94}$ and $FeSe_{0.98}$ sample. SC, M, and PM denote the superconducting, magnetic, and nonmagnetic (paramagnetic) states of the sample.

In conclusion, the magnetic and superconducting properties of $FeSe_{1-x}$ were studied as a function of pressure up to 1.4 GPa by means of ac magnetization and μSR techniques. ac magnetization measurements show that within the pressure range studied the superconductivity is bulk by occupying close to 100% of the whole sample volume. μSR experiments reveal that above ≃ 0.8 GPa superconductivity coexists with magnetism with Néel temperatures $T_N > T_c$. In a narrow pressure range, where a local minimum in $T_c(p)$ is observed, superconductivity competes with magnetism in the sense that the magnetic volume fraction and the magnetic order parameter are suppressed below T_c. At the highest pressure investigated here superconductivity and static commensurate magnetism coexist

on short length scales in the full sample volume. Furthermore, both forms of order seem to be stabilized by pressure, since T_c as well as T_N and the magnetic order parameter simultaneously increase with increasing pressure. This exceptional observation provides a new challenge for theories describing the mechanism of high-temperature superconductivity.

This work was performed at the SμS Paul Scherrer Institute (PSI, Switzerland). The work of M. B. was supported by the Swiss National Science Foundation. The work of E. P. was supported by the NCCR program MaNEP. R. K. acknowledges the discussion with Z. Tesanovic.

*Corresponding author.
rustem.khasanov@psi.ch

[1] Y. Kamihara, T. Watanabe, M. Hirano, and H. Hosono, J. Am. Chem. Soc. **130**, 3296 (2008).
[2] C. de la Cruz, Q. Huang, J. W. Lynn, J. Li, W. Ratcliff, II, J. L. Zarestky, H. A. Mook, G. F. Chen, J. L. Luo, N. L. Wang, and P. Dai, Nature (London) **453**, 899 (2008).
[3] H.-H. Klauss, H. Luetkens, R. Klingeler, C. Hess, F. J. Litterst, M. Kraken, M. M. Korshunov, I. Eremin, S.-L. Drechsler, R. Khasanov, A. Amato, J. Hamann-Borrero, N. Leps, A. Kondrat, G. Behr, J. Werner, and B. Büchner, Phys. Rev. Lett. **101**, 077005 (2008).
[4] H. Luetkens, H.-H. Klauss, M. Kraken, F. J. Litterst, T. Dellmann, R. Klingeler, C. Hess, R. Khasanov, A. Amato, C. Baines, M. Kosmala, O. J. Schumann, M. Braden, J. Hamann-Borrero, N. Leps, A. Kondrat, G. Behr, J. Werner, and B. Büchner, Nature Mater. **8**, 305 (2009).
[5] J. Zhao, Q. Huang, C. de la Cruz, S. Li, J. W. Lynn, Y. Chen, M. A. Green, G. F. Chen, G. Li, Z. Li, J. L. Luo, N. L. Wang, and P. Dai, Nature Mater. **7**, 953 (2008).
[6] J. Zhao, Q. Huang, C. de la Cruz, J. W. Lynn, M. D. Lumsden, Z. A. Ren, J. Yang, X. Shen, X. Dong, Z. Zhao, and P. Dai, Phys. Rev. B **78**, 132504 (2008).
[7] J. P. Carlo, Y. J. Uemura, T. Goko, G. J. MacDougall, J. A. Rodriguez, W. Yu, G. M. Luke, P. Dai, N. Shannon, S. Miyasaka, S. Suzuki, S. Tajima, G. F. Chen, W. Z. Hu, J. L. Luo, and N. L. Wang, Phys. Rev. Lett. **102**, 087001 (2009).
[8] A. J. Drew, Ch. Niedermayer, P. J. Baker, F. L. Pratt, S. J. Blundell, T. Lancaster, R. H. Liu, G. Wu, X. H. Chen, I. Watanabe, V. K. Malik, A. Dubroka, M. Rössle, K. W. Kim, C. Baines, and C. Bernhard, Nature Mater. **8**, 310 (2009).
[9] S. Sanna, R. De Renzi, G. Lamura, C. Ferdeghini, A. Palenzona, M. Putti, M. Tropeano, and T. Shiroka, Phys. Rev. B **80**, 052503 (2009).
[10] A. Jesche, N. Caroca-Canales, H. Rosner, H. Borrmann, A. Ormeci, D. Kasinathan, H.-H. Klauss, H. Luetkens, R. Khasanov, A. Amato, A. Hoser, K. Kaneko, C. Krellner, and C. Geibel, Phys. Rev. B **78**, 180504(R) (2008).
[11] Q. Huang, Y. Qiu, W. Bao, M. A. Green, J. W. Lynn, Y. C. Gasparovic, T. Wu, G. Wu, and X. H. Chen, Phys. Rev. Lett. **101**, 257003 (2008).
[12] J. Zhao, W. Ratcliff, II, J. W. Lynn, G. F. Chen, J. L. Luo, N. L. Wang, J. Hu, and P. Dai, Phys. Rev. B **78**, 140504(R) (2008).
[13] T. Goko, A. A. Aczel, E. Baggio-Saitovitch, S. L. Bud'ko, P. C. Canfield, J. P. Carlo, G. F. Chen, Pengcheng Dai, A. C. Hamann, W. Z. Hu, H. Kageyama, G. M. Luke, J. L. Luo, B. Nachumi, N. Ni, D. Reznik, D. R. Sanchez-Candela, A. T. Savici, K. J. Sikes, N. L. Wang, C. R. Wiebe, T. J. Williams, T. Yamamoto, W. Yu, and Y. J. Uemura, Phys. Rev. B **80**, 024508 (2009).
[14] S. Li, C. de la Cruz, Q. Huang, Y. Chen, J. W. Lynn, J. Hu, Y.-L. Huang, F.-C. Hsu, K.-W. Yeh, M. K. Wu, and P. Dai, Phys. Rev. B **79**, 054503 (2009).
[15] R. Khasanov, M. Bendele, A. Amato, P. Babkevich, A. T. Boothroyd, A. Cervellino, K. Conder, S. N. Gvasaliya, H. Keller, H.-H. Klauss, H. Luetkens, V. Pomjakushin, E. Pomjakushina, and B. Roessli, Phys. Rev. B **80**, 140511 (R) (2009)
[16] S. Medvedev, T. M. McQueen, I. A. Troyan, T. Palasyuk, M. I. Eremets, R. J. Cava, S. Naghavi, F. Casper, V. Ksenofontov, G. Wortmann, and C. Felser, Nature Mater. **8**, 630 (2009).
[17] T. Imai, K. Ahilan, F. L. Ning, T. M. McQueen, and R. J. Cava, Phys. Rev. Lett. **102**, 177005 (2009).
[18] S. Margadonna, Y. Takabayashi, Y. Ohishi, Y. Mizuguchi, Y. Takano, T. Kagayama, T. Nakagawa, M. Takata, and K. Prassides, Phys. Rev. B **80**, 064506 (2009).
[19] K. Miyoshi, Y. Takaichi, E. Mutou, K. Fujiwara, and J. Takeuchi, J. Phys. Soc. Jpn. **78**, 093703 (2009).
[20] F.-C. Hsu, J.-Y. Luo, K.-W. Yeh, T.-K. Chen, T.-W. Huang, P. M. Wu, Y.-C. Lee, Y.-L. Huang, Y.-Y. Chu, D.-C. Yan, and M.-K. Wu, Proc. Natl. Acad. Sci. U.S.A. **105**, 14 262 (2008).
[21] S. Margadonna, Y. Takabayashi, M. T. McDonald, K. Kasperkiewicz, Y. Mizuguchi, Y. Takano, A. N. Fitch, E. Suard, and K. Prassides, Chem. Commun. (Cambridge) 5607 (2008).
[22] E. Pomjakushina, K. Conder, V. Pomjakushin, M. Bendele, and R. Khasanov, Phys. Rev. B **80**, 024517 (2009).
[23] D. Andreica, Ph.D. thesis, IPP/ETH-Zurich, 2001.
[24] A. Schenck, *Muon Spin Rotation: Principles and Applications in Solid State Physics* (Adam Hilger, Bristol, 1986).
[25] R. Khasanov, K. Conder, E. Pomjakushina, A. Amato, C. Baines, Z. Bukowski, J. Karpinski, S. Katrych, H.-H. Klauss, H. Luetkens, A. Shengelaya, and N. D. Zhigadlo, Phys. Rev. B **78**, 220510(R) (2008).
[26] A. T. Savici, Y. Fudamoto, I. M. Gat, T. Ito, M. I. Larkin, Y. J. Uemura, G. M. Luke, K. M. Kojima, Y. S. Lee, M. A. Kastner, R. J. Birgeneau, and K. Yamada, Phys. Rev. B **66**, 014524 (2002).
[27] J. T. Park, D. S. Inosov, Ch. Niedermayer, G. L. Sun, D. Haug, N. B. Christensen, R. Dinnebier, A. V. Boris, A. J. Drew, L. Schulz, T. Shapoval, U. Wolff, V. Neu, X. Yang, C. T. Lin, B. Keimer, and V. Hinkov, Phys. Rev. Lett. **102**, 117006 (2009).
[28] A. B. Vorontsov, M. G. Vavilov, and A. V. Chubukov, Phys. Rev. B **79**, 060508(R) (2009).
[29] V. Cvetkovic and Z. Tesanovic, Phys. Rev. B **80**, 024512 (2009).

4.5.3 Paper III: Evolution of Two-Gap Behavior of the Superconductor $FeSe_{1-x}$

This work is published in:

R. Khasanov, M. Bendele, A. Amato, K. Conder, H. Keller, H.-H. Klauss, H. Luetkens, and E. Pomjakushina, *Evolution of Two-Gap Behavior of the Superconductor $FeSe_{1-x}$*, Phys. Rev. Lett. **104**, 087004 (2010).

Abstract:

The superfluid density, ρ_s, of the iron chalcogenide superconductor, $FeSe_{1-x}$, was studied as a function of pressure by means of muon-spin rotation. The analysis of $\rho_s(T)$ within the two-gap scheme reveals that the effect on both, the transition temperature T_c and $\rho_s(0)$, is entirely determined by the band(s) where the large superconducting gap develops, while the band(s) with the small gap become practically unaffected.

URL: http://link.aps.org/doi/10.1103/PhysRevLett.104.087004
DOI: 10.1103/PhysRevLett.104.087004
PACS: 74.70.-b, 74.25.Jb, 74.62.Fj, 76.75.+i

PRL 104, 087004 (2010) PHYSICAL REVIEW LETTERS week ending 26 FEBRUARY 2010

Evolution of Two-Gap Behavior of the Superconductor $FeSe_{1-x}$

R. Khasanov,[1,*] M. Bendele,[1,2] A. Amato,[1] K. Conder,[3] H. Keller,[2] H.-H. Klauss,[4] H. Luetkens,[1] and E. Pomjakushina[3]

[1]*Laboratory for Muon Spin Spectroscopy, Paul Scherrer Institute, CH-5232 Villigen PSI, Switzerland*
[2]*Physik-Institut der Universität Zürich, Winterthurerstrasse 190, CH-8057 Zürich, Switzerland*
[3]*Laboratory for Developments and Methods, Paul Scherrer Institute, CH-5232 Villigen PSI, Switzerland*
[4]*IFP, TU Dresden, D-01069 Dresden, Germany*

(Received 2 December 2009; published 25 February 2010)

The superfluid density, ρ_s, of the iron chalcogenide superconductor, $FeSe_{1-x}$, was studied as a function of pressure by means of muon-spin rotation. The analysis of $\rho_s(T)$ within the two-gap scheme reveals that the effect on both, the transition temperature T_c and $\rho_s(0)$, is entirely determined by the band(s) where the large superconducting gap develops, while the band(s) with the small gap become practically unaffected.

DOI: 10.1103/PhysRevLett.104.087004 PACS numbers: 74.70.−b, 74.25.Jb, 74.62.Fj, 76.75.+i

Since the discovery of Fe-based high-temperature superconductors (HTS) much effort is devoted to the investigation of their superconducting mechanism. While some properties of Fe-based HTS are reminiscent of the cuprate HTS (as, e.g., their layered structure, the proximity to a magnetic phase, the universal ''Uemura'' scaling between the superfluid density, ρ_s, and the transition temperature, T_c), the differences between both compounds' families are much more remarkable. Hence, the superconductivity in Fe-based HTS originates within the *d* orbitals of the Fe ion, which are normally expected to lead to pair-breaking effects [1]. For the Fe-based HTS, several disconnected Fermi-surface sheets contribute to superconductivity, as revealed by angle-resolved photoemission spectroscopy [2,3]. Furthermore, indications for multigap superconductivity were obtained from tunneling [4,5], magnetic torque [6], point contact [7], infrared spectroscopy [8], NMR [9] and NQR [10] experiments, as well as from specific heat [11], first and second critical field [12,13], and superfluid density [14–17] studies. The multigap superconducting state positions the Fe-based HTS together with MgB_2—the most famous double-gap superconductor discovered to date. However, it is worth mentioning that in spite of the fact that the two-gap superconductivity was detected for Fe-based HTS belonging to different families (as, e.g., 1111: [4,6,13,14]; 122: [2,5,7,11,12,15,16]; 11: [17]) a systematic study of this phenomenon within one given family was not yet performed. In this Letter we report on the evolution of two-gap behavior in the iron chalcogenide superconductor $FeSe_{1-x}$. The transition temperature was changed within the range $8.3 \lesssim T_c \lesssim 12.8$ K by applying an external pressure p between 0 and 0.84 GPa. At each particular pressure the superfluid density ρ_s was obtained from the in-plane magnetic penetration depth $\lambda_{ab}^{-2}(T) \propto \rho_s$ studied by means of muon-spin rotation, μSR. The analysis of $\lambda_{ab}^{-2}(T, p)$, performed by solving self-consistently the gap equations derived within the two-gap scheme [18,19], reveals that the main effect on $T_c(p)$ and $\lambda_{ab}^{-2}(T, p) \propto \rho_s(T, p)$ arises from the energy band(s) where the large superconducting gap, Δ_1, develops. The zero-temperature values of Δ_1, the contribution of this gap to the superfluid density $\lambda_{ab,1}^{-2}$, as well as the effective coupling constant Λ_{11} increase almost linearly with increasing T_c (increasing pressure). In contrast, the contribution of the small gap and thus Δ_2, $\lambda_{ab,2}^{-2}$, and Λ_{22}, are practically pressure independent. Our results imply, therefore, that the transition temperature in $FeSe_{1-x}$ is entirely determined by the intraband interaction within the band(s) where the dominant gap is opened.

The sample with the nominal composition $FeSe_{0.94}$ was prepared by solid state reaction similar to that described in Refs. [20–22]. Hereafter, 0.94 corresponds to the initial Se content. Following our previous studies, the Se stoichiometry of the main (superconducting) phase of our sample corresponds to $1 - x \simeq 0.974$ [22].

The pressure was generated in a CuBe piston-cylinder type of cell especially designed to perform μSR experiments under pressure [23]. As a pressure transmitting medium 7373 Daphne oil was used. The pressure was measured *in situ* by monitoring the pressure shift of the superconducting transition temperature of Pb and/or In.

The μSR experiments were carried out at the $\mu E1$ beam line, Paul Scherrer Institute, Switzerland. Zero-field (ZF) and transverse-field (TF) μSR experiments were performed at temperatures ranging from 0.24 to 50 K. For TF measurements the external magnetic field $\mu_0 H = 10$ mT was applied perpendicular to the muon-spin polarization. The typical counting statistics was ~ 5–7×10^6 positron events for each data point.

The results of the ZF μSR experiments were previously reported in Ref. [24]. It was shown that up to $p \simeq 0.8$ GPa the ZF response of $FeSe_{0.94}$ is determined by the contribution of the dilute Fe moments, in analogy with what was observed for ambient pressure measurements of $FeSe_{0.85}$ [17]. At $p = 0.84$ GPa static magnetism was found to occupy approximately 10% of the sample volume at $T \simeq T_c$ and it decreases down to $\sim 5\%$ at $T \simeq 0.25$ K [24].

Figure 1 shows the TF μSR time spectra measured at $p = 0.76$ GPa above ($T = 20$ K) and below ($T = 0.24$ K) the superconducting transition temperature ($T_c \simeq 13$ K).

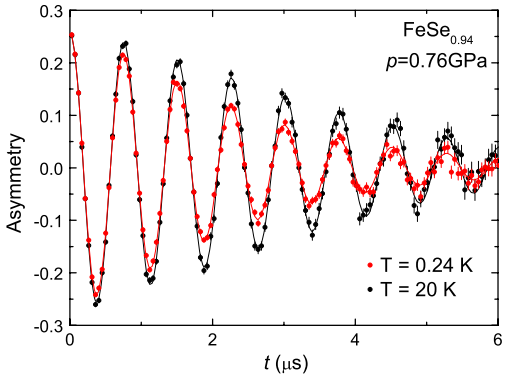

FIG. 1 (color online). TF μSR time spectra ($\mu_0 H = 10$ mT) of $FeSe_{0.94}$ measured below ($T = 0.24$ K) and above ($T = 20$ K) the superconducting transition temperature ($T_c \simeq 13$ K) at $p = 0.76$ GPa. The stronger damping in the superconducting state is due to the formation of the vortex lattice.

The stronger relaxation of the muon-spin polarization at 0.24 K relative to 20 K is due to the formation of the vortex lattice at $T < T_c$. The TF μSR data were analyzed by using the functional form:

$$\begin{aligned} A(t) &= A_S(t) + A_{\mathrm{PS}}(t) \\ &= A_{S,0} e^{-\Lambda t} e^{-\sigma_S^2 t^2/2} \cos(\gamma_\mu B_S t + \phi) \\ &\quad + A_{\mathrm{PS},0} e^{-\sigma_{\mathrm{PS}}^2 t^2/2} \cos(\gamma_\mu B_{\mathrm{PS}} t + \phi). \end{aligned} \tag{1}$$

Here the indexes S and PS denote the sample and the pressure cell, respectively, A_0 is the initial asymmetry, Λ is the exponential relaxation rate caused by the presence of diluted Fe moments [17], $\gamma_\mu = 2\pi \times 135.5$ MHz/T is the muon gyromagnetic ratio, B is the internal field, and ϕ is the initial phase of the muon-spin ensemble. The Gaussian relaxation rate, σ_{PS}, reflects the depolarization due to the nuclear magnetism of the pressure cell, while σ_S represents the depolarization in the sample arising from the nuclear moments and from the vortex lattice (see below). Each set of TF μSR data taken at constant pressure was fitted simultaneously with $A_{S,0}$, $A_{\mathrm{PS},0}$, B_{PS}, σ_{PS}, Λ, and ϕ, as common parameters, and B_S and σ_S as individual parameters for each temperature point. The exponential relaxation rate Λ was assumed to be temperature independent in accordance with the results of ZF μSR experiments [24].

In an anisotropic powder sample the magnetic penetration depth λ can be extracted from the Gaussian relaxation rate $\sigma_{\mathrm{sc}}(T) = [\sigma_S^2(T) - \sigma_{nm}^2]^{1/2} \propto 1/\lambda^2(T)$, which probes the second moment of the magnetic field distribution in a superconductor in the mixed state [17,25,26]. Here σ_{nm} is the nuclear moment contribution measured at $T > T_c$. σ_{sc} can be converted into λ_{ab} via [17,25]

$$\sigma_{\mathrm{sc}}^2/\gamma_\mu^2 = 0.00126\Phi_0^2/\lambda_{ab}^4, \tag{2}$$

where $\Phi_0 = 2.068 \times 10^{-15}$ Wb is the magnetic flux quantum. The measured $\lambda_{ab}^{-2}(T, p)$ of $FeSe_{0.94}$ at $p = 0.0$, 0.28, 0.42, 0.58, 0.76, and 0.84 GPa are shown in Fig. 2.

The experimental $\lambda_{ab}^{-2}(T)$ data were analyzed by using the two-gap model presented recently in Refs. [18,19]. Following [18,19], the coupled gap equations for a superconductor with s-wave energy gaps Δ_1, Δ_2, intraband pairing potentials V_{11}, V_{22}, and interband interaction potentials V_{12}, V_{21} are determined as

$$\Delta_i = \sum_{j=1,2} \int_0^{\omega_{D_i}} \frac{N_j(0) V_{ij} \Delta_j}{\sqrt{E^2 + \Delta_j^2}} \tanh \frac{\sqrt{E^2 + \Delta_j^2}}{2k_B T} dE. \tag{3}$$

Here $i = 1, 2$ is the band index, ω_{D_i} is the phonon cutoff frequency (Debye frequency; note that these cutoffs are expected to be different for both bands $\omega_{D_1} \neq \omega_{D_2}$ [19]) and $N_i(0)$ is the partial density of states at the Fermi level.

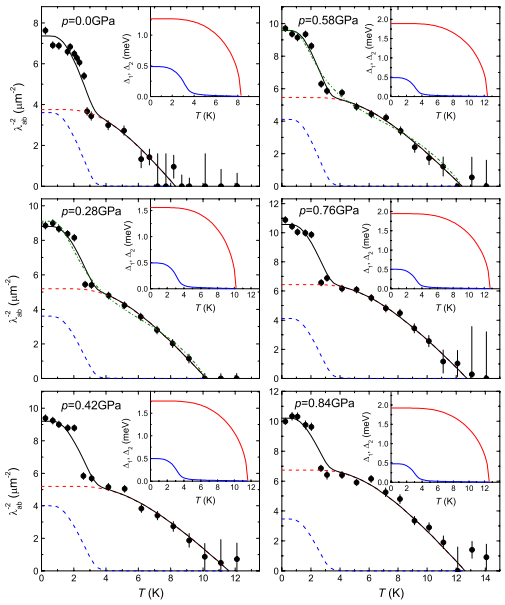

FIG. 2 (color online). Temperature dependence of $\lambda_{ab}^{-2} \propto \rho_s$ of $FeSe_{0.94}$ measured at $p = 0.0$, 0.28, 0.42, 0.58, 0.76, and 0.84 GPa. The solid and the dashed lines are the theoretical curves obtained within the framework of the two-gap model described in the text. The insets show the temperature dependences of the large (Δ_1) and the small (Δ_2) gap. The dash-dotted lines on $p = 0.28$ and 0.58 GPa panels represent the results of the fit by means of the empirical α model [33]. A pure agreement between the theoretical curves and the experimental data is caused by the limitations of the α model as discussed by Kogan *et al.* in [27].

Equation (3) could be simplified by using the notation of the coupling constant $\Lambda_{ij} = N_i(0)V_{ij}$ introduced by Kogan *et al.* [27] and assuming similar cutoff frequencies for both bands ($\omega_{D_1} = \omega_{D_2} = \omega_D$):

$$\Delta_i = \sum_{j=1,2} \Lambda_{ij}\Delta_j \int_0^{\omega_D} \frac{1}{\sqrt{E^2 + \Delta_j^2}} \tanh\frac{\sqrt{E^2 + \Delta_j^2}}{2k_BT} dE. \quad (4)$$

The advantage of using the above equation rather than Eq. (3) is that (i) within the notation of Kogan *et al.* [27] $\Lambda_{12} = \Lambda_{21}$ and (ii) the total number of parameters needed to evaluate $\Delta_1(T)$ and $\Delta_2(T)$ reduces from 8 in case of Eq. (3) to 4 in case of Eq. (4).

With the known $\Delta_1(T)$ and $\Delta_2(T)$, λ_{ab}^{-2} can be obtained by decomposing it into two components $\lambda_{ab,1}^{-2}$ and $\lambda_{ab,2}^{-2}$ so that

$$\lambda_{ab}^{-2}(T) = \lambda_{ab,1}^{-2}(T) + \lambda_{ab,2}^{-2}(T) \quad (5)$$

with [28]

$$\frac{\lambda_{ab,i}^{-2}(T)}{\lambda_{ab,i}^{-2}(0)} = 1 + 2\int_{\Delta_i(T)}^{\infty} \frac{\partial f}{\partial E} \frac{E}{\sqrt{E^2 - \Delta_i(T)^2}} dE.$$

Here $f = [1 + \exp(E/k_BT)]^{-1}$ is the Fermi function.

The analysis of $\lambda_{ab}^{-2}(T, p)$ by using the above described model was made by solely evaluating Λ_{22}, $\lambda_{ab,1}^{-2}(0)$, and $\lambda_{ab,2}^{-2}(0)$. The parameters Λ_{11}, Λ_{12}, and ω_D were taken as follows: Λ_{12}: Our numerical analysis reveals that the step-like change of $\lambda_{ab}^{-2}(T)$ at $T \simeq 2.5$ K (see Fig. 2) requires the interband coupling constant Λ_{12} to be very small ($\Lambda_{12} \sim 10^{-3}$ or smaller). This implies that the band(s), where the large and the small superconducting energy gaps are open, become only weakly coupled. Note that a similarly small interband coupling constant was obtained by Kogan *et al.* for the superconductor V_3Si [27]. Λ_{11}: The fact that the interband coupling in $FeSe_{1-x}$ is weak thus suggests that the transition temperature T_c is mainly determined by the coupling within the band(s) where the large superconducting gap is opened. Assuming that the larger gap is Δ_1, T_c is defined when $\Delta_1(T) = 0$, so that according to Eq. (4)

$$\Lambda_{11} \simeq \left[\int_0^{\omega_D} \frac{dE}{E} \tanh\frac{E}{2k_BT_c}\right]^{-1}. \quad (6)$$

With $T_c(p)$ measured independently (see Ref. [24]) Eq. (6) allows one to obtain the value of the intraband coupling constant Λ_{11} for each particular pressure. ω_D: The ambient pressure value of the cutoff phonon frequency (Debye frequency) $\omega_D(p = 0) \simeq 40$ meV was taken from Ref. [29]. The increase of ω_D with increasing pressure was assumed to follow

$$\omega_D(p) = \omega_D(0)(1 + \gamma p/B), \quad (7)$$

which is the consequence of the Grüneisen equation $\gamma = -d\ln\omega_D/d\ln V$ (γ is the Grüneisen parameter, $B \simeq 31$ GPa is the bulk modulus [21], and V is the sample volume). The Grüneisen parameter was assumed to be $\gamma \approx 1$ in analogy with Ref. [30]. We should also emphasize that the parameters of the above described model are not very sensitive to the exact value of ω_D. As an example, the increase (decrease) of ω_D by a factor of 2 leads to a corresponding decrease (increase) of Λ_{11} obtained from Eq. (6) by $\simeq 15(18)\%$. This makes our assumption about using a similar cutoff phonon frequency for both bands [$\omega_{D_1} = \omega_{D_2}$, see Eq. (4)] to be rather reliable. Note that a similar conclusion was also reached by Kogan *et al.* [31].

The parameters obtained from the analysis of $\lambda_{ab}^{-2}(T)$ by means of the model described above are summarized in Table I. The value of the interband coupling constant $\Lambda_{12} = 0.005$ was kept fixed. The red and the blue dashed lines in Fig. 2 correspond to the contribution of the large, $\lambda_{ab,1}^{-2}$, and the small, $\lambda_{ab,2}^{-2}$, superconducting gaps to the total superfluid density, solid lines. The temperature dependences of the large, Δ_1, and the small, Δ_2, gaps are shown in the corresponding insets.

In order to check how the change of T_c affects the energy bands where the large and the small superconducting gaps are supposed to be open, we plot in Fig. 3 the parameters $\lambda_{ab}^{-2}(0)$, $\lambda_{ab,1}^{-2}(0)$, $\lambda_{ab,2}^{-2}(0)$, $\Delta_1(0)$, $\Delta_2(0)$, $\Lambda_{11} = N_1(0)V_{11}$, and $\Lambda_{22} = N_2(0)V_{22}$ as a function of the transition temperature T_c. From the obtained data the following conclusions can be drawn: (i) The zero-temperature

TABLE I. Summary of the pressure studies of $FeSe_{1-x}$. The meaning of the parameters is p, pressure; T_c, transition temperature; ω_D, Debye frequency; Λ_{12}, interband coupling constant; $\Lambda_{11}/\Lambda_{22}$, $\Delta_1(0)/\Delta_2(0)$, $\lambda_{ab,1}^{-2}(0)/\lambda_{ab,2}^{-2}(0)$, intraband coupling constant, zero-temperature value of the gap, zero-temperature value of superfluid density component within the band 1/2, respectively.

p (GPa)	T_c (K)	ω_D (meV)	Λ_{11}	Λ_{22}	Λ_{12}	$\Delta_1(0)$ (meV)	$\Delta_2(0)$ (meV)	$\lambda_{ab,1}^{-2}(0)$ (μm^{-2})	$\lambda_{ab,2}^{-2}(0)$ (μm^{-2})
0.00	8.3(1)	40.0	0.241(1)	0.195(1)	0.0005	1.27(1)	0.487(6)	3.67(25)	3.53(25)
0.28	10.2(1)	40.36	0.253(1)	0.195(1)	0.0005	1.56(1)	0.494(6)	5.19(23)	3.61(23)
0.42	11.6(1)	40.54	0.261(1)	0.195(1)	0.0005	1.77(1)	0.498(6)	5.20(20)	4.00(18)
0.58	12.4(1)	40.74	0.265(1)	0.194(1)	0.0005	1.89(1)	0.491(6)	5.45(19)	4.11(20)
0.76	12.8(1)	40.98	0.267(1)	0.195(1)	0.0005	1.94(1)	0.504(6)	6.44(29)	4.12(25)
0.84	12.6(1)	41.08	0.266(1)	0.193(1)	0.0005	1.92(1)	0.480(6)	6.74(29)	3.47(29)

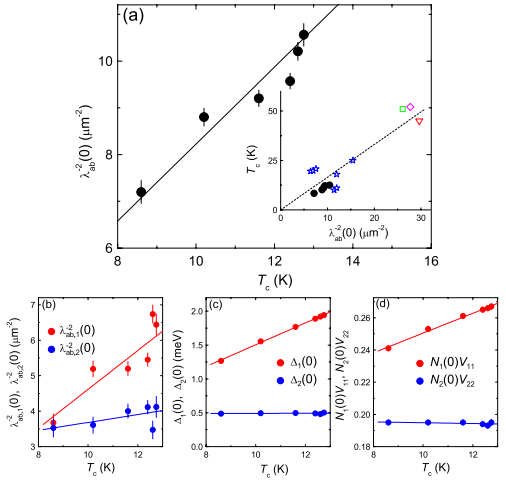

FIG. 3 (color online). (a) Dependence of $\lambda_{ab}^{-2}(T = 0)$ on T_c. The inset is the "Uemura relation" for Fe-based HTS with some of data obtained to date (see Refs. [16,17,25,32]). (b), (c), and (d) Dependence of the parameters obtained in analysis of $\lambda_{ab}^{-2}(T, p)$ within the framework of two-gap model (see text for details).

superfluid density $\rho_s(0) \propto \lambda_{ab}^{-2}(0)$ increases with increasing T_c thus following the Uemura relation established recently for various Fe-based HTS; see Fig. 3(a) and Refs. [16,17,25,32]. (ii) The electronic bands, where the large and the small gap are opened, are affected by the pressure quite differently. The increase of T_c with pressure leads to an almost linear increase of the superfluid density component $\lambda_{ab,1}^{-2}(0)$, the superconducting energy gap $\Delta_1(0)$ as well as the effective coupling constant $\Lambda_{11} = N_1(0)V_{11}$. On the other hand, both $\Delta_2(0)$ and $\Lambda_{22} = N_2(0)V_{22}$ stay almost constant, while $\lambda_{ab,2}^{-2}(0)$ increases with increasing T_c only slightly [see Figs. 3(b)–3(d)]. Bearing in mind that the "large gap" and the "small gap" bands are only weakly coupled (the interband coupling constant Λ_{12} is estimated to be of the order of 5×10^{-4} or less; see Table I) one may conclude that in the range of $0 \leq p \leq 0.84$ GPa the pressure effect on both T_c and λ_{ab}^{-2} is solely determined by the bands exhibiting the large superconducting gap.

To conclude, the superfluid density $\rho_s \propto \lambda_{ab}^{-2}$ was studied as a function of pressure and temperature in the superconductor $FeSe_{1-x}$ by means of μSR. The analysis of $\rho_s(T)$ within a two-gap scheme reveals that the effect on both, T_c and $\rho_s(0)$, is entirely determined by the band(s) where the large superconducting gap develops. Our results suggest that for the 11 family of Fe-based HTS the intraband interaction is most probably the leading pairing interaction determining the superconducting properties.

This work was performed at the SμS Paul Scherrer Institute, Switzerland. The work of MB was supported by the Swiss National Science Foundation. The work of EP was supported by the NCCR program MaNEP.

*Corresponding author.
rustem.khasanov@psi.ch

[1] C. Cao, P. J. Hirschfeld, and H. P. Cheng, Phys. Rev. B **77**, 220506(R) (2008); D. J. Singh and M. H. Du, Phys. Rev. Lett. **100**, 237003 (2008).
[2] H. Ding *et al.*, Europhys. Lett. **83**, 47 001 (2008); L. Zhao *et al.*, Chin. Phys. Lett. **25**, 4402 (2008); V. B. Zabolotnyy *et al.*, Nature (London) **457**, 569 (2009).
[3] T. Kondo *et al.*, Phys. Rev. Lett. **101**, 147003 (2008).
[4] R. S. Gonnelli *et al.*, Physica (Amsterdam) **469C**, 512 (2009).
[5] P. Samuely *et al.*, Physica (Amsterdam) **469C**, 507 (2009).
[6] S. Weyeneth *et al.*, J. Supercond. Novel Magnetism **22**, 347 (2009); S. Weyeneth *et al.*, *ibid.* **22**, 325 (2009).
[7] P. Szabo *et al.*, Phys. Rev. B **79**, 012503 (2009).
[8] G. Li *et al.*, Phys. Rev. Lett. **101**, 107004 (2008).
[9] T. Imai *et al.*, Phys. Rev. Lett. **102**, 177005 (2009).
[10] S. Kawasaki *et al.*, Phys. Rev. B **78**, 220506(R) (2008).
[11] G. Mu *et al.*, Phys. Rev. B **79**, 174501 (2009).
[12] C. Ren *et al.*, Phys. Rev. Lett. **101**, 257006 (2008).
[13] F. Hunte *et al.*, Nature (London) **453**, 903 (2008).
[14] L. Malone *et al.*, Phys. Rev. B **79**, 140501(R) (2009).
[15] M. Hiraishi *et al.*, J. Phys. Soc. Jpn. **78**, 023710 (2009).
[16] R. Khasanov *et al.*, Phys. Rev. Lett. **102**, 187005 (2009); R. Khasanov *et al.*, Phys. Rev. Lett. **103**, 067010 (2009).
[17] R. Khasanov *et al.*, Phys. Rev. B **78**, 220510(R) (2008).
[18] A. Bussmann-Holder *et al.*, Eur. Phys. J. B **37**, 345 (2004).
[19] A. Bussmann-Holder, arXiv:0909.3603.
[20] F.-C. Hsu *et al.*, Proc. Natl. Acad. Sci. U.S.A. **105**, 14 262 (2008).
[21] S. Margadonna *et al.*, Phys. Rev. B **80**, 064506 (2009).
[22] E. Pomjakushina *et al.*, Phys. Rev. B **80**, 024517 (2009).
[23] D. Andreica, Ph.D. thesis, IPP/ETH-Zurich, 2001.
[24] M. Bendele *et al.*, arXiv:0908.2734.
[25] R. Khasanov *et al.*, Phys. Rev. B **78**, 092506 (2008).
[26] E. H. Brandt, Phys. Rev. B **37**, 2349 (1988).
[27] V. G. Kogan, C. Martin, and R. Prozorov, Phys. Rev. B **80**, 014507 (2009).
[28] M. Tinkham, "Introduction to Superconductivity", *Krieger Publishing Company, Malabar, Florida*, 1975.
[29] D. Phelan *et al.*, Phys. Rev. B **79**, 014519 (2009).
[30] C.-L. Huang *et al.*, J. Phys. Soc. Jpn. **78**, 084710 (2009).
[31] V. G. Kogan *et al.*, arXiv:0910.4729.
[32] H. Luetkens *et al.*, Nature Mater. **8**, 305 (2009); A. J. Drew *et al.*, Phys. Rev. Lett. **101**, 097010 (2008); A. Amato *et al.*, Physica (Amsterdam) **469C**, 606 (2009); J. P. Carlo *et al.*, Phys. Rev. Lett. **102**, 087001 (2009); T. Goko *et al.*, Phys. Rev. B **80**, 024508 (2009).
[33] A. Carrington and F. Manzano, Physica (Amsterdam) **385C**, 205 (2003).

4.5.4 Paper IV: Coexistence of incommensurate magnetism and superconductivity in $Fe_{1+y}Se_xTe_{1-x}$

This work is published in:

R. Khasanov, M. Bendele, A. Amato, P. Babkevich, A. T. Boothroyd, A. Cervellino, K. Conder, S. N. Gvasaliya, H. Keller, H.-H. Klauss, H. Luetkens, V. Pomjakushin, E. Pomjakushina, and B. Roessli, *Coexistence of incommensurate magnetism and superconductivity in* $Fe_{1+y}Se_xTe_{1-x}$, Phys. Rev. B **80**, 140511 (2009).

Abstract:

We have studied the superconducting and magnetic properties of $Fe_{1+y}Se_xTe_{1-x}$ single crystals ($0 \leq x \leq 0.5$) by magnetic susceptibility, muon-spin rotation, and neutron diffraction. We find three regimes of behavior: (i) commensurate magnetic order for $x \lesssim 0.1$, (ii) bulk superconductivity for $x \sim 0.5$, and (iii) a range $x \approx 0.25 - 0.45$ in which superconductivity coexists with incommensurate magnetic order. The results are qualitatively consistent with two-band mean-field models in which itinerant magnetism and extended s-wave superconductivity are competing order parameters.

URL: http://link.aps.org/doi/10.1103/PhysRevB.80.140511
DOI: 10.1103/PhysRevB.80.140511
PACS: 74.70.-b, 74.25.Jb, 61.05.F-, 76.75.+i

RAPID COMMUNICATIONS

PHYSICAL REVIEW B **80**, 140511(R) (2009)

Coexistence of incommensurate magnetism and superconductivity in $Fe_{1+y}Se_xTe_{1-x}$

R. Khasanov,[1,*] M. Bendele,[1,2] A. Amato,[1] P. Babkevich,[3,4] A. T. Boothroyd,[3] A. Cervellino,[5] K. Conder,[6] S. N. Gvasaliya,[4] H. Keller,[2] H.-H. Klauss,[7] H. Luetkens,[1] V. Pomjakushin,[4] E. Pomjakushina,[6] and B. Roessli[4]

[1]*Laboratory for Muon Spin Spectroscopy, Paul Scherrer Institute, CH-5232 Villigen PSI, Switzerland*

[2]*Physik-Institut der Universität Zürich, Winterthurerstrasse 190, CH-8057 Zürich, Switzerland*

[3]*Department of Physics, Clarendon Laboratory, Oxford University, Oxford OX1 3PU, United Kingdom*

[4]*Laboratory for Neutron Scattering, Paul Scherrer Institute and ETH Zürich, CH-5232 Villigen PSI, Switzerland*

[5]*Swiss Light Source, Paul Scherrer Institute, CH-5232 Villigen, Switzerland*

[6]*Laboratory for Developments and Methods, Paul Scherrer Institute, CH-5232 Villigen PSI, Switzerland*

[7]*IFP, TU Dresden, D-01069 Dresden, Germany*

(Received 20 July 2009; revised manuscript received 24 August 2009; published 26 October 2009)

We have studied the superconducting and magnetic properties of $Fe_{1+y}Se_xTe_{1-x}$ single crystals ($0 \leq x \leq 0.5$) by magnetic susceptibility, muon-spin rotation, and neutron diffraction. We find three regimes of behavior: (i) commensurate magnetic order for $x \lesssim 0.1$, (ii) bulk superconductivity for $x \sim 0.5$, and (iii) a range $x \approx 0.25-0.45$ in which superconductivity coexists with incommensurate magnetic order. The results are qualitatively consistent with two-band mean-field models in which itinerant magnetism and extended *s*-wave superconductivity are competing order parameters.

DOI: 10.1103/PhysRevB.80.140511 PACS number(s): 74.70.−b, 74.25.Jb, 61.05.F−, 76.75.+i

The recently discovered Fe-based high-temperature superconductors (HTS) host an intriguing competition between magnetic, structural, and superconducting phases. The parent phases, such as *Ln*FeAsO (*Ln*1111, *Ln*=La,Ce,Pr,Sm,...) (Refs. 1–10) and AFe_2As_2 (*A*122, *A*=Ba,Sr,Ca,...) (Refs. 11–15), exhibit commensurate static magnetic order. Upon doping or application of pressure (chemical or mechanical), magnetism is suppressed and superconductivity emerges in a manner that depends on the material. Experiments on fluoride-doped La1111 and Pr1111 indicate that the transition from the superconducting to the magnetic state is of the first order.[3,7] Ce1111 shows a behavior that is more consistent with a quantum-critical point separating magnetic and superconducting states.[5] The experiments on Sm1111 and *A*122 demonstrate the coexistence of magnetism and superconductivity.[9,10,12,16,17]

Recently, Sales *et al.*[18] reported the synthesis of large single crystals of $Fe_{1+y}Se_xTe_{1-x}$ ($0 \leq x \leq 0.5$) belonging to the 011 family of Fe-based HTS. Resistivity measurements showed traces of superconductivity at $T \lesssim 14$ K for all $x \neq 0$ crystals, while bulk superconductivity was detected only for compositions close to $x=0.5$. Nonsuperconducting $Fe_{1+y}Te$ with $y \lesssim 0.1$ exhibits long-range commensurate magnetic order,[19–21] but only short-range incommensurate magnetism survives in Se-doped samples.[20–23] Up to now, however, the relation between the magnetic and superconducting properties has not been studied systematically for the 011 system. Here, we report on a detailed study of $Fe_{1+y}Se_xTe_{1-x}$ single crystals through a combination of magnetic susceptibility, muon-spin rotation (μSR), and neutron diffraction. At the boundary between magnetic and superconducting phases we observe a region of doping in which superconductivity coexists with incommensurate magnetic order. The phase diagram is qualitatively consistent with a two-band itinerant models of the Fe pnictides in which magnetism and extended *s*-wave superconductivity are competing orders.[24,25]

μSR and neutron-diffraction (powder and single crystal) experiments were performed on the πM3 and πE1 beam lines at SμS, and on the HRPT (high resolution powder diffractometer) and TASP (triple-axis spectrometer) instruments at SINQ (all at the Paul Scherrer Institute, Switzerland). ac susceptibility measurements were performed on a Quantum Design PPMS magnetometer with a measuring field $\mu_0 H_{ac}=0.1$ mT and frequency $\nu=1000$ Hz. To reduce the effects of demagnetization thin platelike pieces of $Fe_{1+y}Se_xTe_{1-x}$, cleaved from the main crystals, were oriented with the flat surface (*ab* plane) parallel to the ac field.

Single crystals of $Fe_{1+y}Se_xTe_{1-x}$ were grown by a modified Bridgeman method similar to that reported in Ref. 18. Powders of Fe, Se, and Te of minimum purity 99.99% were mixed in the appropriate ratios, pressed into a rod and vacuum sealed in a double-walled quartz ampule. The rod was first melted and homogenized at 1200 °C for 4 hours and then cooled in a temperature gradient 8 °C/cm at a rate 4 °C/h down to 750 °C followed by 50 °C/h cooling. The crystals had mirrorlike surface and were easily cleaved parallel to the *ab* planes. Several of the crystals were ground into a powder and analyzed by neutron powder diffraction. The amount of the main ($P4/nmm$) fraction was found to be $\simeq$94%, 97%, 98%, and 99% for $x=0.5$, 0.45, 0.4, and 0.25 crystals, respectively. The only impurity phase detected was the hexagonal Fe(SeTe) (space group $P6_3/mmc$).

The ac susceptibility (χ_{ac}) data are shown in Fig. 1. The $x=0.5$ and $x=0.45$ samples are seen to be bulk superconductors with $\chi_{ac}=-1.09$ and -1.18, respectively, at $T \simeq 2$ K. Values of $|\chi_{ac}|$ in excess of unity are likely explained by small nonzero demagnetization factors caused by a slight misalignment of the crystals relative to the direction of the ac field. The $x=0.4$ and 0.25 samples exhibit superconductivity but have a small superconducting fraction of order 10% at low temperature. No trace of superconductivity was detected in the $x=0.1$ and 0.0 samples.

μSR experiments were performed in zero magnetic field

RAPID COMMUNICATIONS

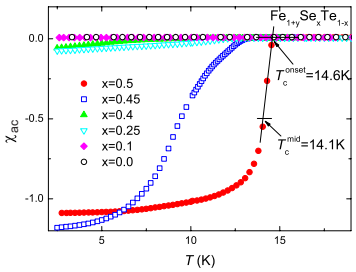

FIG. 1. (Color online) Temperature dependence of the ac volume susceptibility χ_{ac} of $Fe_{1+y}Se_xTe_{1-x}$. The onset T_c^{onset} and the midpoint T_c^{mid} of the superconducting transition are determined from the intersection of straight line fits to the data above and below the transition, and the point corresponding to $\chi_{ac}=-0.5$, respectively.

(ZF), transverse field (TF), and longitudinal field (LF). In TF experiments muons stopping in magnetically ordered parts of the sample lose their polarization rapidly since the magnetic field at the muon stopping site becomes a superposition of the external and the internal fields. ZF experiments provide information on the internal magnetic field distribution, while complementary LF measurements make it possible to discriminate between static and fluctuating fields.

Figure 2 displays μSR results for representative compositions of $Fe_{1+y}Se_xTe_{1-x}$. Figure 2(a) shows that for $x=0.5$ there is no difference between the ZF time spectra measured at $T=1.7$ and 20 K. This suggests that the magnetic state of $FeSe_{0.5}Te_{0.5}$ is the same above and below the superconducting transition temperature. The solid lines correspond to a fit by the function $A^{ZF}(t)=A_0^{ZF}e^{-\Lambda^{ZF}t}$, where A_0^{ZF} is the initial asymmetry and Λ^{ZF} is the exponential relaxation rate. Measurements in LF geometry (not shown) indicate that the exponential character of the muon-spin relaxation is due to randomly oriented local magnetic fields, which are static on the μSR time scale. Such a behavior is consistent with dilute Fe moments as observed recently for another representative of Fe-based HTS $FeSe_{1-x}$.[26] The TF data for $x=0.5$ fit well to the function $A^{TF}(t)=A_0^{TF}e^{-(\Lambda^{TF}t+\sigma^2t^2/2)}\cos(\gamma_\mu Bt+\phi)$. Here, $\gamma_\mu/2\pi=135.5$ MHz/T is the muon gyromagnetic ratio, ϕ is the initial phase of the muon-spin ensemble, and σ is the Gaussian relaxation rate. The right panel of Fig. 2(a) shows that the TF asymmetry A_0^{TF} is almost temperature independent. The slightly stronger relaxation of the muon-spin polarization at 1.7 K relative to 20 K is due to the formation of the vortex lattice at $T<T_c$.

For the $x=0.45$ sample [Fig. 2(b)] there is little change in either the ZF or the TF time spectra on cooling from 20 to $\sim$7 K. At lower temperatures, however, an additional fast relaxing component starts to develop. The solid lines in Fig. 2(b) (left panel) correspond to fits with $A^{ZF}(t)=A_1^{ZF}e^{-\Lambda_1^{ZF}t}+A_2^{ZF}e^{-\Lambda_2^{ZF}t}$ and $A^{TF}(t)=e^{-\sigma^2t^2/2}[A_1^{TF}e^{-\Lambda_1^{TF}t}\cos(\gamma_\mu B_1t+\phi)+A_2^{TF}e^{-\Lambda_2^{TF}t}\cos(\gamma_\mu B_2t+\phi)]$. Here, $A_{1(2)}^{ZF(TF)}$ and $\Lambda_{1(2)}^{ZF(TF)}$ are the initial ZF (TF) asymmetry and the exponential depolarization rate of the slow (fast) relaxing component, respectively. The decrease in A_1^{TF} with

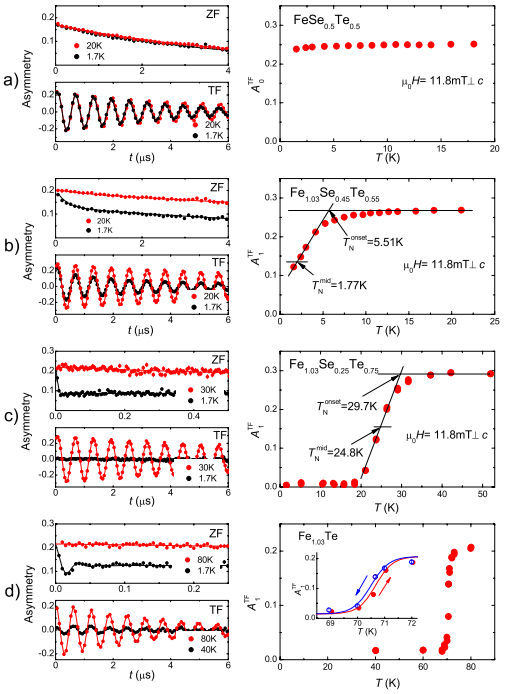

FIG. 2. (Color online) Representative ZF and TF μSR time spectra (left panels) and temperature-dependent initial TF asymmetry of the slow relaxing component (A_0^{TF} and A_1^{TF}, right panels) for single crystals of $Fe_{1+y}Se_xTe_{1-x}$. The onset (T_N^{onset}) and the midpoint (T_N^{mid}) of the magnetic transition are determined from the intersection of straight lines fit to the data above and below the transition and the point where the asymmetry reaches 1/2 of its maximum value, respectively.

decreasing temperature [Fig. 2(b), right panel] is due to the development of magnetic order, which at $T\simeq1.7$ K occupies more than 50% of the whole sample volume. The LF data reveal that the slow relaxing component completely recovers at $\simeq10$ mT (similar to that observed for $x=0.5$), while the asymmetry of the fast relaxing one decreases by $\sim$50% at $B^{LF}=0.4$ T. Since the muon spins become decoupled from the static internal field B_{int} at $B^{LF}\gtrsim10B_{int}$,[27] we may assume that the magnetism that develops in the $x=0.45$ sample below $T\approx7$ K is caused by the static internal field $B_{int}\gtrsim0.1$ T at the muon stopping site.

Magnetism was found to develop in the $x=0.4$, 0.25, 0.1, and 0.0 samples below $T\simeq18$, 30, 40, and 70 K, respectively, as signaled by a fast drop of both A^{ZF} and A^{TF} within the first 100 ns [see Figs. 2(c) and 2(d); the ZF and TF time spectra for $x=0.4$ and $x=0.1$ look very similar to that of the $x=0.25$ sample and are not shown]. The TF and ZF data for $x=0.4$, 0.25, and 0.1 were fitted similarly to $x=0.45$. In order to fit the highly damped oscillations observed for $x=0$ [Fig. 2(d)] the second term in $A^{ZF}(t)$ was multiplied by $\cos(\gamma_\mu B_{int}t)$. This sample shows an abrupt change in

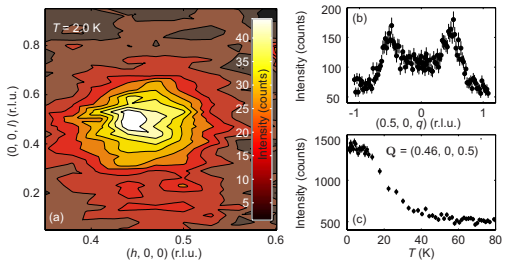

FIG. 3. (Color online) Neutron diffraction from $Fe_{1.03}Se_{0.25}Te_{0.75}$. (a) Intensity of spin-flip scattered polarized neutrons in the $(h,0,l)$ plane. (b) **Q** scan through the magnetic peaks. (c) Temperature dependence of the intensity at (0.46,0,0.5) measured with unpolarized neutrons.

$B_{\rm int} \simeq 0.21$ T at $T \simeq 70.6$ K and hysteresis in $A_1^{\rm TF}(T)$ measured on increasing and decreasing temperature [see inset in the right panel of Fig. 2(d)]. These features are evidence for a first-order magnetic transition in $Fe_{1.03}Te$, which is consistent with the results of Refs. 20 and 21. To within our experimental accuracy there is no hysteresis in the magnetic transition for the $x=0.45$, 0.4, 0.25, and 0.1 samples.

The fact that the ZF time spectra for the $x=0$ sample can be well described by a damped cosine function with *zero* initial phase [see Fig. 2(d)] suggests that the magnetism in $Fe_{1.03}Te$ is commensurate.[28] The absence of ZF oscillations for samples with $x>0$ prevents any firm conclusions being drawn about the type of magnetism in these samples. To learn how the magnetic correlations change with Se doping, we performed neutron-diffraction measurements on the $x=0.25$ crystal. The neutron polarization analysis device MuPAD (Ref. 29) was employed to separate magnetic from nonmagnetic scattering. Figure 3(a) is a color map of the spin-flip (SF) scattering in the $(h,0,l)$ plane in the reciprocal space (referred to the tetragonal unit cell with $a \simeq 3.8$ Å and $c \simeq 6.2$ Å).[21] The sample temperature was 2 K, and the neutron wavelength was 3.2 Å. The neutron polarization **P** was maintained parallel to the scattering vector **Q**, so that the SF scattering is purely magnetic. The map reveals a magnetic peak centered on the incommensurate wave vector (0.46,0,0.5). Figure 3(b) shows a scan along $\mathbf{Q}=(0.5,0,l)$, i.e., displaced slightly from the peak center. Two magnetic Bragg peaks with equal intensities are observed. The peaks are broader than expected from the resolution of the spectrometer and correspond to correlation lengths of $\xi_a = 11.5 \pm 1.0$ Å and $\xi_c = 6.0 \pm 0.5$ Å. Additional Bragg peaks were found at $(0.46,0,-1.5)$, $(1.46,0,-1.5)$, and $(0.46,0,-2.5)$, corresponding to a magnetic arrangement described by the propagation vector $\mathbf{k}=(0.46,0,\pm 0.5)$.

Figure 3(c) shows the temperature dependence of the peak intensity at (0.46,0,0.5) measured with unpolarized neutrons. The magnetic peak emerges below $T \approx 40$ K, which is consistent with the muon asymmetry data [Fig. 2(c)]. A recent study on a crystal of $Fe_{1.07}Se_{0.25}Te_{0.75}$ has also reported incommensurate magnetic order.[22] The incommensurate peaks were observed on one side of the AFM wave vector and were explained in terms of an imbalance of ferromagnetic/antiferromagnetic correlations between nearest-neighbor spins. The incommensurability and ξ_c are consistent with our results, but ξ_a is a factor of 2 smaller than in our sample.

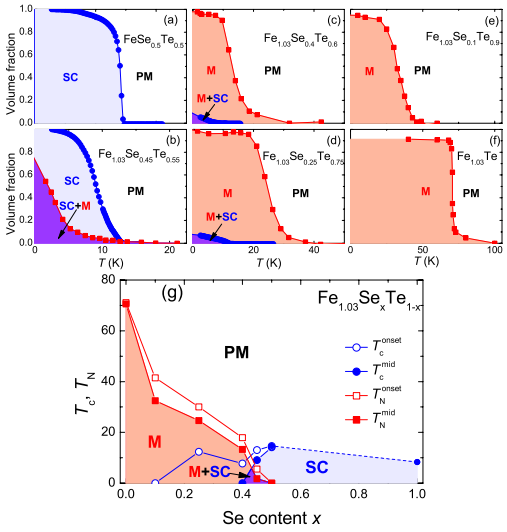

FIG. 4. (Color online) (a)–(f) Temperature dependence of the superconducting (SC) and magnetic (M) volume fractions in $Fe_{1.03}Se_xTe_{1-x}$. PM denotes the paramagnetic phase. (g) Phase diagram showing $T_c^{\rm onset}$, $T_c^{\rm mid}$, $T_N^{\rm onset}$, and $T_N^{\rm mid}$ as functions of x. The datum for $FeSe_{1-x}$ is from Ref. 26.

Figure 4 summarizes our results on the magnetism and superconductivity in $Fe_{1+y}Se_xTe_{1-x}$. The volume fraction curves for the superconducting (SC) and magnetic (M) phases are taken from $\chi_{\rm ac}(T)$ (Fig. 1) and $A_1^{\rm TF}(T)$ (Fig. 2), respectively. The latter represents the fraction of muons experiencing a static local field. Figure 4(g) shows the midpoint and the onset of the superconducting and magnetic transitions, determined as shown in Figs. 1 and 2, as functions of x. It can be seen that superconductivity occurs throughout the bulk of the $x=0.45$ and 0.5 crystals, while it occupies up to $\simeq 10\%$ of the sample volume in the $x=0.25$ and $x=0.4$ samples as $T \to 0$. Magnetic order is present in the $x=0.45$, 0.4, 0.25, 0.1, and 0.0 samples with respective volume fractions of $\simeq 75\%$, 98%, 98%, 95%, and 92% at $T \to 0$.

Most interestingly, superconductivity and magnetism are shown to coexist within certain temperature ranges in the $x=0.45$, 0.4, and 0.25 samples. For $x=0.45$, magnetism starts to develop below the superconducting transition temperature [Fig. 4(b)], while in $x=0.4$ and 0.25 magnetism appears first and superconductivity emerges at a lower temperature [Figs. 4(c) and 4(d)]. The data do not show any evidence that one form of order emerges at the expense of the other, for if that were the case then a growth in one order parameter would coincide with a decrease in the other. This is clearly not the case as may be seen in Figs. 4(b)–4(d). Nor do the data provide any evidence for macroscopic phase separation into superconducting and magnetic clusters (bigger than a few

nm in size), as observed e.g., for $Ba_{1-x}K_xFe_2As_2$.[16] In such a case the sum of magnetic and superconducting volume fractions at a given T should never exceed unity as they do here, especially for $x=0.45$.

To account for the coexistence of superconductivity and magnetism in $Fe_{1+y}Se_xTe_{1-x}$, we consider two scenarios. The first is a *nanoscale* segregation into magnetic domains, similar to that reported for cuprate HTS.[28,30,31] In underdoped cuprate HTS, static, short-range, and stripelike magnetic correlations are thought to exist in the superconducting state and are assumed not to affect the superconducting carriers.[30] Muons are sensitive to dipolar fields at a distance of up to a few lattice spacings, so if nanoscale magnetic domains exist then the fraction of muons experiencing static local magnetic fields could be significantly higher than the fraction of Fe sites carrying an ordered moment. On the other hand, no evidence has been found yet for local magnetic domains in Fe-based compounds. In fact, a recent nuclear magnetic resonance study of $Ba(Fe_{1-x}Co_x)_2As_2$ showed the appearance of magnetic order on *all* Fe sites thus ruling out nanoscale segregation in that material.[17]

The second possibility is a coexistence of the two order parameters on the *atomic* scale. The combination of incommensurate magnetism and superconductivity is compatible with models recently proposed in Refs. 24 and 25. According to Ref. 24, when $T_N^0/T_c^{max} \sim 1$, where T_N^0 is the magnetic ordering temperature at zero doping ($x=0$) and T_c^{max} is the maximum value of the of the superconducting transition temperature for a given family of Fe-based HTS, the magnetic order is commensurate and the transition between the magnetic and superconducting phases with x is first order. However, for larger T_N^0/T_c^{max} the transition between commensurate magnetic order and superconductivity goes through a region of x where superconductivity coexists with incommensurate magnetic order. In the series $Fe_{1+y}Se_xTe_{1-x}$ studied here we find just such a behavior. It is a commensurate magnet without superconductivity at $x=0$ and a nonmagnetic superconductor at $x=0.5$. In between, at $x=0.25$, we observe incommensurate magnetism coexistent with $\sim 10\%$ superconducting fraction. These results are encouraging for the model, but details still need to be worked out. For example, both $LaFeAsO_xF_{1-x}$ and $Fe_{1+y}Se_xTe_{1-x}$ have $T_N^0/T_c^{max} \simeq 5$, yet $LaFeAsO_xF_{1-x}$ apparently exhibits a first-order transition between magnetic and superconducting phases as a function of x without an intermediate region of coexistence.[3]

In conclusion, the phase diagram of $Fe_{1+y}Se_xTe_{1-x}$ bears a strong resemblance to that of other iron pnictide superconductors, but the existence of an intermediate range of doping in which superconductivity coexists with incommensurate magnetic order appears to be specific to $Fe_{1+y}Se_xTe_{1-x}$. The existence of such a phase has been predicted theoretically and is of particular interest in view of the possibility of a Fulde-Ferrell-Larkin-Ovchinnikov state.[25]

This work was performed at the SμS and SINQ, Paul Scherrer Institute (PSI, Switzerland). M.B. was supported by the Swiss National Science Foundation, and E.P. was supported by the NCCR program MaNEP. A.T.B. thanks the PSI for support during an extended visit in 2009. R.K. thanks A. B. Vorontsov for helpful discussions.

*rustem.khasanov@psi.ch

[1] C. de la Cruz *et al.*, Nature (London) **453**, 899 (2008).
[2] H.-H. Klauss *et al.*, Phys. Rev. Lett. **101**, 077005 (2008).
[3] H. Luetkens *et al.*, Nature Mater. **8**, 305 (2009).
[4] G. F. Chen *et al.*, Phys. Rev. Lett. **100**, 247002 (2008).
[5] J. Zhao *et al.*, Nature Mater. **7**, 953 (2008).
[6] J. Zhao *et al.*, Phys. Rev. B **78**, 132504 (2008).
[7] C. Rotundu *et al.*, Phys. Rev. B **80**, 144517 (2009).
[8] J. P. Carlo *et al.*, Phys. Rev. Lett. **102**, 087001 (2009).
[9] A. J. Drew *et al.*, Nature Mater. **8**, 310 (2009).
[10] S. Sanna *et al.*, Phys. Rev. B **80**, 052503 (2009).
[11] A. Jesche *et al.*, Phys. Rev. B **78**, 180504(R) (2008).
[12] A. A. Aczel *et al.*, Phys. Rev. B **78**, 214503 (2008).
[13] Q. Huang *et al.*, Phys. Rev. Lett. **101**, 257003 (2008).
[14] J. Zhao *et al.*, Phys. Rev. B **78**, 140504(R) (2008).
[15] A. I. Goldman *et al.*, Phys. Rev. B **78**, 100506(R) (2008).
[16] J. T. Park *et al.*, Phys. Rev. Lett. **102**, 117006 (2009).
[17] Y. Laplace *et al.*, Phys. Rev. B **80**, 140501(R) (2009).
[18] B. C. Sales *et al.*, Phys. Rev. B **79**, 094521 (2009).
[19] D. Fruchart *et al.*, Mater. Res. Bull. **10**, 169 (1975).
[20] S. Li *et al.*, Phys. Rev. B **79**, 054503 (2009).
[21] W. Bao *et al.*, Phys. Rev. Lett. **102**, 247001 (2009).
[22] J. Wen *et al.*, Phys. Rev. B **80**, 104506 (2009).
[23] M. Lumsden *et al.*, arXiv:0907.2417 (unpublished).
[24] A. B. Vorontsov *et al.*, Phys. Rev. B **79**, 060508(R) (2009).
[25] V. Cvetkovic and Z. Tesanovic, Phys. Rev. B **80**, 024512 (2009).
[26] R. Khasanov *et al.*, Phys. Rev. B **78**, 220510(R) (2008).
[27] A. Schenck, *Muon Spin Rotation: Principles and Applications in Solid State Physics* (Adam Hilger, Bristol, 1986).
[28] A. T. Savici *et al.*, Phys. Rev. B **66**, 014524 (2002).
[29] M. Janoschek *et al.*, Physica B **397**, 125 (2007).
[30] S. Sanna *et al.*, Phys. Rev. Lett. **93**, 207001 (2004).
[31] P. L. Russo *et al.*, Phys. Rev. B **75**, 054511 (2007).

4.5.5 Paper V: Tuning the superconducting and magnetic properties in $Fe_ySe_{0.25}Te_{0.75}$ by varying the Fe-content

This work is published in:

M. Bendele, P. Babkevich, S. Katrych, S. N. Gvasaliya, E. Pomjakushina, K. Conder, B. Roessli, A. T. Boothroyd, R. Khasanov, and H. Keller, *Tuning the superconducting and magnetic properties in $Fe_ySe_{0.25}Te_{0.75}$ by varying the Fe-content*, Phys. Rev. B **82**, 212504 (2010).

Abstract:

The superconducting and magnetic properties of $Fe_ySe_{0.25}Te_{0.75}$ single crystals ($0.9 \leq y \leq 1.1$) were studied by means of x-ray diffraction, superconducting quantum interference device magnetometry, muon-spin rotation, and elastic neutron diffraction. The samples with $y < 1$ exhibit coexistence of bulk superconductivity and incommensurate magnetism. The magnetic order remains incommensurate for $y \geq 1$ but with increasing Fe content superconductivity is suppressed and the magnetic correlation length increases. The results show that the superconducting and the magnetic properties of the $Fe_ySe_{1-x}Te_x$ can be tuned not only by varying the Se/Te ratio but also by changing the Fe content.

URL: http://link.aps.org/doi/10.1103/PhysRevB.82.212504
DOI: 10.1103/PhysRevB.82.212504
PACS: 74.70.Xa, 76.75.+i, 74.25.Dw, 78.70.Nx

PHYSICAL REVIEW B **82**, 212504 (2010)

Tuning the superconducting and magnetic properties of $Fe_ySe_{0.25}Te_{0.75}$ by varying the iron content

M. Bendele,[1,2,*] P. Babkevich,[3,4] S. Katrych,[5] S. N. Gvasaliya,[4] E. Pomjakushina,[6] K. Conder,[6] B. Roessli,[4] A. T. Boothroyd,[3] R. Khasanov,[2] and H. Keller[1]

[1]*Physik-Institut, Universität Zürich, Winterthurerstrasse 190, CH-8057 Zürich, Switzerland*
[2]*Laboratory for Muon Spin Spectroscopy, Paul Scherrer Institut, CH-5232 Villigen PSI, Switzerland*
[3]*Department of Physics, Clarendon Laboratory, Oxford University, Oxford OX1 3PU, United Kingdom*
[4]*Laboratory for Neutron Scattering, Paul Scherrer Institut, CH-5232 Villigen PSI, Switzerland*
[5]*Laboratory for Solid State Physics, ETH Zurich, CH-8093 Zürich, Switzerland*
[6]*Laboratory for Developments and Methods, Paul Scherrer Institut, CH-5232 Villigen PSI, Switzerland*

(Received 1 October 2010; published 7 December 2010)

The superconducting and magnetic properties of $Fe_ySe_{0.25}Te_{0.75}$ single crystals ($0.9 \leq y \leq 1.1$) were studied by means of x-ray diffraction, superconducting quantum interference device magnetometry, muon-spin rotation, and elastic neutron diffraction. The samples with $y < 1$ exhibit coexistence of bulk superconductivity and incommensurate magnetism. The magnetic order remains incommensurate for $y \geq 1$ but with increasing Fe content superconductivity is suppressed and the magnetic correlation length increases. The results show that the superconducting and the magnetic properties of the $Fe_ySe_{1-x}Te_x$ can be tuned not only by varying the Se/Te ratio but also by changing the Fe content.

DOI: 10.1103/PhysRevB.82.212504 PACS number(s): 74.70.Xa, 76.75.+i, 74.25.Dw, 78.70.Nx

The iron chalcogenide family of superconductors Fe_yCh(Ch=Se/Te) was discovered in 2008 (Ref. 1) shortly after the report of high-temperature superconductivity (HTS) in the iron pnictides.[2] This family stands out because of its simple crystal structure relative to other Fe-based superconductors.[3–6] In common with the other Fe-based HTS the parent phase, FeTe, exhibits antiferromagnetic order,[7–9] and superconductivity appears only upon substitution of Te with Se or S.[10,11] The superconducting transition temperature T_c is lower than in most of the other Fe-based superconductors, reaching a value of $\simeq$14 K in $Fe_ySe_{1-x}Te_x$ at optimal Se-Te ratio and $\simeq$36 K at high pressures.[1,12–15] Despite its relatively low T_c, the binary FeCh system is attractive for fundamental investigations of the interplay between magnetism and superconductivity because of (i) its simple crystallographic structure, (ii) the relative ease with which single crystals can be grown, and (iii) the similarity of the Fermi-surface topology with that of other Fe-based superconductors.[16]

Recently, it has been reported that the superconducting and magnetic properties of $Fe_ySe_xTe_{1-x}$ not only depend on the Se-Te ratio but also strongly on the Fe content.[13,17–20] Here we report a systematic investigation of the magnetic and superconducting properties, and their interplay, of $Fe_ySe_{0.25}Te_{0.75}$ with different nominal Fe content in the range $0.9 \leq y \leq 1.1$. Samples with low Fe content ($y < 1$) are found to be bulk superconductors with coexistent magnetic order that sets in at a temperature below T_c. Stoichiometric samples ($y \sim 1$) show filamentary superconductivity and magnetic order. Fe-rich samples ($y > 1$) are almost purely magnetic with only traces of superconductivity. Interestingly, the magnetic order was observed to be incommensurate[12,21] throughout the entire range of nominal Fe content investigated, although the correlation length increases with increasing Fe content.

The $Fe_ySe_xTe_{1-x}$ samples were prepared within a wide range of nominal Fe content from y=0.9 to 1.1 (y=0.90, 0.95, 0.98, 1.00, 1.01, 1.02, 1.03, 1.07, and 1.10), with a fixed Se to Te ratio of x=0.25. The single crystals were prepared in the form of rods with masses of $m \sim 4-5$ g by a modified Bridgman method. For a detailed description of the procedure see Ref. 22.

To establish the crystal structure and the stoichiometry, the samples were investigated by single-crystal x-ray diffraction (XRD) at room temperature. Data reduction and numerical absorption correction were performed using the Bruker AXS Inc. software package.[23] The crystal structure was solved by direct method and refined on F^2, employing the programs SHELXS-97 and SHELXL-97.[24] All crystals reveal a tetragonal lattice (space group $P4/nmm$) with the lattice parameters a and c presented in Table I. The refined Se/Te ratio Se_{occ} is within standard deviation ($\pm 3\%$) close to the nominal content. The three samples with the nominal Fe content of 0.95, 0.98, and 1.03 reveal 100% ($\pm 2\%$) Fe occupation Fe_{occ} at the 2b site [(1/4, 3/4, 1/2) for the space group $P4/nmm$, origin choice 2]. The sample with y=1.07 shows an occupation of 100% Fe at the 2b position and a sharp maximum (2.7 Å from the Se/Te atom) on a difference Fourier map $F_0 - F_c$ indicating that the remaining Fe (8%) par-

TABLE I. Summary of structural parameters obtained from single-crystal XRD of selected compositions of $Fe_ySe_{0.25}Te_{0.75}$. $h_{Se/Te}$ denotes the height of Ch above the Fe plane.

	y=0.95	y=0.98	y=1.03	y=1.07
a axis (Å)	3.8125(5)	3.8096(3)	3.8090(4)	3.8104(3)
c axis (Å)	6.1699(13)	6.1524(6)	6.1562(8)	6.1717(10)
$h_{Se/Te}$ (Å)	1.717(2)	1.709(1)	1.715(1)	1.733(1)
Fe_{occ}	1.00(2)	1.00(2)	1.00(2)	1.00+0.08 [a]
Se_{occ}	0.25(3)	0.26(3)	0.24(3)	0.23(3)

[a]1.00 at the 2b and 0.08 at the 2c site.

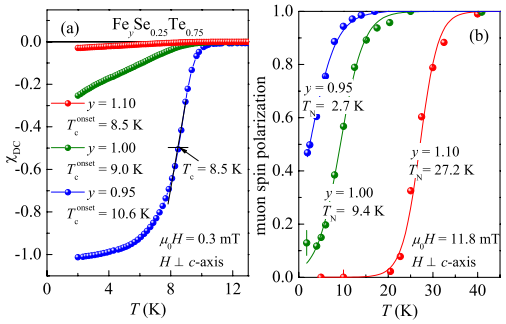

FIG. 1. (Color online) (a) Temperature dependence of the volume susceptibility χ_{dc} of representative compositions (y=0.95, 1.00, and 1.10) of single-crystal $Fe_ySe_{0.25}Te_{0.75}$. The onset of the superconducting transition T_c^{onset} and the midpoint corresponding to χ_{dc}=−0.5 are indicated. (b) Temperature dependence of the muon-spin polarization of the slow relaxing component (P_{slow}^{TF}). The magnetic transition T_N is determined from a fit to a Fermi-type function.

tially occupies the interstitial 2*c* site [3/4, 3/4, 0.2105(2)].

The superconducting properties of $Fe_ySe_{0.25}Te_{0.75}$ were studied on platelike samples with a typical mass ~50 mg that were always mounted with the flat surface (*ab* plane) parallel to the magnetic field to minimize the demagnetization effect on the magnetic moment. The zero-field (ZF) cooled susceptibility measurements were performed with a Quantum Design 7 T magnetic property measurement system (MPMS-XL7) superconducting quantum interference device magnetometer in a magnetic field of μ_0H=0.3 mT using the reciprocating sample option. The data are shown in Fig. 1(a) for samples with representative doping. The measurements indicate that $Fe_ySe_{0.25}Te_{0.75}$ starting from a nominal Fe content of y=0.90 up to y=0.98 exhibits bulk superconductivity since χ_{dc}(2 K)≃−1 close to ideal diamagnetism. However, only the samples with the lowest Fe content (y=0.90 and 0.95) show a saturation of the magnetic moment to χ≃−1 expected for a Meissner state. Already for y=0.98 the transition is broad and tends to saturate only below 2 K. The onset of the superconducting transition decreases with increasing nominal Fe content: T_c^{onset}≃11.5 K, ≃10.6 K, and ≃8 K for y=0.90, 0.95, and 0.98. The samples with a nominal Fe content higher than y≃1 show only traces of superconductivity with a superconducting volume fraction of less than ≈30% at low temperatures for y~1.00 and less than ≈5% for y≥1.03. The onset of the superconducting transition of the samples showing traces of superconductivity is always at T_c^{onset}≈9 K. In order to distinguish samples with bulk superconductivity, T_c was defined as the midpoint of the superconducting transition (namely, χ_{dc}=−0.5). Thus T_c ≃9.7, 8.5, and 6.5 K for the compositions y=0.90, 0.95, and 0.98.

The magnetic response of the samples was investigated by ZF, transverse field (TF), and longitudinal field (LF) muon-spin rotation (μSR) experiments carried out at the πM3 beam line at SμS at the Paul Scherrer Institute (PSI), Switzerland. In TF geometry the muons stopping in magnetic parts of the samples lose their polarization relatively fast because the field at the muon stopping site is a superposition of the internal field and the applied external field of 11.8 mT. The internal field distribution is examined in ZF measurements whereas LF experiments provide information whether the internal field is static or dynamic (fluctuating).

The ZF time spectra (not shown) of the bulk superconducting samples (y=0.90 and 0.95) show no difference between T=20 and 7 K. However, at lower temperatures an additional fast drop of the muon-spin polarization $P(t)$ develops, and the μSR time spectra at 1.8 and 20 K do not coincide any more. This suggests that magnetic ordering observed by μSR develops in the sample at temperatures below T_c. The data were described using the function,

$$P^{ZF}(t) = P_{fast}^{ZF}(0)e^{-\Lambda_{fast}^{ZF}t} + P_{slow}^{ZF}(0)e^{-\Lambda_{slow}^{ZF}t}. \quad (1)$$

Here, $P_{fast(slow)}^{ZF}$ and $\Lambda_{fast(slow)}^{ZF}$ are the initial ZF muon-spin polarization and the exponential depolarization rate of the fast (slow) relaxing component, respectively. Upon increasing the nominal Fe content to y≤0.98 the change in the relaxation occurs at temperatures above T_c. At higher temperatures (T~130 K) an additional change in the ZF depolarization was observed, whose origin requires further investigation.

The magnetic ordering temperature was investigated by means of TF μSR [see Fig. 1(b)]. The TF time spectra (not shown) can be divided into a fast drop of the muon-spin polarization within the first 100 ns and a slow relaxing part below the temperature where magnetism starts to develop. Accordingly, the signal was divided into two parts,

$$P^{TF}(t) = P_{fast}^{TF}(0)\exp[-\Lambda_{fast}^{TF}t]\cos(\gamma_\mu Bt + \phi) + P_{slow}^{TF}(0)\exp[-\Lambda_{slow}^{TF}t]\cos(\gamma_\mu Bt + \phi), \quad (2)$$

where $\gamma_\mu/2\pi$=135.5 MHz/T is the muon gyromagnetic ratio, ϕ is the initial phase of the muon ensemble, and $\Lambda_{fast(slow)}$ the exponential relaxation rate. The fast relaxing component P_{fast}, attributed to the development of magnetism, represents the magnetic volume fraction of the sample and increases with decreasing temperature [Fig. 1(b)]. In the bulk superconducting samples (y=0.90 and 0.95) it occupies at the lowest investigated temperature (T=1.6 K) more than 60% of the signal, indicating that ≥60% of the sample is magnetically ordered. Furthermore, the relaxation of the slow relaxing part increases just below T_c indicating the formation of a vortex lattice in the superconducting state. Upon increasing the nominal Fe content to y≤0.98 the samples were found to be 100% magnetic at 1.6 K as the muon-spin polarization drops to zero within the first 100 ns.

LF measurements reveal that the magnetic order is static in the bulk superconducting samples since the muon-spin polarization recovers almost 100% at B^{LF}=0.64 T and the muon spins decouple from the static internal fields B_{int} at B^{LF}≃10B_{int}.[25] Thus the static internal field in the superconducting samples is B_{int}≳0.1 T at the muon stopping site.

The ordering temperature T_N in Fig. 1(b) was determined by fitting a Fermi-type function $f(T)$={1+exp[$\beta(T_N-T)$]}$^{-1}$ (β^{-1} is the width of transition) to the data [solid lines in Fig. 1(b)].[26] It develops with increasing nominal Fe content from

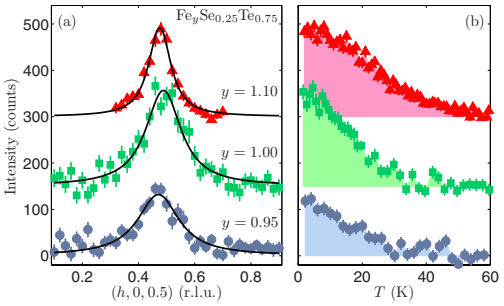

FIG. 2. (Color online) Neutron diffraction from $Fe_ySe_{0.25}Te_{0.75}$ samples for $y=0.95$, 1.00, and 1.10. (a) Intensity profiles along the $(h,0,0.5)$ direction at $T=2$ K after subtraction of a background signal measured at $T\approx 50$ K. The solid line shows a fit to a Lorentzian function convoluted with the resolution function of the instrument. (b) Temperature dependence of the intensity of the magnetic reflection. In both panels the $y=1$ and $y=1.1$ data are displaced vertically for clarity.

$T_N=1.7$ K at the lowest Fe content ($y=0.90$) to 2.7 K, 5 K, 10 K, 12.5 K, and 17 K for $y=0.95$, 0.98, 1.00, 1.01, and 1.02, respectively. Above $y=1.03$ it seems to saturate at $T_N=27$ K (see Ref. 12), 28 K, and 29 K for $y=1.03$, 1.07, and 1.10.

To investigate the change in the magnetic correlations with Fe content, we performed neutron-diffraction measurements on single crystals of $Fe_ySe_{0.25}Te_{0.75}$ for $y=0.95$, 1.00, and 1.10 at 1.5 K. The experiments were performed on the triple-axis spectrometer TASP[27] at the SINQ spallation source (PSI).[28] The instrument was configured for a neutron wave vector of 2.66 $Å^{-1}$ with no collimation. Each sample was aligned on nuclear Bragg reflections to an accuracy of better than 0.008 r.l.u. at 1.5 K. Figure 2(a) shows elastic scans in the $(h,0,l)$ scattering plane. A background recorded at around 50 K (above the magnetic ordering temperature) was subtracted in order to isolate the magnetic contribution to the scattering at 1.5 K. Diffuse incommensurate magnetic peaks centered at $\mathbf{q}=(1/2-\delta,0,1/2)$, with $\delta\approx 0.03$, are observed in all three samples. These results together with our previous neutron-diffraction studies show that samples in the entire range $0.95<y<1.10$ have incommensurate magnetic order.[12,21] We note that our results hint at a possible reduction in incommensurability δ for the $y=1.00$ sample. However, due to the broad nature of the peak this shift may not be related to the sample. As can be seen from Fig. 2(a), the magnetic peaks along $(h,0,0.5)$ appear to become broader with reduced Fe content with correlation lengths along a deduced to be 7.1(5) Å, 8.4(6) Å, and 13.8(8) Å for $y=0.95$, 1.00, and 1.10, respectively. This would suggest that the magnetic correlations become more short ranged on lowering the Fe content.

The temperature at which magnetic order sets in appears also to be dependent on y in $Fe_ySe_{0.25}Te_{0.75}$ as shown in Fig. 2(b). In the $y=1.10$ sample magnetic order is found to develop below ≈ 50 K. However, for $y=1.00$ and $y=0.95$ the transition temperature is reduced to around 30 K. These results are in good agreement with the change in T_N with doping observed by μSR, but due to the difference in fluctuation rates sampled by neutrons and muons, the temperatures at which spin freezing occurs are not the same.

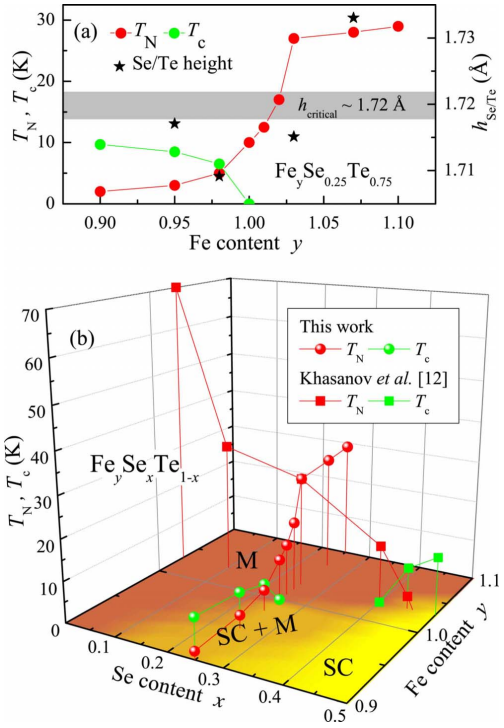

FIG. 3. (Color online) (a) Variation in T_c, T_N, and the Se/Te height $h_{Se/Te}$ in $Fe_ySe_{0.25}Te_{0.75}$ as a function of y. (b) Three-dimensional phase diagram of T_c and T_N of $Fe_ySe_xTe_{1-x}$ as a function of x and y. M and SC denote the magnetic and superconducting phases, respectively. The circles are from this work, and the squares are data taken from Khasanov *et al.* (Ref. 12).

The results of the magnetization and μSR measurements of $Fe_ySe_{0.25}Te_{0.75}$ are summarized in a phase diagram in Fig. 3(a). In the region of $y<1$ a coexistence of superconductivity and magnetism is observed. A recent nuclear-magnetic-resonance study on $BaFe_{2-x}Co_xAs_2$ showed the appearance of magnetic order on all Fe sites and ruled out nanoscale segregation in this material.[29] More reasonable is a coexistence of the two order parameters on atomic scale, as was already suggested earlier[12,29,30] and in agreement with models recently proposed.[31,32]

It has been predicted theoretically that the height of the chalcogenide above the Fe plane $h_{Se/Te}$ can influence the magnetic ordering in $Fe_ySe_xTe_{1-x}$.[33] For that reason $h_{Se/Te}$ derived from XRD measurements is plotted in addition to T_c and T_N in Fig. 3(a). The crossover from the purely magnetic to the coexistence region occurs at $h_{Se/Te}\simeq 1.72$ Å. This result is in good agreement with density-functional theory calculations, which predict a change from double- to single-

stripe antiferromagnetic ordering at $h_{Se/Te} \sim 1.71-1.72$ Å.[33] However, the theoretical calculations are based on Se substitution only and do not take into account any excess Fe. Furthermore, $h_{Se/Te}$ might not be the only contribution since bulk superconductivity appears only for $y \leq 0.98$ whereas the proposed critical height $h_{Se/Te}=1.72$ Å is reached already at $y=1.03$.

The amount of excess Fe seems to play a major role in this system as only for $y \leq 1$ does bulk superconductivity occur. Here the magnetic correlations in the system become more short ranged and lead to less well correlated magnetic order as compared with $y>1$. Thus, only upon reducing the magnetic correlations by lowering the amount of Fe in the system does it become superconducting. Nevertheless, it seems unlikely that the excess Fe acts as isolated magnetic moments that destroy superconductivity. It might on the other hand act as a magnetic electron donor[18] that suppresses superconductivity and induces weakly localized electronic states.[19,20]

The tentative three-dimensional phase diagram of the transition temperatures T_c and T_N of $Fe_ySe_xTe_{1-x}$ for $0 \leq x \leq 0.5$ and $0.9 \leq y \leq 1.1$ is shown in Fig. 3(b). Fe_yTe is always antiferromagnetically ordered.[8,9] Upon substituting Te by Se the order becomes weaker while superconductivity is enhanced and finally the system becomes bulk superconducting. This behavior can be tuned not only by the substitution of Se but also by adjusting the Fe content. The superconductivity is suggested to be of multiband nature, where different doping channels might be involved.[22]

To conclude, we have found that the phase diagram of $Fe_ySe_{0.25}Te_{0.75}$ in the range $0.9 \leq y \leq 1.1$ exhibits a strong dependence of its superconducting and magnetic phases on y. In the low Fe content region $y \leq 1$ bulk superconductivity and incommensurate magnetism coexist. With increasing y the magnetic order becomes correlated over a longer range and superconductivity vanishes. This work emphasizes that not only the Se/Te ratio but also the Fe content is important in controlling the magnetic and superconducting properties of the iron chalcogenides.

This work was performed at the SμS and SINQ, Paul Scherrer Institute (PSI, Switzerland). It was partially supported by the Swiss National Science Foundation and the NCCR program MaNEP.

*markus.bendele@physik.uzh.ch

[1] F. C. Hsu *et al.*, Proc. Natl. Acad. Sci. U.S.A. **105**, 14262 (2008).
[2] Y. Kamihara *et al.*, J. Am. Chem. Soc. **130**, 3296 (2008).
[3] M. Rotter, M. Tegel, and D. Johrendt, Phys. Rev. Lett. **101**, 107006 (2008).
[4] H. Ogino *et al.*, Supercond. Sci. Technol. **22**, 075008 (2009).
[5] X. Zhu, F. Han, G. Mu, B. Zeng, P. Cheng, B. Shen, and H. H. Wen, Phys. Rev. B **79**, 024516 (2009).
[6] X. C. Wang *et al.*, Solid State Commun. **148**, 538 (2008).
[7] D. Fruchart *et al.*, Mater. Res. Bull. **10**, 169 (1975).
[8] W. Bao *et al.*, Phys. Rev. Lett. **102**, 247001 (2009).
[9] S. Li *et al.*, Phys. Rev. B **79**, 054503 (2009).
[10] K.-W. Yeh *et al.*, EPL **84**, 37002 (2008).
[11] Y. Mizuguchi *et al.*, J. Phys. Soc. Jpn. **78**, 074712 (2009).
[12] R. Khasanov *et al.*, Phys. Rev. B **80**, 140511(R) (2009).
[13] T. J. Liu *et al.*, Nature Mater. **9**, 718 (2010).
[14] S. Margadonna, Y. Takabayashi, Y. Ohishi, Y. Mizuguchi, Y. Takano, T. Kagayama, T. Nakagawa, M. Takata, and K. Prassides, Phys. Rev. B **80**, 064506 (2009).
[15] B. C. Sales, A. S. Sefat, M. A. McGuire, R. Y. Jin, D. Mandrus, and Y. Mozharivskyj, Phys. Rev. B **79**, 094521 (2009).
[16] A. Subedi, L. Zhang, D. J. Singh, and M. H. Du, Phys. Rev. B **78**, 134514 (2008).
[17] R. Viennois *et al.*, J. Solid State Chem. **183**, 769 (2010).
[18] L. Zhang, D. J. Singh, and M. H. Du, Phys. Rev. B **79**, 012506 (2009).
[19] J. Wen, G. Xu, Z. Xu, Z. W. Lin, Q. Li, W. Ratcliff, G. Gu, and J. M. Tranquada, Phys. Rev. B **80**, 104506 (2009).
[20] T. J. Liu *et al.*, Phys. Rev. B **80**, 174509 (2009).
[21] P. Babkevich *et al.*, J. Phys.: Condens. Matter **22**, 142202 (2010).
[22] M. Bendele *et al.*, Phys. Rev. B **81**, 224520 (2010).
[23] APEX2 Version 2009.9 (Bruker AXS Inc.). SAINT Version 7.68A (Bruker AXS Inc., 2009). SADABS Version 2008/1 (Sheldrick, Bruker AXS Inc.).
[24] G. Sheldrick, SHELXS-97, Program for the Solution of Crystal Structures, University of Göttingen, Germany, 1997; SHELXL-97, Program for the Refinement of Crystal Structures, University of Göttingen, Germany, 1997.
[25] A. Schenk, *Muon Spin Rotation: Principles and Applications in Solid State Physics* (Adam Hilger, Bristol, 1986).
[26] R. Khasanov, A. Shengelaya, D. Di Castro, E. Morenzoni, A. Maisuradze, I. M. Savic, K. Conder, E. Pomjakushina, A. Bussmann-Holder, and H. Keller, Phys. Rev. Lett. **101**, 077001 (2008).
[27] F. Semadeni, B. Roessli, and P. Böni, Physica B **297**, 152 (2001).
[28] W. E. Fischer, Physica B **234-236**, 1202 (1997).
[29] Y. Laplace, J. Bobroff, F. Rullier-Albenque, D. Colson, and A. Forget, Phys. Rev. B **80**, 140501(R) (2009).
[30] M. Bendele, A. Amato, K. Conder, M. Elender, H. Keller, H. H. Klauss, H. Luetkens, E. Pomjakushina, A. Raselli, and R. Khasanov, Phys. Rev. Lett. **104**, 087003 (2010).
[31] A. B. Vorontsov, M. G. Vavilov, and A. V. Chubukov, Phys. Rev. B **79**, 060508(R) (2009).
[32] V. Cvetkovic and Z. Tesanovic, Phys. Rev. B **80**, 024512 (2009).
[33] C.-Y. Moon and H. J. Choi, Phys. Rev. Lett. **104**, 057003 (2010).

4.5.6 Paper VI: Anisotropic superconducting properties of single-crystalline $FeSe_{0.5}Te_{0.5}$

This work is published in:

M. Bendele, S. Weyeneth, R. Puzniak, A. Maisuradze, E. Pomjakushina, K. Conder, V. Pomjakushin, H. Luetkens, S. Katrych, A. Wisniewski, R. Khasanov, and H. Keller, *Anisotropic superconducting properties of single-crystalline $FeSe_{0.5}Te_{0.5}$*, Phys. Rev. B **81**, 224520 (2010).

Abstract:

Iron-chalcogenide single crystals with the nominal composition $FeSe_{0.5}Te_{0.5}$ and a transition temperature of $T_c \simeq 14.6\,K$ were synthesized by the Bridgman method. The structural and anisotropic superconducting properties of those crystals were investigated by means of single crystal x-ray and neutron powder diffraction, superconducting quantum interference device and torque magnetometry, and muon-spin rotation (μSR). Room temperature neutron powder diffraction reveals that 95% of the crystal volume is of the same tetragonal structure as PbO. The structure refinement yields a stoichiometry of $Fe_{1.045}Se_{0.406}Te_{0.594}$. Additionally, a minor hexagonal Fe_7Se_8 impurity phase was identified. The magnetic penetration depth λ at zero temperature obtained by means of μSR was found to be $\lambda_{ab}(0) = 491(8)\,nm$ in the *ab* plane and $\lambda_c(0) = 1320(14)\,nm$ along the *c* axis. The zero-temperature value of the superfluid density $\rho_s(0) \propto \lambda^{-2}(0)$ obeys the empirical Uemura relation observed for various unconventional superconductors, including cuprates and iron pnictides. The temperature dependences of both λ_{ab} and λ_c are well described by a two-gap $s + s$-wave model with the zero-temperature gap values of $\Delta_S(0) = 0.51(3)\,meV$ and $\Delta_L(0) = 2.61(9)\,meV$ for the small and the large gap, respectively. The magnetic penetration depth anisotropy parameter $\gamma_\lambda(T) = \lambda_c(T)/\lambda_{ab}(T)$ increases with decreasing temperature, in agreement with $\gamma_\lambda(T)$ observed in the iron-pnictide superconductors.

URL: http://link.aps.org/doi/10.1103/PhysRevB.81.224520
DOI: 10.1103/PhysRevB.81.224520
PACS: 74.25.Ha, 74.25.Op, 74.70.Xa, 76.75.+i

PHYSICAL REVIEW B **81**, 224520 (2010)

Anisotropic superconducting properties of single-crystalline $FeSe_{0.5}Te_{0.5}$

M. Bendele,[1,2,*] S. Weyeneth,[1] R. Puzniak,[3] A. Maisuradze,[2] E. Pomjakushina,[4] K. Conder,[4] V. Pomjakushin,[5] H. Luetkens,[2] S. Katrych,[6] A. Wisniewski,[3] R. Khasanov,[2] and H. Keller[1]

[1]*Physik-Institut der Universität Zürich, Winterthurerstrasse 190, CH-8057 Zürich, Switzerland*

[2]*Laboratory for Muon Spin Spectroscopy, Paul Scherrer Institute, CH-5232 Villigen PSI, Switzerland*

[3]*Institute of Physics, Polish Academy of Sciences, Aleja Lotników 32/46, PL-02-668 Warsaw, Poland*

[4]*Laboratory for Developments and Methods, Paul Scherrer Institute, CH-5232 Villigen PSI, Switzerland*

[5]*Laboratory for Neutron Scattering, ETHZ and PSI, CH-5232 Villigen PSI, Switzerland*

[6]*Laboratory for Solid State Physics, ETH Zurich, CH-8093 Zurich, Switzerland*

(Received 1 April 2010; revised manuscript received 8 June 2010; published 28 June 2010)

Iron-chalcogenide single crystals with the nominal composition $FeSe_{0.5}Te_{0.5}$ and a transition temperature of $T_c \approx 14.6$ K were synthesized by the Bridgman method. The structural and anisotropic superconducting properties of those crystals were investigated by means of single crystal x-ray and neutron powder diffraction, superconducting quantum interference device and torque magnetometry, and muon-spin rotation (μSR). Room temperature neutron powder diffraction reveals that 95% of the crystal volume is of the same tetragonal structure as PbO. The structure refinement yields a stoichiometry of $Fe_{1.045}Se_{0.406}Te_{0.594}$. Additionally, a minor hexagonal Fe_7Se_8 impurity phase was identified. The magnetic penetration depth λ at zero temperature obtained by means of μSR was found to be $\lambda_{ab}(0)=491(8)$ nm in the *ab* plane and $\lambda_c(0)=1320(14)$ nm along the *c* axis. The zero-temperature value of the superfluid density $\rho_s(0) \propto \lambda^{-2}(0)$ obeys the empirical Uemura relation observed for various unconventional superconductors, including cuprates and iron pnictides. The temperature dependences of both λ_{ab} and λ_c are well described by a two-gap $s+s$-wave model with the zero-temperature gap values of $\Delta_S(0)=0.51(3)$ meV and $\Delta_L(0)=2.61(9)$ meV for the small and the large gap, respectively. The magnetic penetration depth anisotropy parameter $\gamma_\lambda(T)=\lambda_c(T)/\lambda_{ab}(T)$ increases with decreasing temperature, in agreement with $\gamma_\lambda(T)$ observed in the iron-pnictide superconductors.

DOI: 10.1103/PhysRevB.81.224520 PACS number(s): 74.25.Ha, 74.25.Op, 74.70.Xa, 76.75.+i

I. INTRODUCTION

Since the discovery of superconductivity in $LaFeAsO_{1-x}F_x$ (Ref. 1), high transition temperatures T_c up to 56 K were reported for several Fe-based superconductors with La substituted by other lanthanoids (*Ln*) including, e.g., Ce, Pr, Nd, Sm, and Gd.[2–6] Meanwhile, the family of Fe-based superconductors range from $LnFeAsO_{1-x}F_x$ (the so called "1111" family) over $AeFe_2As_2$ ("122", *Ae*=alkaline earth metal)[7] to the more simple LiFeAs ("111") (Ref. 8) and Fe*Ch* ("11", *Ch*=chalcogenide).[9] The Fe*Ch* system is especially similar to the FeAs-based superconductors, reflecting the ionic nature of the As and chalcogen atoms in these compounds.[10] Recently, two even more complicated families were discovered: the $(Fe_2As_2)(Ae_4M_2O_6)$ ("22426", *M*=transition metal) and the $(Fe_2As_2)(Ae_3M_2O_5)$ ("22325") systems.[11,12] If the parent compound is not already superconducting, superconductivity can be induced by charge carrier doping into either the Fe layers or the spacer layers as well as by applying external or internal pressure.[13–16]

Fe-based superconductors share some common properties with high-T_c cuprates such as a layered crystal structure, the presence of competing orders, a low carrier density, a small coherence length, and an unconventional pairing mechanism. On the other hand, there are some differences: the Fe-based superconductors have metallic parent compounds, the anisotropy is in general lower compared to that of the cuprates, and the order parameter symmetry is claimed to be $\pm s$-wave with Fermi-surface nesting playing a major role.[17–20] Hence, the fundamental question arises whether the mechanisms leading to superconductivity in both families of high-temperature superconductors (HTS) share a common origin.

Among the Fe-based superconductors the "11" system has attracted a lot of attention. The transition temperature T_c of $FeSe_{1-x}$ reaches values up to ≈37 K by applying hydrostatic pressure[9,21] and ≈14 K by partially substituting Se by the isovalent Te or S.[22] In $FeSe_xTe_{1-x}$ the antiferromagnetic order of FeTe is gradually suppressed by increasing *x* and superconductivity emerges with a maximal T_c at $x \approx 0.5$.[16] Additionally, the "11" system has the simplest crystallographic structure among the Fe-based superconductors consisting of layers with a Fe square planar sheet tetrahedrally coordinated by *Ch*.[9] This and the similarity of the Fermi surface to the one of the FeAs-based superconductors[10] make the "11" system an ideal candidate to study the interplay of structure, magnetism, and superconductivity in Fe-based superconductors. In this paper we report on the structural and anisotropic superconducting properties of single crystals with the nominal composition of $FeSe_{0.5}Te_{0.5}$ that were studied by x-ray and neutron powder diffraction, superconducting quantum interference device (SQUID), and torque magnetometry as well as muon-spin rotation (μSR). A part of the present results are in agreement with the findings of a recent μSR study performed on a polycrystalline sample of $FeSe_{0.5}Te_{0.5}$.[23]

II. EXPERIMENTAL DETAILS

A. Single crystal growth

Single crystals with the nominal composition of $FeSe_{0.5}Te_{0.5}$ were grown by the Bridgman method, similar to

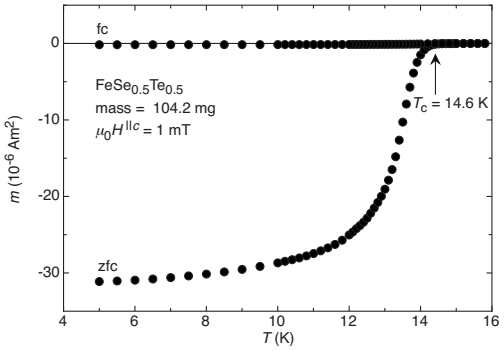

FIG. 1. Magnetic moment m as a function of temperature T in a magnetic field of 1 mT applied parallel to the c axis of single crystal $FeSe_{0.5}Te_{0.5}$, recorded in the Meissner state in zfc mode and in fc mode. The onset transition temperature $T_c \simeq 14.6$ K (vertical arrow) is characteristic for optimal doping $x \simeq 0.5$ of $FeSe_xTe_{1-x}$.

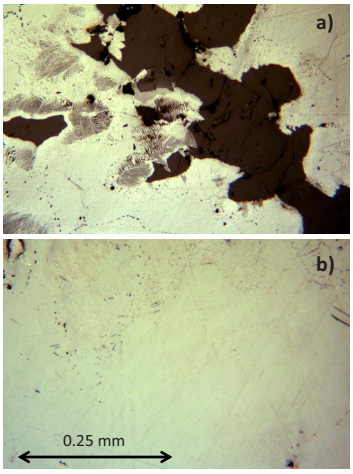

FIG. 2. (Color online) Polarized light microscopic photographs of polished surfaces of the $FeSe_{0.5}Te_{0.5}$ crystal. (a) Microphotography of the crystal surface cut perpendicular to the cleaving facet. Domains with different crystallographic orientations and/or different phases are visible. (b) Micrography of the resulting polished cleaving facet.

that reported by Sales *et al.*[22] Appropriate amounts of Fe, Se, and Te powders with a minimum purity of 99.99 % were mixed together, pressed into a rod (diameter 7 mm), and then evacuated and sealed in a double-wall quartz ampoule for air protection. The ampoule was placed into a vertical furnace with a temperature gradient and annealed at 1200 °C for 4 h. Afterwards the samples were cooled down with a rate of 4 °C/h to 750 °C, followed by a quick cooling (50 °C/h) to room temperature. The so-obtained crystals were easily cleaved from the as-grown crystal along the *ab* plane (cleaving facet).

Figure 1 presents a low-field measurement of the magnetic moment m in a magnetic field of $\mu_0 H = 1$ mT applied along the c axis performed in zero-field-cooled (zfc) and field-cooled (fc) mode. The sample exhibits a clear transition to the superconducting state with an onset transition temperature of $T_c \simeq 14.6$ K. The signal magnitude obtained in the zfc mode reflects a full diamagnetic response of the sample with a calculated susceptibility of $\chi \approx -1$ at $T = 0$ K. The density ρ and the demagnetization factor D were estimated to $\rho = 6.04$ g/cm^3 and $D \approx 0.55$, respectively. Note that a similar result was already observed for a sample of the same batch.[16] The low value of the fc signal indicates strong pinning.

The surface of the as-grown crystal was polished and the surface morphology was examined in a polarized light microscope. Figure 2(a) shows a microphotography of the crystal surface cut perpendicular to the cleaving facet. Distinct domains of different crystallographic orientations and/or different phases are observed. Figure 2(b) shows the polished cleaving facet. No orientation misfit is observed here. In conclusion, the main phase in the material is textured with the c axis perpendicular to the cleaving facet whereas the a and b axes are oriented within domains of irregular shape.

B. Crystal structure

The crystal structure and the phase purity were checked using a single-crystal x-ray diffractometer equipped with a charged-coupled device detector (Xcalibur PX, *Oxford Diffraction*, sample-detector distance 60 mm). Crystallites with approximate dimensions of $1 \times 1 \times 0.2$ mm^3 were cleaved from the as-grown crystal for the single-crystal x-ray diffraction studies. The single crystal diffractographs are shown in Fig. 3. Two distinct crystallographic phases were identified. The major phase of the crystal exhibits a tetragonal lattice [space group: $P4/nmm$ and lattice parameters: $a = 3.7980(2)$ Å and $c = 6.038(1)$ Å]. The reconstruction of the reciprocal space sections of the studied plate-like crystals shows pronounced mosaic spreads with an average mosaicity on the order of about 4°. A small part of the studied crystals with polygonal structure exhibits a hexagonal lattice structure, which is associated with an impurity phase.

Detailed crystal-structure investigations were completed by means of neutron powder diffraction (NPD) at the neutron spallation source SINQ at the Paul Scherrer Institute (PSI, Switzerland) using the High-Resolution Powder diffractometer for Thermal neutrons (HRPT) (Ref. 24), with a neutron wavelength of $\lambda_n = 1.494$ Å. For these experiments, a part of the crystal with the nominal composition of $FeSe_{0.5}Te_{0.5}$ was cleaved, powderized, and loaded into the sample holder in a He-glove box to protect the powder from oxidation. Room-temperature NPD experiments revealed that the sample consists mainly of the tetragonal phase (space group $P4/nmm$) of the PbO type which becomes orthorhomic and superconducting at low temperatures. The results of the Rietveld refinement of the NPD spectra performed with the program FULLPROF (Ref. 25) are shown in Fig. 4. For the refinement it was assumed that all Fe sites are occupied. Additionally, a preferred orientation was assumed as small plate-like grains are created during the pow-

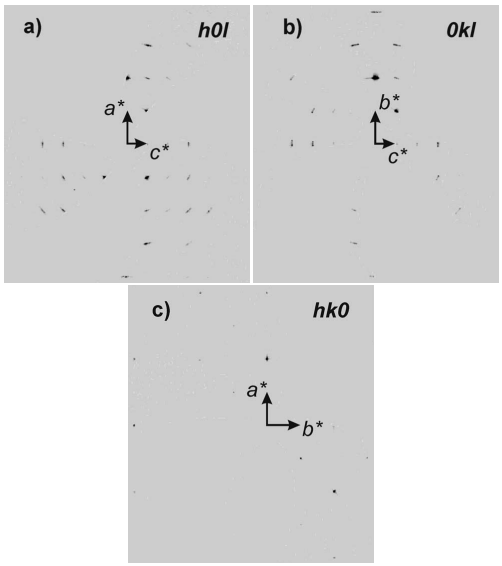

FIG. 3. The reciprocal space sections of the $FeSe_{0.5}Te_{0.5}$ crystal: (a) *h*0*l* reciprocal layer, (b) 0*kl* reciprocal layer, and (c) *hk*0 reciprocal layer.

derization process. The refined stoichiometry is $Fe_{1.045}Se_{0.406(16)}Te_{0.594(16)}$ [a=3.8028(1) Å and c =6.0524(3) Å]. Note that these values were obtained by assuming a texture in the powder sample. As impurity phases hexagonal Fe_7Se_8 (space group $P6_3/mmc$, 5.35(40)% volume fraction) and elemental Fe ($\leq$1%) were identified.

It was shown that in the β-phase additional excess Fe occupies interstitial lattice sites.[26,27] However, introduction of interstitial Fe atoms in the refinement of the data did not improve the fit. This suggests the presence of only a very small amount of such defects, in agreement with the model that in isostructural $FeSe_{1-x}$ (Ref. 28) no interstitial Fe is present. This is in contrast to FeTe where interstitial Fe atoms were detected.[26,27]

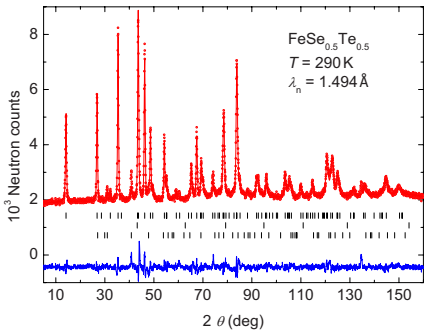

FIG. 4. (Color online) Rietveld refinement pattern (upper–red) and difference plot (lower–blue) of the neutron diffraction data for the crystal with the nominal composition of $FeSe_{0.5}Te_{0.5}$. The rows of ticks show the Bragg peak positions for the main phase and two impurity phases. The refined stoichiometry of the main tetragonal phase is $Fe_{1.045}Se_{0.406}Te_{0.594}$ (see text for details).

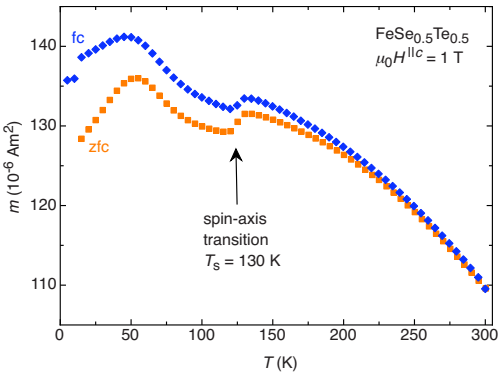

FIG. 5. (Color online) Temperature dependence of the magnetic moment measured in zfc and fc modes in a magnetic field of 1 T applied parallel to the c axis of the crystal with nominal composition $FeSe_{0.5}Te_{0.5}$.

The existence of an impurity phase of Fe_7Se_8 in the studied crystal was confirmed by magnetization measurements. Figure 5 shows the temperature dependence of the magnetic moment recorded for a $FeSe_{0.5}Te_{0.5}$ crystal (mass ~200 mg) in a magnetic field of 1 T, applied parallel to the c axis of the crystal. Fe_7Se_8 is known to undergo a spin-axis transition at 130 K leading to a reduction in magnetization for H parallel to the c axis,[29] as observed in the studied sample (Fig. 5).

III. MAGNETIC PROPERTIES

A. Magnetization measurements

The magnetic properties of the crystals were investigated by a commercial *Quantum Design* 7-T magnetic property measurement system XL SQUID magnetometer at temperatures ranging from 2 K to 300 K and in magnetic fields from 0 T to 7 T using the reciprocating sample option. Magnetic torque measurements were performed with a commercial *Quantum Design* 9-T physical property measurement system equipped with a magnetic torque option.

The magnetization of $FeSe_{0.5}Te_{0.5}$ was measured on a crystal with a mass of the order of 200 mg. The Meissner fraction derived from the magnetic moment in the fc mode as compared to the one from zfc mode is estimated to be ~1% in 1 mT (Fig. 1). This indicates strong vortex pinning in agreement with the weakly field-dependent and pronounced critical current density and with the significant irreversibility in the magnetic torque experiments already present slightly below T_c (as discussed later, Fig. 8). Using Bean's model,[30,31] magnetization hysteresis loop measurements allow to estimate the superconducting critical current density of the order of 10^7 A/m^2. The presence of impurity phases

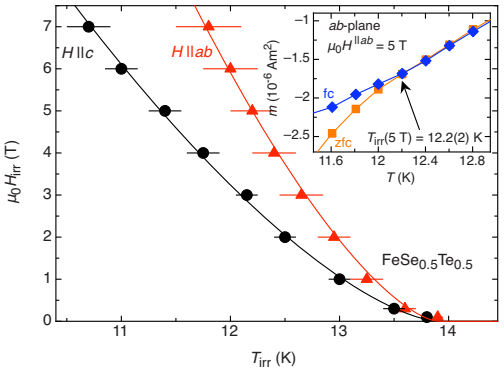

FIG. 6. (Color online) Irreversibility line $H_{irr}(T)$ derived from SQUID measurements for two field configurations, H parallel to the c axis and H parallel to the ab plane of the $FeSe_{0.5}Te_{0.5}$ crystal. The solid black and red lines correspond to fits using the power-law $(1-T/T_c)^n$ with an exponent $n \simeq 1.5$. The inset illustrates how T_{irr} was determined. The lines are guides to the eyes.

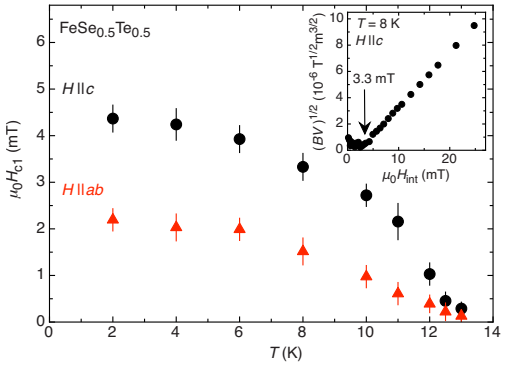

FIG. 7. (Color online) H_{c1} as a function of temperature for both orientations H parallel to the c axis and H parallel to the ab plane for single crystal $FeSe_{0.5}Te_{0.5}$. The inset illustrates the deviation from the linear $B^{1/2}(H)$ dependence plotted as $(BV)^{1/2}$ vs $\mu_0 H_{int}$.

lowers the transport current density as phase separation boundaries prevent to develop a global circulating current. This leads to a relatively low value of the estimated critical-current density as compared to those observed in monocrystalline iron pnictides.[17]

From temperature-dependent magnetization measurements at various magnetic fields the irreversibility line $H_{irr}(T)$ was deduced by following the temperatures for which the zfc and fc branches of the magnetic moment merge. This derivation of $H_{irr}(T)$ is not influenced by the presence of Fe_7Se_8 impurities in the studied samples. Although, the data presented in Fig. 5 indicate that the zfc and fc curves merge only above 200 K, this impurity effect does not affect the determination of T_{irr} here since the temperature range for probing the superconducting irreversibility did not exceed 20 K. No difference between zfc and fc curves, recorded for all magnetic fields in both field configurations, was visible in the temperature range between T_c and maximum applied temperature (inset to Fig. 6). Thus, the influence of an additional phase in the studied samples on the determination of the irreversibility temperature is negligible. The results are presented in Fig. 6, where the inset to the figure illustrates the derivation of T_{irr} in a magnetic field of 5 T parallel to the ab plane. The data were analyzed using the power-law $(1-T/T_c)^n$ with $n \simeq 1.5$, typical for cuprate HTS.[32] The irreversibility line $H_{irr}(T)$ is located at relatively high magnetic fields. Interestingly, H_{irr} is for H parallel to the ab plane almost overlapping, in the studied field range, with the values of the upper critical field $H_{c2}^{\parallel c}$ reported by Fang *et al.*[33]

The temperature dependence of the lower critical field H_{c1} was studied by following the field H_{c1}^{*}, where the first vortices start to penetrate the sample at its surface, which is directly related to H_{c1}. The field dependence of the magnetization was measured at different temperatures for the magnetic field parallel to the ab plane and parallel to the c axis of the sample. For a given shape of the investigated crystal, the demagnetizing factors D were calculated for the magnetic field applied along all of the crystallographic axis. The variation of magnetic induction $B=\mu_0(m/V+H_{int})$ as a function of the internal magnetic field $H_{int}=H_{ext}-DM$ (H_{ext} denotes the external magnetic field) is presented in the inset of Fig. 7. The lower critical fields for H parallel to the ab plane and parallel to the c axis presented in Fig. 7 were determined as the field where the magnetization deviates from the linear behavior. For the case of weak bulk pinning, surface barriers may play a crucial role and determine the first field of flux penetration and the irreversibility line.[34–36] The impact of surface barriers leads to asymmetric $M(H)$ loops. The descending branch is in such a case almost horizontal. For our samples, however, we observe symmetric magnetization loops which means that the bulk pinning controls mainly the entry and exit of the magnetic flux. From these data, the zero-temperature values were found to be $\mu_0 H_{c1}^{\parallel ab}(0) = 2.0(2)$ mT and $\mu_0 H_{c1}^{\parallel c}(0) = 4.5(3)$ mT. In order to extract the values of the magnetic penetration depth from the measured values of H_{c1} the following basic relations were applied:[37]

$$H_{c1}^{\parallel c} = \frac{\Phi_0}{8\pi\mu_0\lambda_{ab}^2}\left[2\ln\left(\frac{\lambda_{ab}}{\xi_{ab}}\right)+1\right], \quad (1)$$

$$H_{c1}^{\parallel ab} = \frac{\Phi_0}{8\pi\mu_0\lambda_{ab}\lambda_c}\left[\ln\left(\frac{\lambda_{ab}\lambda_c}{\xi_{ab}\xi_c}\right)+1\right]. \quad (2)$$

Here, λ_{ab} and λ_c are the magnetic penetration depths parallel to the ab plane and to the c axis, respectively, ξ_{ab} and ξ_c the corresponding coherence lengths, Φ_0 is the elementary flux quantum, and μ_0 the magnetic constant. The values of ξ_{ab} and ξ_c were derived from $H_{c2}^{\parallel ab}$ and $H_{c2}^{\parallel c}$ measurements and found to be approximately 2.8 nm at zero temperature for both field configurations.[33,38] The following zero-temperature values of magnetic penetration depths were obtained: $\lambda_{ab}(0) \simeq 460(100)$ nm and $\lambda_c(0) \simeq 1100(300)$ nm. These values are in good agreement with the values deter-

TABLE I. Summary of the parameters obtained for single crystal $FeSe_{0.5}Te_{0.5}$ by means of μSR and magnetization measurements. The errors of the μSR data are statistical errors and do not take into account for any systematical errors that may be present in the data. Symbol w is defined in the description of Eq. (7).

	μSR		Magnetization	
	ab plane	*c* axis	*ab* plane	*c* axis
T_c (K)	14.1(1)		14.6(1)	
Δ_S^0 (meV)	0.51(3)			
$2\Delta_S^0/k_BT_c$	0.84(4)			
Δ_L^0 (meV)	2.61(9)			
$2\Delta_L^0/k_BT_c$	4.3(1)			
w	0.32(1)	0.36(2)		
$\lambda_{ab,\ c}(0)$ (nm)	491(8)	1320(14)	460(100)	1100(300)
$\mu_0 H_{c1}$ (mT)			2.0(2)	4.5(3)

mined by μSR discussed below (see Table I).

In order to quantify the anisotropy of superconducting state parameters, magnetic torque studies were performed close to T_c, where irreversibility effects are small. The measurements on small crystals ($\sim 1\times1\times0.2$ mm^3) revealed a clear superconducting response, but unfortunately, due to the small amplitude of the superconducting torque signal in the mixed state close to T_c, a relatively strong background component of magnetic origin contributes significantly to the torque signal. The magnetic background signal in the superconducting state is confirmed by following the torque to temperatures above T_c. In order to exclude artifacts in the subsequent analysis, all background components within the superconducting state were subtracted from the torque prior to the analysis (see below). To minimize the influence of pinning the mean reversible torque $\tau_{\rm rev}=[\tau(\theta^+)+\tau(\theta^-)]/2$ was derived from measurements with clockwise and counterclockwise rotating the sample in the field. The superconducting anisotropy parameter $\gamma=\lambda_c/\lambda_{ab}$ may be extracted from the measured torque $\tau(\theta)$ using the relation[39,40]

$$\tau(\theta) = -\frac{V\Phi_0 H}{16\pi\lambda_{ab}^2}\left(1-\frac{1}{\gamma^2}\right)\frac{\sin(2\theta)}{\epsilon(\theta)}\ln\left[\frac{\eta H_{c2}^{\|c}}{\epsilon(\theta)H}\right] + A_\tau \sin(2\theta), \tag{3}$$

where V is the volume of the crystal, λ_{ab} is the in-plane component of the magnetic penetration depth, $H_{c2}^{\|c}$ is the upper critical field along the c axis of the crystal, η denotes a numerical parameter of the order of unity depending on the structure of the flux-line lattice, A_τ is the amplitude of the background torque, and $\epsilon(\theta)=[\cos^2(\theta)+\gamma^{-2}\sin^2(\theta)]^{1/2}$. Since Eq. (3) contains multiple correlated parameters, making a simultaneous fit of all quantities difficult, all $H_{c2}^{\|c}$ values were fixed to those reported in Ref. 33 during the fitting procedure by neglecting any influence of the parameter η. Because the magnetic background contributions tend to influence and alter the fitting parameter $H_{c2}^{\|c}$ strongly,[41,42] the data were fitted by Eq. (3) using the symmetrized expression for the torque $\tau_{\rm symm}(\theta)=\tau(\theta)+\tau(\theta+90°)$.[43] The result of this analysis is depicted in Fig. 8, yielding an anisotropy parameter $\gamma=3.1(4)$ in the vicinity of T_c.

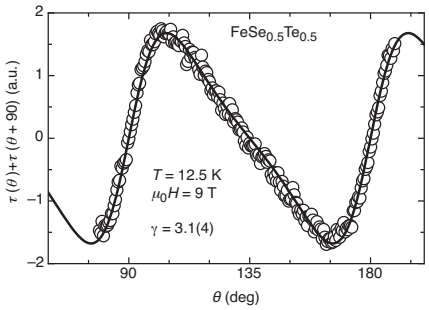

FIG. 8. Symmetrized torque τ_{symm} for the studied crystal of $FeSe_{0.5}Te_{0.5}$ in the superconducting state as a function of the angle θ. The torque data are well described by Eq. (3), yielding an anisotropy parameter $\gamma=3.1(4)$ close to T_c.

B. Muon-spin rotation

μSR is a direct and bulk sensitive probe to investigate local magnetic fields in magnetic solids.[44] Nearly 100% spin-polarized positive muons μ^+ are implanted into the sample and stop at interstitial lattice sites, where the muon spins precess around the local magnetic field B with the Larmor frequency $\omega_{\rm L}=\gamma_\mu B$ ($\gamma_\mu/2\pi=135.5$ MHz/T is the muon gyromagnetic ratio). At the stopping site the muon acts as a magnetic micro probe and measures the internal field distribution. Within the muon's lifetime of $\tau=2.2$ μs it decays into two neutrinos and a positron, which is emitted predominantly along the muon spin polarization at the moment of decay. The direction of the emitted decay positron and the time between the muon implantation and its decay is measured for typically 10^6 positrons. This way the time evolution of the muon spin polarization $P(t)$ is obtained. Zero-field (ZF) μSR experiments probe the magnetic state of a material as the muon spins precess only around the internal field without applying an external magnetic field. In transverse field (TF) μSR experiments, the local magnetic field at the muon site in the sample is probed in the presence of an external magnetic field perpendicular to the initial muon spin polarization. TF μSR is a very powerful tool to investigate the local magnetic field distribution in the vortex state of type-II superconductors. A comprehensive review of the application of μSR to the study of superconductors can be found in Ref. 44.

The μSR experiments were carried out at the πM3 beam line at the Swiss Muon Source (SμS) at PSI. ZF and TF μSR experiments were performed in a temperature range from 1.5 to 20 K. The TF experiments were carried out in two sets of measurements when the external field $\mu_0H=11.8$ mT was applied either parallel to the crystallographic c axis or parallel to the ab plane.

The ZF μSR spectra obtained at 1.6 K and above T_c show no difference [Fig. 9(a)]. This indicates that the magnetic state of $FeSe_{0.5}Te_{0.5}$ below and above T_c is the same. The

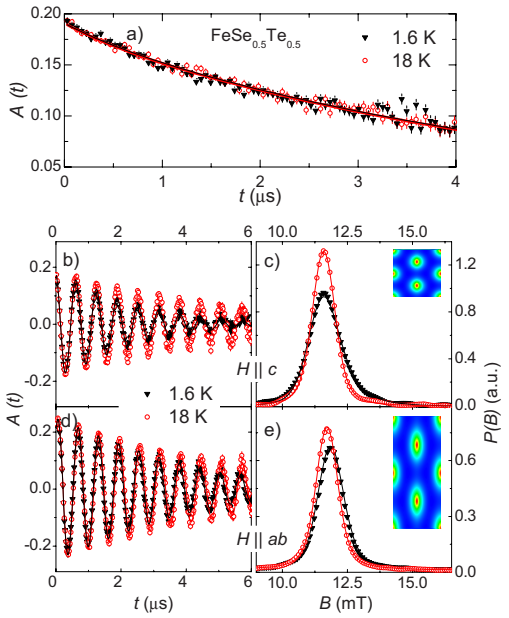

FIG. 9. (Color online) (a) ZF μSR time spectra for $FeSe_{0.5}Te_{0.5}$ recorded at 1.6 K and above T_c. The solid lines represent fits using Eq. (4). [(b) and (d)] TF μSR time spectra for H parallel to the c axis and H parallel to the ab plane, taken at 1.6 K and above T_c. [(c) and (e)] The corresponding magnetic field distributions $P(B)$. The solid lines represent fits using Eq. (5). The insets show the counter plots of the local field variation at 1.6 K, (c) $\lambda_a=\lambda_b$ and (e) $\lambda_c=2.7\lambda_{ab}$.

solid lines in Fig. 9(a) correspond to fits using an exponential decay of the initial muon-spin polarization

$$A^{ZF}(t) = A_{SC} \cdot e^{-\Lambda t} + A_{bg} e^{-\Lambda_{bg} t}. \quad (4)$$

Here, A_{SC} is the asymmetry of the superconducting phase and Λ is the corresponding depolarization rate. The temperature-independent background signal A_{bg}, arising from the Fe_7Se_8 impurity phase was fixed to 6% of the total asymmetry during the fit, corresponding to the results of the NPD refinement. The exponential character of the muon-spin depolarization is typical for diluted and randomly distributed magnetic moments that are static on the muon time scale as shown in Ref. 45.

In the TF geometry muons probe the magnetic field distribution $P(B)$ in the sample. In the mixed state of a type-II superconductor $P(B)$ is determined by the magnetic penetration depth λ and the coherence length ξ. The $P(B)$ distributions obtained from the Fourier transform of the μSR time spectra [Figs. 9(b) and 9(d)] at 1.6 K and above T_c are shown in Figs. 9(c) and 9(e). In the normal state a symmetric $P(B)$ at the position of the applied magnetic field is observed. The broadening of $P(B)$ in the normal state is due to nuclear and diluted electronic magnetic moments. Below T_c an additional

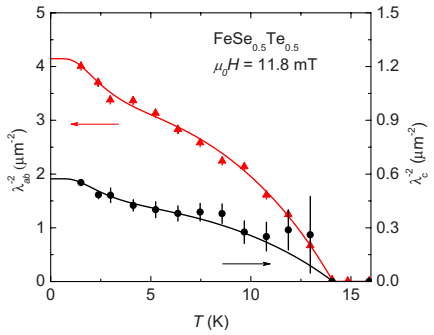

FIG. 10. (Color online) Temperature dependence of the penetration depth components λ_{ab} and λ_c of single crystal $FeSe_{0.5}Te_{0.5}$. The solid lines correspond to fits using Eq. (7). The corresponding fit parameters are listed in Table I.

broadening and an asymmetric line shape $P(B)$ due to the formation of the flux line lattice (FLL) show up. The TF μSR time spectra were analyzed by a theoretical polarization function $A(t)$ by assuming an internal field distribution $P_{FLL}(B)$ and to account for the FLL disorder by multiplying $P_{FLL}(B)$ with a Gaussian function[46,47]

$$A(t) = A_0 e^{i\phi} e^{-(\sigma_g^2+\sigma_{nm}^2)t^2/2-\Lambda_e t} \int P_{FLL}(B) e^{i\gamma_\mu B t} dB. \quad (5)$$

Here, A_0 and ϕ are the initial asymmetry and the phase of the muon-spin ensemble, respectively, σ_g is a parameter related to the FLL disorder,[46,47] σ_{nm} is the nuclear moment contribution measured at $T>T_c$, which is generally temperature independent,[48] and Λ_e is the relaxation rate of the electronic moment contribution, which was obtained from the measurements taken above T_c.

The magnetic field distribution $P_{FLL}(B)$ for a FLL of an anisotropic superconductor was determined from the spatial variation in the magnetic field $B(\mathbf{r})$ calculated in an orthogonal frame x, y, and z with $H\|z$ (z is one of the principal axes a, b, and c) using the expression[49]

$$B(\mathbf{r}) = \langle B \rangle \sum_G \exp(-i\mathbf{G}\cdot\mathbf{r}) B_G(\lambda,\xi,b). \quad (6)$$

Here, $\langle B\rangle$ is the average magnetic field in the superconductor (magnetic induction), $b=\langle B\rangle/B_{c2}$ the reduced field ($B_{c2}=\mu_0 H_{c2}$), and $\mathbf{r}$ the vector coordinate in a plane perpendicular to the applied field. The Fourier components B_G were obtained within the framework of the Ginzburg-Landau model.[49] For a detailed description of the fitting procedure we refer to Ref. 47. The solid lines in Figs. 9(c) and 9(e) correspond to the fast Fourier transforms of the described fits to the μSR time spectra.

The temperature dependences of λ_{ab}^{-2} and λ_c^{-2} extracted from the μSR time spectra using the fitting procedure described above are shown in Fig. 10. These data were analyzed within the framework of the phenomenological α model[50] by assuming that λ^{-2} is a linear combination of two terms

$$\frac{\lambda^{-2}(T)}{\lambda^{-2}(0)} = w\frac{\lambda^{-2}(T,\Delta_S^0)}{\lambda^{-2}(0,\Delta_S^0)} + (1-w)\frac{\lambda^{-2}(T,\Delta_L^0)}{\lambda^{-2}(0,\Delta_L^0)}. \quad (7)$$

Here, Δ_S^0 and Δ_L^0 are the zero-temperature values of the small and the large gap, respectively, and w $(0 \leq w \leq 1)$ is the weighting factor which measures the relative contribution of the two gaps to $\lambda^{-2}(T)/\lambda^{-2}(0)$. For the temperature dependence of λ^{-2} of a London superconductor $(\lambda \gg \xi)$ with a s-wave gap the following relation can be used:[37]

$$\frac{\lambda^{-2}(T,\Delta_{S(L)}^0)}{\lambda^{-2}(0,\Delta_{S(L)}^0)} = 1 + 2\int_{\Delta(T)}^{\infty}\left(\frac{\partial f}{\partial E}\right)\frac{E}{\sqrt{E^2-\Delta^2(T)}}dE. \quad (8)$$

Here, $\lambda(0)$ is the zero-temperature value of the magnetic penetration depth, $f(E)=[1+\exp(E/k_BT)]^{-1}$ is the Fermi function (E is the excitation energy, k_B is the Boltzmann constant), and $\Delta(T)=\Delta(0)\tilde{\Delta}(T/T_c)$ represents the temperature dependence of the gap with $\tilde{\Delta}(T/T_c) = \tanh(1.82[1.018(T_c/T-1)^{0.51}])$.[50] Note that this phenomenological model is only applicable for superconductors in the clean limit.[51] Recent magnetization and resistivity experiments performed on single crystals of $Fe_{1+\delta}Se_{1-x}Te_x$ $(0 \leq x < 1)$ indicate that these superconductors are in the clean limit.[52]

The ratios $2\Delta_S^0/k_BT_c=0.84(4)$ and $2\Delta_L^0/k_BT_c=4.3(1)$ are close to what was reported for isostructural $FeSe_{1-x}$.[45] Based on scanning tunneling spectroscopy measurements, Kato *et al.*[53] reported for $FeSe_{0.4}Te_{0.6}$ only one s-wave gap $\Delta \simeq 2.3$ meV. This value is quite similar to our result of the large gap $[\Delta_L^0=2.61(9)$ meV]. However, a single s-wave gap is not sufficient to describe the present μSR data. The weighting factors w are about the same for $1/\lambda_{ab}^2$ and $1/\lambda_c^2$. Similar results were already reported for isostructural $FeSe_{1-x}$.[45] Recently, Kim *et al.*[54] reported on magnetic penetration depth measurements on $Fe_{1.03}Se_{0.37}Te_{0.63}$ by means of a radio-frequency tunnel diode resonator technique. Their value $\lambda_{ab}(0) \simeq 560(20)$ nm is in good agreement with the value reported here (see Table I). Furthermore, they found a clear signature of multigap superconductivity with comparable gap values ($\Delta_S^0 \simeq 1.2$ meV and $\Delta_L^0 \simeq 2$ meV). In a recent μSR study of polycrystalline $FeSe_{0.5}Te_{0.5}$ the temperature dependence of λ_{ab} was found to be compatible with either a two gap $s+s$-wave or anisotropic s-wave model with $\lambda_{ab}=534(2)$ nm.[23] For the $s+s$-wave analysis, the following results were obtained: $\Delta_L(0)=2.6(1)$ meV, $\Delta_S(0)=0.87(6)$ meV, and $1-w=0.70(3)$.[23] These results are in fair agreement with the present results listed in Table I.

Uemura *et al.*[55] found an empirical relation between the zero-temperature superfluid density $\rho_s(0) \propto \lambda_{ab}^{-2}(0)$ and T_c which seems to be generic for various families of cuprate HTS (Uemura plot). This "universal" relation $T_c(\rho_s)$ has the following features: with increasing carrier doping T_c initially increases linearly $[T_c \propto \rho_s(0)]$, then saturates, and finally is suppressed for high carrier doping. It is interesting to check whether the Uemura relation also holds for iron-based superconductors. For this reason, T_c vs $\lambda_{ab}^{-2}(0)$ is plotted in Fig. 11 for a selection of various Fe-based superconductors investigated so far.[13,14,45,54,57–63] For comparison the linear parts of the Uemura relation for hole-doped (dashed line) and electron-doped (dotted line) cuprate HTS are also shown in Fig. 11. Due to the small number of data points available for a particular family of Fe-based superconductors there is no obvious trend visible. However, all data points are located within an area determined by the straight lines representing the hole-doped and electron-doped cuprates. Whereas several of the Fe-based HTS, including $FeSe_{0.5}Te_{0.5}$ (red star in Fig. 11) investigated here, are located near the hole-doped cuprates in the Uemura plot, the "111" system appears to be close to the electron-doped cuprates.

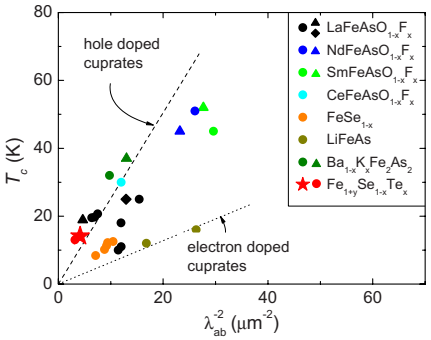

FIG. 11. (Color online) Uemura plot for a selection of some Fe-based HTS. The Uemura relation observed for underdoped cuprates is included for comparison as a dashed line for hole doping and as a dotted line for electron doping (after Ref. 56). $LaFeAsO_{1-x}F_x$ data from Refs. 13 and 57 (●), Ref. 58 (▲), and Ref. 59 (♦); $NdFeAsO_{1-x}F_x$ data from Ref. 60 (●) and Ref. 59 (▲); $SmFeAsO_{1-x}F_x$ data from Ref. 60 (●) and Ref. 14 (▲); $CeFeAsO_{1-x}F_x$ data from Ref. 59, $FeSe_{1-x}$ data from Refs. 45 and 61, LiFeAs data from Ref. 62, $Ba_{1-x}K_xFeAs$ data from Ref. 63, and $Fe_{1+y}Se_{1-x}Te_x$ data from Ref. 54 (●). The red star (⋆) is showing the data for $FeSe_{0.5}Te_{0.5}$ obtained in this work.

IV. TEMPERATURE-DEPENDENT ANISOTROPY PARAMETERS

For a conventional single-band s-wave-layered superconductor, the anisotropy parameter is defined as[37]

$$\gamma = \sqrt{m_c^*/m_{ab}^*} = \lambda_c/\lambda_{ab} = H_{c2}^{\parallel ab}/H_{c2}^{\parallel c} = \xi_{ab}/\xi_c. \quad (9)$$

Here, m_{ab}^* and m_c^* are the effective charge carrier masses related to supercurrents flowing in the ab planes and along the c axis, respectively. Whereas the cuprates were characterized by a well-defined effective mass anisotropy, the observation of two distinct anisotropy parameters in MgB_2 challenged the understanding of anisotropic superconductors.[64–66] Various experiments, such as magnetic torque,[41,42] tunneling,[67,68] point contact and infrared spectroscopy,[69,70] as well as the measurements of the specific heat,[71] the lower and upper critical field,[72,73] and the superfluid density[45,63,74–77] indicate that Fe-based pnictides are multigap superconductors having unconventional anisotropic properties,[41–43] similar to MgB_2.[78,79]

The temperature dependence of the magnetic penetration depth anisotropy parameter $\gamma_\lambda = \lambda_c/\lambda_{ab}$ extracted from the

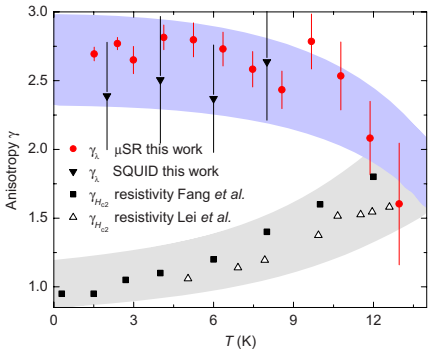

FIG. 12. (Color online) Comparison of the temperature dependence of the magnetic penetration depth anisotropy parameter $\gamma_\lambda = \lambda_c/\lambda_{ab}$ measured by μSR and by SQUID for single crystal $FeSe_{0.5}Te_{0.5}$ with the H_{c2}-anisotropy parameter $\gamma_{H_{c2}} = H_{c2}^{\parallel ab}/H_{c2}^{\parallel c}$ obtained from resistivity measurements for $Fe_{1.11}Se_{0.4}Te_{0.6}$ by Fang *et al.* (Ref. 33) and for $Fe_{1.02}Se_{0.39}Te_{0.61}$ by Lei *et al.* (Ref. 38). The lines are guides to the eyes.

μSR data (see Fig. 10) is shown in Fig. 12. Note that γ_λ increases with decreasing temperature and saturates at $\gamma_\lambda \simeq 2.6(3)$ at low temperatures. This observation is further supported by the temperature dependence of γ_λ determined from the lower critical field measurements presented in Fig. 7. In this case γ_λ is readily obtained from Eqs. (1) and (2) (Ref. 37)

$$\gamma_\lambda = \frac{\lambda_c}{\lambda_{ab}} = \frac{H_{c1}^{\parallel c}}{H_{c1}^{\parallel ab}}\left(1 + \frac{\ln(\gamma_\lambda) + \ln(\gamma_{H_{c2}})}{2\ln(\kappa_{ab}) + 1}\right). \quad (10)$$

Here, $\kappa_{ab} = \lambda_{ab}/\xi_{ab}$ denotes the Ginzburg-Landau parameter. In this work, κ_{ab} was estimated to be $\simeq 180$ from present experiments.[33] The values of γ_λ extracted from the SQUID data using Eq. (10) are also depicted in Fig. 12 and are in fair agreement with those obtained from the μSR data.

The upper critical field anisotropy parameter, $\gamma_{H_{c2}} = H_{c2}^{\parallel ab}/H_{c2}^{\parallel c} = \xi_{ab}/\xi_c$, was studied by Fang *et al.*[33] and Lei *et al.*[38] by resistivity measurements on $Fe_{1+y}Se_{0.4}Te_{0.6}$ ($y = 0.02$ and 0.11). These data are plotted in Fig. 12 as well. Note that $\gamma_{H_{c2}}$ decreases with decreasing temperature. Obviously, the behavior of the two distinct anisotropy parameters γ_λ and $\gamma_{H_{c2}}$ is *not* consistent with Eq. (9). The observed behavior is similar to the one of the two-gap superconductor MgB_2 and other Fe-based superconductors.[42] For MgB_2, however, γ_λ decreases with decreasing temperature while $\gamma_{H_{c2}}$ increases.[65]

V. CONCLUSIONS

Single crystals with a nominal composition of $FeSe_{0.5}Te_{0.5}$ were studied by means of μSR, SQUID and torque magnetometry, and neutron powder diffraction. At room temperature the crystal shows mainly a tetragonal phase of PbO type that becomes orthorombic and superconducting at low temperatures. The stoichiometry was refined to $Fe_{1.045}Se_{0.406}Te_{0.594}$. The onset transition temperature is $T_c = 14.6$ K, and the lower critical field values measured for both crystallographic directions were determined at zero temperature as $H_{c1}^{\parallel ab}(0) = 2.0(2)$ mT and $H_{c1}^{\parallel c}(0) = 4.5(3)$ mT.

By means of μSR it was found that for $FeSe_{0.5}Te_{0.5}$ the temperature dependence of the magnetic penetration depth for both crystallographic directions is best described by a two gap $s+s$-wave model with zero-temperature values of the magnetic penetration depth of $\lambda_{ab}(0) = 491(8)$ nm and $\lambda_c(0) = 1320(14)$ nm, consistent with recent μSR results obtained for a polycrystalline sample.[23] This two-gap scenario is in line with the generally accepted view of multigap superconductivity in Fe-based HTS. Evtushinsky *et al.*[80] pointed out that most Fe-based HTS exhibit two gaps, a large one with $2\Delta/k_BT_c = 7(2)$ and a small one with 2.5(1.5). The magnitudes of the large and the small gap for $FeSe_{0.5}Te_{0.5}$ [$2\Delta_S/k_BT_c = 0.84(4)$ and $2\Delta_L/k_BT_c = 4.3(1)$] are at the lower limit for Fe-based HTS. Moreover, the magnetic penetration depth anisotropy parameter γ_λ determined from penetration depth experiments by means of μSR, is within experimental error the same as the one deduced from H_{c1} measurements. Both techniques yield a temperature-dependent γ_λ that increases with decreasing temperature from 1.6 at $T_c = 14.6$ K to 2.6 at $T = 1.6$ K. Compared to $SmFeAsO_{0.8}F_{0.2}$ and $NdFeAsO_{0.8}F_{0.2}$,[42] superconducting $FeSe_{0.5}Te_{0.5}$ is much more isotropic, but quite comparable to the "122" class of Fe-based superconductors.[63,77,81] This suggests that the direct electronic coupling of the Fe_2Se_2 layers in the 11 system is similar to the one through the intervening Ae layers in the "122" class of superconductors but more effective than the coupling through the LnO layers in the "1111" Fe-based systems. While γ_λ increases with decreasing temperature, the anisotropy parameter of the upper critical field $\gamma_{H_{c2}}$ determined by resistivity measurements decreases.[33,38] The observed behavior is similar to that of the two-gap superconductor MgB_2 and other Fe-based superconductors and supports a two-gap scenario also in $FeSe_{0.5}Te_{0.5}$.[42] Note, however, that for MgB_2 the slopes of $\gamma_\lambda(T)$ and $\gamma_{H_{c2}}(T)$ have reversed signs[64,65] as compared to the Fe-based superconductors. The reason for this difference is still unclear. Furthermore, the value of $\lambda_{ab}^{-2}(0)$ for $FeSe_{0.5}Te_{0.5}$ extracted from μSR data as well as the values of $\lambda_{ab}^{-2}(0)$ obtained for various Fe-based superconductors fall on the Uemura plot[55] within the limits of hole-doped and electron-doped cuprates.[56] This suggests that the pairing mechanism in the Fe-based superconductors is unconventional, as is also the case for the cuprates.

Concluding, $FeSe_{0.5}Te_{0.5}$ shows evidence for two-gap superconductivity, which is reflected in the temperature dependence of λ^{-2} and by the existence of two distinct anisotropy parameters $\gamma_\lambda(T)$ and $\gamma_{H_{c2}}(T)$. The two-gap scenario is observed for most Fe-based superconductors, suggesting that this behavior is generic for layered high-temperature superconductors: it is strongly supported by various experiments for Fe-based superconductors (Ref. 80 and references therein), it is well established for MgB_2,[65,66] and there is firm evidence for two-gap superconductivity also in the cuprates.[82–85] However, it remains to be seen whether superconductivity in these classes of high-temperature superconductors has the same or a similar origin.

ACKNOWLEDGMENTS

The μSR experiments were performed at the Swiss Muon Source, Paul Scherrer Institut, Villigen, Switzerland. This work was partially supported by the Swiss National Science Foundation, the EU Project CoMePhS, the Polish Ministry of Science and Higher Education under the research project No. N N202 4132 33, and by the NCCR Program MaNEP.

*markus.bendele@physik.uzh.ch

[1] Y. Kamihara, T. Watanabe, M. Hirano, and H. Hosono, J. Am. Chem. Soc. **130**, 3296 (2008).
[2] X. H. Chen, T. Wu, G. Wu, R. H. Liu, H. Chen, and D. F. Fang, Nature (London) **453**, 761 (2008).
[3] G. F. Chen, Z. Li, D. Wu, G. Li, W. Z. Hu, J. Dong, P. Zheng, J. L. Luo, and N. L. Wang, Phys. Rev. Lett. **100**, 247002 (2008).
[4] Z.-A. Ren, J. Yang, W. Lu, W. Yi, X.-L. Shen, Z.-C. Li, G.-C. Che, X.-L. Dong, L.-L. Sun, F. Zhou, and Z.-X. Zhao, EPL **82**, 57002 (2008).
[5] Z. A. Ren, J. Yang, W. Lu, W. Yi, G. C. Che, X. L. Dong, L. L. Sun, and Z. X. Zhao, Mater. Res. Innovations **12**, 105 (2008).
[6] P. Cheng, L. Fang, H. Yang, X. Y. Zhu, G. Mu, H. Q. Luo, Z. S. Wang, and H. H. Wen, Sci. China, Ser. G **51**, 719 (2008).
[7] M. Rotter, M. Tegel, and D. Johrendt, Phys. Rev. Lett. **101**, 107006 (2008).
[8] X. C. Wang, Q. Q. Liu, Y. X. Lv, W. B. Gao, L. X. Yang, R. C. Yu, F. Y. Li, and C. Q. Jin, Solid State Commun. **148**, 538 (2008).
[9] F. C. Hsu, J. Y. Luo, K.-W. Yeh, T.-K. Chen, T.-W. Huang, P.-M. Wu, Y.-C. Lee, Y.-L. Huang, Y.-Y. Chu, D.-C. Yan, and M.-K. Wu, Proc. Natl. Acad. Sci. U.S.A. **105**, 14262 (2008).
[10] A. Subedi, L. Zhang, D. J. Singh, and M. H. Du, Phys. Rev. B **78**, 134514 (2008).
[11] H. Ogino, Y. Matsumura, Y. Katsura, K. Ushiyama, S. Horii, K. Kishio, and J. Shimoyama, Supercond. Sci. Technol. **22**, 075008 (2009).
[12] X. Zhu, F. Han, G. Mu, B. Zeng, P. Cheng, B. Shen, and H.-H. Wen, Phys. Rev. B **79**, 024516 (2009).
[13] H. Luetkens, H.-H. Klauss, M. Kraken, F. J. Litterst, T. Dellmann, R. Klingeler, C. Hess, R. Khasanov, A. Amato, C. Baines, M. Kosmala, O. J. Schumann, M. Braden, J. Hamann-Borrero, N. Leps, A. Kondrat, G. Behr, J. Werner, and B. Büchner, Nature Mater. **8**, 305 (2009).
[14] A. J. Drew, Ch. Niedermayer, P. J. Baker, F. L. Pratt, S. J. Blundell, T. Lancaster, R. H. Liu, G. Wu, X. H. Chen, I. Watanabe, V. K. Malik, A. Dubroka, M. Rössle, K. W. Kim, C. Baines, and C. Bernhard, Nature Mater. **8**, 310 (2009).
[15] Y. Mizuguchi, F. Tomioka, S. Tsuda, T. Yamaguchi, and Y. Takano, Appl. Phys. Lett. **93**, 152505 (2008).
[16] R. Khasanov, M. Bendele, A. Amato, P. Babkevich, A. T. Boothroyd, A. Cervellino, K. Conder, S. N. Gvasaliya, H. Keller, H.-H. Klauss, H. Luetkens, V. Pomjakushin, E. Pomjakushina, and B. Roessli, Phys. Rev. B **80**, 140511(R) (2009).
[17] J. Karpinski, N. D. Zhigadlo, S. Katrych, Z. Bukowski, P. Moll, S. Weyeneth, H. Keller, R. Puzniak, M. Tortello, D. Daghero, R. Gonnelli, I. Maggio-Aprile, Y. Fasano, Ø. Fischer, K. Rogacki, and B. Batlogg, Physica C **469**, 370 (2009).
[18] I. I. Mazin and J. Schmalian, Physica C **469**, 614 (2009).
[19] A. Amato, R. Khasanov, H. Luetkens, and H.-H. Klauss, Physica C **469**, 606 (2009).
[20] S. Graser, T. A. Maier, P. J. Hirschfeld, and D. J. Scalapino, New J. Phys. **11**, 025016 (2009).
[21] S. Margadonna, Y. Takabayashi, Y. Ohishi, Y. Mizuguchi, Y. Takano, T. Kagayama, T. Nakagawa, M. Takata, and K. Prassides, Phys. Rev. B **80**, 064506 (2009).
[22] B. C. Sales, A. S. Sefat, M. A. McGuire, R. Y. Jin, D. Mandrus, and Y. Mozharivskyj, Phys. Rev. B **79**, 094521 (2009).
[23] P. K. Biswas, G. Balakrishnan, D. M. Paul, C. V. Tomy, M. R. Lees, and A. D. Hillier, Phys. Rev. B **81**, 092510 (2010).
[24] P. Fischer, G. Frey, M. Koch, M. Könnecke, V. Pomjakushin, J. Schefer, R. Thut, N. Schlumpf, R. Bürge, U. Greuter, S. Bondt, and E. Berruyer, Physica B **276-278**, 146 (2000).
[25] J. Rodríguez-Carvajal, Physica B **192**, 55 (1993).
[26] S. Li, C. de la Cruz, Q. Huang, Y. Chen, J. W. Lynn, J. Hu, Y. L. Huang, F.-C. Hsu, K. W. Yeh, M. K. Wu, and P. Dai, Phys. Rev. B **79**, 054503 (2009).
[27] W. Bao, Y. Qiu, Q. Huang, M. A. Green, P. Zajdel, M. R. Fitzsimmons, M. Zhernenkov, S. Chang, Minghu Fang,B. Qian, E. K. Vehstedt, J. Yang, H. M. Pham, L. Spinu, and Z. Q. Mao, Phys. Rev. Lett. **102**, 247001 (2009).
[28] E. Pomjakushina, K. Conder, V. Pomjakushin, M. Bendele, and R. Khasanov, Phys. Rev. B **80**, 024517 (2009).
[29] T. Kamimura, J. Phys. Soc. Jpn. **43**, 1594 (1977).
[30] C. P. Bean, Phys. Rev. Lett. **8**, 250 (1962).
[31] C. P. Bean, Rev. Mod. Phys. **36**, 31 (1964).
[32] Y. Yeshurun and A. P. Malozemoff, Phys. Rev. Lett. **60**, 2202 (1988).
[33] M. H. Fang, J. H. Yang, F. F. Balakirev, Y. Kohama, J. Singleton, B. Qian, Z. Q. Mao, H. D. Wang, and H. Q. Yuan, Phys. Rev. B **81**, 020509 (2010).
[34] J. R. Clem, in Proceeding of the 13th Conference on Low Temperature Physics (LT 13), edited by K. D. Timmerhaus, W. J. O'Sullivan, and E. F. Hammel (Plenum, New York, 1974), Vol. 3, p. 102.
[35] L. Burlachkov, Phys. Rev. B **47**, 8056 (1993).
[36] L. Burlachkov, V. B. Geshkenbein, A. E. Koshelev, A. I. Larkin, and V. M. Vinokur, Phys. Rev. B **50**, 16770 (1994).
[37] M. Tinkham, *Introduction to Superconductivity* (Krieger, Malabar, Florida, 1975).
[38] H. Lei, R. Hu, E. S. Choi, J. B. Warren, and C. Petrovic, Phys. Rev. B **81**, 094518 (2010).
[39] V. G. Kogan, Phys. Rev. B **24**, 1572 (1981).
[40] V. G. Kogan, M. M. Fang, and S. Mitra, Phys. Rev. B **38**, 11958 (1988).
[41] S. Weyeneth, R. Puzniak, U. Mosele, N. D. Zhigadlo, S. Katrych, Z. Bukowski, J. Karpinski, S. Kohout, J. Roos, and H. Keller, J. Supercond. Novel Magn. **22**, 325 (2009).
[42] S. Weyeneth, R. Puzniak, N. D. Zhigadlo, S. Katrych, Z. Bukowski, J. Karpinski, and H. Keller, J. Supercond. Novel Magn. **22**, 347 (2009).
[43] L. Balicas, A. Gurevich, Y. J. Jo, J. Jaroszynski, D. C. Larbalestier, R. H. Liu, H. Chen, X. H. Chen, N. D. Zhigadlo, S. Katrych, Z. Bukowski, and J. Karpinski, arXiv:0809.4223 (unpublished).
[44] P. Zimmermann, H. Keller, S. L. Lee, I. M. Savić, M. Warden, D.

Zech, R. Cubitt, E. M. Forgan, E. Kaldis, J. Karpinski, and C. Krüger, Phys. Rev. B **52**, 541 (1995).
[45] R. Khasanov, K. Conder, E. Pomjakushina, A. Amato, C. Baines, Z. Bukowski, J. Karpinski, S. Katrych, H.-H. Klauss, H. Luetkens, A. Shengelaya, and N. D. Zhigadlo, Phys. Rev. B **78**, 220510 (2008).
[46] T. M. Riseman, J. H. Brewer, K. H. Chow, W. N. Hardy, R. F. Kiefl, S. R. Kreitzman, R. Liang, W. A. MacFarlane, P. Mendels, G. D. Morris, J. Rammer, J. W. Schneider, C. Niedermayer, and S. L. Lee, Phys. Rev. B **52**, 10569 (1995).
[47] A. Maisuradze, R. Khasanov, A. Shengelaya, and H. Keller, J. Phys.: Condens. Matter **21**, 075701 (2009).
[48] H. Schilling, M. Camani, F. N. Gygax, W. Rüegg, and A. Schenck, J. Phys. F: Met. Phys. **12**, 875 (1982).
[49] A. Yaouanc, P. Dalmas de Réotier, and E. H. Brandt, Phys. Rev. B **55**, 11107 (1997).
[50] A. Carrington and F. Manzano, Physica C **385**, 205 (2003).
[51] A. B. Vorontsov, M. G. Vavilov, and A. V. Chubukov, Phys. Rev. B **79**, 140507(R) (2009).
[52] J. Yang, M. Matsui, M. Kawa, H. Ohta, C. Michioka, C. Dong, H. Wang, H. Yuan, M. Fang, and K. Yoshimura, arXiv:0911.4758 (unpublished).
[53] T. Kato, Y. Mizuguchi, H. Nakamura, T. Machida, H. Sakata, and Y. Takano, Phys. Rev. B **80**, 180507(R) (2009).
[54] H. Kim, C. Martin, R. Gordon, M. Tanatar, J. Hu, B. Qian, Z. Mao, R. Hu, C. Petrovic, N. Salovich, R. Giannetta, and R. Prozorov, Phys. Rev. B **81**, 180503(R) (2010)..
[55] Y. J. Uemura, G. M. Luke, B. J. Sternlieb, J. H. Brewer, J. F. Carolan, W. N. Hardy, R. Kadono, J. R. Kempton, R. F. Kiefl, S. R. Kreitzman, P. Mulhern, T. M. Riseman, D. Ll, Williams, B. X. Yang, S. Uchida, H. Takagi, J. Gopalakrishnan, A. W. Sleight, M. A. Subramanian, C. L. Chien, M. Z. Cieplak, G. Xiao, V. Y. Lee, B. W. Statt, C. E. Stronach, W. J. Kossler, and X. H. Yu, Phys. Rev. Lett. **62**, 2317 (1989).
[56] A. Shengelaya, R. Khasanov, D. G. Eshchenko, D. Di Castro, I. M. Savić, M. S. Park, K. H. Kim, S.-I. Lee, K. A. Müller, and H. Keller, Phys. Rev. Lett. **94**, 127001 (2005).
[57] H. Luetkens, H.-H. Klauss, R. Khasanov, A. Amato, R. Klingeler, I. Hellmann, N. Leps, A. Kondrat, C. Hess, A. Köhler, G. Behr, J. Werner, and B. Büchner, Phys. Rev. Lett. **101**, 097009 (2008).
[58] S. Takeshita and R. Kadono, New J. Phys. **11**, 035006 (2009).
[59] J. P. Carlo, Y. J. Uemura, T. Goko, G. J. MacDougall, J. A. Rodriguez, W. Yu, G. M. Luke, P. Dai, N. Shannon, S. Miyasaka, S. Suzuki, S. Tajima, G. F. Chen, W. Z. Hu, J. L. Luo, and N. L. Wang, Phys. Rev. Lett. **102**, 087001 (2009).
[60] R. Khasanov, H. Luetkens, A. Amato, H.-H. Klauss, Z.-A. Ren, J. Yang, W. Lu, and Z.-X. Zhao, Phys. Rev. B **78**, 092506 (2008).
[61] R. Khasanov, M. Bendele, A. Amato, K. Conder, H. Keller, H.-H. Klauss, H. Luetkens, and E. Pomjakushina, Phys. Rev. Lett. **104**, 087004 (2010).
[62] F. L. Pratt, P. J. Baker, S. J. Blundell, T. Lancaster, H. J. Lewtas, P. Adamson, M. J. Pitcher, D. R. Parker, and S. J. Clarke, Phys. Rev. B **79**, 052508 (2009).
[63] R. Khasanov, D. V. Evtushinsky, A. Amato, H.-H. Klauss, H. Luetkens, Ch. Niedermayer, B. Büchner, G. L. Sun, C. T. Lin, J. T. Park, D. S. Inosov, and V. Hinkov, Phys. Rev. Lett. **102**, 187005 (2009).
[64] J. D. Fletcher, A. Carrington, O. J. Taylor, S. M. Kazakov, and J. Karpinski, Phys. Rev. Lett. **95**, 097005 (2005).
[65] M. Angst, R. Puzniak, A. Wisniewski, J. Jun, S. M. Kazakov, J. Karpinski, J. Roos, and H. Keller, Phys. Rev. Lett. **88**, 167004 (2002).
[66] M. Angst and R. Puzniak, in *Focus on Superconductivity*, edited by B. P. Martines (Nova Science, New York, 2004), Vol. 1, pp. 1–49.
[67] R. S. Gonnelli, D. Daghero, M. Tortello, G. A. Ummarino, V. A. Stepanov, R. K. Kremer, J. S. Kim, N. D. Zhigadlo, and J. Karpinski, Physica C **469**, 512 (2009).
[68] P. Samuely, Z. Pribulová, P. Szabó, G. Pristáš, S. L. Bud'ko, and P. C. Canfield, Physica C **469**, 507 (2009).
[69] P. Szabó, Z. Pribulová, G. Pristáš, S. L. Bud'ko, P. C. Canfield, and P. Samuely, Phys. Rev. B **79**, 012503 (2009).
[70] G. Li, W. Z. Hu, J. Dong, Z. Li, P. Zheng, G. F. Chen, J. L. Luo, and N. L. Wang, Phys. Rev. Lett. **101**, 107004 (2008).
[71] G. Mu, H. Luo, Z. Wang, L. Shan, C. Ren, and H. H. Wen, Phys. Rev. B **79**, 174501 (2009).
[72] C. Ren, Z. S. Wang, H. Q. Luo, H. Yang, L. Shan, and H. H. Wen, Phys. Rev. Lett. **101**, 257006 (2008).
[73] F. Hunte, J. Jaroszynski, A. Gurevich, D. C. Larbalestier, R. Jin, A. S. Sefat, M. A. McGuire, B. C. Sales, D. K. Christen, and D. Mandrus, Nature (London) **453**, 903 (2008).
[74] S. Weyeneth, M. Bendele, R. Puzniak, F. Muranyi, A. Bussmann-Holder, N. D. Zhigadlo, S. Katrych, Z. Bukowski, J. Karpinski, A. Shengelaya, R. Khasanov, and H. Keller, arXiv:0911.5420 (unpublished).
[75] L. Malone, J. D. Fletcher, A. Serafin, A. Carrington, N. D. Zhigadlo, Z. Bukowski, S. Katrych, and J. Karpinski, Phys. Rev. B **79**, 140501(R) (2009).
[76] M. Hiraishi, R. Kadono, S. Takeshita, M. Miyazaki, A. Koda, H. Okabe, and J. Akimitsu, J. Phys. Soc. Jpn. **78**, 023710 (2009).
[77] R. Khasanov, A. Maisuradze, H. Maeter, A. Kwadrin, H. Luetkens, A. Amato, W. Schnelle, H. Rosner, A. Leithe-Jasper, and H.-H. Klauss, Phys. Rev. Lett. **103**, 067010 (2009).
[78] J. Nagamatsu, N. Nakagawa, T. Muranaka, Y. Zenitani, and J. Akimitsu, Nature (London) **410**, 63 (2001).
[79] R. S. Gonnelli, D. Daghero, G. A. Ummarino, V. A. Stepanov, J. Jun, S. M. Kazakov, and J. Karpinski, Phys. Rev. Lett. **89**, 247004 (2002).
[80] D. V. Evtushinsky, D. S. Inosov, V. B. Zabolotnyy, M. S. Viazovska, R. Khasanov, A. Amato, H.-H. Klauss, H. Luetkens, Ch. Niedermayer, G. L. Sun, V. Hinkov, C. T. Lin, A. Varykhalov, A. Koitzsch, M. Knupfer, B. Büchner, A. A. Kordyuk, and S. V. Borisenko, New J. Phys. **11**, 055069 (2009).
[81] Z. Bukowski, S. Weyeneth, R. Puzniak, P. Moll, S. Katrych, N. D. Zhigadlo, J. Karpinski, H. Keller, and B. Batlogg, Phys. Rev. B **79**, 104521 (2009).
[82] R. Khasanov, A. Shengelaya, A. Maisuradze, F. La Mattina, A. Bussmann-Holder, H. Keller, and K. A. Müller, Phys. Rev. Lett. **98**, 057007 (2007).
[83] A. Bussmann-Holder, R. Khasanov, A. Shengelaya, A. Maisuradze, F. La Mattina, H. Keller, and K. A. Müller, EPL **77**, 27002 (2007).
[84] R. Khasanov, A. Shengelaya, J. Karpinski, A. Bussmann-Holder, H. Keller, and K. A. Müller, J. Supercond. Novel Magn. **21**, 81 (2008).
[85] R. Khasanov, S. Strässle, D. Di Castro, T. Masui, S. Miyasaka, S. Tajima, A. Bussmann-Holder, and H. Keller, Phys. Rev. Lett. **99**, 237601 (2007).

5 Isotope effect

The first isotope studies were performed by Kamerlingh-Onnes in 1922 [145]. However, he had only the two natural lead isotopes with the isotope masses $M = 206$u and $M = 207.2$u to his hands. Within the measurement accuracy at that time no difference in the transition temperatures was found. Only almost 30 years later, after some progress in the nuclear physics area, it was possible to create isotopes with larger mass differences in sufficient amount. As a result of these achievements, both Maxwell [8] and Reynolds *et al.* [9] found independent from each other almost at the same time that T_c in mercury is an inverse function of M.
A few years after the first successful isotope experiments of Maxwell and Reynolds *et al.* [8, 9] the BCS-theory was developed [10, 11]. It is able to well explain the isotope effect. T_c in the weak coupling BCS theory is given by:

$$k_B T_c = 1.13 \hbar \omega_D \exp\left(-\frac{1}{N(0)V}\right) \tag{5.1}$$

Here, ω_D is the Debye frequency that is proportional to $M^{-1/2}$. The product $N(0)V$ is the electron-phonon coupling constant, where V is the electron-phonon interaction strength and $N(0)$ the electron density of states at the Fermi level that are both independent from the isotope mass M.
Since $T_c \sim \omega_D \sim M^{-1/2}$ the isotope exponent α can be easily deduced from Eq. (5.1):

$$\alpha = -\frac{\delta \ln T_c}{\delta \ln M} = -\frac{\delta T_c / T_c}{\delta M / M} = \frac{1}{2} \tag{5.2}$$

This relation is fulfilled for a series of conventional superconductors, such as Hg, Sn or In and directly demonstrates the influence of the electron-phonon interaction to the formation of the superconducting state. However, not all classical superconductors show an isotope exponent $\alpha = 0.5$. There are some exceptions that can be explained by the fact that the theory leading to Eq. (5.1) is based on a lot of simplifications, which, however, are valid for most of the conventional low temperature superconductors. By investigating V in Eq. (5.1) in more detail, it is possible to explain the deviations from the BCS value $\alpha = 0.5$. The coupling strength is basically the difference of the attracting electron-phonon interaction and the repulsing Coulomb interaction of the electrons. However, deviations from $\alpha = 0.5$ or even a full absence of the isotope effect cannot be taken as a prove that the electron-phonon coupling is not responsible for pairing.
Also in the newer high temperature superconductors, such as the fullerenes, MgB_2, or the cuprates, isotope effect studies were performed. In fact in all of them isotope effects were found: in the fullerenes $\alpha \simeq 0.3$ was obtained for substituting ^{12}C with ^{13}C which is in good agreement with the electron-phonon coupling by assuming that the intramolecular

oscillations of the C_{60} molecules dominate the pairing effect [146, 147]. In MgB_2 the isotope effect for both Mg and B was investigated. Exchanging the isotopes between ^{11}B and ^{10}B lead to an exponent of $\simeq 0.3$ [148, 149, 150, 151] whereas the variation of the Mg isotopes from ^{24}Mg to ^{26}Mg result only to $\alpha \simeq 0.02$ [149, 150]. These findings reveal that only the electron-phonon coupling of the Boron ions play a major role in the pairing.

In the cuprate superconductors the situation was found to be more complicated; they show an unconventional oxygen isotope effect on T_c. The substitution of ^{16}O to ^{18}O yields to an isotope exponent α that is small, but positive for the optimally doped compounds and increases upon decreasing the doping level. At the phase boundary it even exceeds the BCS value of 0.5 [152, 153, 154]. Interestingly, the values of the copper isotope exponents resulting from the exchange ^{63}Cu to ^{65}Cu are close to the oxygen isotope ones [155, 152, 153, 154]. If the doping is further decreased and the superconducting dome is left also the other thermodynamic quantities as the Néel temperature T_N and the spin glass temperature T_{sg} of the cuprate superconductors show an isotope effect of which the exponent tends to diverge at the phase boundaries [156]. These substantial isotope effects in the cuprate superconductors indicate that lattice effects play a relevant role in the occurrence of superconductivity in the cuprates.

5.1 Isotope effect in the Fe-based superconductors

After the discovery of the Fe-based superconductors immediately the question arouse, whether they also show an isotope effect. Until now only a few studies are available. Liu *et al.* [87] showed an iron isotope effect exponent $\alpha \simeq 0.34$ in $SmFeAsO_{0.85}F_{0.15}$ with $T_c \simeq 42\,K$ by replacing ^{56}Fe with the isotope ^{54}Fe. In contrast Shirage *et al.* [88] published a vanishing small effect in the same family, namely $SmFeAsO_{1-y}$ with a value of $\alpha \simeq -0.018$ by substituting the heavier ^{57}Fe with the lighter ^{54}Fe. However, this sample had a substantially larger T_c of $\simeq 54\,K$ close to optimal doping. Comparing the two isotope effect exponents one could argue that the situation is similar to the cuprate superconductors where the oxygen isotope effect is vanishingly small close to optimal doping, but gets larger with reduced doping [156].

The same groups studied the isotope effect in another system of the Fe-based superconductors, namely in $Ba_{0.6}K_{0.4}Fe_2As_2$. In this system, however, both groups studied samples with the same $T_c \simeq 37\,K$. Again they observed a substantially different isotope effect: The same group finding the positive value in Sm1111 sees again a positive one with a similar value of $\alpha \simeq 0.37$ [87]. This is in severe antithesis to the negative value $\alpha \simeq -0.18$ seen by the other group [89]. This discrepancy in experimental results rises serious questions, which are partly clarified in the following.

Shortly after these works we also found a positive Fe isotope effect on T_c in $FeSe_{1-x}$ with and isotope exponent $\alpha = 0.81(15)$ much larger than the BCS value 0.5 [90]. For this study a series of samples with a nominal composition of $FeSe_{0.98}$ were prepared by a solid state reaction described in Ref. [90]. The superconducting transition temperature of six $^{54}FeSe_{1-x}$ and seven $^{56}FeSe_{1-x}$ samples was investigated. Figure 5.1 shows a typical pair of magnetization curves for the two different Fe isotopes whereas the curve for the lighter ^{54}Fe

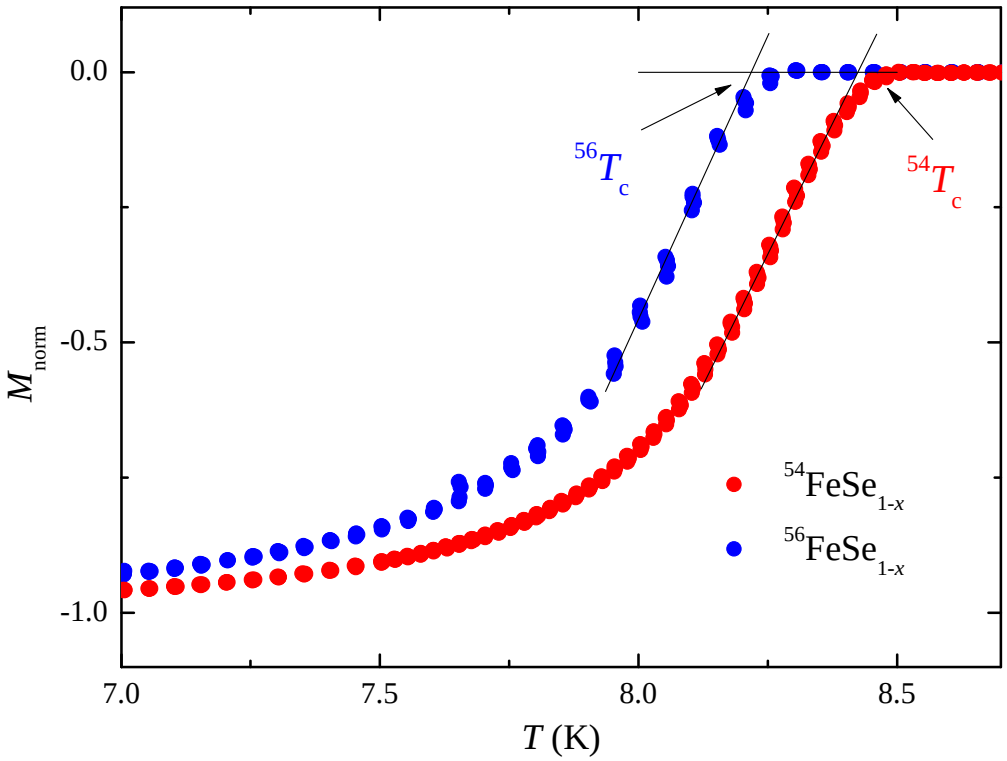

Figure 5.1: Normalized zero field cooled magnetization curves $M_{\mathrm{norm}} = [M(T) - M_{\mathrm{magn}}]/[M(2K) - M_{\mathrm{magn}}]$ for one pair of $^{54}FeSe_{1-x}$ and $^{56}FeSe_{1-x}$ samples. The transition temperature T_c is determined as the intersection of the linearly extrapolated $M_{\mathrm{norm}}(T)$ curve in the vicinity of T_c with the $M = 0$ line. After [90].

is shifted almost parallel to higher temperatures, indicating that T_c of $^{54}FeSe_{1-x}$ is higher than that of $^{56}FeSe_{1-x}$. The superconducting transition temperatures for all the samples investigated are in two specific regions for the two different Fe isotopes in Fig. 5.2 with the corresponding mean values of $\overline{T_c}(^{54}FeSe_{1-x}) = 8.43(3)$ K and $\overline{T_c}(^{56}FeSe_{1-x}) = 8.21(4)$ K. This leads to the unusual large Fe isotope effect exponent of $\alpha = 0.81(15)$ mentioned above.

Neutron powder diffraction on a pair of $^{54}Fe/^{56}Fe$ isotope substituted samples revealed that the lattice parameters are slightly different. Whereas the $^{54}FeSe_{1-x}$ has a slightly larger $a(b)$-axis, the c-axis is smaller compared to $^{56}FeSe_{1-x}$. This results in a shift of the chalcogenide height h above the Fe-plane. It has been shown empirically that only minor changes of the crystal structure, namely the anion height above the Fe-plane may change T_c substantially [54, 90]. An estimation of the change of T_c due to the isotope exchange was done with the help of pressure studies on $FeSe_{1-x}$. The decrease of the Se height, caused by a compression of the Fe_4Se pyramide, leads to an increase in T_c by $\delta T_c^h/(\delta h/h) \simeq 3.4\,\%/\mathrm{K}$ [54, 68]. In addition, an increase in the Se(Te)-Fe-Se(Te) angle β in the $Fe_ySe_xTe_{1-x}$ family (in the superconducting regime of the phase diagram, $x \lesssim 0.5$) results in a decrease in T_c by $\delta T_c^\beta/(\delta\beta/\beta) \simeq 2.9\,\%/\mathrm{K}$ [90]. From these observations a shift in $\delta T_c \approx 0.1$ K due to the structural effects is approximated. Thus $\approx 50\,\%$ of the increase of T_c in the lighter $^{54}FeSe_{1-x}$ compared to $^{56}FeSe_{1-x}$

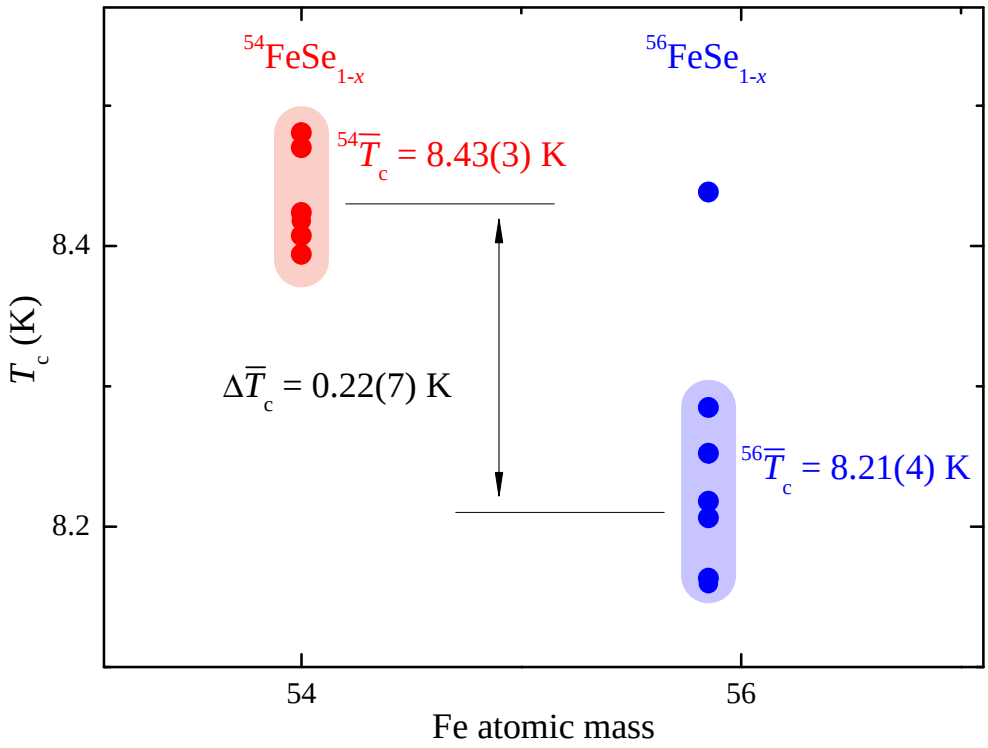

Figure 5.2: The superconducting transition temperature T_c as a function of Fe atomic mass for the $^{54}FeSe_{1-x}/^{56}FeSe_{1-x}$ samples studied. The T_cs fall into the regions marked by the colored stripes with the corresponding mean values $^{54}\overline{T_c} = 8.43(3)$ K and $^{56}\overline{T_c} = 8.21(4)$ K. After [90].

are due to the change of the anion height above the Fe-plane [90]. Taking this additional "structural" isotope effect into account, one may write the total isotope exponent as a sum of two contributions:

$$\alpha_{Fe} = \alpha_{Fe}^{int} + \alpha_{Fe}^{str}. \tag{5.3}$$

Here $\alpha_{Fe}^{int} = -(\delta T_c/T_c)/(\delta M/M)$ is the "intrinsic" component of the isotope effect exponent and $\alpha_{Fe}^{str} = -(\delta T_c/T_c)/(\delta h/h)$ is the contribution related to the change of the lattice parameters. This results in an "intrinsic" iron isotope exponent in $^{54/56}FeSe_{1-x}$ with a value of $\alpha_{Fe}^{int} \approx 0.4$ [90].

The use of the empirical T_c vs. h relation established in Ref. [54] allows to determine the structural related isotope effect. However, the absence of precise structural data complicates the analysis for the studies presented in Refs. [87, 88, 89]. But the intrinsic proportionality between h and the c-axis lattice parameter allows to determine the sign of the structural shift of T_c due to the isotope exchange [68, 99, 157]. Liu *et al.* [87] reported a zero effect on the lattice parameters within experimental accuracy for $Ba_{0.6}K_{0.4}Fe_2As_2$ and in $SmFeAsO_{0.85}F_{0.15}$. Thus $\alpha_{Fe}^{str} \sim 0$ for both studies. This leads to an "intrinsic" α_{Fe}^{int} in the direction of $0.35-0.4$, comparable to $\alpha_{Fe}^{int} \approx 0.4$ in $FeSe_{1-x}$, see Fig. 5.3. In contrary to Liu *et al.* [87], Shirage *et al.* [89] reported a negative isotope effect exponent α_{Fe} in the nominally identical compound $Ba_{0.6}K_{0.4}Fe_2As_2$. In this case, however, the c-axis lattice parameters differ from each other

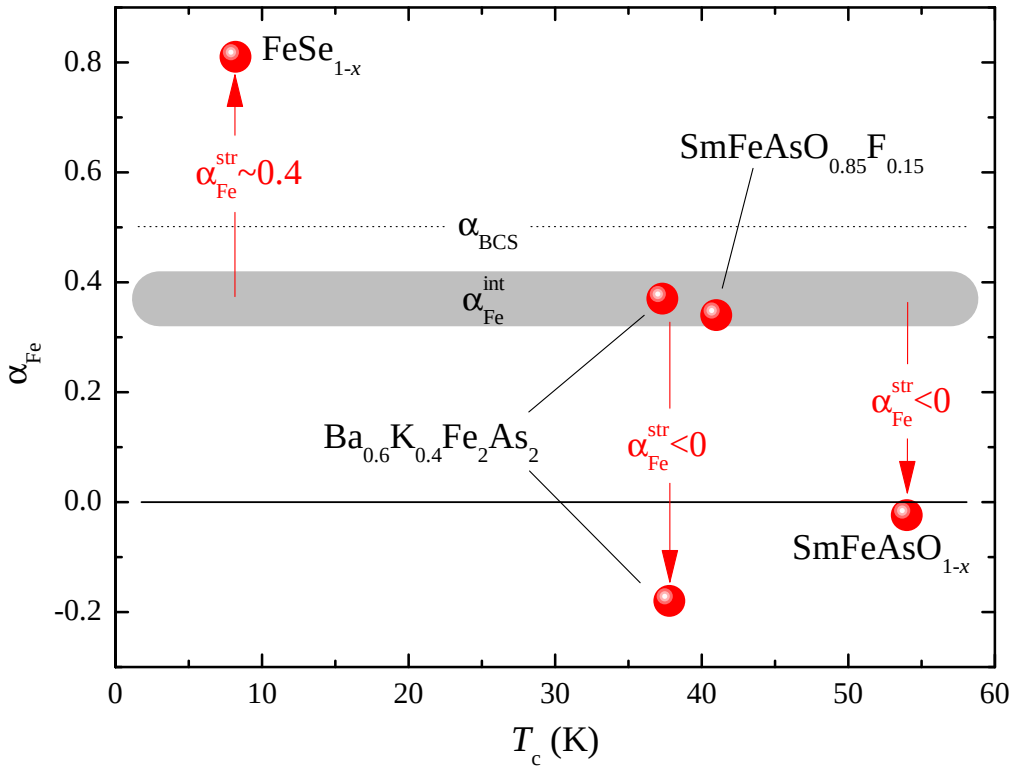

Figure 5.3: Fe isotope effect exponent α_{Fe} as a function of the superconducting transition temperature T_{c} for the samples considered in the present study: $FeSe_{1-x}$ [90], $Ba_{0.6}K_{0.4}Fe_2As_2$ and $SmFeAsO_{0.85}F_{0.15}$ [87], $Ba_{0.6}K_{0.4}Fe_2As_2$ [88], and $SmFeAsO_{1-x}$ [89]. Arrows indicate the direction of the shift from the "intrinsic" Fe isotope effect exponent $\alpha_{\mathrm{Fe}}^{\mathrm{int}} \sim 0.35 - 0.4$ caused by the structural effects. $\alpha_{\mathrm{BCS}} \equiv 0.5$ is the BCS value for electron-phonon mediated superconductivity. After [91].

after the isotope exchange. Consequently, the negative effect stems from the sum of the "structural" and the "intrinsic" effect ($-0.18(\alpha_{\mathrm{Fe}}) = 0.35(\alpha_{\mathrm{Fe}}^{\mathrm{int}}) - 0.53(\alpha_{\mathrm{Fe}}^{\mathrm{str}})$, see Eq. (5.3)). In the case of $SmFeAsO_{1-x}$ [88], however, there are no isotope studies available with the same doping level. But by comparing the c-axis lattice parameters of the isotope exchanged samples, it is possible to estimate the sign of $\alpha_{\mathrm{Fe}}^{\mathrm{str}}$. Based on the other Fe isotope studies [87, 90, 91], also in this case an "intrinsic" Fe isotope effect exponent of $\alpha_{\mathrm{Fe}}^{\mathrm{int}} \sim 0.35 - 0.4$ can be proposed, see Fig. 5.3 [91].

Recently Bussmann-Holder *et al.* [158] investigated a multiple-gap scenario of superconductivity in the Fe-based HTC superconductors to find possible sources of the isotope effect on T_{c}. Electron-phonon mediated superconductivity within the dominant gap channel predicts a T_{c} independent isotope effect with a value of α slightly smaller than 0.5. This is in agreement with the observed $\alpha_{\mathrm{Fe}}^{\mathrm{int}} \sim 0.35 - 0.4$ for superconductors belonging to different families of the Fe-based HTC superconductors after the correction for the structural effect and with T_{c}'s ranging from 8 K to 54 K (see Fig. 5.3).

5.2 Related publications to Chapter 5

5.2.1 Paper I: Iron isotope effect on the superconducting transition temperature and the crystal structure of $FeSe_{1-x}$

This work is published in:

R. Khasanov, M. Bendele, K. Conder, H. Keller, E. Pomjakushina, and V. Pomjakushin, *Iron isotope effect on the superconducting transition temperature and the crystal structure of* $FeSe_{1-x}$, New J. Phys., **12**, 073024 (2010).

Abstract:

The Fe isotope effect (Fe-IE) on the transition temperature T_c and the crystal structure was studied in the Fe chalcogenide superconductor $FeSe_{1-x}$ by means of magnetization and neutron powder diffraction (NPD). The substitution of natural Fe (containing $\simeq 92\%$ of ^{56}Fe) by its lighter ^{54}Fe isotope leads to a shift in T_c of 0.22(5) K corresponding to an Fe-IE exponent of $\alpha_{Fe} = 0.81(15)$. Simultaneously, a small structural change with isotope substitution is observed by NPD, which may contribute to the total Fe isotope shift of T_c.

URL: http://iopscience.iop.org/1367-2630/12/7/073024
DOI: 10.1088/1367-2630/12/7/073024
PACS: 74.62.Dh, 74.25.Ha, 74.62.Bf, 74.72.-h, 75.60.Ej

New Journal of Physics
The open-access journal for physics

Iron isotope effect on the superconducting transition temperature and the crystal structure of $FeSe_{1-x}$

R Khasanov[1,5], M Bendele[1,2], K Conder[3], H Keller[2], E Pomjakushina[2] and V Pomjakushin[4]

[1] Laboratory for Muon Spin Spectroscopy, Paul Scherrer Institute, CH-5232 Villigen PSI, Switzerland
[2] Physik-Institut der Universität Zürich, Winterthurerstrasse 190, CH-8057 Zürich, Switzerland
[3] Laboratory for Developments and Methods, Paul Scherrer Institute, CH-5232 Villigen PSI, Switzerland
[4] Laboratory for Neutron Scattering, ETH Zürich and PSI, CH-5232 Villigen PSI, Switzerland
E-mail: rustem.khasanov@psi.ch

New Journal of Physics **12** (2010) 073024 (8pp)
Received 10 May 2010
Published 22 July 2010
Online at http://www.njp.org/
doi:10.1088/1367-2630/12/7/073024

Abstract. The Fe isotope effect (Fe-IE) on the transition temperature T_c and the crystal structure was studied in the Fe chalcogenide superconductor $FeSe_{1-x}$ by means of magnetization and neutron powder diffraction (NPD). The substitution of natural Fe (containing $\simeq 92\%$ of ^{56}Fe) by its lighter ^{54}Fe isotope leads to a shift in T_c of 0.22(5) K corresponding to an Fe-IE exponent of $\alpha_{Fe} = 0.81(15)$. Simultaneously, a small structural change with isotope substitution is observed by NPD, which may contribute to the total Fe isotope shift of T_c.

Historically, the isotope effect played a crucial role in elucidating the origin of the pairing interaction leading to the occurrence of superconductivity. The discovery of the isotope effect on the superconducting transition temperature T_c in Hg [1] in 1950 provided the key experimental evidence for phonon-mediated pairing as formulated theoretically by Bardeen–Cooper–Schrieffer (BCS) theory subsequently. The observation of unusually high T_cs in the newly discovered Fe-based superconductors immediately raised the question regarding the pairing glue and initiated isotope effect studies. Currently, we are aware of two papers on isotope experiments with, however, contradicting results. Liu *et al* [2] showed that in

[5] Author to whom any correspondence should be addressed.

$SmFeAsO_{0.85}F_{0.15}$ and $Ba_{0.6}K_{0.4}Fe_2As_2$ the Fe isotope effect (Fe-IE) exponent defined as [3]

$$\alpha_{Fe} = -d \ln T_c / d \ln M_{Fe} = -(\Delta T_c / T_c)/(\Delta M_{Fe}/M_{Fe}) \quad (1)$$

reaches values of $\alpha_{Fe} \simeq 0.35$ (M_{Fe} is the Fe atomic mass), while Shirage *et al* [4] found a negative Fe-IE exponent $\alpha_{Fe} \simeq -0.18$ in $Ba_{1-x}K_xFe_2As_2$. Note that the only difference between the $Ba_{1-x}K_xFe_2As_2$ samples studied in [2, 4] was the preparation procedure (low-pressure synthesis in [2] versus high-pressure synthesis in [4]), while the potassium doping ($x \simeq 0.4$) as well as the T_cs for the samples containing natural Fe ($T_c \simeq 37.3$ K in [2] versus $T_c \simeq 37.8$ K in [4]) were almost the same.

In this paper, we study the Fe-IE on T_c and on the structural parameters (such as the lattice parameters a, b and c, the lattice volume V and the distance between the Se atom and Fe plane (Se height) h_{Se}) for another representative of the Fe-based high-temperature superconductors (HTS), namely $FeSe_{1-x}$ [5]–[11]. The substitution of natural Fe (containing $\simeq 92\%$ of ^{56}Fe) by its lighter ^{54}Fe isotope leads to a shift in T_c of 0.22(5) K corresponding to an Fe-IE exponent of $\alpha_{Fe} = 0.81(15)$.

The $^{54}FeSe_{1-x}/^{56}FeSe_{1-x}$ samples (hereafter we denote natural Fe containing $\simeq 92\%$ of ^{56}Fe isotope as ^{56}Fe) with the nominal composition $FeSe_{0.98}$ were prepared by a solid state reaction made in two steps. Pieces of Fe (natural Fe: 99.97% minimum purity, average atomic mass $M_{Fe} = 55.85$ g mol^{-1}, or ^{54}Fe: 99.99% purity, 99.84% isotope enriched, $M_{^{54}Fe} = 54.0$ g mol^{-1}) and Se (99.999% purity) were first sealed in double-walled quartz ampules, heated up to 1075 °C, annealed for 72 h at this temperature and 48 h at 420 °C, and then cooled down to room temperature at a rate of 100 °C h^{-1}. As a next step, the samples, taken out of the ampules, were powderized, pressed into pellets, sealed into new ampules and annealed first at 700 °C for 48 h and then at 400 °C for 36 h, followed by cooling to room temperature at a rate of 200 °C h^{-1}. Due to the extreme sensitivity of $FeSe_{1-x}$ to oxygen [7, 8], all the intermediate steps (grinding and pelletizing), as well as the preparation of the samples for the neutron powder diffraction (NPD) and magnetization experiments, were performed in a glove box in a He atmosphere.

The Fe-IE on the structural properties was studied by NPD experiments by using the high-resolution powder diffractometer HRPT (Paul Scherrer Institute, Switzerland) [12]. The experiments were carried out at a wavelength $\lambda = 1.494$ Å. The $^{54}FeSe_{1-x}/^{56}FeSe_{1-x}$ samples, placed into vanadium containers, were mounted into a He-4 cryostat in order to reach temperatures between 5 and 250 K. High statistics data were taken at 250 and 5 K. Data at $10 \leqslant T \leqslant 240$ K were collected with intermediate statistics.

Figure 1 shows the NPD spectra taken at $T = 250$ K. The differences in peak intensities, clearly visible at small θ, are caused by the different values of the coherent neutron scattering length (b_{coh}) of natural Fe and that of the ^{54}Fe isotope. The refinement of the crystal structure was performed by using the FULLPROF program [13] with $b_{coh}^{Fe} = 9.45 \times 10^{-15}$ m, $b_{coh}^{^{54}Fe} = 4.2 \times 10^{-15}$ m and $b_{coh}^{Se} = 7.97 \times 10^{-15}$ m [15]. The refined structural parameters at $T = 250$ and 5 K are summarized in table 1. The amount of impurity phases and the Se content $(1 - x)$, determined for the data sets taken at $T = 250$ K, were kept fixed during the refinement of the NPD spectra at lower temperatures. The mass fractions of impurity phases, the hexagonal FeSe ($P6_3/mmc$) and Fe ($Im3m$) [14], were found to be 0.50(10)%, 0.31(4)% and 1.13(18)%, 1.06(7)% for $^{54}FeSe_{1-x}$ and $^{56}FeSe_{1-x}$, respectively.

Figure 2 shows the temperature dependence of the lattice parameters a, b and c, the lattice volume V and the Se height h_{Se} of a representative $^{54}FeSe_{1-x}$ and a representative $^{56}FeSe_{1-x}$

IOP Institute of Physics DEUTSCHE PHYSIKALISCHE GESELLSCHAFT

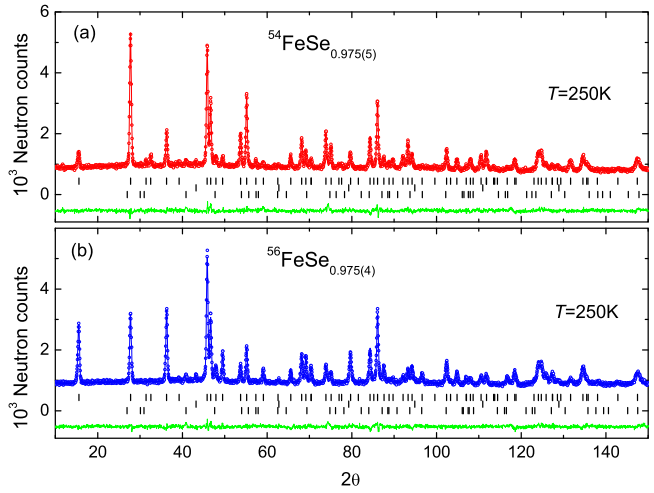

Figure 1. The Rietveld refinement pattern and difference plot of NPD data for $^{54}FeSe_{1-x}$ (panel a) and $^{56}FeSe_{1-x}$ (panel b) at $T = 250$ K. The rows of ticks show the Bragg-peak positions for the main phase FeSe ($P4nmm$) and two impurity phases: Fe ($Im3m$) and hexagonal FeSe ($P6_3/mmc$). The main tetragonal phase corresponds to 0.975(5) and 0.975(4) Se occupancy for $^{54}FeSe_{1-x}$ and $^{56}FeSe_{1-x}$, respectively.

sample (see figure 3). From figure 2(a), it is obvious that at $T_s \simeq 100$ K a transition from a tetragonal to an orthorhombic structure takes place, analogous to that reported in [7, 9, 16]. The Fe-IE on the structural transition temperature T_s could be estimated from the shift of the interception point of the linear fits to $a(T)$ and $b(T)$ in the vicinity of T_s, as denoted by the arrows in the inset of figure 2(a), which was found to be $\Delta T_s = 0.2(2.5)$ K. Within the whole temperature range ($5\,\text{K} \leqslant T \leqslant 250\,\text{K}$), the lattice constants a and b are slightly larger for $^{54}FeSe_{1-x}$ than those for $^{56}FeSe_{1-x}$ (see figure 2(a)). This is in contrast to the lattice parameter c, which within the same range is marginally smaller for $^{54}FeSe_{1-x}$ than for $^{56}FeSe_{1-x}$ (figure 2(b)). The lattice volume remains, however, unchanged. Consequently, substitution of ^{56}Fe by ^{54}Fe leads to a small but detectable *enhancement* of the lattice along the crystallographic a and b directions and a *compression* of it along the c-axis, resulting in a change to the shape of the Fe_4Se pyramid, which is known to influence T_c in Fe-based HTS [17]–[19]. This is shown in figure 2(c), where below 100 K the Se atom is located closer to the Fe plane in $^{54}FeSe_{1-x}$ than in $^{56}FeSe_{1-x}$. The corresponding change to the Fe_4Se pyramid is shown schematically in the inset of figure 2(c). It is important to note that the observed Fe-IEs on the lattice parameters are intrinsic and not just a consequence of slightly different samples. As shown in [7], various samples of $^{56}FeSe_{1-x}$ with $1 - x \simeq 0.98$ and $T_c \simeq 8.2$ K indeed exhibit the same lattice parameters within experimental error.

The Fe-IE on the transition temperature T_c was studied by means of magnetization experiments. Measurements were performed by using a SQUID magnetometer (Quantum Design MPMS-7) in a field of $\mu_0 H = 0.1$ mT for temperatures ranging from 2 to 20 K. In order to avoid artifacts and systematic errors in the determination of the isotope shift of T_c, it is

Table 1. Structural parameters of $^{54}FeSe_{1-x}$ and $^{56}FeSe_{1-x}$ at $T = 250$ and 5 K. Space group $P4/nmm$ (no. 129), origin choice 2: Fe in ($2b$) position (1/4, 3/4, 1/2) and Se in ($2c$) position (1/4, 1/4, z). Space group $Cmma$ (no. 67): Fe in ($4b$) position (1/4, 0, 1/2), Se in ($4g$) position (0, 3/4, z). The atomic displacement parameters (B) for Fe and Se were constrained to be the same. The Bragg R factor is given for the main phase; the other reliability factors are given for the whole refinement.

	$T = 250$ K		$T = 5$ K	
	$^{54}FeSe_{1-x}$	$^{56}FeSe_{1-x}$	$^{54}FeSe_{1-x}$	$^{56}FeSe_{1-x}$
Space group	$P4/nmm$		$Cmma$	
Se content	0.975(5)	0.975(4)	Fixed to 0.975	
a(Å)	3.770 36(3)	3.769 88(5)	5.335 23(10)	5.334 26(10)
b(Å)			5.309 84(10)	5.309 33(10)
c(Å)	5.516 19(9)	5.516 37(9)	5.486 83(9)	5.487 87(9)
Volume (Å^3)	156.883(3)	156.797(3)	155.438(5)	155.424(5)
z−Se	0.2319(2)	0.2326(0.3)	0.2321(2)	0.2322(3)
B(Å^2)	1.02(2)	0.93(2)	0.44(2)	0.36(2)
R_{Bragg}	3.11	2.93	4.13	3.63
R_{wp}	3.93	3.72	5.16	4.62
R_{exp}	3.13	3.05	4.73	4.03
χ^2	1.58	1.49	1.19	1.32

important to perform a *statistical* study: i.e. to investigate the series of $^{54}FeSe_{1-x}/^{56}FeSe_{1-x}$ samples synthesized in exactly the same way (the same thermal history and the same amount of Se in the initial composition). The magnetization experiments were conducted for six $^{54}FeSe_{1-x}$ and seven $^{56}FeSe_{1-x}$ samples, respectively. The inset in figure 3 shows an example of zero-field cooled (ZFC) magnetization curves for a pair of $^{54}FeSe_{1-x}/^{56}FeSe_{1-x}$ samples (M_{norm} was obtained after subtracting the small constant paramagnetic offset M_{magn} measured at $T > T_c$ and further normalization of the obtained curve to the value at $T = 2$ K as $M_{norm} = [M(T) - M_{magn}]/[M(2K) + M_{magn}]$, see also figure 1 in [7] for details). The amount of magnetic impurities responsible for the paramagnetic offset at $T > T_c$ is rather small, which is also confirmed by the small value of the ratio $M_{magn}/M(2K)$ corresponding to $\simeq -0.019$ and -0.023 for the particular $^{54}FeSe_{1-x}$ and $^{56}FeSe_{1-x}$ samples shown in the inset of figure 3. The magnetization curve for $^{54}FeSe_{1-x}$ is shifted almost parallel to higher temperature, implying that T_c of $^{54}FeSe_{1-x}$ is higher than that of $^{56}FeSe_{1-x}$. The resulting transition temperatures determined from the intercept of the linearly extrapolated $M_{norm}(T)$ curves with the $M = 0$ line for all samples investigated are summarized in figure 3. The T_cs for both sets of $^{54}FeSe_{1-x}/^{56}FeSe_{1-x}$ samples fall into two distinct regions: $8.39 \leqslant {}^{54}T_c \leqslant 8.48$ K and $8.15 \leqslant {}^{56}T_c \leqslant 8.31$ K, respectively. The corresponding mean values are ${}^{54}\overline{T}_c = 8.43(3)$ K and ${}^{56}\overline{T}_c = 8.21(4)$ K. Note that one out of the seven $^{56}FeSe_{1-x}$ samples had $T_c \simeq 8.44$ K, which is by more than 5 standard deviations above the average calculated for the rest of the six samples. We have no explanation for this discrepancy, but decided to show this point for completeness of the data collected.

The Fe-IE exponent α_{Fe} was determined from the data presented in figure 3 using equation (1), where the relative Fe isotope shift of the quantity X is defined as

IOP Institute of Physics DEUTSCHE PHYSIKALISCHE GESELLSCHAFT

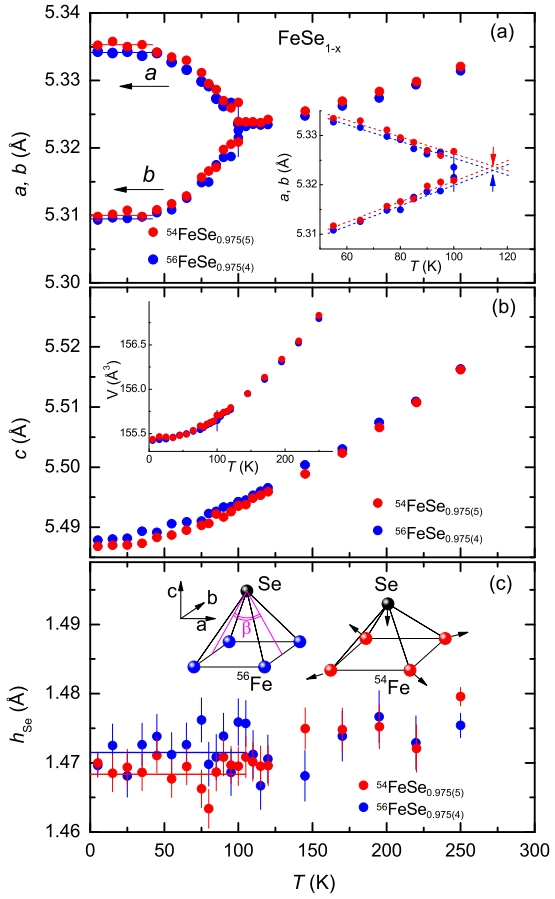

Figure 2. The temperature dependence of the lattice constants a and b (panel (a), in the tetragonal phase a is multiplied by $\sqrt{2}$), lattice constant c (panel (b)) and the distance between the Se atom and Fe plane h_{Se} (panel (c)) for ^{54}FeSe$_{0.975(5)}$ and ^{56}FeSe$_{0.975(4)}$ samples. The inset in panel (a) shows the extended part of $a(T)$ and $b(T)$ in the vicinity of the structural transition temperature T_{s}, together with the linear fits. The inset in panel (b) represents the temperature dependence of the lattice volume V. The inset in panel (c) shows schematically the modification of the Fe$_4$Se pyramid caused by ^{56}Fe/^{54}Fe isotope substitution. The arrows show the direction of atom displacements (see text for details).

$\Delta X/X = (^{54}X - {}^{56}X)/{}^{56}X$ (this definition of $\Delta X/X$ is used throughout the paper). With $^{54}\overline{T}_{\mathrm{c}} = 8.43(3)$ K, $^{56}\overline{T}_{\mathrm{c}} = 8.21(4)$ K, $M_{^{54}\mathrm{Fe}} = 54\,\mathrm{g\,mol^{-1}}$ and $M_{^{56}\mathrm{Fe}} = 55.85\,\mathrm{g\,mol^{-1}}$, one obtains $\alpha_{\mathrm{Fe}} = 0.81(15)$. Three points should be emphasized: (i) the *positive* sign of the Fe-IE exponent α_{Fe} is similar to that observed in phonon-mediated superconductors, such as elemental metals [1]

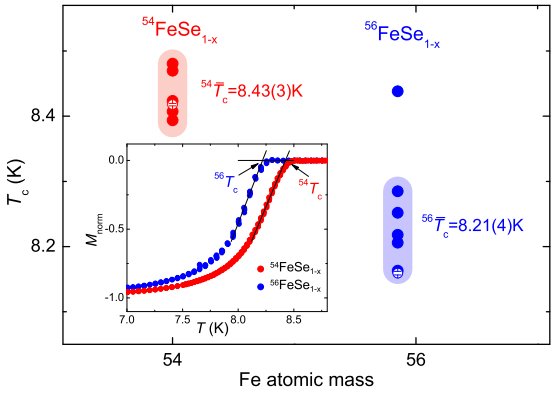

Figure 3. The superconducting transition temperature T_c as a function of Fe atomic mass for $^{54}FeSe_{1-x}/^{56}FeSe_{1-x}$ samples studied in the present work. The open symbols correspond to the samples studied by NPD experiments. The T_cs fall into the regions marked by the colored stripes with the corresponding mean values $^{54}\overline{T}_c = 8.43(3)$ K and $^{56}\overline{T}_c = 8.21(4)$ K. The inset shows the normalized ZFC magnetization curves $M_{norm} = [M(T) - M_{magn}]/[M(2K) + M_{magn}]$ for one pair of $^{54}FeSe_{1-x}$ and $^{56}FeSe_{1-x}$ samples. The transition temperature T_c is determined as the intersection of the linearly extrapolated $M_{norm}(T)$ curve in the vicinity of T_c with the $M = 0$ line.

and MgB_2 [20], as well as in cuprate HTS [21, 22], where the pairing mechanism is still under debate. Bearing in mind that a positive Fe-IE exponent was also observed in $SmFeAsO_{0.85}F_{0.15}$ and $Ba_{0.6}K_{0.4}Fe_2As_2$ [2], we may conclude that, at least for three compounds representing different families of Fe-based HTS (1111, 122 and 11), the sign of the Fe-IE on T_c is conventional. This suggests that the lattice plays an essential role in the pairing mechanism in the Fe-based HTS. (ii) The Fe-IE exponent $\alpha_{Fe} = 0.81(15)$ is larger than the BCS value $\alpha^{BCS} = 0.5$ as well as more than twice as large as $\alpha_{Fe} \simeq 0.35$ reported for $SmFeAsO_{0.85}F_{0.15}$ and $Ba_{0.6}K_{0.4}Fe_2As_2$ [2]. Note that an enhanced value of the oxygen isotope exponent ($\alpha_O \simeq 1$) was also observed in underdoped cuprate HTS [22] and was shown to be a consequence of the polaronic nature of the supercarriers in that class of materials [23]. Recently, Bussmann-Holder *et al* [24] showed that, in the framework of a two-band model, polaronic coupling in the larger gap channel and in the interband interaction induces a T_c (doping)-dependent Fe-IE: α_{Fe} increases strongly with reduced T_c (doping), reaching $\alpha_{Fe} \simeq 0.9$ at $T_c \simeq 10$ K. Note that a similar generic trend is observed in cuprate HTS [21, 22]. (iii) The positive value of the Fe isotope exponent observed in the present study contradicts the results of Shirage *et al* [4], reporting $\alpha_{Fe} \simeq -0.18$ for $Ba_{1-x}K_xFe_2As_2$. As will be shown later, such a difference could arise from the substantial 'structural' contribution to the isotope exponent, which may also allow us to explain the conflicting results of [2] and [4].

Our structural refined NPD data suggest that part of the large Fe-IE $\alpha_{Fe} = 0.81(15)$ may result from the tiny structural changes due to $^{54}Fe/^{56}Fe$ substitution. In the following, we discuss a possible structural effect on the observed Fe-IE on T_c. It is known that in $FeSe_{1-x}$ a decrease

in the Se height caused by compression of the Fe_4Se pyramid leads to an increase in T_c by $\Delta T_c^{h_{Se}}/(\Delta h_{Se}/h_{Se}) \simeq 3.4\,K/\%$ [19, 25]. In contrast, an increase in the Se(Te)–Fe–Se(Te) angle in the $FeSe_{1-y}Te_y$ family (angle β in our notation[6], see the inset of figure 2(c)) results for $y \leqslant 0.5$ in a decrease in T_c by $\Delta T_c^{\beta}/(\Delta\beta/\beta) \simeq 2.9\,K/\%$ [18]. Based on the structural data presented in figure 2, one obtains $\Delta h_{Se}/h_{Se} = 0.22(8)\%$ and $\Delta\beta/\beta = -0.13(4)\%$, leading to $\Delta T_c^{h_{Se}} = 0.7(3)$ K and $\Delta T_c^{\beta} = -0.4(2)$ K (in this estimate, the values of the lattice constants a and b and h_{Se} were averaged over the temperature regions denoted as solid lines in figures 2(a) and (c)). Bearing in mind that all Fe-based HTS are similarly sensitive to structural changes as $FeSe_{1-x}$ (see, e.g., [17]–[19], [26]), we conclude that the shift in T_c caused by tiny modifications of the crystal structure upon isotope exchange may contribute to the total Fe-IE exponent. However, the large errors of $\Delta T_c^{h_{Se}}$ and ΔT_c^{β} do not allow a reliable estimate of this structural effect on the Fe-IE on T_c. A better estimate of this effect can be made based on the empirical relation between T_c and the lattice parameter a for the 11 family $FeSe_{1-y}Te_y$ [18, 26]. Assuming that the relation $T_c(a)$ is also valid for $FeSe_{1-x}$, one obtains from the data presented in [26] for $y \leqslant 0.5$ the relation $\Delta T_c^{a}/(\Delta a/a) \approx 6\,K/\%$. With $(\Delta a + \Delta b)/(a+b) = 0.0195(14)\%$, this gives rise to a *structural* shift in T_c of $\Delta T_c^{str} \approx 0.1$ K (the lattice constants a and b were averaged over the temperature regions marked by a solid line in figure 2(a)). Taking this correction into account yields a rough estimate of the intrinsic Fe-IE exponent of $\alpha_{Fe}^{int} \approx 0.4$. This value is comparable to $\alpha_{Fe} \simeq 0.35$ reported for $SmFeAsO_{0.85}F_{0.15}$ and $Ba_{0.6}K_{0.4}Fe_2As_2$ [2].

To summarize, the $^{56}Fe/^{54}Fe$ isotope effects on the superconducting transition temperature and the crystal structure were studied in the iron chalcogenide superconductor $FeSe_{1-x}$. The following results were obtained: (i) the substitution of the natural Fe ($M_{Fe} = 55.85\,g\,mol^{-1}$) by the ^{54}Fe isotope ($M_{^{54}Fe} = 54.0\,g\,mol^{-1}$) gives rise to a pronounced Fe isotope shift in the transitions temperature T_c as determined by magnetization measurements. The average T_c is found to be $\simeq 0.22$ K higher for the $^{54}FeSe_{1-x}$ samples, as compared to the $^{56}FeSe_{1-x}$ samples, resulting in an Fe-IE exponent of $\alpha_{Fe} = 0.81(15)$. (ii) The $^{56}Fe/^{54}Fe$ isotope substitution leads to an enhancement of the lattice constants a and b and a shrinkage of the lattice constant c. These modifications do not affect the lattice volume. (iii) The tetragonal to orthorhombic structural transition temperature ($T_s \simeq 100$ K) is the same for both $^{54}FeSe_{1-x}$ and $^{56}FeSe_{1-x}$ within the accuracy of the experiment. (iv) For temperatures below 100 K, the distance between the Se atom and Fe plane (Se height) is smaller for the samples with ^{54}Fe. This, together with the results of point (ii), imply that $^{56}Fe/^{54}Fe$ isotope substitution leads to a compression of the Fe_4Se pyramid along the crystallographic c-axis and an enhancement along the a- and b-directions. (v) The structural changes caused by $^{56}Fe/^{54}Fe$ isotope substitution induce a shift in T_c, which may reduce the value of the Fe-IE exponent to ≈ 0.4, in fair agreement with $\alpha_{Fe} \simeq 0.35$ obtained for $SmFeAsO_{0.85}F_{0.15}$ and $Ba_{0.6}K_{0.4}Fe_2As_2$ [2].

In conclusion, from magnetization experiments the Fe-IE exponent of T_c for the $FeSe_{1-x}$ system was determined to be $\alpha_{Fe} = 0.81(15)$. The tiny changes to the structural parameters caused by isotope substitution may contribute to the total Fe-IE exponent, and may help us to clarify, or even be the origin of, the previously reported controversial results [2, 4]. However, more detailed and systematic structural investigations of Fe isotope substituted samples are required in order to draw definite conclusions. Our findings, on the other hand, clearly show that a conventional isotope effect on T_c is present, which highlights the role of the lattice in the pairing mechanism in this new material class.

[6] In the orthorombic phase there are two angles β_1 and β_2, which are different by $\simeq 0.3^\circ$ at $T = 5$ K.

Acknowledgments

We thank A Bussmann-Holder for fruitful discussions and a critical reading of the manuscript. This work was partly performed at SINQ (Paul Scherrer Institute, Switzerland). The work of MB was supported by the Swiss National Science Foundation. The work of EP was supported by the NCCR program MaNEP.

References

[1] Maxwell E 1950 *Phys. Rev.* **78** 477
Reynolds C A, Serin B, Wright W H and Nesbitt L B 1950 *Phys. Rev.* **78** 487
[2] Liu R H *et al* 2009 *Nature* **459** 64
[3] Carbotte J P 1990 *Rev. Mod. Phys.* **62** 1027
[4] Shirage P M, Kihou K, Miyazawa K, Lee C-H, Kito H, Eisaki H, Yanagisawa T, Tanaka Y and Iyo A 2009 *Phys. Rev. Lett.* **103** 257003
[5] Hsu F C *et al* 2008 *Proc. Natl Acad. Sci. USA* **105** 14262
[6] Khasanov R *et al* 2008 *Phys. Rev.* B **78** 2250510(R)
[7] Pomjakushina E, Conder K, Pomjakushin V, Bendele M and Khasanov R 2009 *Phys. Rev.* B **80** 024517
[8] McQueen T M *et al* 2009 *Phys. Rev.* B **79** 014522
[9] McQueen T M, Williams A J, Stephens P W, Tao J, Zhu Y, Ksenofontov V, Casper F, Felser C and Cava R J 2009 *Phys. Rev. Lett.* **103** 057002
[10] Bendele M, Amato A, Conder K, Elender M, Keller H, Klauss H-H, Luetkens H, Pomjakushina E, Raselli A and Khasanov R 2010 *Phys. Rev. Lett.* **104** 087003
[11] Khasanov R, Bendele M, Amato A, Conder K, Keller H, Klauss H-H, Luetkens H and Pomjakushina E 2010 *Phys. Rev. Lett.* **104** 087004
[12] Fischer P 2000 *Physica* B **276–278** 146
[13] Rodríguez-Carvajal J 1993 *Physica* B **192** 55
[14] Okamoto H 1991 *J. Phase Equilib.* **12** 383
[15] http://www.ncnr.nist.gov/resources/n-lengths
[16] Margadonna S, Takabayashi Y, McDonald M T, Kasperkiewicz K, Mizuguchi Y, Takano Y, Fitch A N, Suard E and Prassides K 2008 *Chem. Commun. (Camb.)* 5607
[17] Zhao J *et al* 2008 *Nature Materials* **7** 953
[18] Horigane K, Hiraka H and Ohoyama K 2009 *J. Phys. Soc. Japan* **78** 074718
[19] Mizuguchi Y, Hara Y, Deguchi K, Tsuda S, Yamaguchi T, Takeda K, Kotegawa H, Tou H and Takano Y 2010 *Supercond. Sci. Technol.* **23** 054013
[20] Budko S L, Lapertot G, Petrovic C, Cunningham C E, Anderson N and Canfield P C 2001 *Phys. Rev. Lett.* **86** 1877
Hinks D G, Claus H and Jorgensen J D 2001 *Nature* **411** 457
[21] Batlogg B, Kourouklis G, Weber W, Cava R J, Jayaraman A, White A E, Short K T, Rupp L W and Rietman E A 1987 *Phys. Rev. Lett.* **59** 912
Franck J P, Jung J, Mohamed M A-K, Gygax S and Sproule G I 1991 *Phys. Rev.* B **44** 5318
[22] Khasanov R, Shengelaya A, Di Castro D, Morenzoni E, Maisuradze A, Savic I M, Conder K, Pomjakushina E, Bussmann-Holder A and Keller H 2008 *Phys. Rev. Lett.* **101** 077001
[23] Bussmann-Holder A and Keller H 2005 *Eur. Phys. J.* B **44** 487
[24] Bussmann-Holder A, Simon A, Keller H and Bishop A R 2010 *J. Supercond. Nov. Magn.* **23** 365
Bussmann-Holder A, Simon A, Keller H and Bishop A R 2009 arXiv:0906.2283
[25] Margadonna S, Takabayashi Y, Ohishi Y, Mizuguchi Y, Takano Y, Kagayama T, Nakagawa T, Takata M and Prassides K 2009 *Phys. Rev.* B **80** 064506
[26] Mizuguchi Y, Tomioka F, Tsuda S, Yamaguchi T and Takano Y 2009 *J. Phys. Soc. Japan* **78** 074712

5.2.2 Paper II: Intrinsic and structural isotope effects in Fe-based superconductors

This work is published in:

R. Khasanov, M. Bendele, A. Bussmann-Holder, and H. Keller, *Intrinsic and structural isotope effects in Fe-based superconductors* , Phys. Rev. B **82**, 212505 (2010).

Abstract:

The currently available results of the isotope effect on the superconducting transition temperature T_c in Fe-based high-temperature superconductors (HTSs) are highly controversial. The values of the Fe isotope effect exponent α_{Fe} for various families of Fe-based HTS were found to be as well positive, as negative, or even be exceedingly larger than the BCS value $\alpha_{BCS} \equiv 0.5$. Here we emphasize that the Fe isotope substitution causes small structural modifications which, in turn, affect T_c. Upon correcting the isotope effect exponent for these structural effects, an almost unique value of $\alpha \sim 0.35 - 0.4$ is observed for at least three different families of Fe-based HTS.

URL: http://link.aps.org/doi/10.1103/PhysRevB.82.212505
DOI: 10.1103/PhysRevB.82.212505
PACS: 74.70.Xa, 74.62.Bf, 74.25.Kc

PHYSICAL REVIEW B **82**, 212505 (2010)

Intrinsic and structural isotope effects in iron-based superconductors

R. Khasanov,[1,*] M. Bendele,[1,2] A. Bussmann-Holder,[3] and H. Keller[2]
[1]*Laboratory for Muon Spin Spectroscopy, Paul Scherrer Institute, CH-5232 Villigen PSI, Switzerland*
[2]*Physik-Institut, Universität Zürich, Winterthurerstrasse 190, CH-8057 Zürich, Switzerland*
[3]*Max-Planck-Institut für Festkörperforschung, Heisenbergstrasse 1, D-70569 Stuttgart, Germany*
(Received 26 August 2010; revised manuscript received 17 September 2010; published 8 December 2010)

The currently available results of the isotope effect on the superconducting transition temperature T_c in Fe-based high-temperature superconductors (HTSs) are highly controversial. The values of the Fe isotope effect exponent α_{Fe} for various families of Fe-based HTS were found to be as well positive, as negative, or even be exceedingly larger than the BCS value $\alpha_{BCS} \equiv 0.5$. Here we emphasize that the Fe isotope substitution causes small structural modifications which, in turn, affect T_c. Upon correcting the isotope effect exponent for these structural effects, an almost unique value of $\alpha \sim 0.35-0.4$ is observed for at least three different families of Fe-based HTS.

DOI: 10.1103/PhysRevB.82.212505 PACS number(s): 74.70.Xa, 74.62.Bf, 74.25.Kc

The isotope effect on the transition temperature T_c traditionally plays an important role in identifying the superconducting pairing mechanism. As a rule, an impact of the isotope substitution and, consequently, an involvement of the lattice degrees of freedom in formation of the supercarriers are determined by comparing the isotope effect exponent $\alpha = -(\Delta T_c/T_c)/(\Delta M/M)$ (M is the atomic mass) with the universal value $\alpha_{BCS} \equiv 0.5$ as predicted within the framework of BCS theory of electron-phonon-mediated superconductivity.

In conventional phonon-mediated superconductors such as simple metals, alloys, etc., α, typically, ranges from 0.2 to 0.5, see, e.g., Ref. 1, and references therein. The only exceptions are Ru and Zr exhibiting zero isotope effect and PdH(D) with $\alpha_{H(D)} = -0.25$.[2] The negative isotope effect of PdH(D) is explained, however, by the presence of strong lattice anharmonicity caused by the double-well potential in the proton (deuteron) bond distribution.[3] This was confirmed by neutron scattering data where the large zero-point motion of H in comparison with that of deuterium results in 20% change in the lattice force constants.[4] A similar finding exists in organic superconductors where the H(D) isotope effect changes sign as compared, e.g., to ^{34}S, ^{13}C, and ^{15}N isotope replacements, see Ref. 5, and references therein. Again, an unusually strong anharmonic lattice dynamics are attributed to this observation.[5,6] The cuprate high-temperature superconductors (HTSs) are characterized by a vanishingly small but positive isotope effect exponent in optimally doped compounds which increases in a monotonic way upon decreasing doping for almost all cuprate families[7–13] with the exception of the doped $La_{2-x}Sr_xCuO_4$ system, where at 1/8th an anomaly appears,[14,15] most likely caused by the low-temperature tetragonal phase transition. For the optimally doped cuprate HTS the smallest value of the oxygen-isotope exponent $\alpha_O \simeq 0.02$ was obtained for $YBa_2Cu_3O_{7-\delta}$ and $Bi_2Sr_2Ca_2Cu_3O_{10+\delta}$ while it reaches $\alpha_O \simeq 0.25$ for $Bi_2Sr_{1.6}La_{0.4}CuO_{6+\delta}$.[7–9,12,13] In addition, it was demonstrated that in underdoped materials α_O exceeds substantially the BCS limit $\alpha_{BCS} \equiv 0.5$.[8,13,15] It is important to note here that the values of both, the oxygen and the copper isotope exponents in cuprate HTS are *always* positive. Similar tendencies, with the only few above-mentioned exceptions, are realized in a case of conventional phonon-mediated superconductors.

Since the discovery of superconductivity in Fe-based compounds few attempts to measure the isotope effect on T_c in these materials were made. Currently we are aware of four papers reporting, however, rather contradictory results.[16–19] Liu *et al.*[16] and Khasanov *et al.*[19] have found a *positive* Fe isotope effect (Fe-IE) exponent α_{Fe} for $Ba_{0.6}K_{0.4}Fe_2As_2$, $SmFeAsO_{0.85}F_{0.15}$, and $FeSe_{1-x}$ with the corresponding values $\alpha_{Fe} = 0.34(3)$, 0.37(3), and 0.81(15), respectively. Note that $\alpha_{Fe} = 0.81(15)$ for $FeSe_{1-x}$ exceeds grossly the BCS value. In the other two studies Shirage *et al.*[17] have reported a *negative* $\alpha_{Fe} = -0.18(3)$ and $-0.024(15)$ for $Ba_{0.6}K_{0.4}Fe_2As_2$ and $SmFeAsO_{1-y}$,[18] respectively. These controversial results are unlikely to stem from different pairing mechanisms to be realized in different Fe-based superconductors. Especially, in the case of $Ba_{0.6}K_{0.4}Fe_2As_2$, nominally identical samples were isotope replaced with one exhibiting a positive[16] and the other a negative isotope exponent.[17] Note, that the sign reversed isotope exponent seen by Shirage *et al.*[17,18] was attributed to multiband superconductivity with different pairing channels, namely, a phononic one and an antiferromagnetic (AF) fluctuation dominated one.[20] However, as shown by Bussmann-Holder and Keller,[21] the model presented in Ref. 20 and its extensions cannot give rise to *any* sign reversed isotope effect even if both pairing channels stem from AF fluctuations.

In the present study we demonstrate that the very controversial results for α_{Fe} are caused by small structural changes occurring simultaneously with the Fe isotope exchange. As such, we decompose the Fe-IE exponent into one related to the structural changes α_{Fe}^{str} and the genuine (intrinsic) one α_{Fe}^{int} to arrive at

$$\alpha_{Fe} = \alpha_{Fe}^{int} + \alpha_{Fe}^{str}. \quad (1)$$

By comparing the c-axis lattice constants for the pairs of isotopically substituted samples we observe that α_{Fe}^{str} is negative for $Ba_{0.6}K_{0.4}Fe_2As_2$ and $SmFeAsO_{1-y}$ studied by Shirage *et al.* in Refs. 17 and 18, positive for $FeSe_{1-x}$ from Ref. 19 and close to 0 for $Ba_{0.6}K_{0.4}Fe_2As_2$ and $SmFeAsO_{0.85}F_{0.15}$ measured in Ref. 16. By taking into account the sign of α_{Fe}^{str}

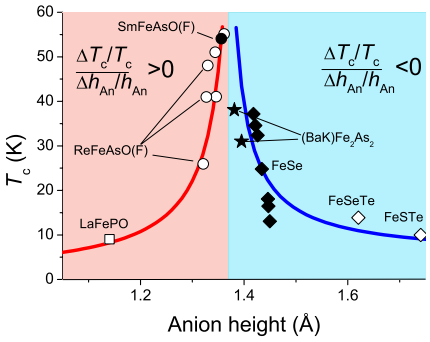

FIG. 1. (Color online) Dependence of the superconducting transition temperature T_c on the height of the anion atom (h_{An}, An=As, Se, P) for various families of Fe-based HTS, after Mizuguchi *et al.* (Ref. 22). The closed symbols represent the samples which are relevant for the present study. The lines are guide for the eyes. Shaded areas on the left (right) side of the figure represent the regions of T_c vs h_{An} diagram where T_c increases (decreases) with increasing h_{An}.

we arrive at the conclusion that α_{Fe}^{int} is positive for all so far studied Fe-based HTS.

Our motivation to separate the isotope coefficient into the above-mentioned two components, see Eq. (1), stems from the fact that superconductivity in these compounds is intimately related to small structural changes as reported in various works. As an example, we mention the strong nonlinear dependence of the superconducting transition temperature on the anion atom height (h_{An}, An=As, P, S, or Se) with a sharp maximum of T_c at $h_{An} \simeq 1.38$ Å, see Mizuguchi *et al.*[22] and Fig. 1. The influence of the Fe isotope substitution on the crystal structure, on the other hand, was considered by Granath *et al.*[23] based on the results of Raman studies of $CaFeAsO_{1-x}$ and $NdFeAsO_{1-x}$ and further confirmed by Khasanov *et al.*[19] in neutron powder-diffraction experiments on ^{54}Fe to ^{56}Fe substituted $FeSe_{1-x}$.

The c-axis lattice constants for the pairs of Fe isotope substituted samples $Ba_{0.6}K_{0.4}Fe_2As_2$, $SmFeAsO_{0.85}F_{0.15}$, $SmFeAsO_{1-y}$, and $FeSe_{1-x}$ studied in Refs. 16–19, are summarized in Table I. The choice of the c-axis lattice constant as the relevant quantity in deriving the structural isotope effect might appear to be rather arbitrary since T_c is influenced by all structural details, namely, tetrahedral angle, a-axis lattice constant, internal bond lengths, etc. However, the c-axis lattice constant provides a very sensitive probe since its compression (expansion) is directly accompanied by the corresponding variation in the distance from the Fe planes to the above (below) lying anions which, in turn, is a well characterized property for many Fe-based compounds.[22] A survey of the literature shows that the proportionality between the anion atom height and the c-axis lattice constant indeed holds for $FeSe_{1-x}$, $(BaK)Fe_2As_2$, and SmFeAsO(F) families of Fe-based HTS considered in the present study.[24–26] From Table I it is obvious that in $Ba_{0.6}K_{0.4}Fe_2As_2$ and $SmFeAsO_{0.85}F_{0.15}$ (Ref. 16) the c-axis constants are the same within the experimental error for both isotopically substituted sets of the samples.[27] In $FeSe_{1-x}$ (Ref. 19) the c-axis constant is larger while in $Ba_{0.6}K_{0.4}Fe_2As_2$ (Ref. 17) it is smaller for the sample with the heavier Fe isotope. In $SmFeAsO_{1-y}$, studied by Shirage *et al.*,[18] both c-axis lattice constants seem to coincide within the experimental resolution. However, since the difference between them is 1.5 times larger than one standard deviation, it is conceivable to attribute an increase in the c-axis lattice constant in $SmFeAsO_{1-y}$ with the heavier Fe isotope.

The use of the empirical T_c vs h_{An} relation from Ref. 22 combined with the intrinsic relation of the proportionality between the c-axis constant and the anion atom height ($\Delta c \propto \Delta h_{An}$, see Refs. 24–26) enables us to determine the sign of the structurally related shift of T_c induced by isotopic exchange. By defining the shift of a given quantity X as $\Delta X/X = (^{light}_{Fe}X - ^{heavy}_{Fe}X)/^{heavy}_{Fe}X$ and following Mizuguchi *et al.*,[22] see also Fig. 1, the sign of $(\Delta T_c/T_c)/(\Delta h_{An}/h_{An})$ is positive for SmFeAsO(F) as well as for various Fe-based HTS belonging to ReFeAsO(F) family (Re=Nd, Ce, La) and negative for $(BaK)Fe_2As_2$ and $FeSe_{1-x}$. Consequently the change in the c-axis constant caused by Fe isotope substitution as presented in Table I results in an additional structurally related shift of T_c being positive for $FeSe_{1-x}$,[19] negative for $Ba_{0.6}K_{0.4}Fe_2As_2$ and $SmFeAsO_{1-y}$,[17,18] and close to 0 for $Ba_{0.6}K_{0.4}Fe_2As_2$ and $SmFeAsO_{0.85}F_{0.15}$.[16] It is rather remarkable that the corresponding "structural" Fe-IE exponents α_{Fe}^{str} would lead to the shift of genuine (intrinsic) α_{Fe}^{int} in the direction of 0.35–0.4, see Fig. 2.

TABLE I. Summary of Fe isotope effect studies for $FeSe_{1-x}$ (Ref. 19), $SmFeAsO_{0.85}F_{0.15}$ and $Ba_{0.6}K_{0.4}Fe_2As_2$ (Ref. 16), $Ba_{0.6}K_{0.4}Fe_2As_2$ (Ref. 17), and $SmFeAsO_{1-x}$ (Ref. 18). The parameters are: T_c—superconducting transition temperature for the sample with the natural Fe isotope (^{nat}Fe); α_{Fe}-Fe isotope effect exponent; c—the c-axis lattice constant for the sample with the lighter ($^{light}Fe$) and the heavier ($^{heavy}Fe$) Fe isotope; $\Delta c/c$—the relative shift of the c-axis constant caused by the Fe isotope substitution; α_{Fe}^{str} and α_{Fe}^{int}—the structural and the intrinsic contributions to α_{Fe}. See text for details.

Sample	Reference	$T_c(^{nat}Fe)$ (K)	α_{Fe}	c axis ($^{light}Fe$) (Å)	c axis ($^{heavy}Fe$) (Å)	$\Delta c/c$	α_{Fe}^{str}	α_{Fe}^{int}
$FeSe_{1-x}$	19	8.21(4)	0.81(15)	5.48683(9)	5.48787(9)	>0	≃0.4	≃0.4
$Ba_{0.6}K_{0.4}Fe_2As_2$	16	37.30(2)	0.37(3)	13.289(7)	13.288(7)	~0	~0	~0.35
$Ba_{0.6}K_{0.4}Fe_2As_2$	17	37.78(2)	−0.18(3)	13.313(1)	13.310(1)	<0	~−0.5	~0.35
$SmFeAsO_{0.85}F_{0.15}$	16	41.40(2)	0.34(3)	8.490(2)	8.491(2)	~0	~0	~0.35
$SmFeAsO_{1-y}$	18	54.02(13)	−0.024(15)	8.4428(8)	8.4440(8)	≳0	<0	

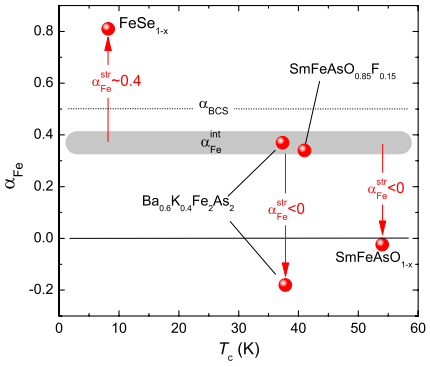

FIG. 2. (Color online) Fe isotope effect exponent α_{Fe} as a function of the superconducting transition temperature T_c for the samples considered in the present study: $FeSe_{1-x}$ (Ref. 19), $Ba_{0.6}K_{0.4}Fe_2As_2$ and $SmFeAsO_{0.85}F_{0.15}$ (Ref. 16), $Ba_{0.6}K_{0.4}Fe_2As_2$ (Ref. 17), and $SmFeAsO_{1-x}$ (Ref. 18). Arrows indicate the direction of the shift from the "intrinsic" Fe-isotope effect exponent α_{Fe}^{int} $\sim 0.35-0.4$ caused by the structural effects. $\alpha_{BCS} \equiv 0.5$ is the BCS value for electron-phonon-mediated superconductivity. See text for details

Note that the above-mentioned discussion allows only to determine the sign of the structurally related isotope effect but not the absolute value. The reasons are the following. First, the relative change in the c-axis constant is proportional but not identical to the one of h_{An}. As an example, ^{56}Fe to ^{54}Fe isotope substitution in $FeSe_{1-x}$ leads to an increase in the c-axis constant by approximately 0.02% while the change of the Se height amounts to $\simeq$0.22%, see Ref. 19. Second, the height of the anion atom is clearly not the only parameter which is crucial for T_c of Fe-based HTS as already mentioned above. However, the lack of a consistent structural characterization limits this study to a single parameter which was emphasized to be of uppermost relevance to T_c.

The analysis of the structural data together with the dependence of T_c on Se height in $FeSe_{1-x}$, as well as on Se(Te)-Fe-Se(Te) angle and the a-axis constant in $FeSe_{1-y}Te_y$ for $y \leq 0.5$ admits to extract the "structural" Fe isotope effect exponent $\alpha_{Fe}^{str} \simeq 0.4$ for ^{56}Fe to ^{54}Fe substituted $FeSe_{1-x}$ samples.[19] The absence of precise structural data complicates the analysis as outlined in Refs. 16–18. However, a zero, within the experimental accuracy, Fe isotope shift of the c-axis lattice constant for $Ba_{0.6}K_{0.4}Fe_2As_2$ as reported by Liu *et al.*[16] is a clear indication that no structural effect is present for this particular set of the samples. Consequently, the negative isotope effect exponent $\alpha_{Fe} \simeq -0.18$ obtained for nominally identically doped $Ba_{0.6}K_{0.4}Fe_2As_2$ by Shirage *et al.*[17] stems from summing both effects, i.e., $-0.18(\alpha_{Fe}) = 0.35(\alpha_{Fe}^{int}) - 0.53(\alpha_{Fe}^{str})$, see Eq. (1). It is important to recognize that for SmFeAsO(F) a similar analysis is impossible since samples with different doping levels (different T_c's, see Table I and Fig. 2) were studied in Refs. 16 and 18.

Recently Bussmann-Holder *et al.*[28] investigated a multiple gap scenario of superconductivity in Fe-based HTS with the aim to search for possible sources of the isotope effect on T_c. Typical phonon-mediated scenarios were contrasted to polaronic effects and found to have very different impacts on the isotope effect. While phonon mediated superconductivity slightly suppresses the isotope effect as compared to the BCS value $\alpha_{BCS} \equiv 0.5$, polaronic effects can largely enhance it. The scenario of electron-phonon-mediated superconductivity within the dominant gap channel predicts a T_c independent isotope effect with the α value being slightly smaller than 0.5 thus agreeing rather well with that observed for $FeSe_{1-x}$,[19] $Ba_{0.6}K_{0.4}Fe_2As_2$,[16,17] and $SmFeAsO_{0.85}F_{0.15}$.[16] Indeed, for these particular samples, which belong to three different families of Fe-based HTS and have T_c's ranging from 8 to 44 K, the "intrinsic" Fe isotope exponent is almost constant with $\alpha_{Fe}^{int} \sim 0.35-0.4$, see Table I and Fig. 2. As such, the independent on T_c value of α_{Fe}^{int} would suggest $\alpha_{Fe}^{str} \sim -0.4$ for $SmFeAsO_{1-x}$ studied by Shirage *et al.*[18]

To conclude, the currently available Fe isotope effect data on the superconducting transition temperature T_c for various Fe-based HTS were reanalyzed by separating the measured Fe-IE exponent α_{Fe} into a structural and an intrinsic (unrelated to the structural changes) component. Accounting for the empirical relation between T_c and the anion atom height h_{An} (Ref. 22) we have demonstrated that the structural contribution to the Fe-IE exponent is negative for $Ba_{0.6}K_{0.4}Fe_2As_2$ and $SmFeAsO_{1-x}$ studied by Shirage *et al.*,[17,18] positive for $FeSe_{1-x}$,[19] and close to 0 for $SmFeAsO_{0.85}F_{0.15}$ and $Ba_{0.6}K_{0.4}Fe_2As_2$ measured by Liu *et al.*[16] By taking such corrections into account we infer that the value of the genuine Fe-IE exponent is close to $\alpha_{Fe}^{int} \sim 0.35-0.4$ for compounds belonging to at least three different families of Fe-based HTS. We are convinced that the analysis presented in our Brief Report helps in clarifying the existing controversy on the isotope effect in Fe-based superconductors.

*Corresponding author: rustem.khasanov@psi.ch

[1] C. P. Poole, *Handbook of Superconductivity* (Academic Press, London, 2000).
[2] W. Buckel and B. Strizker, Phys. Lett. **43A**, 403 (1973); J. E. Schirber and C. J. M. Northrup, Jr., Phys. Rev. B **10**, 3818 (1974).
[3] M. Yussouff, B. K. Rao, and P. Jena, Solid State Commun. **94**, 549 (1995).
[4] A. Rahman, K. Sköld, C. Pelizzari, S. K. Sinha, and H. Flotow, Phys. Rev. B **14**, 3630 (1976).
[5] J. A. Schlueter, A. M. Kini, B. H. Ward, U. Geiser, H. H. Wang, J. Mohtasham, R. W. Winter, and G. L. Gard, Physica C **351**, 261 (2001).
[6] M. H. Whangbo, J. M. Willimas, A. J. Schultz, T. J. Emge, and M. A. Beno, J. Am. Chem. Soc. **109**, 90 (1987).
[7] B. Batlogg, G. Kourouklis, W. Weber, R. J. Cava, A. Jayaraman,

A. E. White, K. T. Short, L. W. Rupp, and E. A. Rietman, Phys. Rev. Lett. **59**, 912 (1987).
[8] J. P. Franck, J. Jung, M. A.-K. Mohamed, S. Gygax, and G. I. Sproule, Phys. Rev. B **44**, 5318 (1991); J. P. Franck, in *Physical Properties of High Temperature Superconductors IV*, edited by D. M. Ginsberg (World Scientific, Singapore, 1994), pp. 189–293.
[9] D. Zech, H. Keller, K. Conder, E. Kaldis, E. Liarokapis, N. Poulakis, and K. A. Müller, Nature (London) **371**, 681 (1994).
[10] R. Khasanov, A. Shengelaya, E. Morenzoni, K. Conder, I. M. Savić, and H. Keller, J. Phys.: Condens. Matter **16**, S4439 (2004); R. Khasanov, S. Strässle, K. Conder, E. Pomjakushina, A. Bussmann-Holder, and H. Keller, Phys. Rev. B **77**, 104530 (2008).
[11] J. L. Tallon, R. S. Islam, J. Storey, G. V. M. Williams, and J. R. Cooper, Phys. Rev. Lett. **94**, 237002 (2005).
[12] X.-J. Chen, B. Liang, C. Ulrich, C.-T. Lin, V. V. Struzhkin, Z. Wu, R. J. Hemley, H.-k. Mao, and H.-Q. Lin, Phys. Rev. B **76**, 140502 (2007).
[13] R. Khasanov, A. Shengelaya, D. Di Castro, E. Morenzoni, A. Maisuradze, I. M. Savic, K. Conder, E. Pomjakushina, A. Bussmann-Holder, and H. Keller, Phys. Rev. Lett. **101**, 077001 (2008).
[14] M. K. Crawford, M. N. Kunchur, W. E. Farneth, E. M. McCarron III, and S. J. Poon, Phys. Rev. B **41**, 282 (1990).
[15] G.-M. Zhao, H. Keller, and K. Conder, J. Phys.: Condens. Matter **13**, R569 (2001).
[16] R. H. Liu, T. Wu, G. Wu, H. Chen, X. F. Wang, Y. L. Xie, J. J. Yin, Y. J. Yan, Q. J. Li, B. C. Shi, W. S. Chu, Z. Y. Wu, and X. H. Chen, Nature (London) **459**, 64 (2009).
[17] P. M. Shirage, K. Kihou, K. Miyazawa, C.-H. Lee, H. Kito, H. Eisaki, T. Yanagisawa, Y. Tanaka, and A. Iyo, Phys. Rev. Lett. **103**, 257003 (2009).
[18] P. M. Shirage, K. Miyazawa, K. Kihou, H. Kito, Y. Yoshida, Y. Tanaka, H. Eisaki, and A. Iyo, Phys. Rev. Lett. **105**, 037004 (2010).
[19] R. Khasanov, M. Bendele, K. Conder, H. Keller, E. Pomjakushina, and V. Pomjakushin, New J. Phys. **12**, 073024 (2010).
[20] T. Yanagisawa, K. Odagiri, I. Hase, K. Yamaji, P. M. Shirage, Y. Tanaka, A. Iyo, and H. Eisaki, J. Phys. Soc. Jpn. **78**, 094718 (2009).
[21] A. Bussmann-Holder and H. Keller, arXiv:1009.2590 (unpublished).
[22] Y. Mizuguchi, Y. Hara, K. Deguchi, S. Tsuda, T. Yamaguchi, K. Takeda, H. Kotegawa, H. Tou, and Y. Takano, Supercond. Sci. Technol. **23**, 054013 (2010).
[23] M. Granath, J. Bielecki, J. Holmlund, and L. Börjesson, Phys. Rev. B **79**, 235103 (2009).
[24] S. Margadonna, Y. Takabayashi, M. T. McDonald, M. Brunelli, G. Wu, R. H. Liu, X. H. Chen, and K. Prassides, Phys. Rev. B **79**, 014503 (2009).
[25] M. Rotter, M. Pangerl, M. Tegel, and D. Johrendt, Angew. Chem., Int. Ed. **47**, 7949 (2008).
[26] T. M. McQueen, Q. Huang, V. Ksenofontov, C. Felser, Q. Xu, H. W. Zandbergen, Y. S. Hor, J. Allred, A. J. Williams, D. Qu, J. Checkelsky, N. P. Ong, and R. J. Cava, Phys. Rev. B **79**, 014522 (2009).
[27] The c-axis lattice constants in isotopically substituted samples are the same within $\sim 1 \times 10^{-3}$ Å while the absolute errors are larger by the factor of 7 for $SmFeAsO_{85}F_{0.15}$ and by the factor of 2 for $Ba_{0.6}K_{0.4}Fe_2As_2$.
[28] A. Bussmann-Holder, A. Simon, H. Keller, and A. Bishop, arXiv:0906.2283 (unpublished).

6 Conclusion and Outlook

The investigations of the FeCh system by means of μSR, magnetization, and neutron diffraction measurements presented in this thesis provide a detailed insight into the superconducting and magnetic properties of the system.

The hydrostatic pressure effect on the superconducting and magnetic properties of the binary $FeSe_{1-x}$ was studied. The system exhibits one of the highest known pressure effects on the superconducting transition temperature T_c and an unusual pressure dependence with a local maximum at $p \simeq 0.8\,\mathrm{GPa}$ and a local minimum at a slightly higher pressure of $p \simeq 1.2\,\mathrm{GPa}$. The system is bulk superconducting within the pressure range investigated. The μSR experiments reveal the appearance of magnetism that coexist with superconductivity above $p \simeq 0.8\,\mathrm{GPa}$ whereat the Néel temperature $T_N > T_c$. In a narrow pressure range where the local minimum in $T_c(p)$ is observed, magnetism competes with superconductivity in the sense that T_c is decreasing, and the magnetic volume fraction and the internal magnetic field decrease below T_c. However, at pressures above the local minimum of $T_c(p)$, superconductivity and magnetism coexist on short length scales in the entire sample volume with superconducting and magnetic volume fractions reaching both 100%. In addition both T_c and T_N as well as the magnetic order parameter increase with increasing pressure. This extraordinary behavior needs further investigation and provides a new challenge for theories of superconductivity.

The substitution of Se by Te in $FeSe_{1-x}$ induces a chemical pressure effect. The resulting phase diagram of $Fe_ySe_xTe_{1-x}$ is very similar to that of other Fe-based superconductors. First T_c increases until at an intermediate range of substitution superconductivity and incommensurate magnetism coexist. Finally, the fully substituted FeTe is a commensurate antiferromagnet. Furthermore, the superconducting and magnetic properties depend strongly on the Fe content of the system in the coexistence region of superconductivity and magnetism. In the low Fe content region bulk superconductivity and incommensurate magnetism coexist. With increasing y the magnetic order becomes more correlated over a longer range and superconductivity vanishes. It will be important to investigate the role of excess Fe and accompanying Fe vacancies and how the local atomic structure and the Fermi-surface are affected.

The μSR studies of superconducting $FeSe_{0.5}Te_{0.5}$ indicate multi-gap superconductivity as observed for most Fe-based superconductors. Comparing the Fe-based high temperature (HTC) superconductors with other classes suggests that the two gap scenario is generic for high temperature superconductors while the order parameter is different in every class: In MgB_2 and most probably in the Fe-based superconductors it is $s + s$-wave like, whereas in the latter case the situation is not fully resolved yet whether the fully gaped s-wave states have a different phase or not ($s_{\pm}$- or s_{++}-wave). It is even possible, that the Fe-based

superconductors have a nodal $s_{\pm}$ gap structure. In the cuprate HTC superconductors, on the other hand, nodes are present in the gap structure that is $d + s$-wave like. However, even if the symmetry of the gap-structure is known, one cannot conclude on the nature of the pairing mechanism in the Fe-based superconductors.

Isotope effect studies show a significant difference in T_c after the iron-isotope substitution (^{54}Fe/^{56}Fe) in all families of Fe-based superconductors. The isotope effect exponents reach values as large as $\alpha_{Fe} = 0.81(15)$ in $FeSe_{1-x}$. However, a minor change in the lattice parameters was observed in the isotope exchanged samples. It turned out that T_c is extremely sensitive to any changes in the lattice parameters, in particular the anion (Se) height above the Fe-plane. Taking this structural effect into account, α_{Fe} reduces to an intrinsic isotope exponent $\alpha_{Fe}^{int} \simeq 0.4$. Careful comparison of the lattice structure in the other families of Fe-based superconductors, resulted in intrinsic isotope exponents of comparable values: $\alpha_{Fe}^{int} \simeq 0.35 - 0.4$. These findings clearly show a conventional isotope effect on T_c and highlight the role of the lattice in the pairing mechanism in this new material class. However, only four experimental studies are available up to now. It will be interesting to gain more detailed information on the local atomic structure and binding valence in order to get more insight on the origin of the structural isotope effect. Furthermore, the impact of the anions (As/P and Se/Te) on the pairing must be tested with isotope exchange experiments.

In conclusion, the FeCh system investigated in the framework of the present thesis shows a substantial sensitivity of the superconducting and magnetic properties for small variations of various physical parameters of the system. Application of hydrostatic pressure drives T_c up to 36 K and commensurate magnetism occurs in the system, coexisting with superconductivity. Chemical pressure, induced by substitution of Se with the isovalent Te, leads to similar effects, whereas the FeTe parent compound is not superconducting. Even the isotope substitution of ^{56}Fe by ^{54}Fe gives rise to slightly different lattice parameters that substantially contribute to the isotope exponent. Combining all these observations made for the FeCh system leads to the conclusion that the lattice and its parameters play a major, if not the most important role in determining whether the system is superconducting, magnetically ordered, or even in a state where both phenomena are coexisting on a microscopic scale.

More than three year after the discovery of the Fe-based superconductors, the origin of superconductivity in this novel class of superconductors remains a challenging field of modern condensed matter physics research. At the end it remains to be seen whether superconductivity in these classes of high-temperature superconductors has the same or a similar origin.

Bibliography

[1] H. Kamerlingh Onnes, *The liquefaction of helium*, Proc. K. Akad. Amsterdam **11**, 168 (1908).

[2] H. Kamerlingh Onnes, *Further experiments with liquid helium D - On the change of the electrical resistance of pure metals at very low temperatures, etc. V The disappearance of the resistance of mercury*, Proc. K. Akad. Amsterdam **14**, 113 (1911).

[3] W. Meissner and R. Ochsenfeld, *Short initial announcements*, Naturwissenschaften **21**, 787 (1933).

[4] F. London and H. London, *The electromagnetic equations of the supraconductor*, Proc. R. Soc. A **149**, 71 (1935).

[5] F. London and H. London, *Supra conduction and diamagnetism*, Physica (Amsterdam) **2**, 341 (1935).

[6] V. L. Ginzburg and L. D. Landau, *On the theory of superconductivity*, Zh. Eksp. Theor. Fiz. **20**, 1064 (1950).

[7] A. Abrikosov, *On the magnetic properties of superconductors of the second group*, Sov. Phys. JETP **5**, 1174 (1957).

[8] E. Maxwell, *Isotope effect in the superconductivity of mercury*, Phys. Rev. **78**, 477 (1950).

[9] C. A. Reynolds, B. Serin, W. H. Wright, and L. B. Nesbitt, *Superconductivity of isotopes of mercury*, Phys. Rev. **78**, 487 (1950).

[10] J. Bardeen, L. N. Cooper, and J. R. Schrieffer, *Microscopic theory of superconductivity*, Phys. Rev. **106**, 162 (1957).

[11] J. Bardeen, L. N. Cooper, and J. R. Schrieffer, *Theory of superconductivity*, Phys. Rev. **108**, 1175 (1957).

[12] L. P. Gorkov, *Microscopic deruvation of the Ginzburg-Landay equations int the theory of superconductivity*, Soviet Physics JETP-USSR **9**, 1364 (1959).

[13] J. P. Carbotte, *Properties of boson-exchange superconductors*, Rev. Mod. Phys. **62**, 1027 (1990).

[14] J. G. Bednorz and K. A. Müller, *Possible high-T_c superconductivity in the Ba-La-Cu-O system*, Z. Phys. B - Condens. Matter **64**, 189 (1986).

[15] A. Schilling, M. Cantoni, J. D. Guo, and H. R. Ott, *Superconductivity above 130 K in the Hg-Ba-Ca-Cu-O system*, Nature (London) **363**, 56 (1993).

[16] L. Gao, Y. Y. Xue, F. Chen, Q. Xiong, R. L. Meng, D. Ramirez, C. W. Chu, J. H. Eggert, and H. K. Mao, *Superconductivity up to 164 K in* $HgBa_2Ca_{m-1}Cu_mO_{2m+2+\delta}$ *(m=1, 2, and 3) under quasihydrostatic pressures*, Phys. Rev. B **50**, 4260 (1994).

[17] A. Bussmann-Holder and H. Keller, *Polaron formation as origin of unconventional isotope effects in cuprate superconductors*, Eur. Phys. J. B **44**, 487 (2005).

[18] A. Bussmann-Holder, H. Keller, A. R. Bishop, A. Simon, R. Micnas, and K. A. Müller, *Unconventional isotope effects as evidence for polaron formation in cuprates*, EPL **72**, 423 (2005).

[19] H. Keller, A. Bussmann-Holder, and K. A. Müller, *Jahn-Teller physics and high-*T_c *superconductivity*, Materials Today **11**, 38 (2008).

[20] K. A. Müller, *On the superconductivity in hole doped cuprates*, J. Phys.: Condens. Matter **19**, 251002 (2007).

[21] J. Nagamatsu, N. Nakagawa, T. Muranaka, Y. Zenitani, and J. Akimitsu, *Superconductivity at 39 K in magnesium diboride*, Nature (London) **410**, 63 (2001).

[22] A. Y. Liu, I. I. Mazin, and J. Kortus, *Beyond Eliashberg superconductivity in* MgB_2*: Anharmonicity, two-phonon scattering, and multiple gaps*, Phys. Rev. Lett. **87**, 087005 (2001).

[23] Y. Kamihara, T. Watanabe, M. Hirano, and H. Hosono, *Iron-based layered superconductor* $La[O_{1-x}F_x]FeAs$ *(x=0.05-0.12) with* T_c*=26 K*, J. Am. Chem. Soc. **130**, 3296 (2008).

[24] P. J. Hirschfeld, M. M. Korshunov, and I. I. Mazin, *Gap symmetry and structure of Fe-based superconductors*, Reports on Progress in Physics **74**, 124508 (2011).

[25] A. Subedi, L. Zhang, D. J. Singh, and M. H. Du, *Density functional study of FeS, FeSe, and FeTe: Electronic structure, magnetism, phonons, and superconductivity*, Phys. Rev. B **78**, 134514 (2008).

[26] M. Tinkham, *Introduction to superconductivity*, McGraw-Hill, New York, 1996.

[27] W. Buckel and R. Kleiner, *Supraleitung: Grundlagen und Anwendungen*, Wiley-VCH, Wernheim, 2004.

[28] T. Schneider, *The physics of superconductors*, edited by K. Bennemann and J. B. Ketterson, Springer, Berlin, 2004.

[29] L. D. Landau, *The theory of phase transitions*, Nature (London) **138**, 840 (1936).

[30] L. N. Cooper, *Bound electron pairs in a degenerate Fermi gas*, Phys. Rev. **104**, 1189 (1956).

[31] A. Schenck, *Muon Spin Rotation Spectroscopy: Principles and Applications in Solid State Physics*, Adam Hilger, Bristol, 1985.

[32] A. Yaouanc and P. D. de Réotier, *Muon Spin Rotation, Relaxation, and Resonance*, Oxford Science Publications, 2011.

[33] R. Kubo and T. Toyabe, *A stochastic model for low field resonance and relaxation*, in *A stochastic model for low field resonance and relaxation*, pages 810–823, North-Holland, Amsterdam, 1967.

[34] J. Major, J. Mundy, M. Schmolz, A. Seeger, K. Döring, K. Fürderer, M. Gladisch, D. Herlach, and G. Majer, *Zero-field muon spin rotation in monocrystalline chromium*, Hyperfine Interactions **31**, 259 (1986).

[35] A. Amato, *Heavy-fermion systems studied by μSR technique*, Rev. Mod. Phys. **69**, 1119 (1997).

[36] R. S. Hayano, Y. J. Uemura, J. Imazato, N. Nishida, T. Yamazaki, and R. Kubo, *Zero-and low-field spin relaxation studied by positive muons*, Phys. Rev. B **20**, 850 (1979).

[37] J. E. Sonier, J. H. Brewer, and R. F. Kiefl, *μSR studies of the vortex state in type-II superconductors*, Rev. Mod. Phys. **72**, 769 (2000).

[38] A. Maisuradze, R. Khasanov, A. Shengelaya, and H. Keller, *Comparison of different methods for analyzing SR line shapes in the vortex state of type-II superconductors*, J. Phys.: Condens. Matter **21**, 075701 (2009).

[39] E. H. Brandt, *Flux distribution and penetration depth measured by muon spin rotation in high-Tc superconductors*, Phys. Rev. B **37**, 2349 (1988).

[40] Z. Hao, J. R. Clem, M. W. McElfresh, L. Civale, A. P. Malozemoff, and F. Holtzberg, *Model for the reversible magnetization of high-κ type-II superconductors: Application to high-T_c superconductors*, Phys. Rev. B **43**, 2844 (1991).

[41] A. Yaouanc, P. Dalmas de Réotier, and E. H. Brandt, *Effect of the vortex core on the magnetic field in hard superconductors*, Phys. Rev. B **55**, 11107 (1997).

[42] E. H. Brandt, *Magnetic field density of perfect and imperfect flux line lattices in type II superconductors. I. Application of periodic solutions*, Journal of Low Temperature Physics **73**, 355 (1988).

[43] Y. Kamihara, H. Hiramatsu, M. Hirano, R. Kawamura, H. Yanagi, T. Kamiya, and H. Hosono, *Iron-based layered superconductor: LaOFeP*, J. Am. Chem. Soc. **128**, 10012 (2006).

[44] B. S. Chandrasekhar and J. K. Hulm, *The electrical resistivity and superconductivity of some uranium alloys and compounds*, J. Phys. Chem. Solids **7**, 259 (1958).

[45] I. Shirotani, Y. Shimaya, K. Kihou, C. Sekine, N. Takeda, M. Ishikawa, and T. Yagi, *Superconductivity of new filled skutterudite YFe_4P_{12} prepared at high pressure*, J. Phys.: Condens. Matter **15**, 2201 (2003).

[46] G. P. Meisner, *Superconductivity and magnetic order in ternary rare-earth transition metal phosphides*, Physica B & C **108**, 763 (1981).

[47] H. Takahashi, K. Igawa, K. Arii, Y. Kamihara, M. Hirano, and H. Hosono, *Superconductivity at 43 K in an iron-based layered compound $LaO_{1-x}F_xFeAs$*, Nature (London) **453**, 376 (2008).

[48] V. Johnson and W. Jeitschko, *ZrCiSiAs - Filled PbFCl-type*, J. Solid State Chem. **11**, 161 (1974).

[49] X. H. Chen, T. Wu, G. Wu, R. H. Liu, H. Chen, and D. F. Fang, *Superconductivity at 43 K in $SmFeAsO_{1-x}F_x$*, Nature (London) **453**, 761 (2008).

[50] Z.-A. Ren, J. Yang, W. Lu, W. Yi, X.-L. Shen, Z.-C. Li, G.-C. Che, X.-L. Dong, L.-L. Sun, F. Zhou, and Z.-X. Zhao, *Superconductivity in the iron-based F-doped layered quaternary compound $Nd[O_{1-x}F_x]FeAs$*, EPL **82**, 57002 (2008).

[51] G. F. Chen, Z. Li, D. Wu, G. Li, W. Z. Hu, J. Dong, P. Zheng, J. L. Luo, and N. L. Wang, *Superconductivity at 41 K and its competition with spin-density-wave instability in layered $CeO_{1-x}F_xFeAs$*, Phys. Rev. Lett. **100**, 247002 (2008).

[52] Z.-A. Ren, G.-C. Che, X.-L. Dong, J. Yang, W. Lu, W. Yi, X.-L. Shen, Z.-C. Li, L.-L. Sun, F. Zhou, and Z.-X. Zhao, *Superconductivity and phase diagram in iron-based arsenic-oxides $ReFeAsO_{1-\delta}$ (Re = rare-earth metal) without fluorine doping*, EPL **83**, 17002 (2008).

[53] J. Karpinski, N. D. Zhigadlo, S. Katrych, Z. Bukowski, P. Moll, S. Weyeneth, H. Keller, R. Puzniak, M. Tortello, D. Daghero, R. Gonnelli, I. Maggio-Aprile, Y. Fasano, O. Fischer, K. Rogacki, and B. Batlogg, *Single crystals of $LnFeAsO_{1-x}F_x$ (Ln = La, Pr, Nd, Sm, Gd) and $Ba_{1-x}Rb_xFe_2As_2$: Growth, structure and superconducting properties*, Physica C **469**, 370 (2009).

[54] Y. Mizuguchi, Y. Hara, K. Deguchi, S. Tsuda, T. Yamaguchi, K. Takeda, H. Kotegawa, H. Tou, and Y. Takano, *Anion height dependence of T_c for the Fe-based superconductor*, Supercond. Sci. Technol. **23**, 054013 (2010).

[55] M. Rotter, M. Tegel, and D. Johrendt, *Superconductivity at 38 K in the iron arsenide $(Ba_{1-x}K_x)Fe_2As_2$*, Phys. Rev. Lett. **101**, 107006 (2008).

[56] K. Sasmal, B. Lv, B. Lorenz, A. M. Guloy, F. Chen, Y.-Y. Xue, and C.-W. Chu, *Superconducting Fe-based compounds ($A_{1-x}Sr_x$)Fe_2As_2 with A = K and Cs with transition temperatures up to 37 K*, Phys. Rev. Lett. **101**, 107007 (2008).

[57] G. Wu, H. Chen, T. Wu, Y. L. Xie, Y. J. Yan, R. H. Liu, X. F. Wang, J. J. Ying, and X. H. Chen, *Different resistivity response to spin-density wave and superconductivity at 20 K in $Ca_{1-x}Na_xFe_2As_2$*, J. Phys.: Condens. Matter **20**, 422201 (2008).

[58] H. S. Jeevan, Z. Hossain, D. Kasinathan, H. Rosner, C. Geibel, and P. Gegenwart, *High-temperature superconductivity in $Eu_{0.5}K_{0.5}Fe_2As_2$*, Phys. Rev. B **78**, 092406 (2008).

[59] Y. Qi, Z. Gao, L. Wang, D. Wang, X. Zhang, and Y. Ma, *Superconductivity at 34.7 K in the iron arsenide $Eu_{0.7}Na_{0.3}Fe_2As_2$*, New J. Phys. **10**, 123003 (2008).

[60] X. C. Wang, Q. Q. Liu, Y. X. Lv, W. B. Gao, L. X. Yang, R. C. Yu, F. Y. Li, and C. Q. Jin, *The superconductivity at 18 K in LiFeAs system*, Solid State Comm. **148**, 538 (2008).

[61] D. R. Parker, M. J. Pitcher, P. J. Baker, I. Franke, T. Lancaster, S. J. Blundell, and S. J. Clarke, *Structure, antiferromagnetism and superconductivity of the layered iron arsenide NaFeAs*, Chem. Comm. **16**, 2189 (2009).

[62] H. Ogino, Y. Matsumura, Y. Katsura, K. Ushiyama, S. Horii, K. Kishio, and J. Shimoyama, *Superconductivity at 17 K in (Fe_2P_2)($Sr_4Sc_2O_6$): A new superconducting layered pnictide oxide with a thick perovskite oxide layer*, Supercond. Sci. Technol. **22**, 075008 (2009).

[63] X. Zhu, F. Han, G. Mu, B. Zeng, P. Cheng, B. Shen, and H.-H. Wen, *$Sr_3Sc_2Fe_2As_2O_5$ as a possible parent compound for FeAs-based superconductors*, Phys. Rev. B **79**, 024516 (2009).

[64] F.-C. Hsu, J.-Y. Luo, K.-W. Yeh, T.-K. Chen, T.-W. Huang, P. M. Wu, Y.-C. Lee, Y.-L. Huang, Y.-Y. Chu, D.-C. Yan, and M.-K. Wu, *Superconductivity in the PbO-type structure α-FeSe*, Proc. Nat. Acad. Sci. USA **105**, 14262 (2008).

[65] K.-W. Yeh, T.-W. Huang, Y. l. Huang, T.-K. Chen, F.-C. Hsu, P. M. Wu, Y.-C. Lee, Y.-Y. Chu, C.-L. Chen, J.-Y. Luo, D.-C. Yan, and M.-K. Wu, *Tellurium substitution effect on superconductivity of the α-phase iron selenide*, EPL **84**, 37002 (2008).

[66] B. C. Sales, A. S. Sefat, M. A. McGuire, R. Y. Jin, D. Mandrus, and Y. Mozharivskyj, *Bulk superconductivity at 14 K in single crystals of $Fe_{1+y}Te_xSe_{1-x}$*, Phys. Rev. B **79**, 094521 (2009).

[67] Y. Mizuguchi, F. Tomioka, S. Tsuda, T. Yamaguchi, and Y. Takano, *Substitution Effects on FeSe Superconductor*, J. Phys. Soc. Jap. **78**, 074712 (2009).

[68] S. Margadonna, Y. Takabayashi, Y. Ohishi, Y. Mizuguchi, Y. Takano, T. Kagayama, T. Nakagawa, M. Takata, and K. Prassides, *Pressure evolution of the low-temperature crystal structure and bonding of the superconductor FeSe ($T_c = 37\,K$)*, Phys. Rev. B **80**, 064506 (2009).

[69] J. Guo, S. Jin, G. Wang, S. Wang, K. Zhu, T. Zhou, M. He, and X. Chen, *Superconductivity in the iron selenide $K_xFe_2Se_2$ ($0 \leq x \leq 1.0$)*, Phys. Rev. B **82**, 180520 (2010).

[70] A. Krzton-Maziopa, Z. Shermadini, E. Pomjakushina, V. Pomjakushin, M. Bendele, A. Amato, R. Khasanov, H. Luetkens, and K. Conder, *Synthesis and crystal growth of $Cs_{0.8}(FeSe_{0.98})_2$: a new iron-based superconductor with $T_c = 27\,K$*, Journal of Physics: Condensed Matter **23**, 052203 (2011).

[71] A. F. Wang, J. J. Ying, Y. J. Yan, R. H. Liu, X. G. Luo, Z. Y. Li, X. F. Wang, M. Zhang, G. J. Ye, P. Cheng, Z. J. Xiang, and X. H. Chen, *Superconductivity at 32 K in single-crystalline $Rb_xFe_{2-y}Se_2$*, Phys. Rev. B **83**, 060512 (2011).

[72] S. Weyeneth, *Anisotropic properties and critical behavior of high-temperature superconductors*, Ph.D. thesis, University of Zurich, 2009.

[73] L. Boeri, O. V. Dolgov, and A. A. Golubov, *Is $LaFeAsO_{1-x}F_x$ an Electron-Phonon Superconductor?*, Phys. Rev. Lett. **101**, 026403 (2008).

[74] D. V. Evtushinsky, D. S. Inosov, V. B. Zabolotnyy, M. S. Viazovska, R. Khasanov, A. Amato, H.-H. Klauss, H. Luetkens, C. Niedermayer, G. L. Sun, V. Hinkov, C. T. Lin, A. Varykhalov, A. Koitzsch, M. Knupfer, B. Büchner, A. A. Kordyuk, and S. V. Borisenko, *Momentum-resolved superconducting gap in the bulk of $Ba_{1-x}K_xFe_2As_2$ from combined ARPES and μSR measurements*, New Journal of Physics **11**, 055069 (2009).

[75] K. Kuroki, H. Usui, S. Onari, R. Arita, and H. Aoki, *Pnictogen height as a possible switch between high- Tc nodeless and low- Tc nodal pairings in the iron-based superconductors*, Phys. Rev. B **79**, 224511 (2009).

[76] K. Seo, B. A. Bernevig, and J. Hu, *Pairing Symmetry in a Two-Orbital Exchange Coupling Model of Oxypnictides*, Phys. Rev. Lett. **101**, 206404 (2008).

[77] S. Onari, H. Kontani, and M. Sato, *Structure of neutron-scattering peaks in both s_{++}-wave and $s_{\pm}$ -wave states of an iron pnictide superconductor*, Phys. Rev. B **81**, 060504 (2010).

[78] I. I. Mazin, D. J. Singh, M. D. Johannes, and M. H. Du, *Unconventional superconductivity with a sign reversal in the order parameter of $LaFeAsO_{1-x}F_x$*, Phys. Rev. Lett. **101**, 057003 (2008).

[79] A. V. Chubukov, *Renormalization group analysis of competing orders and the pairing symmetry in Fe-based superconductors*, Physica C **469**, 640 (2009).

[80] A. V. Chubukov, M. G. Vavilov, and A. B. Vorontsov, *Momentum dependence and nodes of the superconducting gap in the iron pnictides*, Phys. Rev. B **80**, 140515 (2009).

[81] A. B. Vorontsov, M. G. Vavilov, and A. V. Chubukov, *Superconductivity and spin-density waves in multiband metals*, Phys. Rev. B **81**, 174538 (2010).

[82] R. M. Fernandes and J. Schmalian, *Competing order and nature of the pairing state in the iron pnictides*, Phys. Rev. B **82**, 014521 (2010).

[83] A. B. Vorontsov, M. G. Vavilov, and A. V. Chubukov, *Interplay between magnetism and superconductivity in the iron pnictides*, Phys. Rev. B **79**, 060508 (2009).

[84] T. Yildirim, *Origin of the 150-K Anomaly in LaFeAsO: Competing Antiferromagnetic Interactions, Frustration, and a Structural Phase Transition*, Phys. Rev. Lett. **101**, 057010 (2008).

[85] T. Yildirim, *Frustrated magnetic interactions, giant magneto-elastic coupling, and magnetic phonons in iron-pnictides*, Physica C **469**, 425 (2009).

[86] F. Yndurain and J. M. Soler, *Anomalous electron-phonon interaction in doped LaFeAsO: First-principles calculations*, Phys. Rev. B **79**, 134506 (2009).

[87] H. Liu, T. Wu, H. Chen, X. F. Wang, Y. L.Xie, J. J. Ying, Y. J. Yan, Q. J. Li, B. C. Shi, W. S. Chu, Z. Y. Wu, and X. H. Chen, *A large iron isotope effect in $SmFeAsO_{1-x}F_x$ and $Ba_{1-x}K_xFe_2As_2$*, Nature (London) **459**, 64 (2008).

[88] P. M. Shirage, K. Miyazawa, K. Kihou, H. Kito, Y. Yoshida, Y. Tanaka, H. Eisaki, and A. Iyo, *Absence of an Appreciale Iron Isotope Effect on the Transition Temperature of the Optimally Doped $SmFeAsO_{1-y}$ Superconductor*, Phys. Rev. Lett. **105**, 037004 (2010).

[89] P. M. Shirage, K. Kihou, K. Miyazawa, C.-H. Lee, H. Kito, H. Eisaki, T. Yanagisawa, Y. Tanaka, and A. Iyo, *Inverse Iron Isotope Effect on the Transition Temperature of the (Ba,K)Fe_2As_2 Superconductor*, Phys. Rev. Lett. **103**, 257003 (2009).

[90] R. Khasanov, M. Bendele, K. Conder, H. Keller, E. Pomjakushina, and V. Pomjakushin, *Iron isotope effect on the superconducting transition temperature and the crystal structure of $FeSe_{1-x}$*, New J. Phys. **12**, 073024 (2010).

[91] R. Khasanov, M. Bendele, A. Bussmann-Holder, and H. Keller, *Intrinsic and structural isotope effects in Fe-based superconductors*, Phys. Rev. B **82**, 212505 (2010).

[92] K. Terashima, Y. Sekiba, J. H. Bowen, K. Nakayama, T. Kawahara, T. Sato, P. Richard, Y.-M. Xu, L. J. Li, G. H. Cao, Z.-A. Xu, H. Ding, and T. Takahashi, *Fermi surface nesting induced strong pairing in iron-based superconductors*, Proc. Nat. Acad. Sci. USA **106**, 7330 (2009).

[93] D. C. Johnston, *The puzzle of high temperature superconductivity in layered iron pnictides and chalcogenides*, Advances In Physics **59**, 803 (2010).

[94] M. D. Lumsden and A. D. Christianson, *Magnetism in Fe-based superconductors*, J. Phys.: Condens. Matter **22**, 203203 (2010).

[95] S.-H. Lee, G. Xu, W. Ku, J. S. Wen, C. C. Lee, N. Katayama, Z. J. Xu, S. Ji, Z. W. Lin, G. D. Gu, H.-B. Yang, P. D. Johnson, Z.-H. Pan, T. Valla, M. Fujita, T. J. Sato, S. Chang, K. Yamada, and J. M. Tranquada, *Coupling of spin and orbital excitations in the iron-based superconductor* $FeSe_{0.5}Te_{0.5}$, Phys. Rev. B **81**, 220502 (2010).

[96] P. Babkevich, M. Bendele, A. T. Boothroyd, K. Conder, S. N. Gvasaliya, R. Khasanov, E. Pomjakushina, and B. Roessli, *Magnetic excitations of* $Fe_{1+y}Se_xTe_{1-x}$ *in magnetic and superconductive phases*, J. Phys.: Condens. Matter **22**, 142202 (2010).

[97] J. Zhang, R. Sknepnek, R. M. Fernandes, and J. Schmalian, *Orbital coupling and superconductivity in the iron pnictides*, Phys. Rev. B **79**, 220502 (2009).

[98] E. Pomjakushina, K. Conder, V. Pomjakushin, M. Bendele, and R. Khasanov, *Synthesis, crystal structure, and chemical stability of the superconductor* $FeSe_{1-x}$, Phys. Rev. B **80**, 024517 (2009).

[99] T. M. McQueen, Q. Huang, V. Ksenofontov, C. Felser, Q. Xu, H. Zandbergen, Y. S. Hor, J. Allred, A. J. Williams, D. Qu, J. Checkelsky, N. P. Ong, and R. J. Cava, *Extreme sensitivity of superconductivity to stoichiometry in* $Fe_{1+\delta}Se$, Phys. Rev. B **79**, 014522 (2009).

[100] S. Margadonna, Y. Takabayashi, M. T. McDonald, K. Kasperkiewicz, Y. Mizuguchi, Y. Takano, A. N. Fitch, E. Suard, and K. Prassides, *Crystal structure of the new* $FeSe_{1-x}$ *superconductor*, Chem. Commun. , 5607 (2008).

[101] S. Medvedev, T. M. McQueen, I. A. Troyan, T. Palasyuk, M. I. Eremets, R. J. Cava, S. Naghavi, F. Casper, V. Ksenofontov, G. Wortmann, and C. Felser, *Electronic and magnetic phase diagram of* β-$Fe_{1.01}Se$ *with superconductivity at 36.7 K under pressure*, Nature Materials **8**, 630 (2009).

[102] M. Bendele, A. Amato, K. Conder, M. Elender, H. Keller, H.-H. Klauss, H. Luetkens, E. Pomjakushina, A. Raselli, and R. Khasanov, *Pressure Induced Static Magnetic Order in Superconducting* $FeSe_{1-x}$, Phys. Rev. Lett. **104**, 087003 (2010).

[103] K. Miyoshi, Y. Takaichi, E. Mutou, K. Fujiwara, and J. Takeuchi, *Anomalous Pressure Dependence of the Superconducting Transition Temperature in* $FeSe_{1-x}$ *Studied by DC Magnetic Measurements*, J. Phys. Soc. Jap. **78**, 093703 (2009).

[104] S. Masaki, H. Kotegawa, Y. Hara, H. Tou, K. Murata, Y. Mizuguchi, and Y. Takano, *Precise Pressure Dependence of the Superconducting Transition Temperature of FeSe: Resistivity and* ^{77}*Se-NMR Study*, J. Phys. Soc. Jap. **78**, 063704 (2009).

[105] M. Bendele, A. Ichsanow, Y. Pashkevich, L. Keller, T. Strässle, A. Gusev, E. Pomjakushina, K. Conder, R. Khasanov, and H. Keller, *Coexistence of superconductivity and magnetism in $FeSe_{1-x}$ under pressure*, Phys. Rev. B **85**, 064517 (2012).

[106] A. Ichsanow, *Magnetic and Superconducting properties of $FeSe_{1-x}$, dependency on sample preparation*, Master thesis, University of Zurich, 2010.

[107] A. Bussmann-Holder, R. Micnas, and A. Bishop, *Enhancements of the superconducting transition temperature within the two-band model*, Eur. Phys. J. B **37**, 345 (2004).

[108] V. G. Kogan, C. Martin, and R. Prozorov, *Superfluid density and specific heat within a self-consistent scheme for a two-band superconductor*, Phys. Rev. B **80**, 014507 (2009).

[109] A. Bussmann-Holder, *Comment on: Superfluid density and specific heat within a self-consistent scheme for a two-band superconductor*, arXiv:0909.3603v1 (2009).

[110] R. Khasanov, M. Bendele, A. Amato, K. Conder, H. Keller, H.-H. Klauss, H. Luetkens, and E. Pomjakushina, *Evolution of Two-Gap Behavior of the Superconductor $FeSe_{1-x}$*, Phys. Rev. Lett. **104**, 087004 (2010).

[111] M. Bendele, S. Weyeneth, R. Puzniak, A. Maisuradze, E. Pomjakushina, K. Conder, V. Pomjakushin, H. Luetkens, S. Katrych, A. Wisniewski, R. Khasanov, and H. Keller, *Anisotropic superconducting properties of single-crystalline $FeSe_{0.5}Te_{0.5}$*, Phys. Rev. B **81**, 224520 (2010).

[112] A. T. Savici, Y. Fudamoto, I. M. Gat, T. Ito, M. I. Larkin, Y. J. Uemura, G. M. Luke, K. M. Kojima, Y. S. Lee, M. A. Kastner, R. J. Birgeneau, and K. Yamada, *Muon spin relaxation studies of incommensurate magnetism and superconductivity in stage-4 $La_2CuO_{4.11}$ and $La_{1.88}Sr_{0.12}CuO_4$*, Phys. Rev. B **66**, 014524 (2002).

[113] I. M. Reznik, F. G. Vagizov, and R. Troć, *Chemical bonding in the $UFe_{1-x}Ni_xAl$ alloys*, Phys. Rev. B **51**, 3013 (1995).

[114] P. W. Anderson, *Antiferromagnetism. Theory of Superexchange Interaction*, Phys. Rev. **79**, 350 (1950).

[115] J. B. Goodenough, *Theory of the Role of Covalence in the Perovskite-Type Manganites [La, M(II)]MnO_3*, Phys. Rev. **100**, 564 (1955).

[116] J. Kanamori, *Superexchange interaction and symmetry properties of electron orbitals*, Journal of Physics and Chemistry of Solids **10**, 87 (1959).

[117] M. J. Han, Q. Yin, W. E. Pickett, and S. Y. Savrasov, *Anisotropy, Itineracy, and Magnetic Frustration in High-T_c Iron Pnictides*, Phys. Rev. Lett. **102**, 107003 (2009).

[118] T. Imai, K. Ahilan, F. L. Ning, T. M. McQueen, and R. J. Cava, *Why Does Undoped FeSe Become a High-T_c Superconductor under Pressure?*, Phys. Rev. Lett. **102**, 177005 (2009).

[119] J. T. Park, D. S. Inosov, C. Niedermayer, G. L. Sun, D. Haug, N. B. Christensen, R. Dinnebier, A. V. Boris, A. J. Drew, L. Schulz, T. Shapoval, U. Wolff, V. Neu, X. Yang, C. T. Lin, B. Keimer, and V. Hinkov, *Electronic Phase Separation in the Slightly Underdoped Iron Pnictide Superconductor* $Ba_{1-x}K_xFe_2As_2$, Phys. Rev. Lett. **102**, 117006 (2009).

[120] R. Khasanov, S. Sanna, G. Prando, Z. Shermadini, M. Bendele, A. Amato, P. Carretta, R. De Renzi, J. Karpinski, S. Katrych, H. Luetkens, and N. D. Zhigadlo, *Tuning of competing magnetic and superconducting phase volumes in* $LaFeAsO_{0.945}F_{0.055}$ *by hydrostatic pressure*, Phys. Rev. B **84**, 100501 (2011).

[121] H. Maeter, H. Luetkens, Y. G. Pashkevich, A. Kwadrin, R. Khasanov, A. Amato, A. A. Gusev, K. V. Lamonova, D. A. Chervinskii, R. Klingeler, C. Hess, G. Behr, B. Büchner, and H.-H. Klauss, *Interplay of rare earth and iron magnetism in* $RFeAsO$ *(R = La, Ce, Pr, and Sm): Muon-spin relaxation study and symmetry analysis*, Phys. Rev. B **80**, 094524 (2009).

[122] R. Khasanov, H. Luetkens, A. Amato, H.-H. Klauss, Z.-A. Ren, J. Yang, W. Lu, and Z.-X. Zhao, *Muon spin rotation studies of* $SmFeAsO_{0.85}$ *and* $NdFeAsO_{0.85}$ *superconductors*, Phys. Rev. B **78**, 092506 (2008).

[123] R. Khasanov, M. Bendele, A. Amato, P. Babkevich, A. T. Boothroyd, A. Cervellino, K. Conder, S. N. Gvasaliya, H. Keller, H.-H. Klauss, H. Luetkens, E. Pomjakushina, and B. Roessli, *Coexistence of incommensurate magnetism and superconductivity in* $Fe_{1+y}Se_xTe_{1-x}$, Phys. Rev. B **80**, 140511 (2009).

[124] Y. Laplace, J. Bobroff, F. Rullier-Albenque, D. Colson, and A. Forget, *Atomic coexistence of superconductivity and incommensurate magnetic order in the pnictide* $Ba(Fe_{1-x}Co_x)_2As_2$, Phys. Rev. B **80**, 140501 (2009).

[125] Z. Shermadini, A. Krzton-Maziopa, M. Bendele, R. Khasanov, H. Luetkens, K. Conder, E. Pomjakushina, S. Weyeneth, V. Pomjakushin, O. Bossen, and A. Amato, *Coexistence of Magnetism and Superconductivity in the Iron-Based Compound* $Cs_{0.8}(FeSe_{0.98})_2$, Phys. Rev. Lett. **106**, 117602 (2011).

[126] R. Hu, K. Cho, H. Kim, H. Hodovanets, W. E. Straszheim, M. A. Tanatar, R. Prozorov, S. L. Bud'ko, and P. C. Canfield, *Anisotropic magnetism, resistivity, London penetration depth and magneto-optical imaging of superconducting* $K_{0.80}Fe_{1.76}Se_2$ *single crystals*, Superconductor Science and Technology **24**, 065006 (2011).

[127] B. Wei, H. Qing-Zhen, C. Gen-Fu, M. A. Green, W. Du-Ming, H. Jun-Bao, and Q. Yi-Ming, *A Novel Large Moment Antiferromagnetic Order in* $K_{0.8}Fe_{1.6}Se_2$ *Superconductor*, Chinese Physics Letters **28**, 086104 (2011).

[128] R. Khasanov, K. Conder, E. Pomjakushina, A. Amato, C. Baines, Z. Bukowski, J. Karpinski, S. Katrych, H.-H. Klauss, H. Luetkens, A. Shengelaya, and N. D. Zhi-

gadlo, *Evidence of nodeless superconductivity in $FeSe_{0.85}$ from a muon-spin-rotation study of the in-plane magnetic penetration depth*, Phys. Rev. B **78**, 220510 (2008).

[129] M. G. Vavilov, A. V. Chubukov, and A. B. Vorontsov, *Coexistence between superconducting and spin density wave states in iron-based superconductors: Ginzburg-Landau analysis*, Superconductor Science and Technology **23**, 054011 (2010).

[130] V. Cvetkovic and Z. Tesanovic, *Valley density-wave and multiband superconductivity in iron-based pnictide superconductors*, Phys. Rev. B **80**, 024512 (2009).

[131] A. Carrington and F. Manzano, *Magnetic penetration depth of MgB_2*, Physica C **385**, 205 (2003).

[132] P. K. Biswas, G. Balakrishnan, D. M. Paul, C. V. Tomy, M. R. Lees, and A. D. Hillier, *Muon-spin-spectroscopy study of the penetration depth of $FeTe_{0.5}Se_{0.5}$*, Phys. Rev. B **81**, 092510 (2010).

[133] H. Lei, R. Hu, E. S. Choi, J. B. Warren, and C. Petrovic, *Pauli-limited upper critical field of $Fe_{1+\delta}Te_{1-x}Se_x$*, Phys. Rev. B **81**, 094518 (2010).

[134] M. Fang, J. Yang, F. F. Balakirev, Y. Kohama, J. Singleton, B. Qian, Z. Q. Mao, H. Wang, and H. Q. Yuan, *Weak anisotropy of the superconducting upper critical field in $Fe_{1.11}Te_{0.6}Se_{0.4}$ single crystals*, Phys. Rev. B **81**, 020509 (2010).

[135] T. Kato, Y. Mizuguchi, H. Nakamura, T. Machida, H. Sakata, and Y. Takano, *Local density of states and superconducting gap in the iron chalcogenide superconductor $Fe_{1+\delta}Se_{1-x}Te_x$ observed by scanning tunneling spectroscopy*, Phys. Rev. B **80**, 180507 (2009).

[136] H. Kim, C. Martin, R. T. Gordon, M. A. Tanatar, J. Hu, B. Qian, Z. Q. Mao, R. Hu, C. Petrovic, N. Salovich, R. Giannetta, and R. Prozorov, *London penetration depth and superfluid density of single-crystalline $Fe_{1+y}(Te_{1-x}Se_x)$ and $Fe_{1+y}(Te_{1-x}S_x)$*, Phys. Rev. B **81**, 180503 (2010).

[137] S. Weyeneth, R. Puzniak, U. Mosele, N. D. Zhigadlo, S. Katrych, Z. Bukowski, J. Karpinski, S. Kohout, J. Roos, and H. Keller, *Anisotropy of superconducting single crystal $SmFeAsO_{0.8}F_{0.2}$ studied by torque magnetometry*, J. Supercond. Nov. Magn. **22**, 325 (2009).

[138] S. Weyeneth, R. Puzniak, N. D. Zhigadlo, S. Katrych, Z. Bukowski, J. Karpinski, and H. Keller, *Evidence for two distinct anisotropies in the oxypnictide superconductors $SmFeAsO_{0.8}F_{0.2}$ and $NdFeAsO_{0.8}F_{0.2}$*, J. Supercond. Nov. Magn. **22**, 347 (2009).

[139] M. Bendele, P. Babkevich, S. Katrych, S. N. Gvasaliya, E. Pomjakushina, K. Conder, B. Roessli, A. T. Boothroyd, R. Khasanov, and H. Keller, *Tuning the superconducting and magnetic properties of $Fe_ySe_{0.25}Te_{0.75}$ by varying the iron content*, Phys. Rev. B **82**, 212504 (2010).

[140] Y. J. Uemura, G. M. Luke, B. J. Sternlieb, J. H. Brewer, J. F. Carolan, W. N. Hardy, R. Kadono, J. R. Kempton, R. F. Kiefl, S. R. Kreitzman, P. Mulhern, T. M. Riseman, D. L. Williams, B. X. Yang, S. Uchida, H. Takagi, J. Gopalakrishnan, A. W. Sleight, M. A. Subramanian, C. L. Chien, M. Z. Cieplak, G. Xiao, V. Y. Lee, B. W. Statt, C. E. Stronach, W. J. Kossler, and X. H. Yu, *Universal Correlations between T_c and n_s/m^* (Carrier Density over Effective Mass) in High-T_c Cuprate Superconductors*, Phys. Rev. Lett. **62**, 2317 (1989).

[141] A. Shengelaya, R. Khasanov, D. G. Eshchenko, D. Di Castro, I. M. Savić, M. S. Park, K. H. Kim, S.-I. Lee, K. A. Müller, and H. Keller, *Muon-Spin-Rotation Measurements of the Penetration Depth of the Infinite-Layer Electron-Doped $Sr_{0.9}La_{0.1}CuO_2$ Cuprate Superconductor*, Phys. Rev. Lett. **94**, 127001 (2005).

[142] R. Viennois, E. Giannini, D. van der Marel, and R. Černý, *Effect of Fe excess on structural, magnetic and superconducting properties of single-crystalline $Fe_{1+x}Te_{1-y}Se_y$*, Journal of Solid State Chemistry **183**, 769 (2010).

[143] W. Bao, Y. Qiu, Q. Huang, M. A. Green, P. Zajdel, M. R. Fitzsimmons, M. Zhernenkov, S. Chang, M. Fang, B. Qian, E. K. Vehstedt, J. Yang, H. M. Pham, L. Spinu, and Z. Q. Mao, *Tunable ($\delta\pi$, $\delta\pi$)-Type Antiferromagnetic Order in α-Fe(Te,Se) Superconductors*, Phys. Rev. Lett. **102**, 247001 (2009).

[144] S. Li, C. de la Cruz, Q. Huang, Y. Chen, J. W. Lynn, J. Hu, Y.-L. Huang, F.-C. Hsu, K.-W. Yeh, M.-K. Wu, and P. Dai, *First-order magnetic and structural phase transitions in $Fe_{1+y}Se_xTe_{1-x}$*, Phys. Rev. B **79**, 054503 (2009).

[145] H. Kamerlingh Onnes and W. Tuyn, *Measurements Concerning the Electrical Resistance or Ordinary Lead and of Uranium Lead Below 14K*, Comm. Phys. Lab. Leiden **160b**, 13 (1922).

[146] K. Prassides, J. Tomkinson, C. Christides, M. J. Rosseinsky, D. W. Murphy, and R. C. Haddon, *Vibrational spectroscopy of superconducting K_3C_{60} by inelastic neutron scattering*, NAT **354**, 462 (1991).

[147] A. P. Ramirez, A. R. Kortan, M. J. Rosseinsky, S. J. Duclos, A. M. Mujsce, R. C. Haddon, D. W. Murphy, A. V. Makhija, S. M. Zahurak, and K. B. Lyons, *Isotope effect in superconducting Rb_3C_{60}*, Phys. Rev. Lett. **68**, 1058 (1992).

[148] S. L. Bud'ko, G. Lapertot, C. Petrovic, C. E. Cunningham, N. Anderson, and P. C. Canfield, *Boron Isotope Effect in Superconducting MgB_2*, Phys. Rev. Lett. **86**, 1877 (2001).

[149] D. G. Hinks, H. Claus, and J. D. Jorgensen, *The complex nature of superconductivity in MgB_2 as revealed by the reduced total isotope effect*, NAT **411**, 457 (2001).

[150] D. G. Hinks and J. D. Jorgensen, *The isotope effect and phonons in MgB_2*, Physica C **385**, 98 (2003).

[151] D. D. Castro, M. Angst, D. G. Eshchenko, R. Khasanov, J. Roos, I. M. Savić, A. Shengelaya, S. L. Bud'ko, P. C. Canfield, K. Conder, J. Karpinski, S. M. Kazakov, R. A. Ribeiro, and H. Keller, *Absence of a boron isotope effect in the magnetic penetration depth of* MgB_2, Phys. Rev. B **70**, 014519 (2004).

[152] G.-M. Zhao, K. Ghosh, and R. L. Greene, *Colossal oxygen isotope shift of the charge-ordering transition in Nd 0.5 Sr 0.5 MnO 3*, J. Phys.: Condens. Matter **10**, L737 (1998).

[153] G. meng Zhao, H. Keller, and K. Conder, *Unconventional isotope effects in the high-temperature cuprate superconductors*, J. Phys.: Condens. Matter **13**, R569 (2001).

[154] H. Keller, *Unconventional Isotope Effects in Cuprate Superconductors*, in *Unconventional Isotope Effects in Cuprate Superconductors*, edited by K. A. Müller and A. Bussmann-Holder, Vol. 114 of *Structure & Bonding*, pages 1336–1338, Springer Berlin / Heidelberg, 2005.

[155] J. P. Franck, S. Harker, and J. H. Brewer, *Copper and oxygen isotope effects in* $La_{2-x}Sr_xCuO_4$, Phys. Rev. Lett. **71**, 283 (1993).

[156] R. Khasanov, A. Shengelaya, D. Di Castro, E. Morenzoni, A. Maisuradze, I. M. Savić, K. Conder, E. Pomjakushina, A. Bussmann-Holder, and H. Keller, *Oxygen Isotope Effects on the Superconducting Transition and Magnetic States Within the Phase Diagram of* $Y_{1-x}Pr_xBa_2Cu_3O_{7-\delta}$, Phys. Rev. Lett. **101**, 077001 (2008).

[157] M. Rotter, M. Pangerl, M. Tegel, and D. Johrendt, *Superconductivity and crystal structures of* $Ba_{1-x}K_xFe_2As_2$ *(*$x = 0 - 1$*)*, Angew. Chem. Int. Ed. **47**, 7949 (2008).

[158] A. Bussmann-Holder, A. Simon, H. Keller, and A. Bishop, *Identifying the Pairing Mechanism in Fe-As Based Superconductors: Gaps and Isotope Effects*, Journal of Superconductivity and Novel Magnetism **24**, 1099 (2011), 10.1007/s10948-010-0864-z.

Acknowledgments

In this place, it is time to say thank you to everybody who contributed and helped this work to succeed. Working at the *Physik-Institut der Universität Zürich* and at the *Paul Scherrer Institut* was a great experience. Thanks to many people there, I had a delightful learning time in a friendly and constructive working atmosphere.

Zu Beginn möchte ich Prof. Hugo Keller für die Möglichkeit danken, in seiner Forschungsgruppe diese Arbeit durchzuführen. Trotz seiner knappen Zeit hatte er immer eine offene Tür für mich und immer einen wertvollen Rat bereit. Die gewährte Freiheit zusammen mit den vielfältigen Möglichkeiten sowie der Unterstützung in wissenschaftlicher und finanzieller Hinsicht haben es mir erlaubt, unzählige sehr wertvolle Erfahrungen zu sammeln.

Many thanks to Dr. Rustem Khasanov for the introduction to μSR and valuable discussions. The various beamtimes together were enlightening and it was a great pleasure to work with him. His enthusiasm is really catching to me.

The measurements would not have been possible without the high quality samples prepared by PD. Dr. Kazimirz Conder and Dr. Ekaterina Pomjakushina at PSI. It was a great pleasure to work with them. Furthermore, I would like to thank Dr. Nikolai Zhigadlo for the samples prepared at ETH.

Thanks to Prof. Roman Puzniak for the fruitful discussions and his great support in various fields of this work. It was always a great pleasure to work with him.

Herzlich möchte ich mich bei Stephen für die vielen wunderbaren Diskussionen, die Teamarbeit und seine Freundschaft bedanken.

Merci Simon und Nastja. Ich habe unsere Freundschaft und die damit verbundenen Bierchen immer sehr genossen.

Danke an Matthias Elender, der mir jederzeit, auch sehr spontan, mit einer helfenden Hand zur Verfügung stand. Auch dem Werkstatt Team um Kurt Bösiger gilt ein grosses Dankeschön. Ohne die Arbeiten, welche immer zu meiner vollsten Zufriedenheit ausgeführt wurden, wäre so manches nicht möglich gewesen.

Ein grosses dankeschön gilt meinen Mitbewohnern (umgekehrt alphabetisch): Thomas, Simon, Philipp, Nicole, Ivan und Giancarlo für ihre Geduld mit mir und so manches sehr

leckere Essen. Meine Zeit in der WG-Bergün war unbeschreiblich.

Grazie Ilaria for inspiring me to finish so fast. The thoughts to you always renewed my motivation.

I would like to thank my collegues from Univeristy of Zurich, PSI and ETH for the great working atmosphere (in alphabetic order): Alex Amato, Saskia Bosma, Zurab Guguchia, Severin Gvsaelle, Francis Froborg, Sergij Katrich, Lukas Keller, Hubertus Luetkens, Elvezio Morenzoni, Ferenc Muranyi, Volodja Pomjakushin, Bertrand Roessli, Robert Scheuermann, Evelyin Stilp, Stefan Sigrist, Thierry Strässle, Andreas Suter, and Bastian Wojek.

Ein besonderer Dank geht an meine Familie. Wo immer und wann immer sie konnte hat sie mich liebevollst unterstützt. Ohne sie wäre dies alles nicht möglich gewesen.

This work was supported by the Swiss National Science Foundation.

Curriculum vitae

Name	Markus Michael Bendele
Date of birth	January 12^{th}, 1982
Place of birth	Heidenheim, Germany
Citizenship	German

Education

12/11	University of Zurich, Switzerland, Ph.D. thesis The superconducting and magnetic properties of the iron-chalcogenides Supervisors: Prof. Dr. Hugo Keller, Dr. Rustem Khasanov
01/09 - 12/11	University of Zurich, Switzerland, Ph.D. student in physics Superconductivity and Magnetism group of Prof. Dr. Hugo Keller
09/08	University of Ulm, Germany, Dilpoma thesis Optimization of epitaxial FePt thin films Supervisors: Prof. Dr. Paul Ziemann, Dr. Ulf Wiedwald
10/07 - 09/08	University of Ulm, Germany, Diploma work Institut für Festkörperphysik, Prof. Dr. Paul Ziemann
10/02 - 09/08	University of Ulm, Germany, undergrad studies in physics Main focus: Condensed matter physics
09/92 - 06/01	Werkgymnasium Heidenheim, Germay, Abitur (high school diploma)

List of publications

Issued March 1st, 2012.

- *Atomic coexistence of superconductivity and magnetism in $FeSe_{1-x}$ under pressure*
  M. Bendele, A. Ichsanov, Yu. Pashkevich, L. Keller, T. Strässle, A. A. Gusev, E. Pomjakushina, K. Conder, R. Khasanov, and H. Keller,
  Phys. Rev. B **85**, 064517 (2012).

- *Magnetic-Field Tuned Anisotropy in superconducting $Rb_xFe_{2-y}Se_2$*
  S. Bosma, R. Puzniak, A. Krzton-Maziopa, M. Bendele, K. Pomjakushina, K. Conder, H. Keller, and S. Weyeneth,
  Phys. Rev. B **85**, 064509 (2012).

- *Interplay of composition, structure, magnetism, and superconductivity in $SmFeAs_{1-x}P_xO_{1-y}$*
  N. D. Zhigadlo, S. Katrych, M. Bendele, P. J. W. Moll, M. Tortello, S. Weyeneth, V. Yu. Pomyakushin, J. Kanter, R. Puzniak, Z. Bukowski, H. Keller, R. S. Gonnelli, R. Khasanov, J. Karpinski, and B. Batlogg,
  Phys. Rev. B **84**, 134526 (2011).

- *Tuning of competing magnetic and superconducting phase volumes in $LaFeAsO_{0.945}F_{0.055}$ by hydrostatic pressure*
  R. Khasanov, S. Sanna, G. Prando, Z. Shermadini, M. Bendele, A. Amato, P. Carretta, R. De Renzi, J. Karpinski, S. Katrych, H. Luetkens, and N.D. Zhigadlo,
  Phys. Rev. B **84**, 100501(R)(2011).

- *Muon spin rotation study of the intercalated graphite superconductor CaC_6 at low temperatures*
  F. Murányi, M. Bendele, R. Khasanov, S. Weyeneth, Z. Guguchia, A. Shengelaya, C. Baines, and H. Keller,
  J. Supercond. Nov. Magn., published Online (2011).
  DOI: 10.1007/s10948-011-1358-3

- *Coexistence of Magnetism and Superconductivity in the Iron-based Compound $Cs_{0.8}(FeSe_{0.98})_2$*
  Z. Shermadini, A. Krzton-Maziopa, M. Bendele, R. Khasanov, H. Luetkens, K. Conder, E. Pomjakushina, S. Weyeneth, V. Pomjakushin, O. Bossen, and A. Amato,
  Phys. Rev. Lett. **106**, 117602 (2011).

- *Synthesis and crystal growth of $Cs_{0.8}(FeSe_{0.98})_2$: a new iron-based superconductor with $T_c = 27\,K$*

A. Krzton-Maziopa, Z. Shermadini, E. Pomjakushina, V. Pomjakushin, M. Bendele, A. Amato, R. Khasanov, H. Luetkens, and K. Conder,
J. Phys.: Condens. Matter **23**, 052203 (2011).

- *Tuning the superconducting and magnetic properties in $Fe_ySe_{0.25}Te_{0.75}$ by varying the Fe-content*
M. Bendele, P. Babkevich, S. Katrych, S. N. Gvasaliya, E. Pomjakushina, K. Conder, B. Roessli, A. T. Boothroyd, R. Khasanov, and H. Keller,
Phys. Rev. B **82**, 212504 (2010).

- *Intrinsic and structural isotope effects in Fe-based superconductors*
R. Khasanov, M. Bendele, A. Bussmann-Holder, and H. Keller,
Phys. Rev. B **82**, 212505 (2010).

- *Microscopic Study of the Superconducting State of the Iron Pnictide $RbFe_2As_2$ via muon spin rotation*
Z. Shermadini, J. Kanter, C. Baines, M. Bendele, Z. Bukowski, R. Khasanov, H.-H. Klauss, H. Luetkens, H. Maeter, G. Pascua, B. Batlogg, and A. Amato,
Phys. Rev. B **82**, 144527 (2010).

- *Field-dependent superfluid density in the optimally doped $SmFeAsO_{1-x}F_y$ superconductor*
S. Weyeneth, M. Bendele, R. Puzniak, F. Muranyi, A. Bussmann-Holder, N. D. Zhigadlo, S. Katrych, Z. Bukowski, J. Karpinski, A. Shengelaya, R. Khasanov, and H. Keller,
EPL **91**, 47005 (2010).

- *Iron isotope effect on the superconducting transition temperature and the crystal structure of $FeSe_{1-x}$*
R. Khasanov, M. Bendele, K. Conder, H. Keller, E. Pomjakushina, and V. Pomjakushin,
New J. Phys., **12**, 073024 (2010).

- *Suppression of the antinodal coherence of superconducting $(Bi,Pb)_2(Sr,La)_2CuO_{6+\delta}$ as revealed by muon spin rotation and angle-resolved photoemission*
R. Khasanov, Takeshi Kondo, M. Bendele, Yoichiro Hamaya, A. Kaminski, S. L. Lee, S. J. Ray, and Tsunehiro Takeuchi,
Phys. Rev. B **82**, 020511 (2010).

- *Identification of magnetic properties of few nm sized FePt crystalline particles by characterizing the intrinsic atom order using aberration corrected S/TEM Ultramicroscopy*
J. Biskupek, J. R. Jinschek, U. Wiedwald, M. Bendele, L. Han, P. Ziemann, and U. Kaiser,
Ultramicroscopy, **110**, 820 (2010).

- *Anisotropic superconducting properties of single-crystalline $FeSe_{0.5}Te_{0.5}$*
M. Bendele, S. Weyeneth, R. Puzniak, A. Maisuradze, E. Pomjakushina, K. Conder, V. Pomjakushin, H. Luetkens, S. Katrych, A. Wisniewski, R. Khasanov, and H. Keller,
Phys. Rev. B **81**, 224520 (2010).

- *Magnetic excitations of $Fe_{1+y}Se_xTe_{1-x}$ in magnetic and superconductive phases*
  P. Babkevich, M. Bendele, A. T. Boothroyd, K. Conder, S. N. Gvasaliya, R. Khasanov, E. Pomjakushina, and B. Roessli,
  J. Phys.: Condens. Matter 22 142202 (2010).

- *Evolution of Two-Gap Behavior of the Superconductor $FeSe_{1-x}$*
  R. Khasanov, M. Bendele, A. Amato, K. Conder, H. Keller, H.-H. Klauss, H. Luetkens, and E. Pomjakushina,
  Phys. Rev. Lett. **104**, 087004 (2010).

- *Pressure Induced Static Magnetic Order in Superconducting $FeSe_{1-x}$*
  M. Bendele, A. Amato, K. Conder, M. Elender, H. Keller, H.-H. Klauss, H. Luetkens, E. Pomjakushina, A. Raselli, and R. Khasanov,
  Phys. Rev. Lett. **104**, 087003 (2010).

- *Coexistence of incommensurate magnetism and superconductivity in $Fe_{1+y}Se_xTe_{1-x}$*
  R. Khasanov, M. Bendele, A. Amato, P. Babkevich, A. T. Boothroyd, A. Cervellino, K. Conder, S. N. Gvasaliya, H. Keller, H.-H. Klauss, H. Luetkens, V. Pomjakushin, E. Pomjakushina, and B. Roessli,
  Phys. Rev. B **80**, 140511 (2009).

- *Synthesis, crystal structure, and chemical stability of the superconductor $FeSe_{1-x}$*
  E. Pomjakushina, K. Conder, V. Pomjakushin, M. Bendele, and R. Khasanov,
  Phys. Rev. B **80**, 024517 (2009).